Characteristics and origin of subaqueous pumice-rich pyroclastic facies: Ohanapecosh Formation (USA) and Dogashima Formation (Japan)

By

Martin Jutzeler

M.Sc. Joint Schools of Earth and Environmental Sciences of the

Geneva and Lausanne Universities (ELSTE), Switzerland

Submitted in fulfilment of the requirements for the degree of

Doctor in Philosophy

Australia

April, 2012

Statement

This thesis contains no material which has been accepted for a degree or diploma by the University or any other institution, except by way of background information and duly acknowledged in the thesis, and to best of my knowledge and belief no material previously published or written by another person except where due acknowledgment is made in the text of the thesis, nor does the thesis contain any material that infringes copyright.

Authority of Access

This thesis may be made available for loan and limited copying and communication in accordance with the Copyright Act 1968.

Date: 11th April 2012

Signature:

ABSTRACT

This thesis discusses the processes that generate subaqueous, pumice-rich pyroclastic facies in below wave-base environments. The principal method is field-based facies analysis. I also present grain size distributions and hydraulic sorting ratios of selected samples using a new technique that combines image analysis and functional stereology. Two Tertiary volcaniclastic successions have been studied. The Ohanapecosh Formation (Washington State, United States) is dominated by subaqueous pumice-rich facies derived from subaerial explosive eruptions and subaqueous sediment remobilisation in a continental basin environment. The Dogashima Formation (Izu Peninsula, Japan) contains well-preserved examples of subaqueous pumice-rich facies produced by subaqueous explosive eruptions and below wave-base sediment remobilisation in an oceanic arc setting.

The common processes of lithification and welding prevent quantification of grain size by conventional sieving for most clastic rocks in the geological record. In addition, the true grain size distribution of clastic rocks is finer grained than its representation in a random 2D section. I show that image analysis combined with functional stereology can be used to infer 3D volume fractions and weight percent of clast populations >0.25-2 mm from 2D cross-sectional images. Data from synthetic rocks correlate well with results from sieving of the same samples while still unconsolidated. The method can be applied to any type of coarse grained clastic rock, regardless of age, and therefore has a wide application in volcanology and clastic sedimentology.

The >800-m-thick Ohanapecosh Formation records voluminous sedimentation of volcanic clasts during the Eocene-Oligocene in the Central Cascades. Most volcaniclastic beds are dominated by angular pumice clasts and fiamme of intermediate composition, now entirely devitrified and altered. Very thick to extremely thick (1–50 m) and very thin to thick (0.001–1 m) beds are laterally continuous and have even thickness; erosion surfaces, cross-beds and other traction structures are almost entirely absent, which strongly suggests a below wave-base environment of deposition for most of the succession. The Chinook Pass Member is mostly composed of extremely thick, graded, matrix-supported, pumice-and-fiamme-rich beds that commonly include a coarse basal breccia comprising sub-rounded dense clasts. The abundance of angular pumice clasts and extreme thickness suggest that this facies was generated by magmatic volatile-driven explosive eruptions, and the sub-rounded dense clasts were probably rounded above wave-base. Thus, these beds are interpreted to have been deposited in a below wave-base setting by subaerial pyroclastic flows that crossed the shoreline, and transformed into eruption-fed, water-supported subaqueous volcaniclastic density currents. Reversely to normally graded pumice breccia facies that contains sub-rounded pumice clasts, wood and accretionary lapilli is interpreted to have formed by settling from pumice rafts, also related to subaerial explosive eruptions. The White Pass Member chiefly contains massive

to normally graded volcanic breccia and coarse volcanic breccia that suggest deposition from subaqueous high-concentration density currents and subaqueous debris flows. The abundance of angular pumice clasts suggests minor reworking above wave-base. Very thin to thick interbeds of fine sandstone to mudstone are interpreted to be derived from subaqueous and subaerial sources, and to have mostly been deposited from low density turbidity currents and suspension. The presence of shallow basaltic intrusions and mafic volcanic breccia composed of scoria lapilli and that contains rare beds of accretionary lapilli indicate the presence of intra-basinal scoria cones that may have been partly subaerial. The lateral transition to thinner and finer-grained facies in the Johnson Creek Member and western part of the White Pass Member suggests that the principal sources were to the east of the preserved exposures of the Ohanapecosh Formation.

The Pliocene Dogashima Formation (Izu Peninsula, Japan) is composed of three volcaniclastic sequences erupted under water. Dogashima 1 is mostly composed of pumice breccia, shard-rich siltstone, and cross-bedded and planar bedded pumice breccia/sandstone. The base of Dogashima 2 is dominated by very thick, clast-supported, massive grey andesite breccia composed of very coarse andesite clasts with quenched margins. It is gradationally overlain by very thick, clast-supported white pumice breccia. The massive grey andesite breccia is confined to a palæo-valley eroded into beds of Dogashima 1. The white pumice breccia is hydraulically sorted and stratified in proximity to the wall of this palæo-valley, and is stratified and finer grained in the adjacent overbank setting. The top of Dogashima 2 is dominated by very thick cross-bedded pumice breccia-conglomerate and planar bedded pumice breccia that contains coarse pumice clasts. Dogashima 2 has an erosive contact with overall monomictic andesite breccia of Dogashima 3. The similar mineralogy and composition of white andesite pumice and grey andesite clasts in Dogashima 1 and 2 suggests they were co-magmatic and erupted from the same vent. Dogashima 2 is interpreted to record explosive destruction of a subaqueous hot lava dome by a subaqueous, magmatic volatile-driven explosive eruption. Most of the products of this eruption were deposited in two gradational units from cohesionless, water-supported volcaniclastic density currents. Coarse pumice clasts and ash present in overlying planar beds were settled from suspension. This sequence demonstrates that lava or dome effusion on the sea floor can switch to an open-vent, pumice-forming, magmatic volatile-driven explosive activity, as in subaerial analogues. Pumice breccia of Dogashima 1 is interpreted to be the product of precursory explosive activity, whereas Dogashima 3 records a late, dome-building episode. Pumice breccia and dome-related clasts indicate cyclic effusive and explosive activity throughout the Dogashima Formation. Cross-bedded pumice breccia/breccia conglomerate facies in the Dogashima Formation are most likely to be products of resedimentation of pumiceous aggregates, and development and destruction of subaqueous dune fields in a below wave-base, canyon setting.

I apply the image analysis and functional stereology method to pumiceous volcaniclastic rocks of the Ohanapecosh and Dogashima formations and the Manukau Sub-Group (New Zealand) and the Sierra La Primavera caldera (Mexico). Samples from these water-lain successions were grouped into three broad facies, on the basis of bed thickness, abundance of matrix and clast size sorting. The volume of pumice clasts, dense clasts and matrix (<2 mm), modal grain size distribution and hydraulic sorting ratio between pumice and dense clasts were used to characterise these three facies. On plots of sorting versus median diameter, the three facies overlap, which suggests that all three facies have overall good hydraulic sorting in their coarse clasts (>2 mm), and that the pumice clasts were fully waterlogged during transport and deposition. In addition, the studied subaqueous volcaniclastic samples overlap with the fields defined by matrix-free subaerial pyroclastic flow deposits, which confirms that outputs from functional stereology and conventional sieving give comparable results.

The volcaniclastic successions in the Ohanapecosh and the Dogashima formations include good examples of subaqueous, pumice-rich pyroclastic facies that were erupted onland or under water, and deposited in below wave-base settings. Eruption-fed facies generated by subaqueous pumice-forming explosive eruptions are exemplified by the extremely thick and graded sequence in Dogashima 2 (Dogashima Formation), which contains dense clasts that were deposited hot. Numerous beds of graded, extremely thick, pumice-rich facies in the Ohanapecosh Formation are interpreted to be deposited from eruption-fed, water-supported high concentration density currents that were fed by subaerial pyroclastic flows, primarily because rounded dense clasts, accretionary lapilli and wood in these and associated facies imply that the source vents were subaerial.

Resedimentation events can occur during eruptions and after, especially after eruptions that produce large volumes of pyroclasts in unstable environments. However, resedimented facies can be difficult to distinguish from eruption-fed facies in below wave-base successions, essentially because clast reworking below wave-base is minimal during resedimentation. In addition, eruption-fed facies can contain clasts that were previously abraded in above wave-base settings, for example during long-distance transport in subaerial pyroclastic flows, in pumice rafts (e.g. Chinook Pass Member, Ohanapecosh Formation) or during transport in the dense-clast-dominated bedload of subaqueous volcaniclastic density currents (e.g. Dogashima 2). Short-distance transport in pyroclastic flows might not be able to abrade pumice clasts (e.g. the eruption-fed facies in the Chinook Pass Member, Ohanapecosh Formation).

ACKNOWLEDGEMENTS

To my supervisors Jocelyn McPhie and Sharon Allen who have contributed greatly to this thesis with their constant support throughout my stay in Tasmania. Thank you for the confidence you had in me by accepting me at CODES, and being my advisors during this thesis. Thank you both for your ability to patiently teach me loads on volcanic processes and textures, scientific research and writing. Your ability to turn around my sentences and rigorously edit my numerous manuscripts has been a tremendous experience in learning how to write in English. Thanks to Jocelyn for field experiences - sometimes surreal - in New Zealand, Japan, Iceland and in the United States.

To Alexander Proussevitch for his enormous support on the functional stereology technique. Alexander processed hundreds of samples and very patiently assisted me on issues in statistics, through epic Skype meetings and emails.

To the Centre of Excellence in Ore Deposits (CODES) and the Australian Research Council for financial support on this PhD thesis. To the USGS 2009 Jack Kleinman Grant for Volcano Research for partial financial support.

To the professional staff at CODES and the School of Earth Sciences at the University of Tasmania, for their professionalism to keep me away from diverse administrative, financial and computer technology labyrinths. To the Science library for their attentive support. To Karsten Goemann who helped me at the electron microprobe and to Philippe Robinson who conducted X-Ray Fluorescence analyses.

To Richard Fiske and Paul Hammond for their enthusiastic support in the field, in the Ohanapecosh Formation. To the National Park Services (United States) for authorisation to sample. To the staff at the Mount Rainier National Park for their assistance, in particular Mimi Gorman and Martin at the Ohanapecosh campground. To Lee Walking, for her perseverance in seeking dusty articles for me in the Washington Geology Library.

To Ken-Ichi Kano-San for logistic support in Japan. To the Shimoda Marine Research Center (Japan) for accommodation. To Bruce Hayward for his help in the field in the Manukau Sub-Group, New Zealand. To Mathias Ort and Alain Burgisser for helpful advice on palæo-magnetism and hydraulic sorting, respectively. To Rebecca Carey for friendship and sampling of volcaniclastic samples in the Taupo Volcanic Zone. To Dork Sahagian, Bruce Houghton and Colin Wilson for their careful review of an earlier version of a manuscript.

To numerous music composers and their interpreters that strengthen my focus, relaxed my mind and inspired me during the entire PhD thesis. Special thanks to H. Purcell, G.-F. Haendel, J. Des Prez, G.P. Palestrina, J.S. Bach, W.A. Mozart, D. Buxtehude, T. Albinoni, A. Vivaldi and G. Brassens amongst many others.

To friends and colleagues at CODES who shared these four years of my life. Special thanks to Andrea, Bronto, Chris, Dave H., Emily, Gisela, Heidi B., Heidi P., Hugo, Isabelle, Jacqueline, Olga, Roisin and Wojtek for the fantastic support throughout this time in Hobart. To izzy for friendship and help with the rock catalogue. To Lindsey and Mathieu for friendship, chocolate sharing, and making our office very special. To Sarah Gordee for hysterical moments during fieldwork in Japan. Special thanks to Susan Belford for coffee time including chocolate-coated coffee beans expansively shared in the very early mornings, during passionate discussions.

To my family in Switzerland, my parents Nelly and Jean-François, my sister Sandrine and her husband Nicolas and my brother Andy, who supported my life choice despite the distance between us.

To my wife-to-be Sarah Quine, who had the great task to patiently cope with the flip sides of this thesis, and who continuously gave me support and balance in my life. Thanks to you with all my love. I would like to dedicate this thesis to you and to our newborn daughter Armelle.

Table of Contents

4
Effusive-to-explosive transition during an underwater eruption: Dogashima revisited (Japan)

5
Image analysis and grain size stereology on rocks: Application to subaqueous volcaniclastic facies and characterisation of deposition processes

---

6
Synthesis

References

Appendices

1

Introduction

1. AIMS AND SIGNIFICANCE

This thesis characterises eruption, transport and sedimentation processes of two Tertiary intermediate-to-felsic, subaqueous pumice-rich volcaniclastic successions. It addresses questions regarding the lithofacies characteristics generated by explosive eruptions that occurred on land versus under water. The Ohanapecosh Formation (Washington, United States) and the Dogashima Formation (Izu Peninsula, Japan) were chosen because of the high influence they have had in the literature dedicated to subaqueous explosive eruptions [*Fiske*, 1963; 1969; *Cashman and Fiske*, 1991; *Tamura et al*., 1991].

The quantification of the grain size distributions of subaerial pyroclastic deposits has provided data that underpin eruption and emplacement interpretations [*Kuno et al*., 1964; *Walker*, 1971; 1983; 1984]. This thesis presents a new technique for statistically calculating the grain size distribution of clastic rocks based on image analysis and functional stereology of photographs and scans. The technique is tested on natural samples, and applied to the major facies of the Ohanapecosh and Dogashima formations.

The principal aims of this thesis are to:

1. re-assess the origins of the Ohanapecosh and Dogashima formations, in terms of eruption, transport and depositional processes;

2. develop a technique based on image analysis and functional stereology to calculate the grain size distribution of clastic rocks, and to apply it to the rocks of the Ohanapecosh and Dogashima formations;

3. identify lithofacies characteristics that distinguish between subaqueous versus subaerial source vents for subaqueous pumice-rich pyroclastic facies;

4. identify lithofacies characteristics that distinguish between eruption-fed versus resedimented origins of a subaqueous pyroclastic deposit.

For the last five decades, research on felsic-intermediate explosive eruptions has been mostly dedicated to the eruptive mechanisms, and transport and depositional processes of such eruptions in subaerial settings. These events and their products are easily accessible, often witnessed, and an obvious source of hazardous phenomena [e.g. *Schmincke*, 2004]. Underwater, most volcanoes are basaltic, and most of the subaqueous volcanology conducted to date is overwhelmingly biased to processes of basaltic eruptions, in particular effusion of lavas [e.g. *Batiza et al*., 1984; *Soule et al*., 2007].

Subaqueous deposits from subaerial explosive eruptions

Felsic-intermediate subaqueous pyroclastic successions incorporate a complication that does not occur for small-volume basaltic pyroclastic subaqueous successions that are easily constrained to intra-basinal settings. Medium- to large-volume subaqueous pyroclastic units can be derived from extra-basinal or basin-margin subaerial sources, such as volcanic islands (Krakatau, Martinique, Dominica, Montserrat), or from intra-basinal, subaqueous sources [*Whitham and Sparks*, 1986; *Cas and Wright*, 1991; *Mandeville et al*., 1996; *Legros and Druitt*, 2000; *White*, 2000; *Freundt*, 2003; *Trofimovs et al*., 2006; *Dufek et al*., 2007; *Freundt et al*., 2007; *Sohn and Yoon*, 2010]. Onland eruptions producing pyroclastic flows that entered the sea have been witnessed [*Tanguy*, 1994; *Mandeville et al*., 1996; *Trofimovs et al*., 2006], but only a handful of the offshore deposits have been sampled in comparison to the large number of felsic-intermediate volcanic islands and volcanoes in proximity to the sea [*Carey and Sigurdsson*, 1980; *Whitham*, 1989; *Mandeville et al*., 1996; *Trofimovs et al*., 2008]. Therefore, subaqueous products from felsic-intermediate volcanic eruptions may contain complex transitions and/or combinations of fragmentation, transport and depositional processes in both air and in water, generating a large variety of subaqueous facies. A major challenge in studies of ancient subaqueous pyroclastic deposits is to discriminate between those sourced onland versus those from subaqueous vents.

Factors such as the type of pyroclastic flow, the density and temperature of the juvenile pyroclasts and the slope at the shore influence the transformation of gas-supported pyroclastic flows into water-supported density currents [e.g. *Freundt*, 2003; *Trofimovs et al*., 2006] or not [*Mandeville et al*., 1996]. Fallout of pyroclasts onto the sea produces rafts that will progressively waterlog and sink as suspension settling or in vertical density currents [e.g. *Carey*, 1997; *Manville et al*., 1998; *White et al*., 2001; *Manville et al*., 2002; *Manville and Wilson*, 2004; *Wetzel*, 2009].

Subaqueous explosive eruptions

Very little is known about explosive eruptions from underwater felsic-intermediate volcanoes [*Allen and McPhie*, 2009; *Allen et al*., 2010]. Shallow- and deep-submarine explosive eruptions are, however, attested to by numerous pumice-dominated volcaniclastic deposits that were erupted under water, demonstrating that such eruptions are physically possible.

A few modern felsic-intermediate, explosive, shallow sea-floor eruption columns have been witnessed breaching the water surface, but vent processes remain unseen, thus current understanding of the frequency, intensity, and styles of explosive activity underwater is largely based on ancient, well exposed successions [*Fiske*, 1963; *Fiske and*

Matsuda, 1964; *Fiske*, 1969; *Kano et al*., 1994; *Kano*, 1996; *Kano et al*., 1996; *Allen and McPhie*, 2000; *Allen and Stewart*, 2003; *Kano*, 2003; *McPhie and Allen*, 2003; *Stewart and McPhie*, 2004; *Tani et al*., 2008; *Allen and McPhie*, 2009; *Allen et al*., 2010], samples recovered from drill core, dredging, and submersible and geophysical studies of the sea floor [*Wright*, 1996; *Wright et al*., 2003; *Tani et al*., 2008; *Allen et al*., 2010]. However, interpretations of ancient successions and modern sea floor deposits have limitations, related to poor constraints on the water depth at the vent and vent location [*Tani et al*., 2008]. Only recently have very small, ~550-m-deep explosive eruptions of mafic composition been witnessed, at NW Rota-1 volcano [Mariana arc; *Chadwick et al*., 2008] and at West Mata (Tonga arc).

Subaerial explosive eruptions cannot be used as analogues for submarine explosive eruptions. Because of the different physical proprieties of air (gas, mainly N_2 and O_2) versus liquid water (H_2O), the eruption jet at a vent underwater behaves very differently. The higher density (1,025 kg/m^3), higher viscosity (8.9×10^{-4} Pa x s at 25°C) and poor compressibility of water (4.6×10^{-10} Pa^{-1} at 25°C) compared with air act against formation of a buoyant, gas-supported eruption column [*Kano et al*., 1996; *Downey and Lentz*, 2006; *Allen et al*., 2008; *Woods*, 2010]. In addition, water is a very efficient cooling agent, because of its high heat capacity (4.2×10^3 J x kg^{-1} x K^{-1}) and thermal conductivity (0.6 W/m^{-1} x K^{-1}), which allows quick and efficient transfer of thermal energy. Water will quench the magma and rapidly change its physical proprieties before, during and after the fragmentation. Rapid waterlogging of small vesicular pyroclasts (scoria, pumice) that are hot results from a suction effect associated with the condensation of magmatic gases, dominantly steam, that infill pyroclast vesicles [*Whitham and Sparks*, 1986; *Kano et al*., 1996; *Allen et al*., 2008]. Hence, underwater eruption columns quickly become negatively buoyant and prone to collapse [*Allen et al*., 2008]. The pyroclasts may then be transported in subaqueous density currents over large distances from vent.

Resedimented and reworked subaqueous pyroclastic facies

Pumice-rich facies deposited in subaqueous environments are likely to include the products of resedimentation and reworking. Sediment remobilisation can be generated by mass-wasting events, products of erosion from waves, and deep water currents [*Allen and McPhie*, 2000; *White et al*., 2001; *Allen and Freundt*, 2006; *Allen et al*., 2007]. Both subaerial and/or subaqueous parts of volcanic edifices may be sources of subaqueous resedimented facies. Cold, air-filled pumice clasts can float for months if highly-vesicular and buoyant (~700 kg/m^3). They sink as soon as their bulk air content is lower than 40 vol.% [*White et al*., 2001; *Manville et al*., 2002], which is likely to happen once waterlogged [*Whitham and Sparks*, 1986; *Cas and Wright*, 1991; *Allen et al*., 2008].

Resedimentation of volcaniclastic aggregates under water is effective in upper wave-base environments [e.g. *Kano*, 1991], but can also happen in deeper water, although the

full spectrum of mechanisms is poorly understood [e.g. *Wright*, 2001; *Stow et al.*, 2002; *Gardner*, 2010; *Leat et al.*, 2010]. Remobilisation events can include small (<1 m^3) to large [>5,000 km^3; *Moore et al.*, 1994] volumes, span from minutes to decades, be transported by subaqueous debris flows, high-concentration density currents, turbidity currents and/or clear water currents, and commonly involve multiple events [e.g. *Stow*, 1994; *Piper et al.*, 1999; *Stow et al.*, 2002; *Piper and Normark*, 2009].

Types of transport

Finally, the literature dedicated to particle transport and depositional processes, which is part of clastic sedimentology, does not generally take in account the special characteristics of volcaniclastic transport and deposition [e.g. *Hampton*, 1972; *Lowe*, 1982; *Postma et al.*, 1988; *Middleton*, 1993; *Iverson*, 1997; *Shanmugam*, 1997; *Mulder and Alexander*, 2001; *Shanmugam*, 2002; *Talling et al.*, 2007; *Baas et al.*, 2009; *Piper and Normark*, 2009; *Sumner et al.*, 2009; *Meiburg and Kneller*, 2010; *Sequeiros et al.*, 2010; *Talling et al.*, 2010]. This point is critical, because pyroclasts have a wide range of grain sizes (extrema from $>10^1$ to $<10^{-6}$ m), shapes (very angular to rounded) and densities (<500–2,500 kg/m^3) that make them very difficult to be compared with common siliciclastic deposits. In addition, particle supply rates and volumes generated by pumice-forming explosive eruptions greatly exceed those of other types of sedimentation. Hence, transport and depositional processes dynamics may be very different from those that explain the characteristics of conventional clastic sediments.

2. METHODS

This research is primarily field-based, and uses data obtained from outcrops and rock samples. Stratigraphic logs are used to correlate between localities, and for comparison of the principal facies with similar facies in the literature. The stratigraphic logs use textural characteristics recorded from outcrops, polished slabs and thin sections on numerous sections through the Dogashima and Ohanapecosh formations. Bed form, grading, sorting, and clast types and abundance were described in the field. Fine-grained components were further characterised from study of polished slab, and thin sections.

The analysis of volcanic textures in Dogashima and Ohanapecosh formations was limited by the abundance of natural exposures and the preservation state of the rocks. In particular, alteration of most samples of the Ohanapecosh Formation precludes description of the matrix (<2 mm). Chemical analyses of bulk clasts and feldspar crystals give the composition of clasts from the Dogashima Formation.

I develop a new method to quantify the abundance and grain size distribution of rock samples from the Dogashima and Ohanapecosh formations, using image analysis and

the code of functional stereology developed by Dr. Alexander Proussevitch (chapter 2). The grain size and componentry data complement field observations and contributes to interpretations based on facies analysis.

3. DEFINITION OF TERMS

In this thesis, several technical terms are used under a precise definition.

Subaqueous pyroclast

A subaqueous pyroclast describes a product from explosive eruption and deposited under water. It is not necessarily juvenile, and its source can either be subaerial or subaqueous.

Subaqueous volcaniclastic density currents

The term subaqueous volcaniclastic density currents is used for a group of sea-floor-hugging, water-supported density currents that vary in particle types, particle concentrations and rheology, but are chiefly composed of volcanic particles. Such currents may be eruption-fed or not, and can be derived from subaerial or subaqueous settings.

Eruption-fed pyroclastic facies

Eruption-fed pyroclastic facies are produced directly from the vent. There is no interruption between their eruption and their deposition. For pumice-forming explosive eruptions, the final deposition will happen seconds, minutes to hours after eruption.

Resedimented pyroclastic facies

An eruption-fed pyroclastic facies that is not welded or otherwise consolidated may be resedimented i.e. after initial deposition, and enter another transport system. Resedimentation does not need to involve reworking. Commonly, resedimentation is initiated by mass-wasting events that produce density currents.

Reworking pyroclastic facies

Reworking pyroclastic facies consist in above wave-base surface processes (especially erosion and traction transport) that modify grain size, grain shape, sorting and bed forms of an initial pyroclastic facies. Reworking may involve resedimentation, but it is not necessary. Reworking of delicate pumice clasts may occur in special conditions below wave-base, but is reduced to environments where high-energy currents can occur, such as channels.

4. STRUCTURE OF THE THESIS

This thesis consists of six chapters. Chapter 1 is introduces and discusses the aims of the thesis.

Chapter 2 describes a new technique that combines image analysis and functional stereology to infer the grain size distributions of clastic rocks. Grain size data generated by functional stereology are compared with results from the conventional sieving method. This technique was developed in collaboration with Dr. Alexander Proussevitch, University of New Hampshire (USA), who built the functional stereology code and adapted it to phi-scale measurements.

Chapter 3 describes volcaniclastic facies of the Ohanapecosh Formation (Washington State, USA). This formation includes eruption-fed and resedimented pyroclastic facies deposited in a wide and probably deep continental basin. Facies analysis and facies architecture are used to reconstruct the palæo-environment and depositional processes. This formation was previously studied by Fiske [1963], in a landmark paper on subaqueous pyroclastic deposits.

Chapter 4 describes the Dogashima Formation (Izu Peninsula, Japan). This formation consists of subaqueous, explosive eruption-fed and resedimented pumice-rich deposits. The middle part of the formation records transitions between effusive and explosive eruptions. The distinctive sorting in part of the section was previously studied in the highly influential work of Cashman and Fiske [1991]. This paper greatly advanced the understanding of the depositional processes that form submarine pyroclastic deposits. Thermoremanent temperatures of coarse dense blocks were calculated by Tamura et al. [1991] and confirmed their juvenile nature. This study examines the eruption and the depositional processes of the entire formation and reassesses the conclusions from these two papers.

Chapter 5 explores the application of the functional stereology technique to a variety of volcaniclastic facies. Image analysis and functional stereology are carried out on the samples rocks of the Ohanapecosh Formation (chapter 3), the Dogashima Formation (chapter 4), the Manukau Sub-Group (Northland, New Zealand; Appendix E) and Sierra La Primavera caldera (Jalisco, Mexico). Statistical values extracted from these various distributions allow comparison between the subaqueous volcaniclastic facies, and sieve data from subaerial unconsolidated pyroclastic facies. The results may have significance with respect to transport and depositional processes. The functional stereology code was processed by Dr. Alexander Proussevitch, following the detailed method outlined in chapter 2.

Chapter 6 discusses the major scientific advances achieved by this research in understanding the lithofacies characteristics of subaqueous volcaniclastic facies of different origins.

2

Image analysis and grain size stereology on clastic rocks: Procedures and tests

1. INTRODUCTION

The grain size distribution of pyroclastic deposits reflects processes of fragmentation, transport and deposition [*Walker*, 1971; 1973; *Wohletz et al*., 1989], and is a fundamental input to inverse physical models of explosive eruptions [e.g. *Bonadonna and Houghton*, 2005; *Dufek and Bergantz*, 2007; *Macedonio et al*., 2008; *Volentik et al*., 2010]. Presently, grain size distributions of pyroclastic deposits are obtained by sieving coarse fractions (>64 μm), and by laser diffraction and optical devices for finer ash [e.g. *Evans et al*., 2009]. These methods are exclusively used for loose, unconsolidated deposits, and the grain (or clast) population is represented as a function of the intermediate feret diameter of each particle and its weight. Consequently, most physical models of explosive volcanic eruptions are based on modern deposits and are almost exclusively based on subaerial examples, because available data are limited to unwelded and unconsolidated aggregates. The grain size distributions of the largest part of the accessible volcaniclastic deposits on Earth – the rock record – have not been quantitatively studied, as clastic rocks cannot be sieved. The same basic problem occurs in traditional detrital sedimentology [*Boggs*, 2006], so solutions found for pyroclastic deposits can be applied to other volcaniclastic and non-volcanic clastic deposits as well.

Pyroclastic deposits incorporate a wide range of grain sizes (extrema from 10^{1} to $<10^{-6}$ m). They can form and be deposited in both subaerial and subaqueous environments [*Cas and Wright*, 1987; *McPhie et al*., 1993; *Schmincke*, 2004], and be transported by various fluids (high-temperature volcanic gas, air, water, ice and mixtures). Pyroclasts may be composed partly or entirely of volcanic glass.

The lithification of pyroclastic deposits is accomplished by welding of hot juvenile pyroclasts, and/or by diagenetic or hydrothermal alteration. Most pyroclastic deposits have undergone unidirectional compaction during welding and/or diagenesis [*Quane and Russell*, 2005]. The inherent porosity of pumice and scoria clasts makes them very susceptible to flattening prior to or during lithification. Lithification may be accompanied by an irreversible obliteration of part to all of the original fine-grained particles, the minimum preserved grain size being commonly around 0.5–2 mm. Therefore, only the coarse-grained fraction (>2 mm) of clastic rocks is considered in this study.

Here, I describe a new method to statistically calculate the three-dimensional grain size distribution of clastic rocks. This method involves two steps (1) *image analysis*, that is the processing of photographs taken in the field or scans of samples to select and calculate the particle characteristics (feret diameters, aspect ratio) of clasts of the same type; (2) *functional stereology* that is, conversion of two-dimensional (2D) diameters of a population of the same clasts into a three-dimensional (3D) dataset. This method uses the functional stereology technique that is based on a new approach developed by Dr. Alexander Proussevitch (University of New Hampshire, USA), and builds on earlier

research based on stereology applications [*Sahagian and Proussevitch*, 1998; *Proussevitch et al*., 2007a; *Proussevitch et al*., 2007b]. The output of this method is the grain size distribution density, and can be approximated in volume per phi and weight percent. The application of the method to subaqueous and subaerial volcaniclastic facies is the subject of chapter 5. In this chapter, I consider only two main clast types: (1) pumice clasts, which are 60–90% vesicular and are intermediate to silicic in composition; (2) dense clasts, which comprise all non-vesicular clasts.

2. IMAGE ANALYSIS

Digital image processing of clastic textures is a powerful tool for quantification of clast proprieties [e.g. *Capaccioni et al*., 1997; *Karatson et al*., 2002]. Image analysis can be used from any medium, including field photographs or scans of rock slabs and thin sections (Figs 2.1, 2.2). The original images must be taken at right angles to the studied surface, or artificially corrected with specialized software. The images must be scaled with a known object length (ruler, hammer, person, etc.), or by predefined scanning resolution or microscope magnification. In contrast to most grain size acquisition methods, the functional stereology technique does not depend on the scale of the sample. This implies that input images for image analysis can range over several orders of magnitude (tens of m to mm). I have used similar image nesting strategy similar to that used in vesicularity studies [*Shea et al*., 2010] because the entire clast size range could not be described from a single image, which is common (Fig. 2.1).

Use of automated recognition software [e.g. *Proussevitch and Sahagian*, 2001; *Van Den Berg et al*., 2002] is a rapid technique, but accurate only for images that contain distinct object boundaries. In most of my natural samples, clast-clast contacts and additional "noise" within the clasts and the fine-grained matrix (including variations in colour, slight compaction and presence of secondary crystals) precluded an automated procedure. I "manually" outlined single clasts in every image, using the multiple selection tools of *Adobe Photoshop* software (Fig. 2.1). The time needed for manual image acquisition depends on the complexity of the rock, but commonly require <0.5–4 hours per image for an experienced user. For ideal samples in which clasts are not touching each other, use of an automated method considerably reduces this time to a couple of minutes. Once clasts were outlined, discrete clast parameters were acquired with image analysis software *AnalySIS*, including area, perimeter, various types of maximum and intermediate diameters, aspect ratio, shape factor and angle of the long-axis relative to a defined line, commonly perpendicular to the main axis of compaction.

Few errors are associated with this method and can reasonably be minimised, including the representativeness of the sample, the randomness of clast orientation, the orthogonal projection of the image, the clarity of grain boundaries, estimation of the density of each

type of clast, and the approximation of the grain shapes to a common geometry [*Sahagian and Proussevitch*, 1998]. The shapes of volcanic clasts is much less complex than highly tortuous shapes of vesicles in pumice clasts [e.g. *Shea et al*., 2010], and are simplified to oblate rotational ellipsoids [*Sahagian and Proussevitch*, 1998]. The functional stereology technique requires populations of at least a couple of hundred grains. Generally, one outcrop photo and one rock slab scan gave good precision for functional stereology, and were sufficient to obtain a representative clast population, as well as acceptable data overlap. The precision of the stereology technique for the coarsest and finest tails of the distribution may be low. Out-sized clasts on a 2D section cannot be statistically reproduced in 3D if their abundance is too low. The grain size study of clastic rocks is limited by the state of texture preservation. The cut-off grain size that can be analysed depends on the rock but is commonly 2 mm. The systematic use of high-definition digital photos (>6*10^6 pixels) and scans (1,200 ppi) prevented pixellated aspect for clasts in this size, thus the clasts shapes and diameters are sufficiently accurate. In addition, the image should only be taken from a reasonably even rock surface. The density of each type of clast is needed where using weights of particles. This remains difficult to evaluate without study of the density and vesicularity of each grain (e.g. heterogeneously vesicular pumice clasts can be less dense than others by a factor of ~2).

3. THE STEREOLOGY TECHNIQUE

The clast dimensions found on a 2D section do not statistically represent true three-dimensional clast diameters. Stereology is the reconstruction of 3D objects from 2D imagery, and has been the subject of numerous contributions concerned with crystal populations in igneous rocks [e.g. *Cashman*, 1988; *Sahagian and Proussevitch*, 1998; *Higgins*, 2000; *Castro et al*., 2003; *Mock and Jerram*, 2005; *Jerram and Davidson*, 2007] and bubbles in magma [*Sahagian and Proussevitch*, 1998; *Proussevitch et al*., 2007a; *Proussevitch et al*., 2007b; *Shea et al*., 2010]. Stereology is an efficient alternative to sieving in grain size studies and to 3D imaging by X-ray tomography [e.g. *Degruyter et al*., 2010; *Gualda et al*., 2010; *Jerram et al*., 2010; *Kervyn et al*., 2010; *Ketcham et al*., 2010].

The concept of stereology lies in the difference in apparent grain diameter on a 2D section compared to the real 3D grain size population [*Kellerhals et al*., 1975; *Sahagian and Proussevitch*, 1998; *Proussevitch et al*., 2007b]. For instance, cross-section size almost never represents the true size, as a random 2D section rarely crosses through a grain centre. This means 2D sections are particularly poor for acquiring the maximum clast diameter in a population. Additional bias is introduced because small-diameter particles in a randomly distributed grain population have lower probability to appear in a random 2D section than coarser particles, thus causing a significant shift towards a coarser apparent grain size distribution.

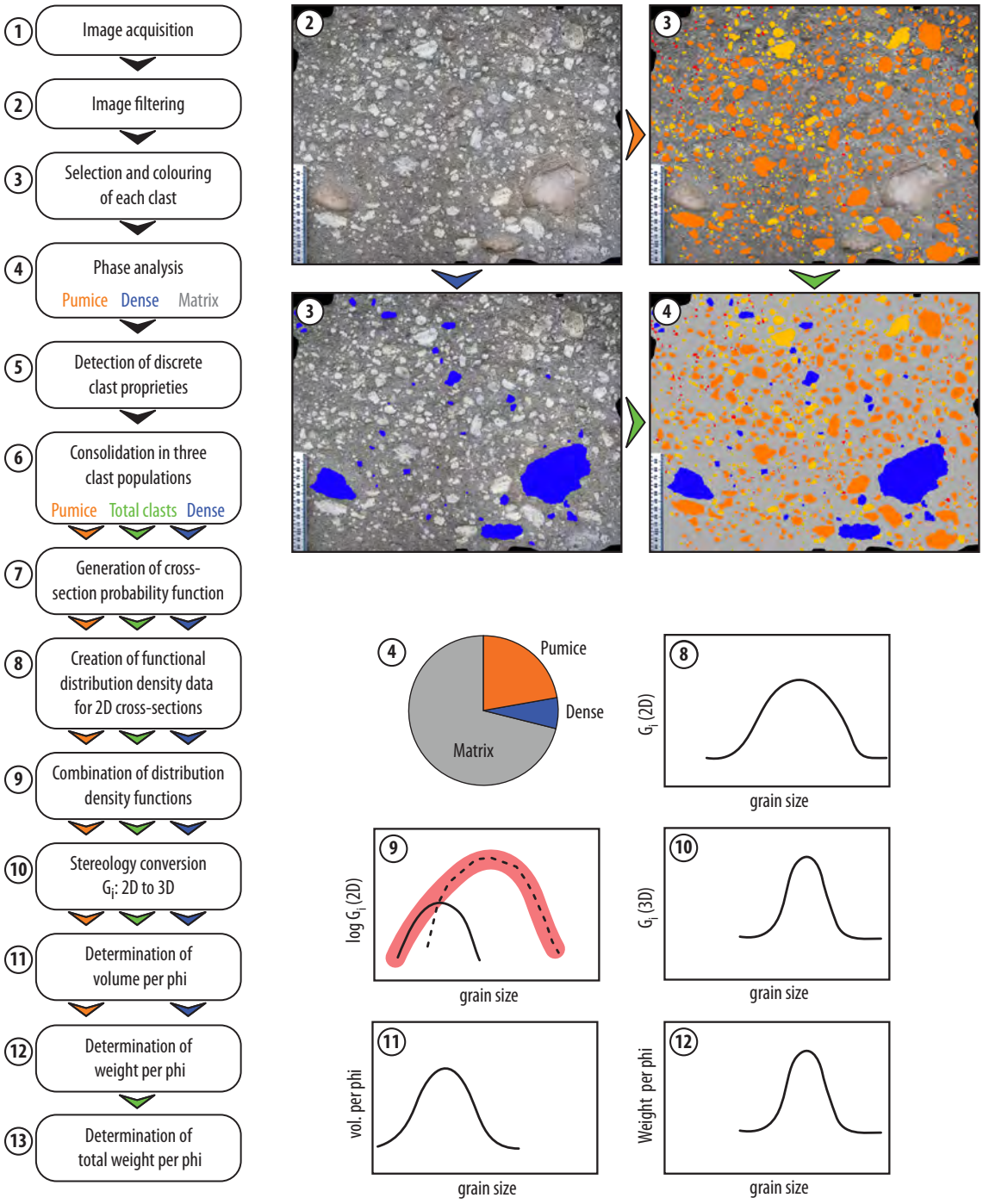

Fig. 2.1 Step-by-step procedure for the image analysis and stereology techniques, using an example of pumice-rich volcaniclastic bed in the Manukau Sub-Group (New Zealand). Numbers 7 to 11 are run by the functional stereology code (Appendix A); numbers in photos and graphs refer to steps at left. **1)** The representative population of clasts to analyse is selected from an original photo, rock slab scan or thin section scan. The image must contain tens to hundreds of identifiable objects. The surface photographed should be perpendicular to the angle of view and not have clasts standing out. The photograph must be scaled with an object of reference, or with a known scanning resolution; **2)** Photograph is filtered to enhance contrasts and clast boundaries. Depending on the image, Photoshop filters may be used: contrast, brightness, colour, levels, sharpen, median. Filtering may decrease image resolution and modify the shape of clasts [Shea et al., 2010]. The original photograph (left, top),shows pumice clasts (white) and dense clasts (pale brown) in a matrix (grey) in the Manukau Sub-Group, New Zealand; **3)** Selection and colouring of discrete clasts. Multiple colours and layers are usually needed for each clast type, because clasts are commonly touching each other. Photoshop tools mostly used comprise: quick selection tool, magic wand tool, paint bucket. Coarse pumice clasts are filled in yellow and orange, coarse dense clasts in dark blue over original photos in background; **4)** Phase analysis of each clast type with AnalySIS software, for detection of pumice clasts (yellow and orange), dense clasts (dark blue) and matrix (pale grey). Pie diagram shows relative abundance of pumice clast, dense clast and matrix; **5)** Detection of discrete clast properties with AnalySIS software for pumice and dense clast populations, after image scaling and selection of the colour threshold. Detection

of clast diameters (maximum feret and minimum feret), area and aspect ratio; **6)** Consolidation of dataset in a .txt file for three categories: "pumice", "dense" and "total clasts". Discrete clast data comprise minimum and maximum feret diameters, area, aspect ratio and average aspect ratio; **7)** Selection of clast shape [ellipsoid, rectangular solid or random; Sahagian and Proussevitch, 1998] and input of the average aspect ratio of each clast population, and generation of empirical cross-section probability function, with manual selection of the most appropriate distribution function [Gaussian, log-normal, exponential, gamma, logistic, Weibull; Proussevitch et al., 2007a]; **8)** Conversion of discrete clast diameters in ¼ ϕ bin size in a distribution density. Generation of cross-section distribution function parameters using Amoeba minimization algorithm. Creation of functional distribution density data (best fit curve). Manual choice of the number of modes (up to three); **9)** If the analysed image is not representative enough of the sample, combination (red curve in graph) of distribution density functions from other analysed images at same scale, and nesting at different scales on a log-scaled diagram [Shea et al., 2010]; **10)** Conversion of 2D to 3D and building of 3D distribution density data (3D G_i) by functional stereology. Generation of 3D distribution function parameters using Amoeba minimization algorithm; **11)** Determination of volume fraction per ϕ from 3D G_i; **12)** Determination of weight per ϕ from estimation of the density of each clast type (density=mass/volume); **13)** Determination of total weight per ϕ by addition of the separate weight of all types of clast.

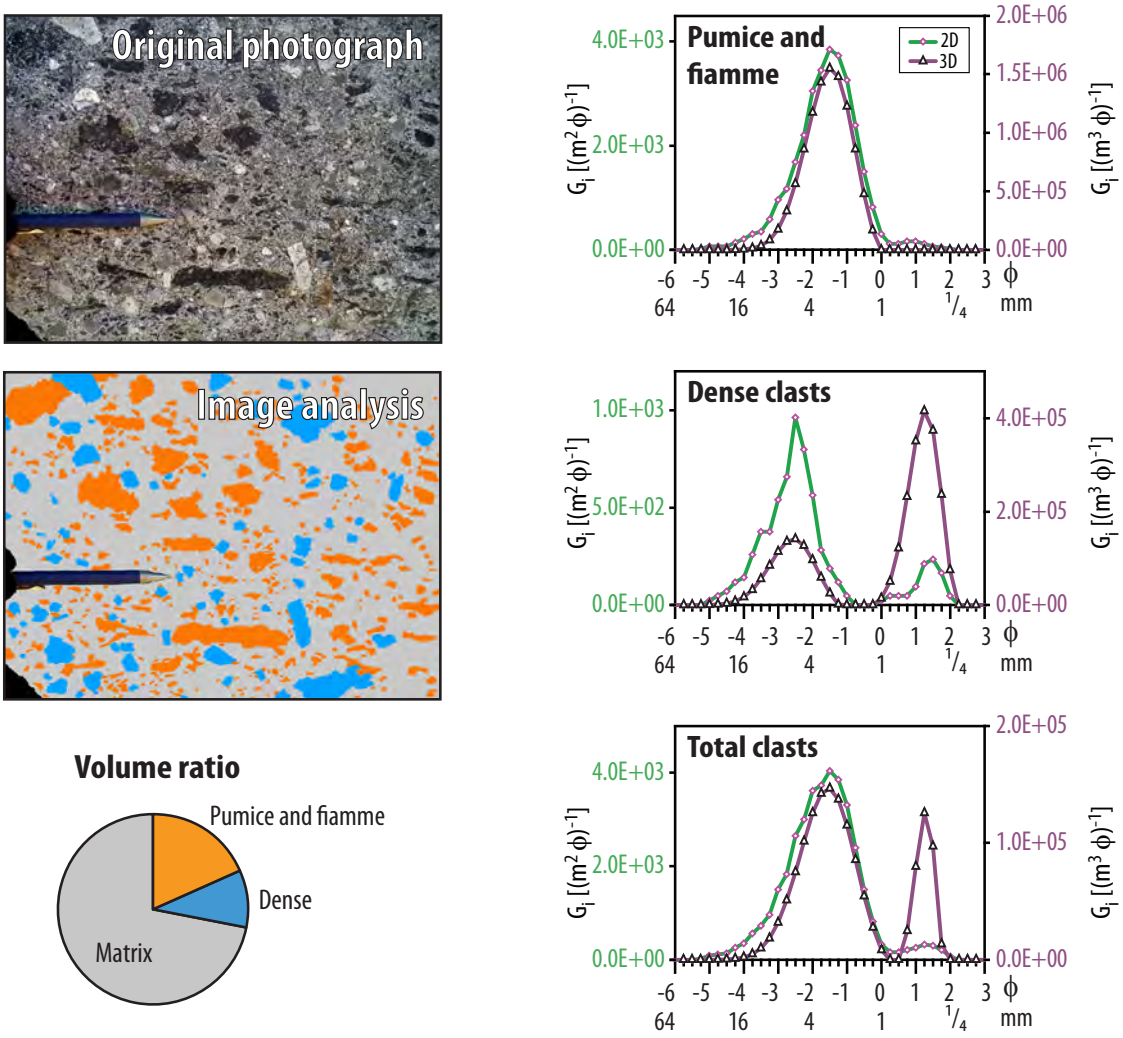

Fig. 2.2 Example of the method of acquisition of grains (pumice clasts and fiamme in orange; dense volcanic clasts in blue) from an outcrop photograph of a normally graded fiamme-lithic breccia in the Ohanapecosh Formation at Cayuse Pass (WA, USA). Minimum detection limit is 0.5 mm. Note the shift in grain size from 2D to 3D populations towards finer grained values, and the substantial increase of clasts probability in the finer mode. Average grain diameters of G_i in green line and diamonds are for the 2D population (left vertical scale), purple line and triangles are for calculated 3D population (right vertical scale). Bin interval ¼ ϕ. Visible part of the pencil is 10.0 cm long.

In order to correct for the misrepresentation of grain size distributions involved in the examination of cross sections, the embedded basic tools of functional stereology can be applied, thus deriving inferred 3D volume information from simple 2D observations. Here, the stereology approach of Sahagian and Proussevitch [1998] was improved for developing a new method, the functional stereology, that converts measurements of grain cross-sections by deconvolution of pre-defined functions of their 3D sizes (Fig. 2.1). Amongst the various distribution functions available in the embedded functional stereology code (Gaussian, log-normal, exponential, gamma, logistic, Weibull), the samples studied in this paper match a log-normal behaviour the best, as do a large selection of natural object sizing categories [*Proussevitch et al*., 2007a; *Proussevitch et al*., 2007b]. Generic clast shape [ellipsoid, rectangular solid or random; *Sahagian and Proussevitch*, 1998] and aspect ratio corresponding to the average of the discrete aspect ratio of each clasts are used as input in the functional stereology code.

The output of the stereology method gives values of G_i, which represent the *grain number distribution density*, and equal the number of particles per m^2 or m^3 and per bin width, in $(m^2\ \phi)^{-1}$ or $(m^3\ \phi)^{-1}$, respectively (Fig. 2.1). The governing formulae from Dr. Alexander Proussevitch are developed in Appendix A.

As such, stereology is an inexpensive, rapid and straightforward technique, which only necessitates discrete clast dimensions extracted by image analysis and a special routine for functional stereology [*Proussevitch et al*., 2007b].

4. VALIDATION OF THE METHOD

4.1. Samples, sieving and synthetic rock preparation

To compare functional stereology results with those from sieving, I constructed synthetic rocks by embedding clasts in epoxy cement (Fig. 2.3). This test complements the theoretical tests of the stereology technique undertaken on bubble populations [*Proussevitch et al*., 2007a]. The samples consisted of ~10 cm^3 of various populations of clasts (Fig. 2.4) from industrial sites in Tasmania (Australia) and from various pumice-rich pyroclastic deposits in the Taupo Volcanic Zone (New Zealand).

First, the unconsolidated samples were sieved and weighed to generate conventional weight percent histograms of grain size [Fig. 2.4; e.g. *Folk*, 1980]. The diverse samples were sieved at 1 ϕ intervals on the range -5 to 1 ϕ to simplify sieving and image analysis procedures on extreme grain sizes; the finer particles (>1 ϕ) were discarded. Each sample comprised clasts of assumed similar densities to allow the direct conversion of weight percent into volume fractions.

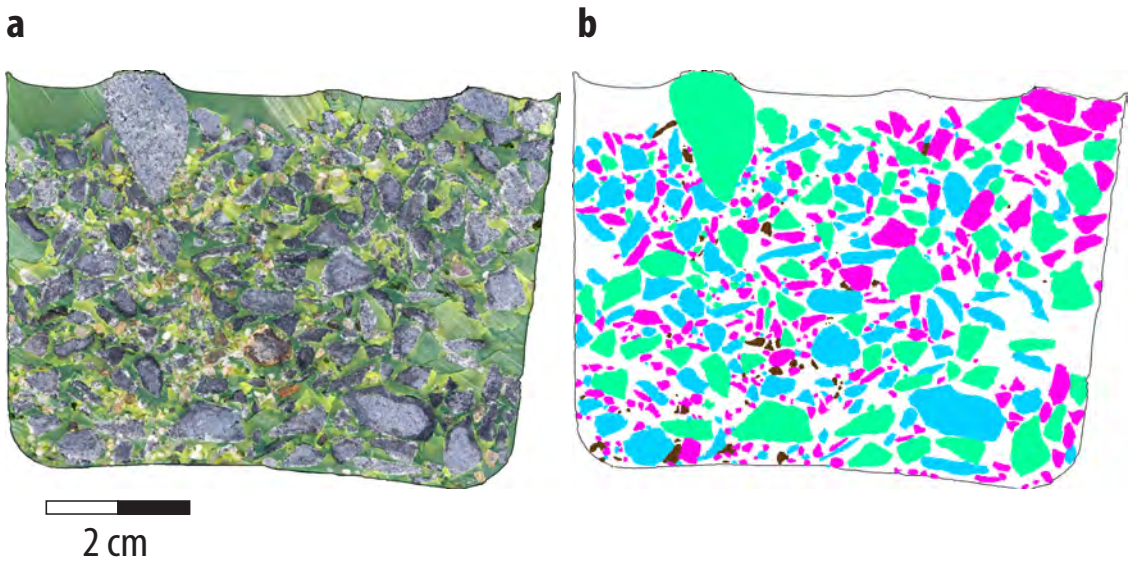

Fig. 2.3 Example of a slab of synthetic rock with industrial clasts from Tasmania (Australia), which is part of the population (d) in Figure 2.4. **a)** Original polished slab, cemented in green-dyed epoxy; **b)** Image analysis of a single clast population, using numerous colours to separate touching clasts.

The sieve samples were then placed in a vessel and gently shaken until clasts were randomly spread. Samples were immersed in coloured epoxy and placed under 80 kPa vacuum for an hour to remove any porosity, then left to dry for several days. Once solid, the samples were sawn in to one or multiple parallel slabs, polished and digitized at 1,200 dpi on a flat screen scanner. Spacing between adjacent slabs was wide enough to avoid clasts to be cross-cut twice and appear on multiple slabs. The slab grain-size distribution was acquired using the image analysis and functional stereology methods detailed earlier, to be compared with the sieving data (Figs 2.3, 2.4).

4.2. Advantages of the functional stereology technique

The functional stereology technique has several advantages. This cheap method allows fast calculation of statistical values from pre-selected samples on 2D sections. It allows for narrow bin sizes and can therefore be very effective in studies of clastic rocks that have subtle variations in grain size. Small size increments between bins should be used when multiple modes are suspected (e.g. ¼ ϕ, as used with this technique).

Calculation of up to three modes is included in the functional stereology code. Calculating the modes of grain size populations was avoided in the early stages of research on the statistical treatment of sieving data, because of the complexity of the task [*Folk*, 1980]; hence values of the median and standard deviation were preferred [*Krumbein*, 1936; *Murai*, 1961; *Walker*, 1971; *Folk*, 1980]. Grain size distributions are commonly multi-modal [e.g. *Folk*, 1980] and the mode has been demonstrated to be a more robust parameter than the median [*Sahagian and Maus*, 1994], because it is less affected by the presence or absence of a few large grains in the population, or limits in resolution of the smallest

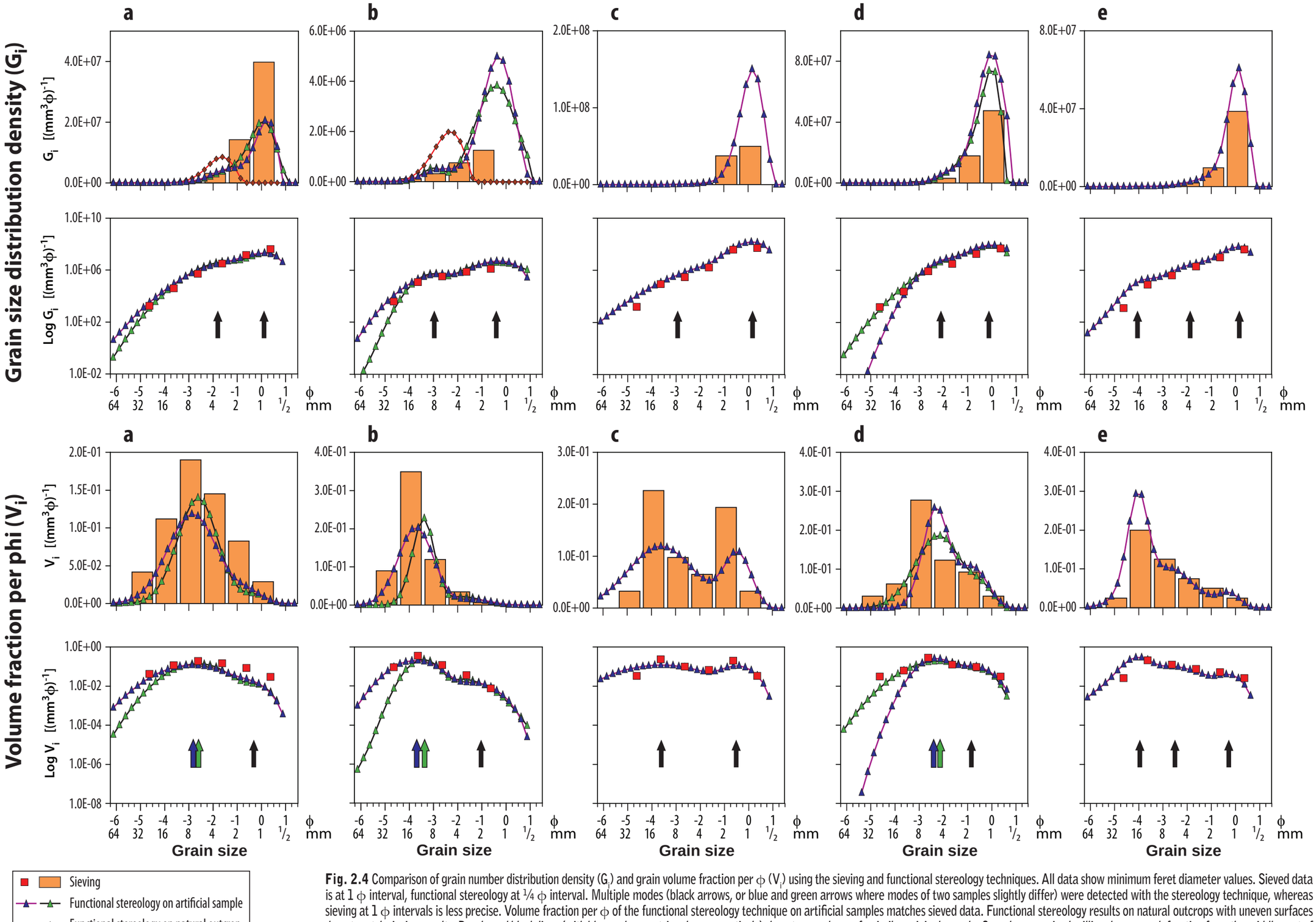

Fig. 2.4 Comparison of grain number distribution density (G_i) and grain volume fraction per ϕ (V_i) using the sieving and functional stereology techniques. All data show minimum feret diameter values. Sieved data is at 1 ϕ interval, functional stereology at ¼ ϕ interval. Multiple modes (black arrows, or blue and green arrows where modes of two samples slightly differ) were detected with the stereology technique, whereas sieving at 1 ϕ intervals is less precise. Volume fraction per ϕ of the functional stereology technique on artificial samples matches sieved data. Functional stereology results on natural outcrops with uneven surfaces do not match sieving results. Purple and black lines (with blue and green triangles, respectively) show two analyses of a similar original sample. Sample **a**: pumice lapilli and coarse ash fraction from the middle part of the rhyolitic Taupo ignimbrite (New Zealand); sample **b**: gravel and coarse sand fraction of reworked pumice deposit (Taupo Volcanic Zone, New Zealand); samples **c**, **d** and **e**: artificial samples of industrial gravels.

particles.

For simplicity, this study follows the logarithmic grain size scale to the base two (ϕ) commonly used for sieved samples, where *d* is the clast diameter [*Wentworth*, 1922; *Krumbein*, 1936; *Walker*, 1971; 1973; *Folk*, 1980].

$$\phi = -log_2(d) \quad (2\text{-}1)$$

The typical aspect ratio (A = length / thickness) of pyroclasts is in the range of 1.5 to 2.5 (chapter 5). To fit the conventional sieving technique which sorts clasts by intermediate feret diameter [*Walton*, 1948], the average grain diameter output is corrected by the functional stereology technique using:

$$\phi_{sieving} = \phi_{average} + log_2\left(\frac{A+1}{2}\right) \quad (2\text{-}2)$$

The conversion of a G_i bin population into a bin volume fraction under a ϕ scale is approximated by:

$$V_i^g = G_i \, \Delta\phi \, V^g(\phi)_i \quad (2\text{-}3)$$

where V_i is the bin *i* (in m^3 and ϕ scale), G_i is in $(m^3\ \phi)^{-1}$, Δϕ is the bin interval (in ϕ scale), and ϕ_i is a class size or average clast size in the bin *i* (in ϕ scale). The volume of a single grain (V^g) in the bin *i* with average size ϕ_i:

$$V(\phi)_i = 10^{-9} \cdot \frac{\pi}{6}\left(2^{-\phi_i}\right)^3 \quad (2\text{-}4)$$

Conversion of volume *V* [m^3] into a weight *W* [kg] requires a known or assumed bulk density (ρ) for each clast type in the sample:

$$W = \rho \, V \quad (2\text{-}5)$$

Functional stereology overcomes flaws documented in the sieving technique, such as poor reproducibility of the method due to the shape and roughness of the grains [*Sahu*, 1965; *Kennedy et al.*, 1985; *Fernlund*, 1998]. The disparity in the density of each type of clast needs to be estimated in both the sieving and stereology methods.

The optical methods of functional stereology enable continuation of the distribution to particle sizes that belong to the identified modes. Most pyroclastic deposits are sieved at 1 ϕ intervals. The precision of the image analysis is arbitrarily set at ¼ ϕ intervals, which equals that used for detailed sediment grain size analysis [e.g. *Evans et al.*, 2009] because it may reveal subtle features in the grain size distribution such as hidden secondary modes.

4.3. Results of the tests of stereology vs. sieving

The functional stereology technique consistently reproduced the form of the grain size distributions obtained from sieving, demonstrating the accuracy of the image analysis and functional stereology methods (Fig. 2.4). The modes of the G_i and volume per ϕ (V_i) are reproduced with accuracy.

A bin increment of 1 ϕ was used in the sieving method, following conventional studies of volcanic deposits. However, the stereology data are presented with ¼ ϕ increments. This discrepancy in the sieve aperture does not modify the conclusions drawn from the comparisons of results, but demonstrates the precision of the stereology method. In the functional stereology technique, the bin size at ¼ ϕ permits definition of the distribution curve with a better precision than for sieving at 1 ϕ, and various secondary modes are defined. As expected from equations (2-3) and (2-4), there is a large quantity of fine-grained clasts (G_i spans -1 to 1 ϕ) but they take less volume in proportion to the coarse clasts (V_i spans -5 to -1 ϕ), because volume scales to the cube of the clast radius.

A few stereology curves do not perfectly fit the sieving data (Fig. 2.4). These small shifts reflect the natural discrepancies in shape of a few clasts, or that the grain size distribution does not perfectly follow a log-normal behaviour.

Functional stereology cannot be used on images of uneven surfaces. Tests made on images of natural outcrops of unconsolidated pyroclastic deposits are inconsistent with sieving data where the coarsest clasts are standing out of a vertical cliff face (Figs 2.4a, 2.4b), because the coarse clasts seem to out-number the finer grained clasts. This can be addressed in the future studies by developing correction routines for such coarse clasts.

5. CONCLUSIONS

The application of functional stereology to consolidated pyroclastic rocks enables quantification of the grain size distribution of coarse clast populations, provided that a significant amount of clasts can be separately resolved on a 2D image. The stereological technique described here dramatically increases the number of potential samples because it can be used on consolidated pyroclastic deposits (rocks). This should broaden the realm of research on pyroclastic deposits, including clast-forming processes, transport and deposition.

The good match between sieving and stereology results, as well as those undertaken by Proussevitch et al. [2007a], demonstrate the validity of the method for various natural object populations. Because natural clasts have highly variable

shape and density, both sieving and stereology give only a statistical estimate of the grain size distribution in a given population. This technique that uses image analysis and functional stereology is more precise than sieving because it can handle data in smaller bins. The major limitation of this technique resides in the state of texture preservation of the rock, which excludes fine grain sizes (<0.5-2 mm). As such, functional stereology should represent a major step forward in our ability to quantify grain size of any clastic aggregate, including volcaniclastic deposits of concern to the volcanic modelling and hazards communities.

3

Reappraisal of the Ohanapecosh Formation (Washington, USA): a facies model for subaqueous deposition of pumice-dominated density currents in a below wave-base basin

1. INTRODUCTION

The Eocene-Oligocene Ohanapecosh Formation (Washington State, USA) has been a key reference in the literature on subaqueous explosive volcanism [e.g. *Fiske*, 1963; *Fiske et al*., 1963]. The highly influential work of Fiske [1963] explored general concepts on the nature of explosive subaqueous volcaniclastic density currents – then called "subaqueous pyroclastic flows" – and related them to sources, and transport and depositional processes. Despite the widespread extent of the Ohanapecosh Formation in the Central Cascades (>400 km^2), and mapping of various sections, the depositional processes and palæo-environment remain debated, in part due to vegetation cover. I use facies analysis and the facies architecture of this succession to reassess the eruption styles and palæo-environments of eruption, transport and deposition. I focus on the range of volcanic and sedimentation processes that can reasonably be inferred for voluminous pumice-rich units deposited in a quiet water environment. These processes include subaqueous deposition from subaerial pyroclastic flows that entered water and from subaqueous explosive eruptions, and subaqueous remobilisation of unconsolidated pumice-rich aggregates. Previous interpretations are re-evaluated. The new facies models based on the Ohanapecosh Formation can be translated to the architecture of subaqueous basins associated with volcanic arcs elsewhere.

2. GEOLOGICAL SETTING OF THE OHANAPECOSH FORMATION

2.1. Cascades volcanism during the Tertiary

Subduction of the Pacific plate under the North American plate began in the Palaeozoic era and is still continuing today [*Dickinson*, 2009]. During the Cenozoic, the extremely long (>1,250 km) Cascades arc developed on the Palaeozoic and Mesozoic continental terranes of western North America. Clockwise rotation of the subducted Pacific plate around a pole situated in southern Washington induced compressional deformation in British Columbia, transpression in Washington, and extension in Oregon, which was accommodated by the formation of the Basin and Range province during the same period [*McBirney*, 1978; *Duncan and Kulm*, 1989; *Wells*, 1990; 1998; *Sonder and Jones*, 1999]. The Cenozoic history of the Cascade arc and studies of volcanic products of the arc have been established through an extended period of research on major geological units [e.g. *McBirney*, 1978; *Hammond*, 1979; *Vance et al*., 1987; *Tabor et al*., 2000], stratigraphic unconformities [e.g. *Hammond*, 1979; *Johnson*, 1985; *Tabor et al*., 2000], sedimentation within large basins [e.g. *Fiske et al*., 1963; *Johnson*, 1985; *Smith*, 1989; *Tabor et al*., 2000; *Schuster*, 2005] and palaeomagnetic orientations [*Bates et al*., 1981; *Beck*, 1986; *Wells*, 1990; 1998]. Uncertainties regarding the early Cenozoic history of southern Washington are partly due to loss of the geological record by erosion in response to regional uplift of the

northern Cascades [e.g. *McBirney*, 1978; *Hammond*, 1979; *Reiners et al.*, 2002], and burial under Quaternary volcanoes [*Hildreth*, 2007].

2.2. Regional tectonic and stratigraphic context of the Ohanapecosh Formation

From the Eocene to the middle Oligocene, regional extension and transtension affected the northwestern part of the North American continent, in which the Ohanapecosh Formation was deposited [*Frizzell et al.*, 1984; *Tabor et al.*, 1984; *Johnson*, 1985; *Tabor et al.*, 2000]. In the Puget lowland, southern Washington, the inferred Puget fault is a major north-striking dextral transcurrent fault that offset the pre-Tertiary continental basement during late Cretaceous to Eocene [*Johnson*, 1984; *Johnson*, 1985; *Armstrong and Ward*, 1991]. The inferred fault coincides with a prominent gravity anomaly [*Bonini et al.*, 1974; *Blakely et al.*, 2002] and is buried by upper Eocene and younger formations.

To the east of the Puget lowland, vertical mid-Cretaceous north- and northwest-striking faults (Straight Creek Fault, Entiat-Leavenworth Fault) formed in response to oblique subduction of the Kula and Farallon plates beneath the North American plate as early as late Cretaceous. Evidence of these major faults is well preserved in the northern part of Washington, where they cut the pre-Tertiary basement rocks. They probably extend north into Canada and Alaska [*Tabor et al.*, 2000]. The northward transport of this part of the North American plate is consistent with the palaeomagnetic inclination data that also imply northwestern movement [*Bates et al.*, 1981]. From 57 to 43 Ma [*Cheney and Hayman*, 2009], the faults promoted the formation of separate basins (Chuckanut, Puget-Naches, Chiwaukum Graben and Swauk) that have distinct sedimentary and deformation histories [*Johnson*, 1984; *Johnson*, 1985]. The basins (Appendix C) occur in forearc or intra-arc settings with respect to the Cascade arc. They are mainly composed of very thick (up to >6 km) terrigenous conglomerate and sandstone, commonly of fluviatile origin. These non-marine facies are interbedded with volcaniclastic units and lavas of mostly mafic to intermediate composition [*Tabor et al.*, 1984]. Local and/or temporary connection of the basins probably occurred. High sediment accumulation rates, extensive unconformities and abrupt changes in facies or bed thickness in these basin successions suggest a tectonically active environment in which subsidence and uplift were rapid, as in strike-slip or pull-apart basins [*Johnson*, 1984; *Johnson*, 1985; *Vance et al.*, 1987; *Evans*, 2010]. Cheney and Hayman [2009] proposed that the Eocene formations were preserved in regional synclines belonging to the same basin, rather than in multiple pull-apart basins.

The Puget-Naches Basin contains the middle to late Eocene Puget Group, Renton Formation, Spiketon Formation and Naches Formation [*Tabor et al.*, 2000]. McBirney [1978] proposed that compression (uplift and folding) of the Puget Group occurred in the late-middle Eocene (i.e. ~45-50 Ma). Tabor et al. [2000] suggested that the Puget Group and Naches Formation formed in the same fluvial-deltaic system. Palæo-currents in the

fluviatile facies of the Puget Group indicate westward sediment transport [*Gard*, 1968].

To the west, a chain of basaltic seamounts was accreted to the forearc of the Cascade arc in Washington and Oregon during the middle to late Eocene (48 to 36 Ma), producing a mountain range parallel to the coast [*Duncan*, 1982]. The seamounts were originally part of a ridge separating the Farallon (south) and Kula (north) oceanic plates.

2.3. The Ohanapecosh Formation

The mostly volcaniclastic Ohanapecosh Formation [*Fiske et al.*, 1963] is early to middle Oligocene [36 to 28 Ma; *Tabor et al.*, 2000] and thought to record an early stage of volcanism in the Cascade arc [*Fiske*, 1963; *McBirney*, 1978]. However, such span of time includes a much wider area than the volcaniclastic facies described by Fiske et al. [1963] and this study. Tabor et al. [1984] and Johnson [1985] interpreted this formation to mark the end of the Eocene strike-slip faulting and magmatism of the Cascades arc in southern Washington. It is up to ~3 km thick [*Fiske et al.*, 1963], exposed over >400 km^2 in an area >700 km^2 [*Schuster*, 2005] throughout Mt Rainier National Park and its surroundings, and is the basement upon which Mt Rainier volcano was built (Fig. 3.1). The formation has been recognised from the Snoqualmie area (north) to Columbia River Gorge (south to Mt St Helens and Mt Adams), and from Mt Rainier and Lake Tapps (west) to Little Naches River area (east) [e.g. *Fisher*, 1961b; *Fiske et al.*, 1963; *Gard*, 1968; *Wise*, 1970; *Ellingson*, 1972; *Simmons et al.*, 1983; *Frizzell et al.*, 1984; *Evarts et al.*, 1987; *Schasse*, 1987; *Vance et al.*, 1987; *Smith*, 1989; *Swanson*, 1996; *Swanson et al.*, 1997; *Tabor et al.*, 2000; *Hammond*, 2005; *Schuster*, 2005; *Hammond*, 2008 unpubl. data].

The contact of the Ohanapecosh Formation on the Puget Group (Appendix C) is everywhere conformable and commonly gradational [*Fiske et al.*, 1963; *Gard*, 1968; *Simmons et al.*, 1983; *Vance et al.*, 1987]. The Spiketon Formation [*Gard*, 1968; *Vance et al.*, 1987] and Renton Formation [*Tabor et al.*, 2000] are also conformably overlain by the Ohanapecosh Formation (Appendix C). In contrast, the contact with the underlying Naches Formation is an unconformity [*Johnson*, 1985; *Vance et al.*, 1987; *Tabor et al.*, 2000]. The middle to late Eocene Summit Creek Sandstone [~43 to 37 Ma; *Vance et al.*, 1987] consists of various sandstone units conformably underlying the Ohanapecosh Formation in the areas from eastern side of White Pass to the Naches River to the east [Fig. 1, Appendix C; *Ellingson*, 1972; *Vance et al.*, 1987; *Hammond*, 2005].

In the Mt Rainier National Park area, the Ohanapecosh Formation is overlain by the Oligocene (25-27 Ma) Stevens Ridge Member, that is the lower part of the Fifes Peak Formation [*Vance et al.*, 1987; *Hammond*, 2008 unpubl. data]. This member is composed of multiple, quartz-bearing, rhyolitic, 5- to >100–m-thick ignimbrites. Columnar joints occur in the thickest ignimbrite units. At Backbone Ridge, southeast of Mt Rainier,

clasts of the Ohanapecosh Formation and tree trunks occur in the base of the lowest ignimbrite of the Stevens Ridge Member. In the Mt Rainier National Park, the Stevens Ridge Member was originally defined as a formation by Fiske et al. [1963]. However, Tabor [2000] found a gradational boundary between it and the overlying Fifes Peak Formation, and consequently re-defined the Stevens Ridge Formation as a Member of the Fifes Peak Formation.

On the basis of the angular unconformity between the Ohanapecosh Formation and the Stevens Ridge Member and the presence of a syncline in the Ohanapecosh Formation in the Mt Rainier National Park, Fiske et al. [1963] suggested that a "regional fold, alteration and erosion event" directly followed deposition of the Ohanapecosh Formation. However, Tabor et al. [2000] could not find evidence for this event outside the Mt Rainier National Park.

The early Miocene Fifes Peak Formation was first described by Warren [1941] as a heterogeneous assemblage of lavas and volcaniclastic rocks of mafic to intermediate composition. The Fifes Peak Formation covers large areas around Mt Rainier, at Fifes Peak and Tieton [*Warren*, 1941; *Fiske et al*., 1963; *Swanson*, 1965; 1966; 1978; *Schasse*, 1987; *Vance et al*., 1987; *Tabor et al*., 2000; *Hammond*, 2005; 2008 unpubl. data]. Regional disconformities and unconformities separate the Fifes Peak Formation and the Pliocene formations in the Cascades. In southern Washington, the Ohanapecosh Formation is unconformably overlain by the early Miocene Eagle Creek Formation [*Wise*, 1970], composed of very poorly sorted conglomerate containing pumice fragments, thin-bedded sandstone and pebble conglomerate.

Various late Oligocene and Miocene eruptive centres are preserved in central Washington. The Mount Aix caldera (late Oligocene), Tieton volcano (Miocene) and Columbia River Basalt Group (Miocene) are, respectively, at 15 km, 30 km and >30 km to the east of the Mt Rainier National Park [*Swanson*, 1966; *Hammond*, 2005; 2008 unpubl. data]. Fifes Peak volcano (Oligocene) is situated at 15 km to the northeast of the national park, and the Miocene Tatoosh pluton (late Miocene) is ~10 km south of Mt Rainier volcano. The Oligocene-Miocene Snoqualmie plutons in central Washington record the northern continuation of the igneous activity in the Tertiary Cascades arc.

The apparently lower magma rate of production in the central Cascades during the early Miocene and the Pleistocene-Quaternary [*Fiske et al*., 1963; *McBirney*, 1978; *Hammond*, 1979; *Smith*, 1989; *Tabor et al*., 2000] has been attributed to the change in direction and rate of the subduction [*Hammond*, 1979; *Evarts et al*., 1987; *Verplanck and Duncan*, 1987]. However, the geological record of this period is incomplete due to erosion in response to uplift [*McBirney*, 1978; *Hammond*, 1979; *Smith*, 1989]. On the basis of (U-Th)/He and apatite fission-track ages, Reiners et al. [2002] proposed a low exhumation rate during the Oligocene to late Miocene, followed by an increase in the exhumation, uplift and cooling

rates of the western Cascades during late Miocene (8-12 Ma). Consequently, the paucity of 5-15 Ma igneous rocks could mostly be the consequence of lack of preservation.

The Eocene-Miocene formations are covered by thick Quaternary volcaniclastic deposits and lavas. Major volcanoes in and around the studied area (Fig. 3.1) are Mt Rainier, Goat Rocks, Mt Adams, Indian Heaven and Mt St Helens [*Crandell*, 1976; *Hildreth*, 2007].

2.4. Previous work on facies of the Ohanapecosh Formation

The volcaniclastic facies of the Ohanapecosh Formation in the Mt Rainier area was studied extensively by Fiske [1963] and Fiske et al. [1963; 1964] and various processes and origins were proposed [*Fiske*, 1963; *Fiske et al*., 1963; *Winters*, 1984; *Stine*, 1987; *Vance et al*., 1987; *Swanson*, 1996; *Swanson et al*., 1997]. The formation is mainly composed of andesitic and dacitic volcaniclastic facies; minor lavas, "arkose" and "sandstone" are present locally [*Wise*, 1970; *Winters*, 1984; *Stine*, 1987; *Vance et al*., 1987]. The volcanic clasts were originally glassy tube pumice clasts, crystals, non-vesicular glassy fragments and glass shards, but all glass has devitrified [*Fiske*, 1963]. Dense volcanic clasts, dominantly andesitic, are ubiquitous. Broken and unbroken accretionary lapilli are common in a few facies. Fossils of wood, leaves and poorly preserved benthic shells ["ostracods, gastropods, and perhaps even Foraminifera"; *Fiske et al*., 1963] are present, but not indicative of marine or lacustrine environment. Fiske [1963] divided the volcaniclastic facies in the Ohanapecosh Formation into two types, thick and thin, depending on bed thickness.

The "thick" beds [*Fiske*, 1963] are well defined and laterally extensive (>hundreds of metres), and 3 to 60 m thick (average thickness of 10 m). No welding textures or columnar joints were documented. The two varieties described by Fiske [1963] are: (1) rich in dense lava fragments and containing less than 50 vol.% "fine matrix" and (2) pumice-rich facies, with up to 70 vol.% "fine matrix".

The "thin" beds [*Fiske*, 1963] are well defined, laterally extensive over tens of metres, commonly normally graded, and mostly 50-60 cm thick. The most common facies is "coarse tuff, with subordinate fine tuff and fine lapilli tuff". "Well-sorted tuff or lapilli tuff with no matrix" was also recorded. Some "thin" beds are internally stratified, but sole marks, slump structures and cross laminae are uncommon.

Fiske [1963], followed by Wise [1970], proposed that most of the formation was emplaced subaqueously, in quiet water such as a lake or sheltered embayment of the sea, and sourced from several underwater or subaerial volcanoes. The quiet subaqueous depositional setting was argued on the basis of: the laterally extensive, even thickness bed geometry, internal grading, and the complete absence of unconformities, erosion surfaces and large-scale cross beds. The absence of typically marine fossils suggested a

lacustrine rather than marine environment. The "thick" beds were thought to be deposits of "subaqueous pyroclastic flows" or "debris flows". The "thin" beds were interpreted to be turbidity current or water-settled ash fall deposits [*Fiske*, 1963]. However, more recent interpretations have favoured a subaerial environment of deposition, such as a fluviatile and alluvial apron in which lakes were minor, shallow and temporary [*Frizzell et al*., 1984; *Winters*, 1984; *Stine*, 1987; *Vance et al*., 1987; *Swanson*, 1996; *Swanson et al*., 1997; *Tabor et al*., 2000].

Flow-banded rhyolitic and andesitic coherent facies occur in the Ohanapecosh Formation at Indian Bar, on the eastern foot of Mt Rainier (Fig. 3.2) and in central Washington [*Fiske et al*., 1963; *Wise*, 1970]. Andesitic lavas of Angry Mountain southeast of Packwood [*Swanson*, 1996; *Swanson et al*., 1997] are also possibly related to the Ohanapecosh Formation. Northeast of Mt Rainier, the Ohanapecosh Formation contains sedimentary units derived from a granitic-metamorphic basement, bordering the northern end of the Cascade volcanic arc [*Hammond*, 1979]. A crystalline basement source in eastern Washington and Idaho was suggested by Winters [1984] for feldspathic sandstone that occurs in the Ohanapecosh Formation southeast of Packwood.

Major differences in thickness of sections in the White Pass area (east) and in the Lake Tapps area (northwest; Fig. 3.1) were interpreted to result from horst structures controlling sediment accumulation [*Gard*, 1968; *Vance et al*., 1987]. Bed pinch-out structures were documented locally southeast of Packwood [*Winters*, 1984; *Stine*, 1987]. However, no major faults have been identified in previous studies of the Ohanapecosh Formation.

The Ohanapecosh Formation is well indurated and has a secondary mineral assemblage consistent with low-grade regional metamorphism (zeolite facies). All original glass and most original ferromagnesian and plagioclase phenocrysts have been replaced by secondary minerals. The overall greenish-grey colour is caused by the presence of fine-grained laumontite-albite-quartz, wairakite-albite-quartz and prehnite-albite-quartz [*Fiske et al*., 1963]. Other common secondary minerals include epidote, chlorite, carbonate, sphene, leucoxene, celadonite, saponite and other montmorillonoids [*Fiske et al*., 1963]. The alteration has been attributed to higher temperature and pressure associated with deep burial and contact metamorphism from intrusions, especially the Tatoosh and Snoqualmie plutons [*Fiske et al*., 1963; *Tabor et al*., 2000]. Johnson [1985] proposed that peak metamorphism was associated with the emplacement of these large plutons.

3. GEOLOGICAL OVERVIEW OF THE OHANAPECOSH FORMATION

In the studied area (Figs 3.1, 3.2), the Ohanapecosh Formation records deposition of almost exclusively volcaniclastic facies. The duration of the sedimentation is unsure, but probably much shorter than the apparently ~8 million years proposed for the entire Ohanapecosh Formation [*Tabor et al*., 2000]. A remarkable feature throughout the

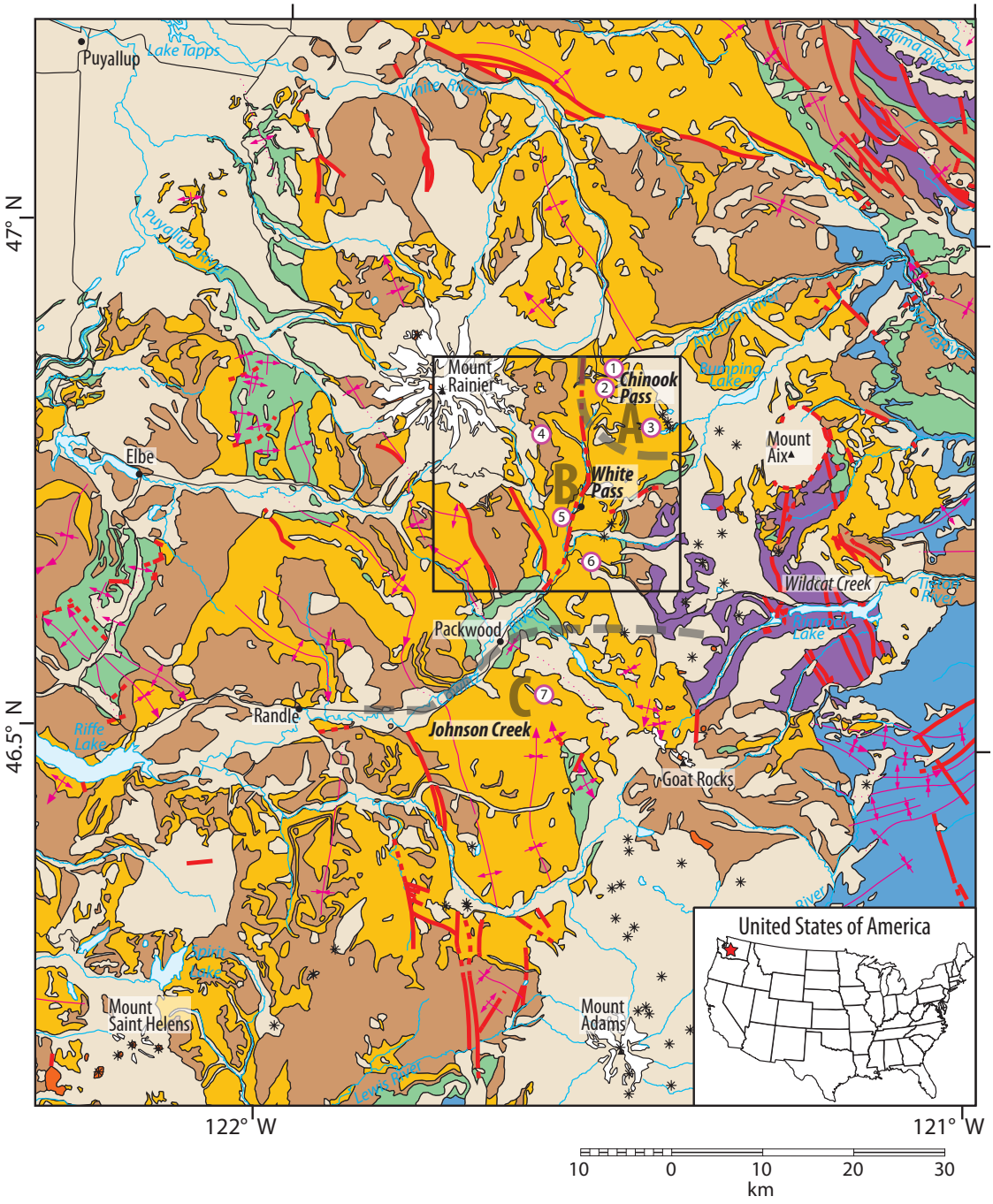

Fig. 3.1 Regional geological map of the Mt Rainier area (Washington State, USA), simplified and modified after Schuster [2005]. Inset shows map location (red star). Logged section locations 1: Chinook Pass, 2: Cayuse Pass, 3: Cougar Lake, 4: Indian Bar, 5: Backbone Ridge and Ohanapecosh Campground, 6: White Pass; 7: southern Packwood. Thick grey lines are boundaries between the members of the Ohanapecosh Formation, with Chinook Pass Member (large grey letter A, locations 1–3), White Pass Member (large grey letter B, locations 4–6) and Johnson Creek Member (large grey letter C, location 7). The main study area (black outlined square) is shown in more detail in Figure 3.2.

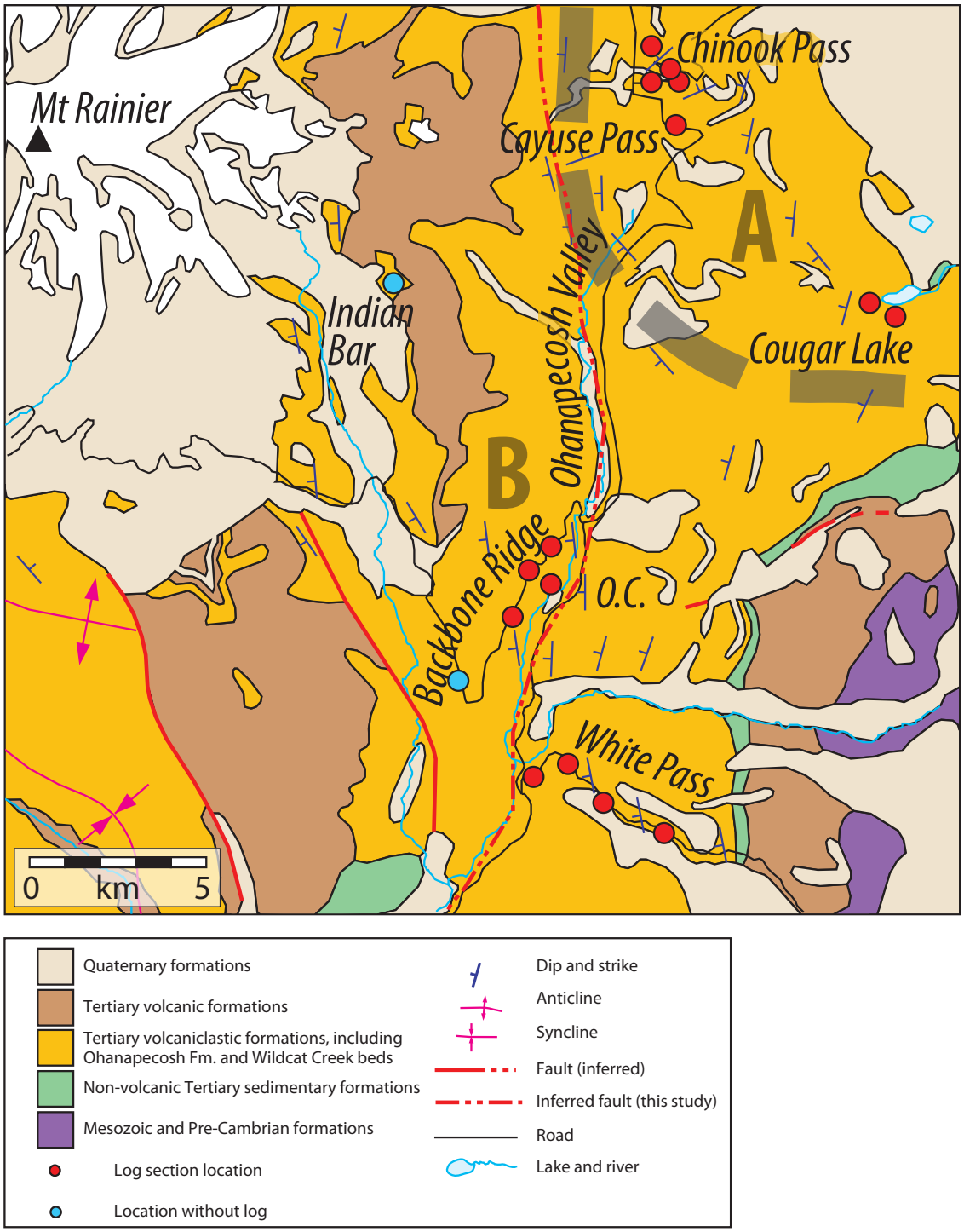

Fig. 3.2 Local geological map of the Ohanapecosh Formation in the Mt Rainier area; simplified and modified after Schuster [2005] and Fiske [1964]. Red dots are logged section locations. Thick grey lines are boundaries between the members of the Ohanapecosh Formation: Chinook Pass Member (large grey letter A) and White Pass Member (large grey letter B). Dips are in the range 20–45° [Fiske et al., 1963]. O.C. for Ohanapecosh campground.

Ohanapecosh Formation is the occurrence of laterally continuous very thin to thick beds intercalated with thick to extremely thick units, and the absence of large-scale cross-beds and bed discontinuities [*Fiske*, 1963]. A dominant intermediate composition of the volcanic rocks is suggested by abundant plagioclase and minor ferromagnesian phenocrysts in fiamme, pumice and dense clasts. A minor part of the succession is mafic in composition (probably basaltic) and characterized by abundant ferromagnesian and

rare feldspar phenocrysts in scoria and dense clasts. I have subdivided the Ohanapecosh Formation into three main areas that overall consist of similar volcaniclastic facies, and are tentatively named members of the Ohanapecosh Formation: the Chinook Pass Member, the White Pass Member and the Johnson Creek Member. Intrusions occur at various places in these three areas and most of them are associated with the younger Miocene Tatoosh pluton. Due to widespread vegetation cover, well-exposed outcrops mostly occur on road cuts and in sub-vertical cliffs.

The White Pass Member consists of thick to very thick, coarse-grained beds, and voluminous sequences of fine-grained, very thin to thick beds (Fig. 3.3). The rocks of the White Pass Member are much darker-green compared to the Chinook Pass Member, and contain volcaniclastic facies with different thickness, texture and mineralogy than the Chinook Pass Member. The presence of chlorite as the secondary mineral in the White Pass and Johnson Creek Members but absence in the Chinook Pass Member indicates a different style and intensity of alteration.

3.1. Chinook Pass Member

The Chinook Pass Member comprises >350-m-thick volcaniclastic sequences exposed at Cayuse and Chinook Passes (Appendix C). The total thickness of the Chinook Pass Member is unknown. These sequences dip at 20° towards the north-northwest <4 km to the southwest of the hinge of the Chinook Pass anticline (Figs 3.1, 3.2). The base of the sequence is the Cayuse Pass section which comprises multiple very thin to thick beds, overlain by a succession of extremely thick, graded beds (>20 m each; Fig. 3.4). The >200–m-thick Chinook Pass section overlies the Cayuse Pass section after a couple of hundred metres of hidden stratigraphy and is composed of very thin to thick beds that are overlain by numerous extremely thick (>30 m) beds (Fig. 3.5). Major natural cliffs at Cougar Lake on the Pacific Crest trail expose >150 m of Ohanapecosh Formation volcaniclastic facies (Fig. 3.6). The Cougar Lake section is several km to the southeast of the Cayuse and Chinook Pass sections and cannot be firmly correlated with these sections. However, these facies are broadly similar, and are grouped together in the Chinook Pass Member.

3.2. White Pass Member

The White Pass Member comprises the road cuts of White Pass and Backbone Ridge, as well as the section exposed on the slope from near the Ohanapecosh Campground up to the Backbone Ridge road (Fig. 3.2; Appendix C). The >850-m-thick White Pass section consists of very thick to extremely thick and very thin to thick, dark green volcaniclastic facies, but part of the stratigraphy remains obscured by vegetation (Fig. 3.7). Overall, the

Fig. 3.3 Typical outcrop of the Ohanapecosh Formation at Backbone Ridge (White Pass Member). Double arrows and blue line show volcaniclastic beds, single blue arrow indicates a Miocene dyke (facies 18).

sequence strikes 160° and dips 45° towards the west. However, a >100-m-thick sequence of mafic volcanic breccia (unit 137, White Pass section) shows local changes in facies, dip and strike.

More to the northwest, the Ohanapecosh Formation can be followed from the Ohanapecosh Campground (Fig. 3.8) up to the Backbone Ridge road cut (>200 m of stratigraphy; Appendix C). This area could be mapped due to the exceptional removal of the dense vegetation by floods in 2006. A sequence of mafic volcanic breccia (unit 22, Ohanapecosh Campground) similar to that in the White Pass section is locally non-conformable with the stratigraphy. Southwest along the Backbone Ridge road (Fig. 3.9), beds strike 180° and dip 35° towards the west (>230 m of stratigraphy, in addition to 200 m of hidden stratigraphy). Outcrops of the Ohanapecosh Formation found at Indian Bar (Fig. 3.2; Appendix C) presumably belong to a higher stratigraphic level [*Fiske*, 1963]. The top of the Ohanapecosh Formation at Backbone Ridge has been eroded and the contact is overlain by the Stevens Ridge Member [*Fiske et al.*, 1963], and the last logged sections are very poorly preserved.

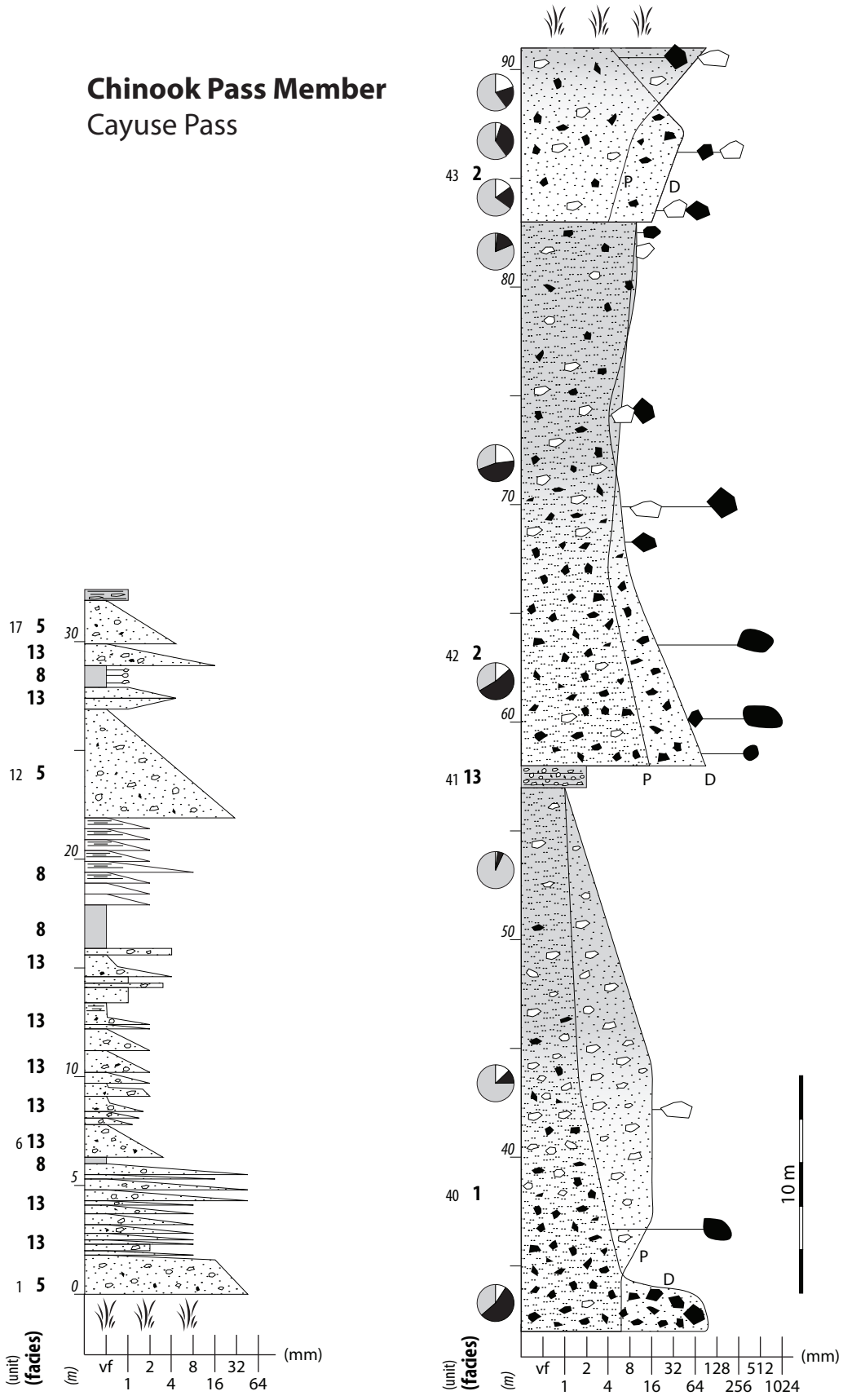

Fig. 3.4 Stratigraphy of the Chinook Pass Member of the Ohanapecosh Formation at Cayuse Pass. Graphic log features and key as in Figure 3.5. Pumice clasts and fiamme (P), dense clasts (D).

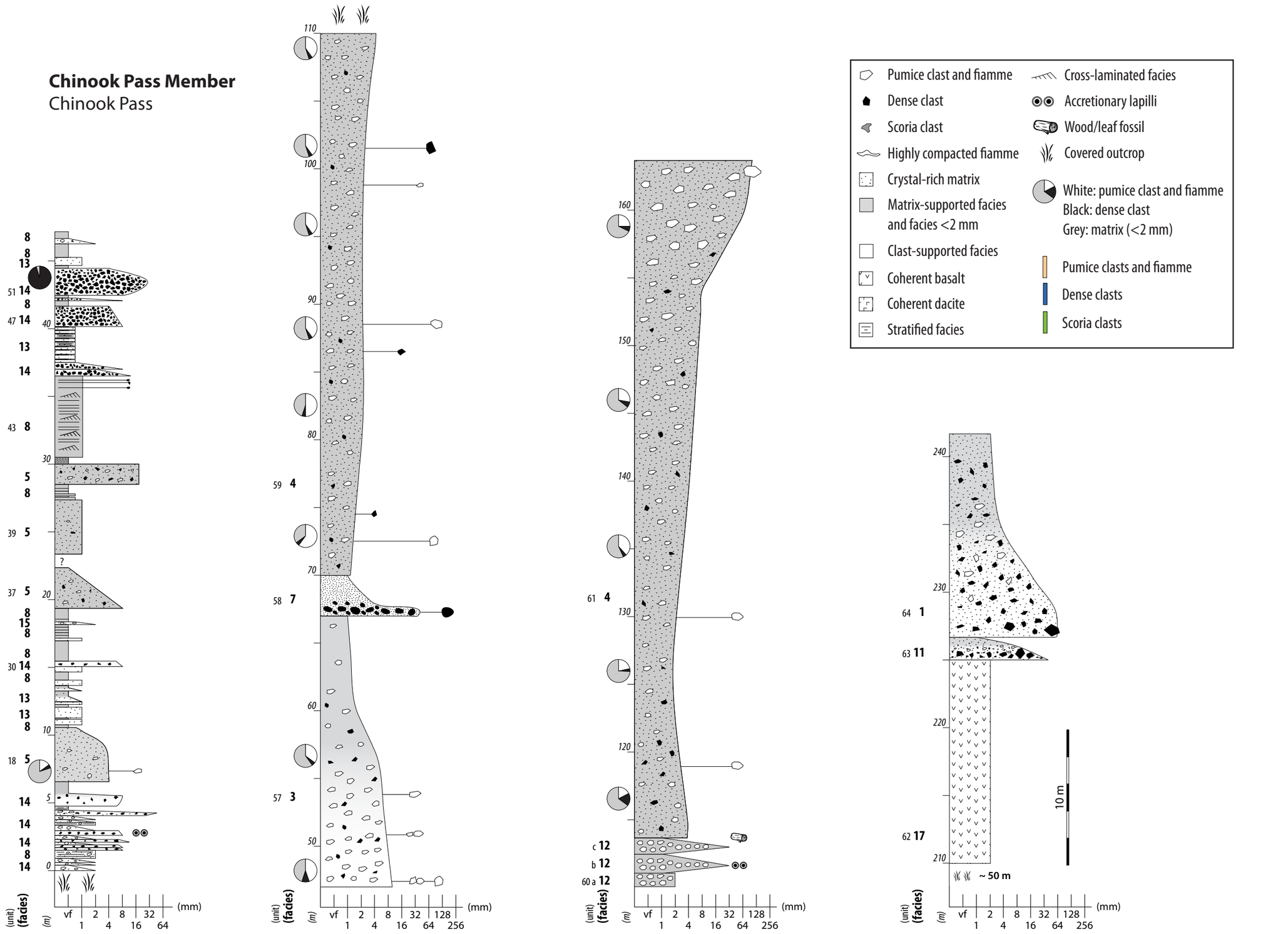

Fig. 3.5 Stratigraphy of the Chinook Pass Member of the Ohanapecosh Formation at Chinook Pass. The log outlines the mean of clast intermediate diameter on horizontal scale (in mm); isolated clasts on right-hand side give outsized clast dimensions. Logs are in direct upward continuity from left to right. Unit number (italic type), facies number (bold type) and stratigraphic thickness (plain type) are given on the left-hand side of logs. Pie diagrams give vol.% of different clast types from image analysis (field and rock slabs): white for pumice clasts and fiamme, black for dense clasts, grey for matrix (<2 mm), including free broken crystals.

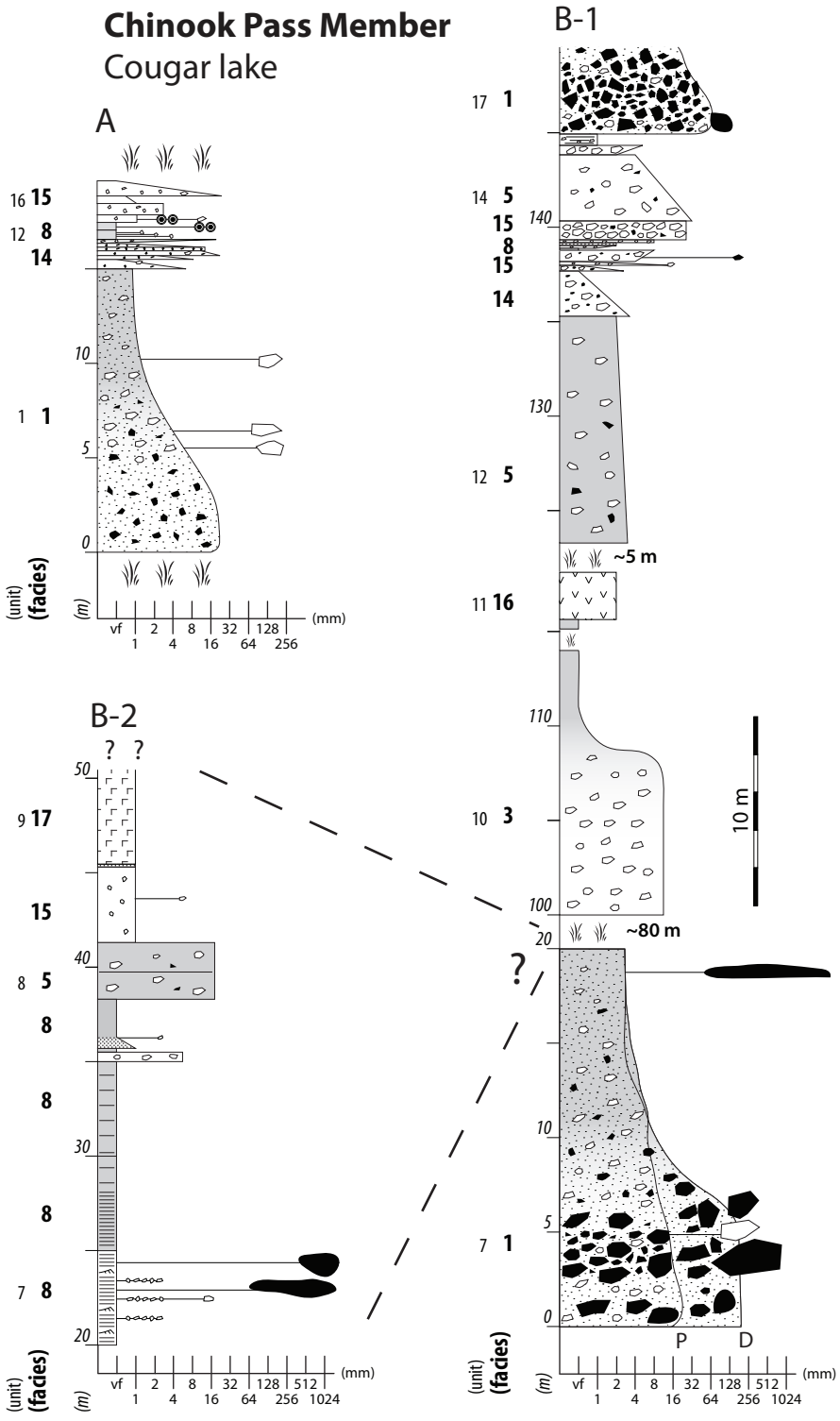

Fig. 3.6 Stratigraphy of the Chinook Pass Member of the Ohanapecosh Formation at Cougar Lake. Log B-2 probably corresponds to the covered top of the basal unit of log B-1. Log A is below log B in the stratigraphy. Graphic log features and key as in Figure 3.5. Pumice clasts and fiamme (P), dense clasts (D).

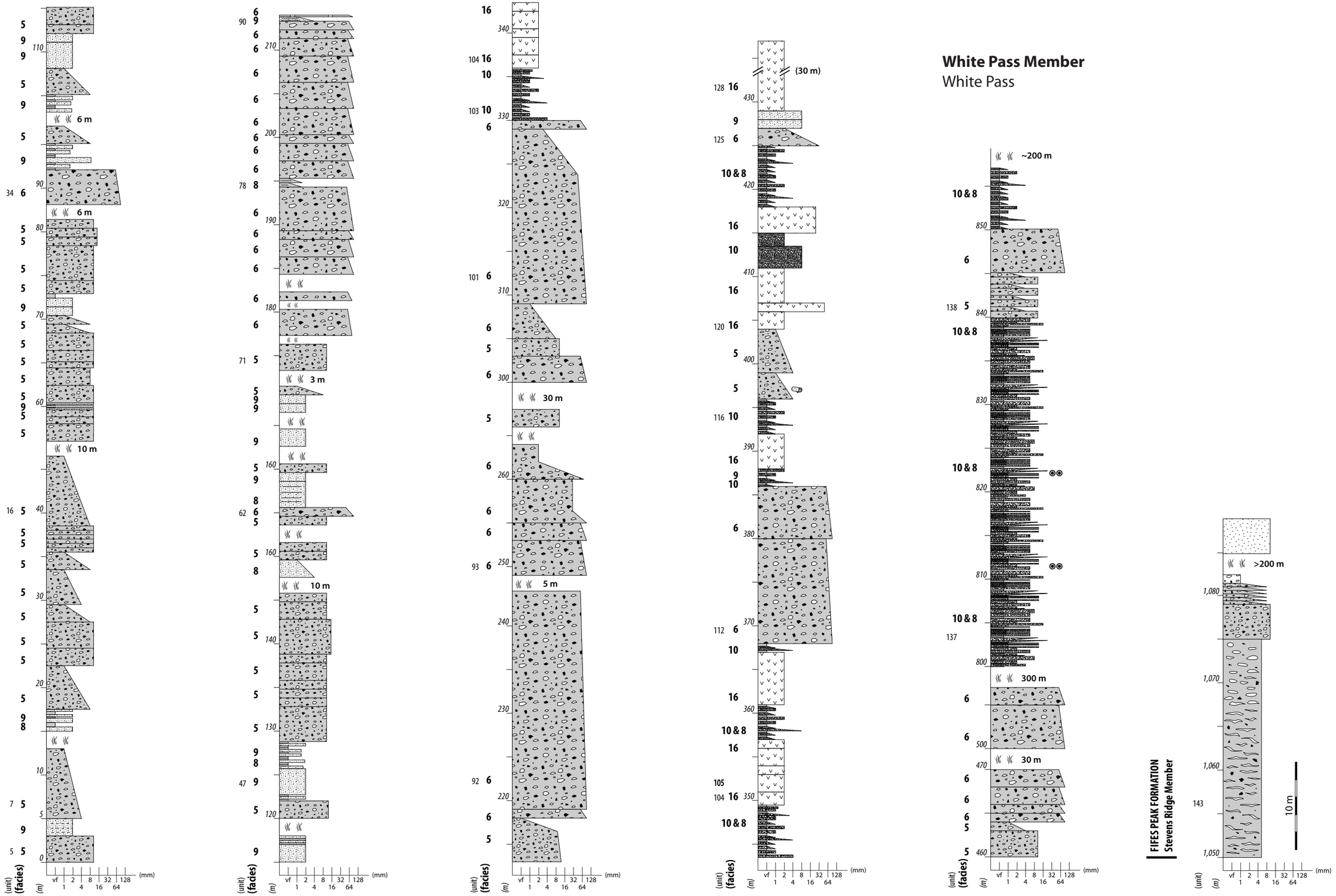

Fig. 3.7 Stratigraphy of the White Pass Member of the Ohanapecosh Formation at White Pass, from lowest mappable volcaniclastic units on the White Pass road (road 12) westward to the intersection with north-south road towards Cayuse Pass (road 123). About 500 m of stratigraphy is covered by vegetation between the Summit Creek sandstone and this log. Graphic log features and key as in Figure 3.5.

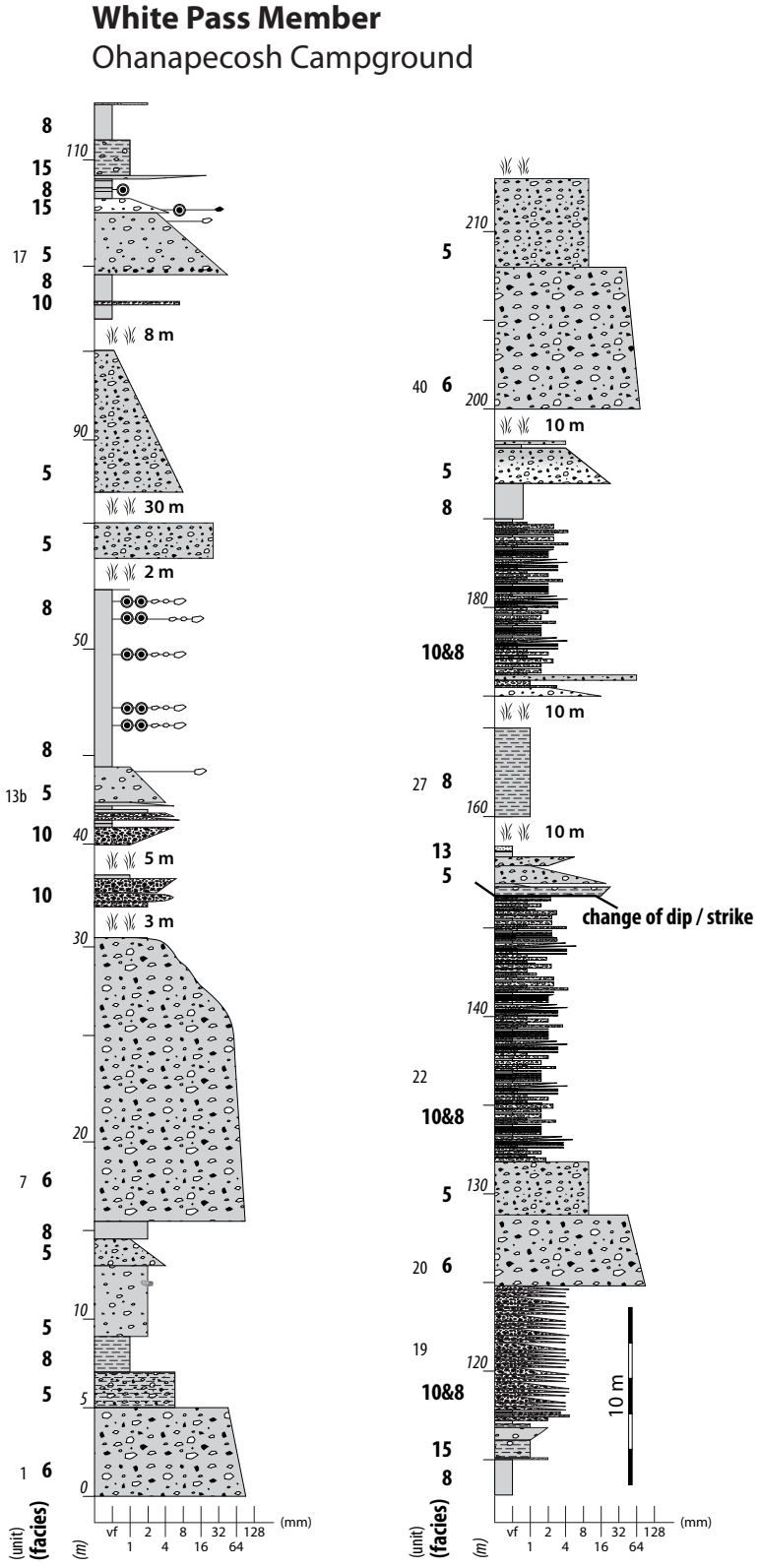

Fig. 3.8 Stratigraphy of the White Pass Member of the Ohanapecosh Formation from Ohanapecosh Campground up to Backbone Ridge road, on the site of the 2006 floods. This section is a lateral equivalent up to the ~100 m gap (at 130 m of stratigraphy) at the base of the Backbone Ridge section (Fig. 3.10). Graphic log features and key as in Figure 3.5.

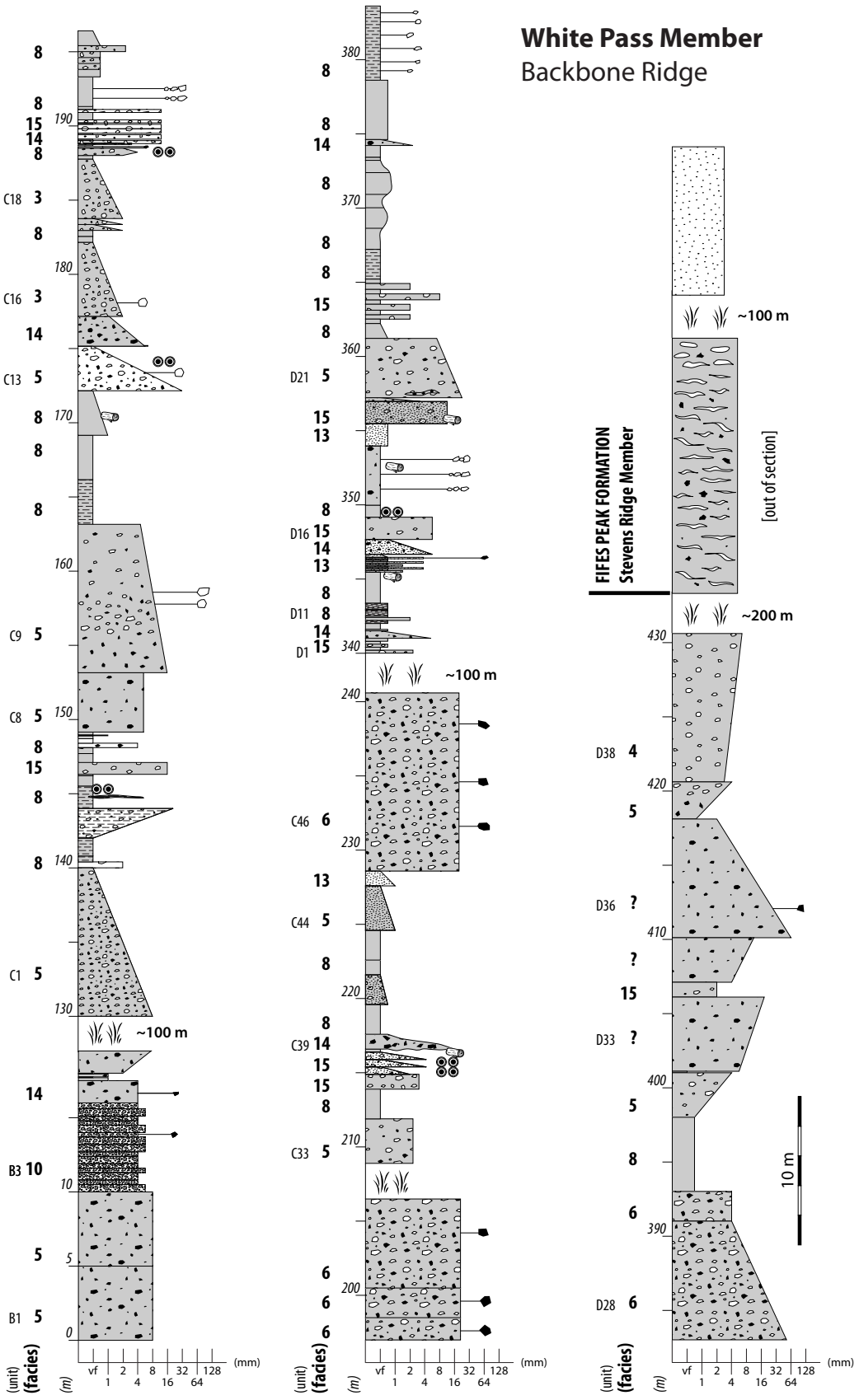

Fig. 3.9 Stratigraphy of the White Pass Member of the Ohanapecosh Formation on Backbone Ridge road. Graphic log features and key as in Figure 3.5. Prefix of unit number C and D refer to different sections.

3.3. Johnson Creek Member

The Johnson Creek Member is exposed in scattered road cut outcrops to the southeast of Packwood (Fig. 3.10; Appendix C). Only one section has been logged and the facies are mostly similar to those in the Ohanapecosh Campground and Backbone Ridge sections (White Pass Member), but beds are thinner and show rare cross-laminae and channel-like features.

3.4. Contact with the overlying Fifes Peak Formation

Despite poor exposure of the White Pass section at the bottom of the Ohanapecosh valley (Fig. 3.2), two units are used as stratigraphic markers. An extremely thick (>15 m) red fiamme breccia (unit 143, White Pass section) is attributed to the Stevens Ridge Member of the Fifes Peak Formation. The red colour and grading in compaction help distinguish this facies from all other facies in the Ohanapecosh Formation. The basal facies of the red fiamme breccia contains very elongate white and red fiamme (aspect ratio >20) that are aligned parallel to bedding and deformed around dense clasts and alkali feldspar and minor plagioclase crystals in a red-oxidised matrix. The feldspar phenocryst content of the fiamme is <5 vol.%. The fiamme in the upper facies are substantially less compacted (aspect ratio ~5) and also contain <5 vol.% feldspar phenocrysts. The red colour is not associated to a nearby intrusion that could have oxidised the unit. Red fiamme breccia attributed to the Stevens Ridge Member found outside the logged area at Backbone Ridge probably correlates with the red fiamme breccia in the lower White Pass section (Fig. 3.11).

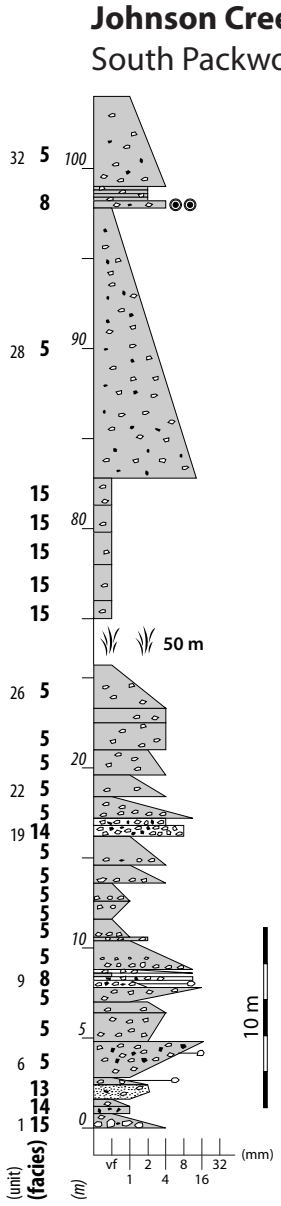

At the base of White Pass (top of the White Pass section), after more than 200 m of hidden exposures from bed 143, a poorly exposed, pale-coloured, 5-m-thick quartz-rich, fine-grained ignimbrite occurs and is also attributed to the Stevens Ridge Member, part of the Fifes Ridge

Fig. 3.10 Stratigraphy of the Johnson Creek Member of the Ohanapecosh Formation at southern Packwood. Graphic log features and key as in Figure 3.5.

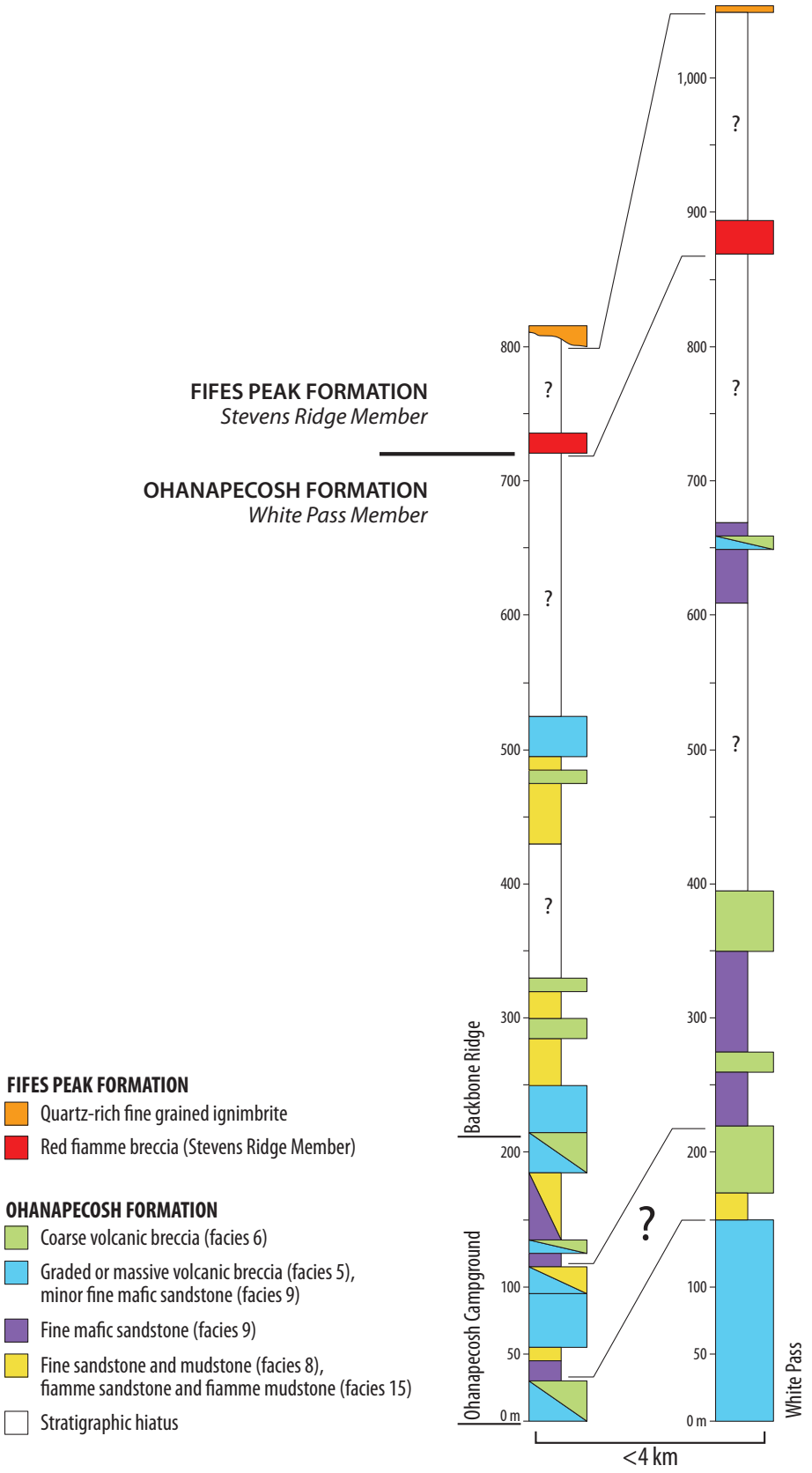

Fig. 3.11 Simplified stratigraphy in the White Pass Member, comparing joint Ohanapecosh Campground and Backbone Ridge (left; Fig. 3.8) and White Pass (right; Fig. 3.9) sections. Facies at White Pass are overall thicker and coarser than at Backbone Ridge. Red fiamme breccia and quartz-rich fine grained ignimbrite of the Stevens Ridge Member (Fifes Peak Formation) constrain stratigraphic relations, whereas mafic volcanic breccia and vesicular basalt are tentative. Only most voluminous facies are shown; simplified clast coarseness shown by log width. Real thicknesses of stratigraphic hiatus are rough estimates, and dependant on unknown dips. In addition, stratigraphic hiatus may hide fault repeating stratigraphy. White Pass and Ohanapecosh Campground logs are shown entirely; Backbone Ridge log starts at 130 m from its base (Fig. 3.11). Less than 4 km separates top of White Pass from base of Ohanapecosh Campground (Fig. 3.2).

Formation. These outcrops of the Stevens Ridge Member are not shown on any geological maps at my knowledge [*Fiske et al.*, 1963; *Schuster*, 2005; *Hammond*, 2008 unpubl. data].

The stratigraphic position and concordance of the felsic coherent facies at Indian Bar could not be determined from the poorly preserved outcrops available, and no radiometric dates have been published. Hence, this unit could be part of the Ohanapecosh Formation, or of the Fifes Peak Formation.

3.5. Ohanapecosh Valley Fault

On the basis of stratigraphic correlations in the White Pass Member (Fig. 3.11), I infer that a major north-south fault separates the White Pass and Backbone Ridge sections. This fault follows the Ohanapecosh Valley and is here named the Ohanapecosh Valley Fault (Fig. 3.12). Its exact location and dip are unknown. The Ohanapecosh Valley Fault accounts for repetition of red fiamme breccia and quartz-rich fine grained ignimbrite in the Stevens Ridge Member (Fifes Peak Formation; Fig 11). This fault doubles the apparent thickness of the Ohanapecosh Formation between White Pass and Backbone Ridge (Fig. 3.2). On the basis of the White Pass and Backbone Ridge sections, Fiske et al. [1963] proposed a thickness of ~3 km for the entire Ohanapecosh Formation. The fault repetition proposed here dramatically decreases the maximum thickness of the formation to 800 m (Fig. 3.11), because the inferred Ohanapecosh Valley Fault increases the apparent thickness

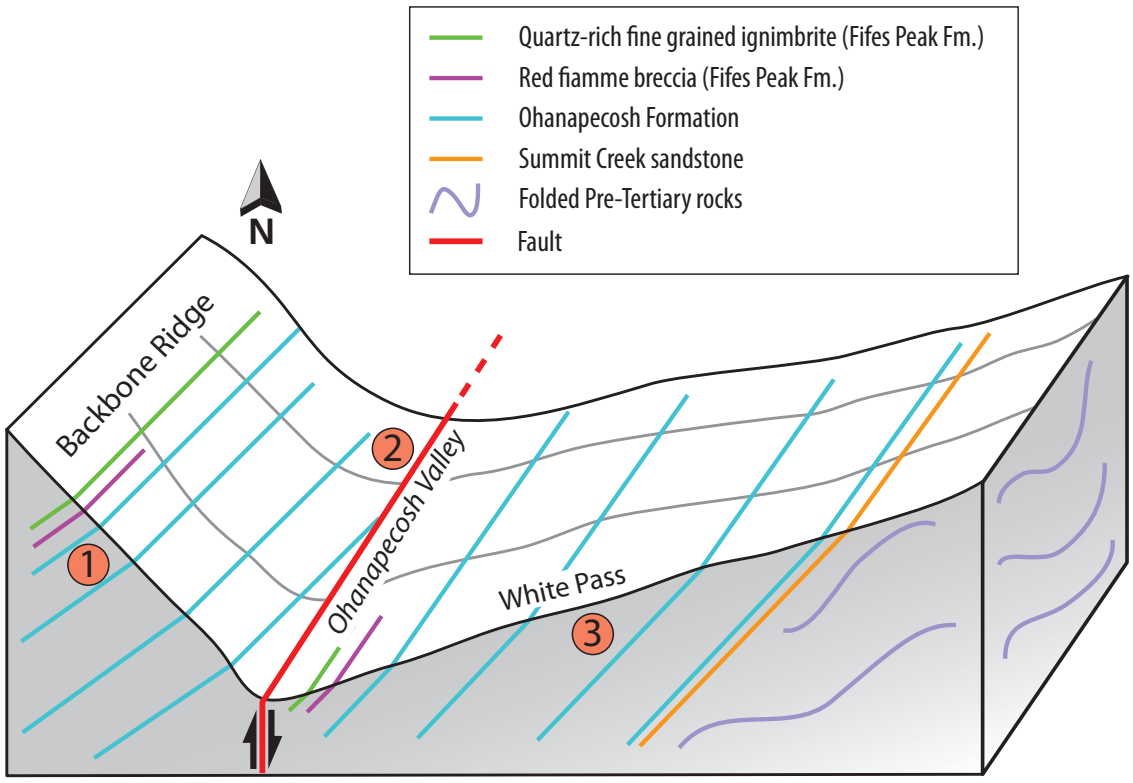

Fig. 3.12 Block diagram of the structure in the Ohanapecosh Valley. A major sub-vertical fault is concealed in the valley and separates the White Pass Member into two blocks. The western side contains Backbone Ridge (1) and Ohanapecosh Campground (2), the eastern block contains White Pass (3). The red fiamme breccia and quartz-rich fine grained ignimbrite of the Stevens Ridge Member (Fifes Peak Formation) were used as stratigraphic markers.

of the White Pass Member (Fig. 3.11). No other faults were recognised, but they could occur in the numerous gaps in stratigraphic sections. This thickness better matches the ~800-m-thick section of the Ohanapecosh Formation in the Lake Tapps area to the northwest [*Gard*, 1968].

4. COMPONENTS OF THE OHANAPECOSH FORMATION

4.1 Definitions

The bed thickness nomenclature follows Ingram [1954], with the addition of "extremely thick" for beds >10 m thick. Breccia is used as a non-genetic term to describe any clastic facies composed of angular clasts coarser than 2 mm [*Fisher*, 1961a]. Similarly, sandstone (1/16–2 mm) and mudstone (<1/16 mm) are used to designate grain size classes [*Wentworth*, 1922; *Fisher*, 1961a]. I have used the term "facies" instead of "facies association", for simplicity.

Most components of the Ohanapecosh Formation are volcanogenic. Primary volcaniclastic facies are generated directly by volcanic eruptions, and are not remobilized [*White and Houghton*, 2006], and may include juvenile and non-juvenile clasts. The term juvenile refers the products of volcanic eruptions that were at magmatic temperature when erupted [*White and Houghton*, 2006], i.e. on first contact with the atmosphere or the hydrosphere. Pumice clast refers to a highly vesicular (>60 vol.%) volcanic fragment that is intermediate to felsic in composition, whereas a scoria clast is less vesicular (<60 vol.%) and mafic in composition. Where compacted by diagenesis or welding, pumice clasts lose porosity and are transformed into fiamme [*Bull and McPhie*, 2007]. Dense clasts are not now and never were vesicular.

The proportions of clasts and matrix of representative samples of facies were estimated in the field, and on polished rock slabs and thin sections in the laboratory. Grain size distribution was determined following the technique described in Chapter 2. The best examples were also studied by image analysis from scans and field photographs at 1,200 dpi. The detection limit of fine-grained particles is generally around 2 mm, due to rock alteration, and this limit was used as a boundary between clasts and matrix. Thus, the term matrix is used broadly for interstitial fine clasts <2 mm. Alteration on feldspar and ferromagnesian crystals prevented making precise estimates of their volumes. Volumetric data are presented as pie diagrams.

The average diameter of clasts measured in the field corresponds to the mean diameter population, i.e. most common long-axis dimension of clasts. Maximum clast diameter corresponds to long-axis dimension of the coarsest clast. However, these values are in fact an apparent diameter on the rock face (chapter 2, Appendix B).

4.2. Pumice clasts and fiamme

Pumice clasts (Fig. 3.13a) are ubiquitous throughout the Ohanapecosh Formation. They are pale to dark green to black, and the formerly glassy groundmass is entirely devitrified and composed of secondary minerals. They span 1–300 mm in length and their aspect ratios (clast length/thickness) are 1–2.5 (max 5), reflecting the minimal effect of regional compaction. Coarse fiamme (up to 200 mm in length) are also present and have their long axes oriented parallel to bedding (Fig. 3.13b); they are considered to be former pumice clasts, now compacted because of their relic vesicular texture, their content in largely euhedral phenocrysts, and their similar alteration colour compared to pumice clasts. The pumice clasts range from aphyric to phenocryst-rich. Plagioclase and minor ferromagnesian (including pyroxene) phenocrysts are commonly partially to fully replaced by secondary minerals and can reach 10-20 vol.% of the pumice clast volume. No quartz as a phenocryst phase in pumice clasts and fiamme was found.

In the Chinook Pass Member, most pumice clasts have 25-30 vol.% euhedral to subhedral plagioclase phenocrysts (2 mm, up to 5 mm). The pumice clasts are vesicular (Fig. 3.13a) and fiamme show moderate collapse of the vesicles parallel to the bedding. In contrast, small pumice clasts (<5 mm) are angular, blocky and equant, and are generally too small to contain phenocrysts (Fig. 3.13b). Preservation of vesicular texture in the small pumice clasts is rare (Fig. 3.13a). In the White Pass Member, pumice clasts are poorly to moderately (<30 vol.%) porphyritic. The pumice clasts can be tube pumice, and few specimens of "woody" type [*Kato*, 1987; *Allen et al*., 2010] were found, in which well-preserved vesicles are exceptionally elongate (aspect ratio >>100).

4.3. Free broken crystals

Fragments of plagioclase crystals (average 1-2 mm) are abundant in many facies (Figs 3.13b, 3.13d), and reflect the mineralogy of the coarser pumice clasts and fiamme. Relic ferromagnesian minerals are commonly too altered to identify. Very rare volcanic quartz crystals were found in the volcaniclastic facies (<3 grains over tens of thin sections).

4.4. Scoria clasts

Scoria clasts are present in the White Pass Member, and interpreted to be basaltic in composition by their mineralogy, vesicularity and colour (Fig. 3.13c). They are sub-angular to very angular, 2–10 mm in average size, range from red or dark grey to black, and are poorly to moderately vesicular (<40 vol.% of vesicles). They contain feldspar microlites arranged in a trachytic texture, and rare plagioclase phenocrysts (<1 vol.%). Ferromagnesian crystals occur in many scoria clasts, but are commonly altered and

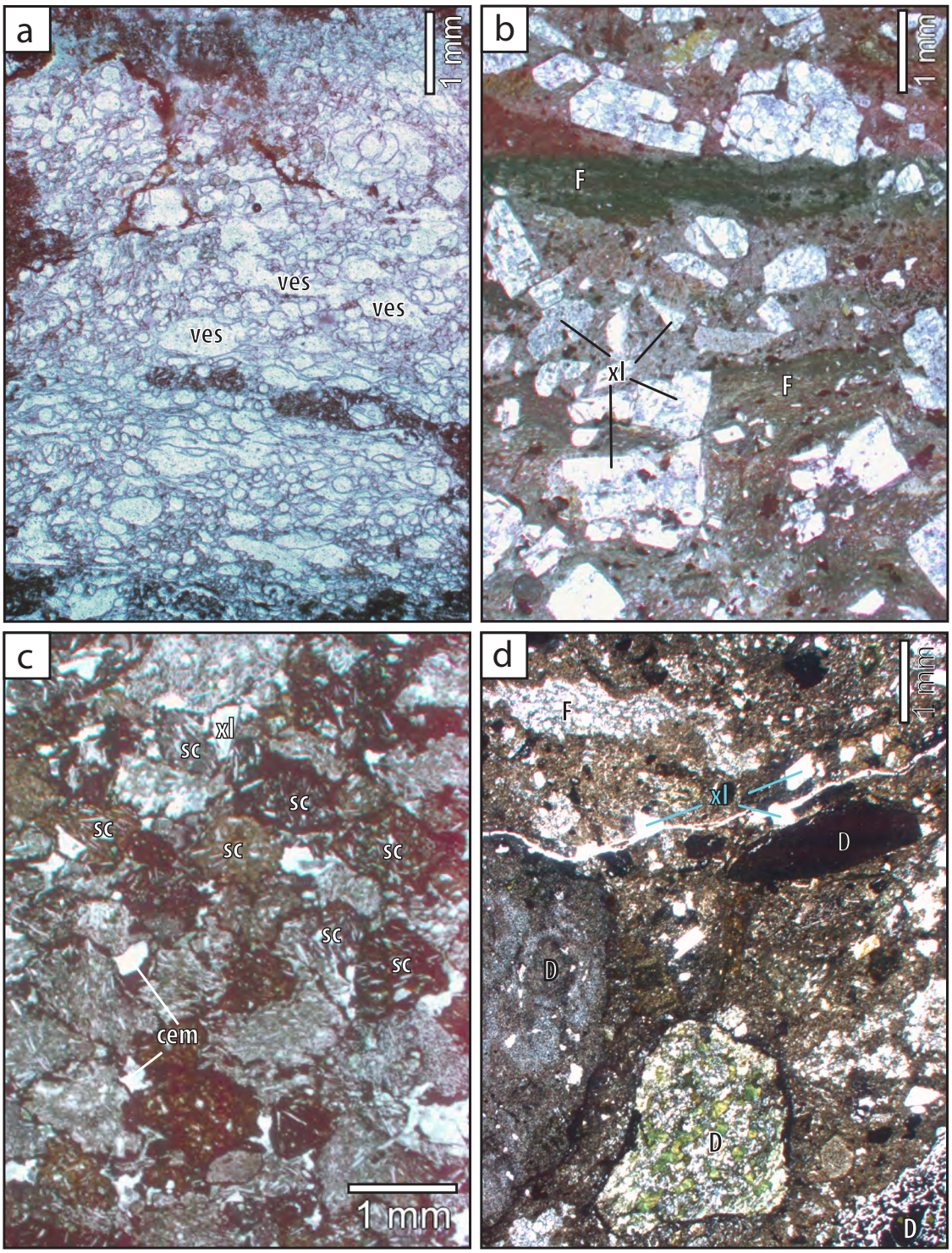

Fig. 3.13 Clasts in the Ohanapecosh Formation. **a)** Highly-vesicular pumice clast in normally graded or massive volcanic breccia (facies 5; unit 30, sample WA-03), White Pass section; **b)** Fiamme, broken feldspar crystals and fine (<2 mm) matrix in the middle sub-facies of normally graded fiamme-andesite breccia (facies 1) in the Cayuse Pass section, sample WA-22; **c)** Clast-supported scoria clasts in mafic volcanic breccia (facies 10) at White Pass (unit 137, sample WA-09). A few broken feldspar crystals and zeolite cement are present; **d)** Dense clasts and fiamme in a finer matrix with broken feldspar crystals in coarse volcanic breccia (facies 6, sample WA-07). Dense clast (D), scoria clast (Sc), fiamme (F), feldspar crystal (xl), cement (cem), vesicles (ves).

difficult to distinguish from the ubiquitous altered groundmass. Vesicles are round to highly contorted in shape, commonly <0.1–1 mm across and filled with zeolites and other secondary minerals.

4.5. Dense clasts

Numerous types of dense clasts occur in the Ohanapecosh Formation. The mineralogy of the dense clasts reflects mafic to intermediate compositions and they lack quartz crystals. They are aphyric to moderately porphyritic with up to 50 vol.% feldspar crystals and minor amounts of relic ferromagnesian crystals. Dense clasts span <1–1,000 mm in size and show different types of alteration (Fig. 3.13d). The White Pass Member is rich in red, dark red, dark green, and dark brown dense clasts, whereas the Chinook Pass Member abounds with white, green or dark green to dark brown aphyric dense clasts, and lacks red dense clasts, except where in contact with Miocene Tatoosh sills. Dense clasts are mostly angular to very angular. Sub-rounded dense clasts are minor, and only occur in five facies, and they are restricted to basal dense clast breccia in three of them. Rare perlitic textures occur in some equant clasts and indicate that they were formerly glassy.

4.6. Plant fossils

Fossils and casts of leaves and silicified tree fragments were found at various places, but in minor quantities. An isolated trunk fragment was found at lower Cayuse Pass (Fig. 3.14a); it is silicified, >60 cm long, and contains minor pyrite and possible anthracite. The growth rings suggest a former trunk diameter of >60 cm.

4.7 Accretionary lapilli

Rim-type accretionary and armoured lapilli [*Schumacher and Schmincke*, 1991] were found in few places, and can reach 20 mm across. They commonly show multiple rims and their cores are up to 10 mm (American Lake, Ohanapecosh Campground; Fig. 3.14b) or absent (e.g. Backbone Ridge, Ohanapecosh Campground, White Pass). Accretionary and armoured lapilli are commonly spread throughout the thickness of thin beds, and are in places concentrated in layers within very thin beds. They are absent in the thick to extremely thick beds. Intact and broken accretionary lapilli are found together in most beds (Fig. 3.14b).

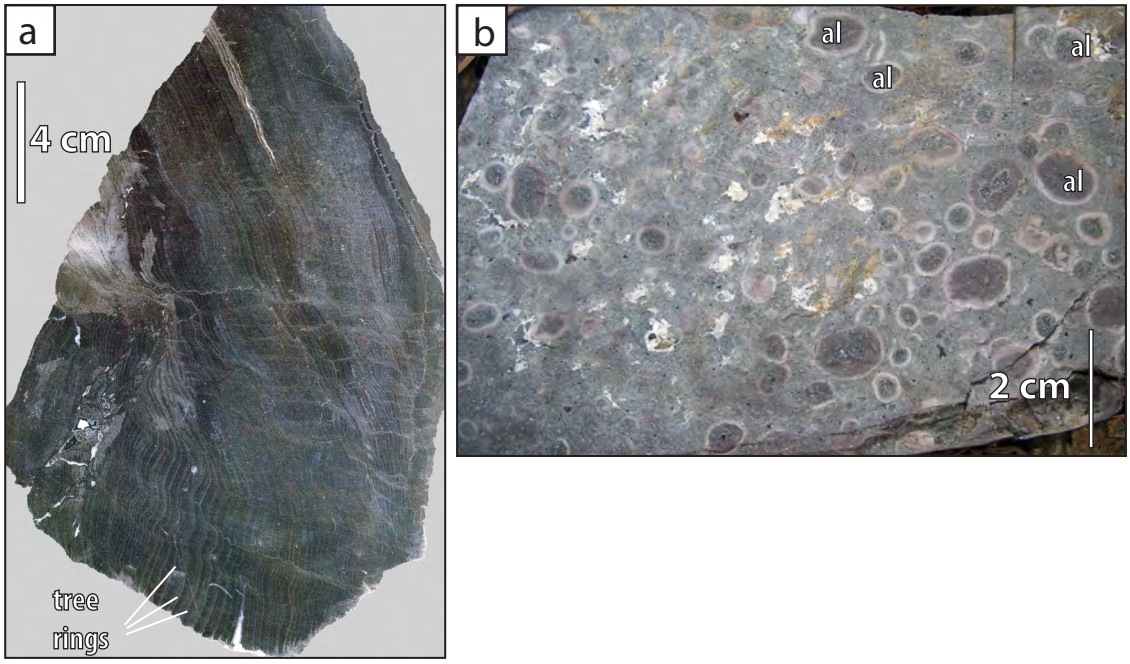

Fig. 3.14 Clasts in the Ohanapecosh Formation. **a)** Silicified wood from fine sandstone and mudstone beds (facies 8) in the lower Chinook Pass section. Some outer tree rings are made of anthracite and pyrite, sample WA-01; **b)** Red-altered, rim-type accretionary lapilli (al) and armoured lapilli in bed of fine sandstone and mudstone (facies 8) within a sequence of mafic volcanic breccia (facies 10) at Ohanapecosh Campground. Cores of armoured lapilli are made of mafic scoria clasts. Note that some accretionary lapilli are broken.

4.8. Matrix

Although probably entirely composed of fine particles originally, matrix now includes secondary crystals formed during diagenesis. The matrix is ubiquitously altered, but its similar colour and texture compared to the preserved clasts strongly suggest that the original components were all volcanic, and had the same bulk composition (Figs 3.13, 3.14). The grain size is dependant on the preservation state of the rock, and is commonly <2 mm.

5. FACIES IN THE OHANAPECOSH FORMATION

The Ohanapecosh Formation consists of eight very thickly to extremely thickly bedded (>1 m thick in general), and eight very thinly to thickly bedded (<1 m thick) volcaniclastic facies, and three coherent facies. In addition to bed thickness, facies have been distinguished by depositional structures (grading, lamination), clast type, clast proportion and mineralogy (Tables 3.1, 3.2). The descriptions of the best preserved examples include bed thickness, grading, clast colour, clast shape, clast types and their approximate volume, average and maximum grain size and volumetric proportion of matrix. With the exception of some poorly preserved beds, all the beds included in the stratigraphic sections belong to a described facies. Miocene intrusions are described, but not shown on the stratigraphic logs for simplicity; covered stratigraphy is also indicated.

	Name	Major components	Minor components	Thickness	Sedimentary textures	Location (Member)	Initiation and sedimentary processes
1	Normally graded fiamme-andesite breccia	Fiamme/pumice clast, feldspar crystal fragment, andesite clast, matrix	-	>20 m	Tabular, normally graded, basal andesite breccia Basal dense clast-supported breccia	Cayuse Pass, Chinook Pass, Cougar Lake (Chinook Pass)	Subaqueous volcaniclastic density current Derived from subaerial pyroclastic flow
2	Fiamme-andesite breccia	Fiamme/pumice clast, feldspar crystal fragment, andesite clast, matrix	-	>20 m	Tabular, normally graded, basal andesite breccia Basal dense clast-supported breccia	Cayuse Pass (Chinook Pass)	Subaqueous volcaniclastic density current Derived from subaerial pyroclastic flow
3	Normally graded fiamme breccia	Fiamme/pumice clast, feldspar crystal fragment, matrix	Dense clast	20 m	Tabular, normally graded Basal dense clast-supported breccia	Chinook Pass, Cougar Lake, ?Backbone Ridge (Chinook Pass and ?White Pass)	Subaqueous volcaniclastic density current Derived from subaerial pyroclastic flow
4	Reversely graded fiamme breccia	Fiamme/pumice clast, feldspar crystal fragment, matrix	Dense clast	40-50 m	Tabular, reversely graded	Chinook Pass, Backbone Ridge (Chinook Pass and White Pass)	Subaqueous volcaniclastic density current Derived from subaerial pyroclastic flow
5	Graded or massive volcanic breccia	Fiamme/pumice clast, dense clast, matrix	Feldspar crystal fragment	0.5–15 m	Tabular, normally graded, massive or reversely graded	Cayuse Pass, Chinook Pass, Cougar Lake, White Pass, Ohanapecosh Campground, Backbone Ridge, south Packwood (Chinook Pass, White Pass and Johnson Creek)	Subaqueous volcaniclastic density current Derived from subaqueous remobilisation, subaerial pyroclastic flow or subaqueous explosive eruption
6	Coarse volcanic breccia	Fiamme/pumice clast, dense clast, matrix	Feldspar crystal fragment	1–20 m	Tabular, normally graded	White Pass, Ohanapecosh Campground, Backbone Ridge (White Pass)	Subaqueous volcaniclastic density current Derived from subaqueous remobilisation, subaerial pyroclastic flow or subaqueous explosive eruption
7	Clast-supported polymictic breccia-conglomerate	Dense clast	Matrix	3 m	Normally graded	Chinook Pass (Chinook Pass)	Subaqueous volcaniclastic density current Remobilisation from upper wave-base source
8	Fine sandstone and mudstone	Matrix	Fiamme, dense clasts, feldspar crystal fragment, wood fragment, accretionary lapilli	<1 mm–2 m	Tabular, massive or normally graded or laminated, planar or cross-bedded	Cayuse Pass, Chinook Pass, Cougar Lake, White Pass, Ohanapecosh Campground, Backbone Ridge, south Packwood (Chinook, White Pass and Johnson Creek)	Turbidity current, suspension settling or background sedimentation Derived from subaerial fallout, remobilisation or non-volcanogenic processes
9	Fine mafic sandstone	Vesicular basaltic clast	zeolitic cement	0.1–2 m	Tabular, massive or normally graded	White Pass (White Pass)	Subaqueous volcaniclastic density current, or suspension settling Derived from subaerial plume fallout or subaqueous remobilisation
10	Mafic volcanic breccia	Vesicular basaltic clast	accretionary lapilli, zeolitic cement	3 cm–1 m	Tabular, normally graded	White Pass, Ohanapecosh Campground, Backbone Ridge (White Pass)	Grain flow or subaqueous suspension Derived from eruption-fed fallout or from remobilisation
11	Normally graded andesite breccia to fiamme breccia	Fiamme, dense clast, feldspar crystal fragment, matrix	-	60 cm	Tabular, normally graded, basal dense clast breccia	Chinook Pass, Cougar Lake (Chinook Pass)	Subaqueous volcaniclastic density current or rock fall Probably derived from remobilisation
12	Reversely to normally graded pumice breccia	Pumice clasts, mudstone matrix	Fiamme, accretionary lapilli, wood fragment	1–1.5 m	Tabular, reversely to normally graded, numerous mudstone interbeds Basal dense clast-supported breccia	Chinook Pass (Chinook Pass)	Suspension settling Derived from abrasion and progressive waterlogging of pumice clasts in rafts, derived from subaerial fallout or dilute pyroclastic flow over water
13	Crystal-rich sandstone	Feldspar crystal fragment, matrix	Dense clast, fiamme, wood, accretionary lapilli	<1m	Tabular, massive or normally graded	Chinook Pass, Cayuse Pass, Ohanapecosh Campground, Backbone Ridge, south Packwood (Chinook Pass, White Pass and Johnson Creek)	Subaqueous volcaniclastic density current or turbidity current Derived from eruption-fed or remobilisation processes
14	Poorly porphyritic andesite breccia	Dense andesite clast	Fiamme, matrix	0.1–2 m	Tabular, normally graded	Chinook Pass, Cougar Lake, Backbone Ridge, south Packwood (Chinook Pass, White Pass and Johnson Creek)	Subaqueous volcaniclastic density current, or suspension settling Derived from remobilisation of parts of dome or lava
15	Fiamme sandstone and fiamme mudstone	Fiamme/pumice clast, matrix	Accretionary lapilli, dense clast, wood fragment	0.1–2 m	Tabular, normally or reversely graded, rare cross-beds	Cougar Lake, Ohanapecosh Campground, Backbone Ridge, south Packwood (Chinook Pass, White Pass and Johnson Creek)	Subaqueous turbidity current or subaqueous volcaniclastic density current Derived from eruption-fed or remobilisation processes

Table 3.1 Volcaniclastic facies in the Ohanapecosh Formation, description and interpretation.

	Name	Thickness	Textures	Location (Member)	Emplacement processes
16	Vesicular basalt	0.3–3 m	Coherent, possible local peperitic margins	Chinook Pass, White Pass (Chinook Pass, White Pass and Johnson Creek)	Intrusive, syn-sedimentary (White Pass) and/or post-sedimentary with the Ohanapecosh Formation
17	Flow-banded dacite	?30 m	Coherent, flow banded	Cougar lake (Chinook Pass)	Intrusive, possibly syn-sedimentary with the Ohanapecosh Formation
18	Miocene intrusions (silicic)	0.5 m to >50m	Coherent	All localities (Chinook Pass, White Pass and Johnson Creek)	Intrusive dyke or sill, Miocene age

Table 3.2 Intrusive facies in the Ohanapecosh Formation, description and interpretation.

The abundance of pumice and dense clasts versus matrix was documented by image analysis and functional stereology (chapter 2) in various bed of the Chinook Pass Member. These data quantify the volume and grain size distribution of pumice and dense clasts and are used as complement to the facies analysis description.

5.1. Very thick to extremely thick beds (1–50 m)

Facies 1 - Normally graded fiamme-andesite breccia

Unit 40 at Cayuse Pass (Chinook Pass Member) consists of a >20-m-thick, tabular bed laterally continuous over >400 m (Fig. 3.15). It overlies a sequence of very thin to thick beds with a sharp contact (Fig. 3.4) and is made of three massive, gradational sub-facies. The basal sub-facies consists of 3 m of clast-supported, normally graded polymictic breccia, mostly composed of a variety of coarse dense angular to sub-rounded volcanic clasts (50 vol.%; some with all edges modified), dominated by dark aphyric dense clasts (Fig. 3.16a). The size of the dense clasts gradually decreases upward from 60–80 mm to 6–10 mm, and rare sub-rounded outsized clasts occur (up to 1 m). The other components are abundant free broken feldspar crystals (Fig. 3.16b; >10 vol.% of the rock), black moderately porphyritic fiamme and pumice clasts (Fig. 3.16a; 6–10 mm, 15 vol.%; 15–20 vol.% feldspar phenocrysts) and matrix (<20 vol.%). The middle sub-facies (10 m thick) is matrix-supported, normally graded breccia. The volume of dense clasts decreases to 10–15 vol.%, whereas fiamme become abundant (>15 vol.%); they have an average size of 10-20 mm and are rarely up to 400x150 mm (Figs 3.16c, 3.16d). The content of free broken crystals in the matrix remains high (Fig. 3.16d; >10 vol.%). The upper sub-facies is also normally graded, matrix-supported breccia but finer grained (average diameter 6–2 mm, max 20 mm) and occupies the upper third (6–7 m) of the unit. Fiamme are minor (< 5 vol.%) and the matrix is up to 90 vol.% and includes 20 vol.% of free broken feldspar crystals (Figs 3.16e, 3.16f). The hydraulic sorting ratio (comparing both the size and density between pumice and dense clasts; chapter 5) is lower than 1 (Fig. 3.15g), indicating that dense clasts are too coarse to be in hydraulic equivalence with the pumice clasts.

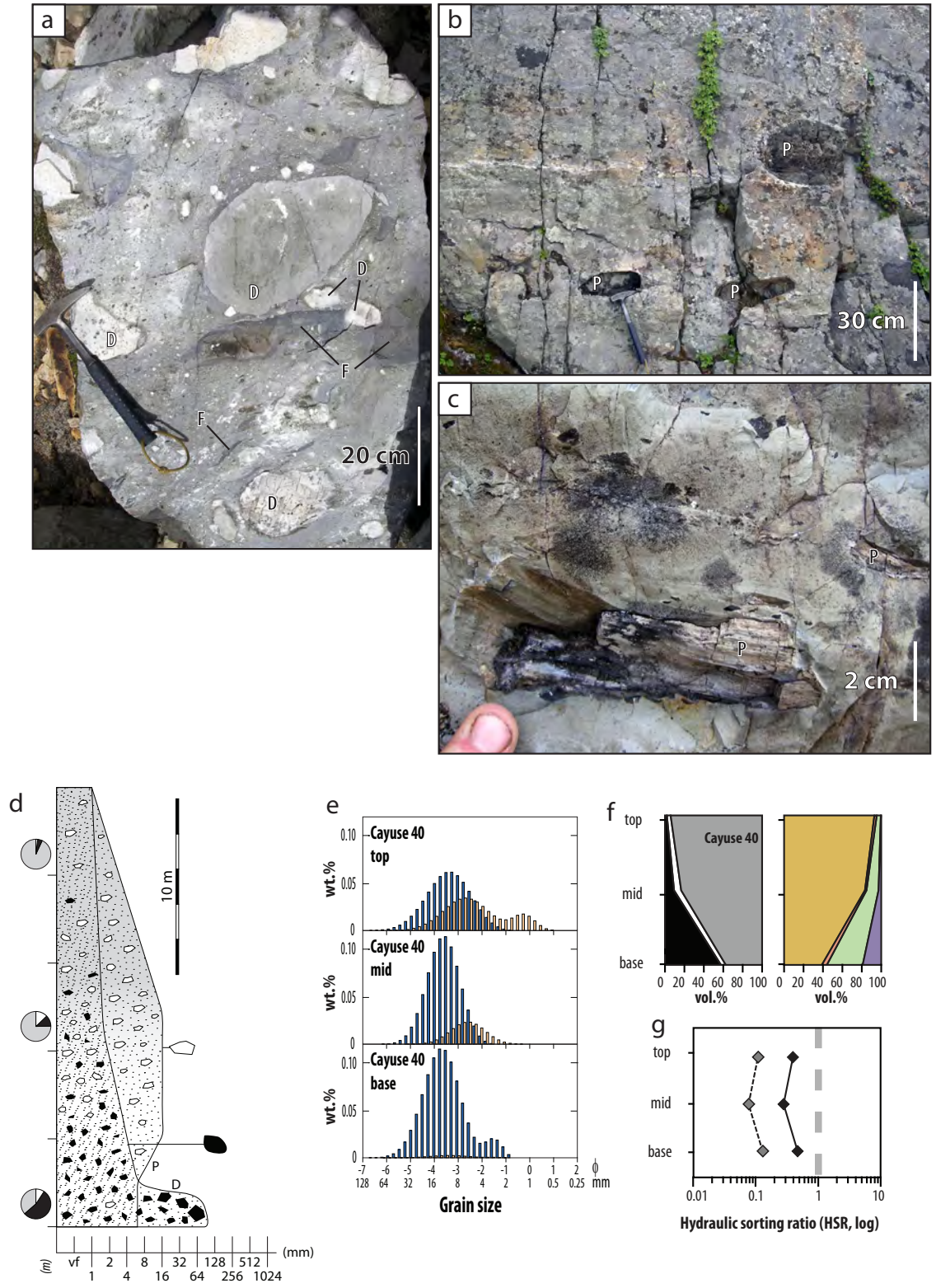

Fig. 3.15 Facies 1 - Normally graded fiamme-andesite breccia. **a,** Base of unit 7 of section B at Cougar Lake in the Chinook Pass Member; coarse, sub-angular dense clasts (white and pale grey) and coarse fiamme (black) in a grey matrix of similar clasts and broken feldspar crystals. Fiamme are parallel to bedding; **b)** Exceptionally coarse tube pumice clasts in middle of facies 1 (unit 1 of section A) at Cougar Lake in the Chinook Pass Member; **c)** Tube pumice clast in facies 1 (unit 1 of section A) at Cougar Lake in the Chinook Pass Member; **d)** Typical stratigraphic log of facies 1 in unit 40 at Cayuse Pass section; **e)** Grain size distribution (chapter 2) of the three sub-facies in unit 40 at Cayuse Pass section. Pumice clast distribution is bimodal at base and top of the facies, whereas dense clasts are bimodal at base only. Both pumice and dense clasts show normal grading; **f)** Volume of clasts and matrix, and volume per size; **g)** Hydraulic sorting ratio (comparing both the size and density between pumice and dense clasts; chapter 5) is very small in facies 1. Graphic log features and key as in Figures 3.5 and 3.17; chapters 2 and 5 for techniques used for grain size distribution, volume and hydraulic sorting. Dense clast (D), fiamme (F) and pumice (P).

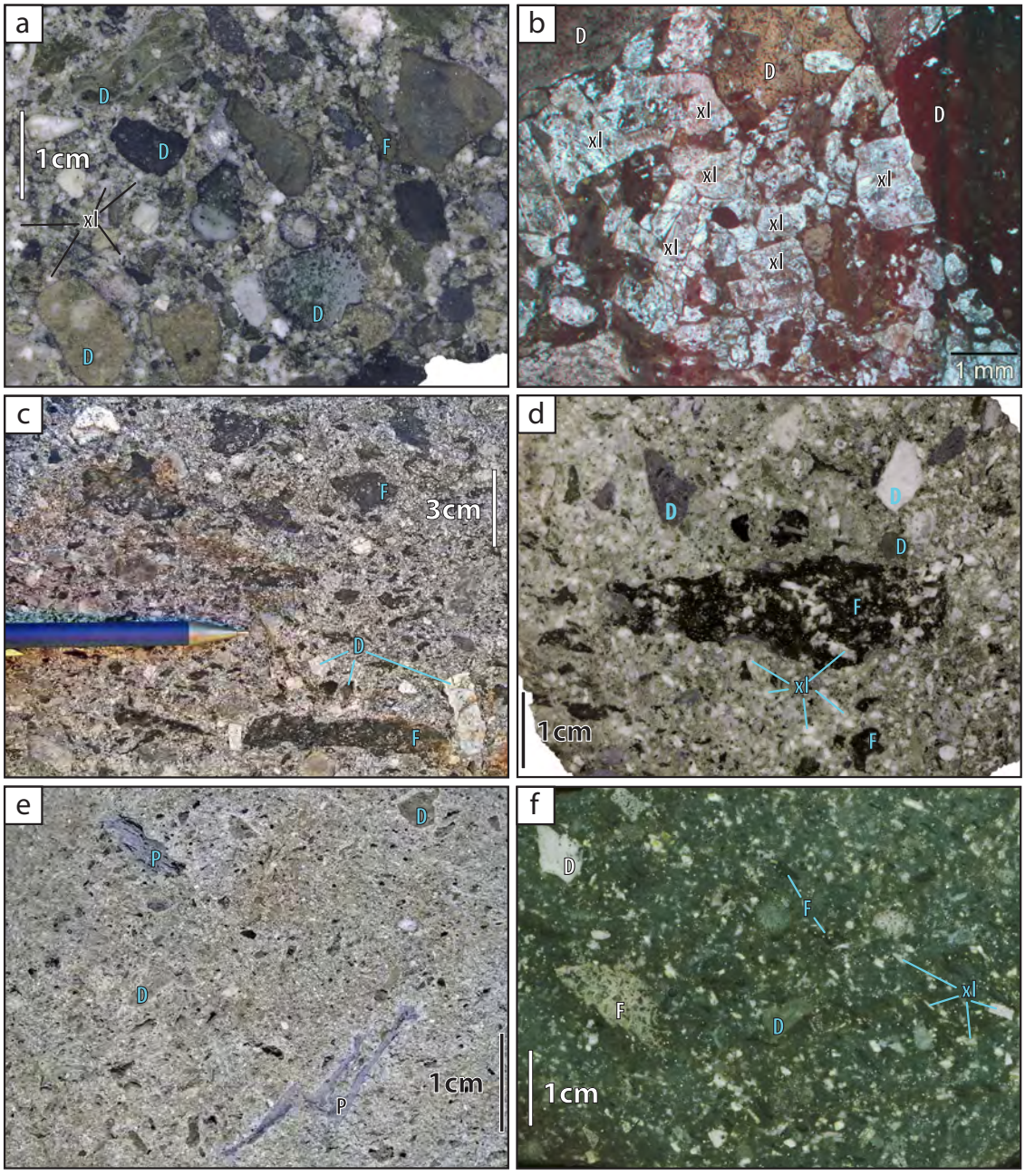

Fig. 3.16 Facies 1 - Normally graded fiamme-andesite breccia (continuing). **a)** Basal facies 1 (unit 40, sample WA-23b) composed of dense clasts (green, white, black) and rare fiamme (yellow-green) and free broken feldspar crystals (white) in a green matrix; **b)** Basal facies of normally graded fiamme-andesite breccia (unit 40, facies 1, sample WA-23b) at Cayuse Pass. Broken feldspar crystals make up most of the matrix of the coarse dense-clast-supported facies; **c)** Middle facies 1 (unit 40) with fiamme (black) and dense clasts (white and grey) in a grey matrix; **d)** Middle facies 1 (unit 40) with porphyritic fiamme (black) and dense clasts (white, green, purple) and free broken feldspar crystals (white) in a pale green matrix (unit 40, sample WA-22); **e)** Upper facies 1 (unit 40), elongate tube pumice clasts and minor dense clasts in a pale-green matrix; **f)** Upper facies 1 (unit 40, sample WA-21) with pumice clasts (black and pale green), and free broken feldspar crystals (white) in a green matrix. Dense clast (D), fiamme (F) and feldspar crystal (xl).

Unit 40 in the Cayuse Pass section show a massive facies that contain a bimodal grain size distribution (Figs 3.15d, 3.15e). The clast-supported basal sub-facies of unit 40 is the coarsest clastic facies (~50 vol.% clasts coarser than 4 mm) found in the Ohanapecosh Formation. The middle and upper parts are matrix-supported (Fig. 3.15d) and weakly normally graded in pumice clasts.

Unit 64 at Chinook Pass (Chinook Pass Member) is composed of similar facies, but less rich in pumice clasts and fiamme, and exposed in 15-m-high cliff (Fig. 3.5) that overlies a thick (~1 m) bed of normally graded andesite breccia to fiamme breccia (facies 11). It also grades from being clast-supported to matrix-supported up section.

Three 20-m-thick units at Cougar Lake (Chinook Pass Member) are composed of very coarse basal breccia, made of 60–80 vol.% angular, black or white to grey dense clasts (average diameter 20 cm, max >70 cm), in a matrix of finer, angular dense clasts, poorly feldspar-phyric dark fiamme (<10 mm, max 250 mm), free broken feldspar crystals (1–2 mm) and mudstone clasts (Figs 3.6, 3.15). Pumice clasts have well-preserved tube vesicles. Grain size diminishes drastically in the upper half of the units and the units grade from clast-supported to matrix-supported up section; fiamme are more abundant and reversely to normally graded in size (<30 cm long). Dense clasts are normally graded in the top half of the deposit. Coarse tube pumice clasts (max 30 cm) occur in the upper sub-facies at Cougar Lake (unit 1 of section A; Figs 3.15b, 3.15c). Several m-long altered, tabular clasts (possibly stratified mudstone or coarse fiamme) are present at the top of unit 7 in section B. Poorly exposed, laminated or cross-laminated mudstone (>10 m thick) above may be part of the unit.

Facies 2 - Fiamme-andesite breccia

Fiamme-andesite breccia is very similar to the normally graded fiamme-andesite breccia (facies 1) at Cayuse Pass, but has a higher content of fiamme and pumice clasts, less matrix in the middle and top (Fig. 3.17b), and different types of dense clasts. Fiamme-andesite breccia is exposed in the Cayuse Pass section (ChinookPass Member; Fig. 3.4). It is >20 m thick, tabular and laterally continuous over >400 m, and divided into two gradational sub-facies. Unit 42 at Cayuse Pass directly overlies a 1-m–thick interval of laminated crystal-rich sandstone (facies 13) with a sharp boundary. The lower sub-facies is <10 m thick, and consists of clast-supported coarse breccia chiefly composed of angular to sub-rounded dense volcanic clasts, of which a green aphyric type is dominant. The dense clasts are normally graded from 80 to 10 mm in average size and account for 40–60 vol.%. Outsized clasts (up to 1 m) are sub-rounded, some with all edges modified (Fig. 3.17a). Fiamme (up to 15 mm) are relatively abundant (15–20 vol.%). The matrix includes free broken feldspar crystals and dense clasts. The upper sub-facies is matrix-rich (80 vol.%). Angular pumice clasts (8–10 mm) make 15 vol.% of the rock; minor outsized dense clasts (up to 25 mm), small fiamme (<5 vol.%; <4 mm) and minor dense clasts (<5 vol.%) are also

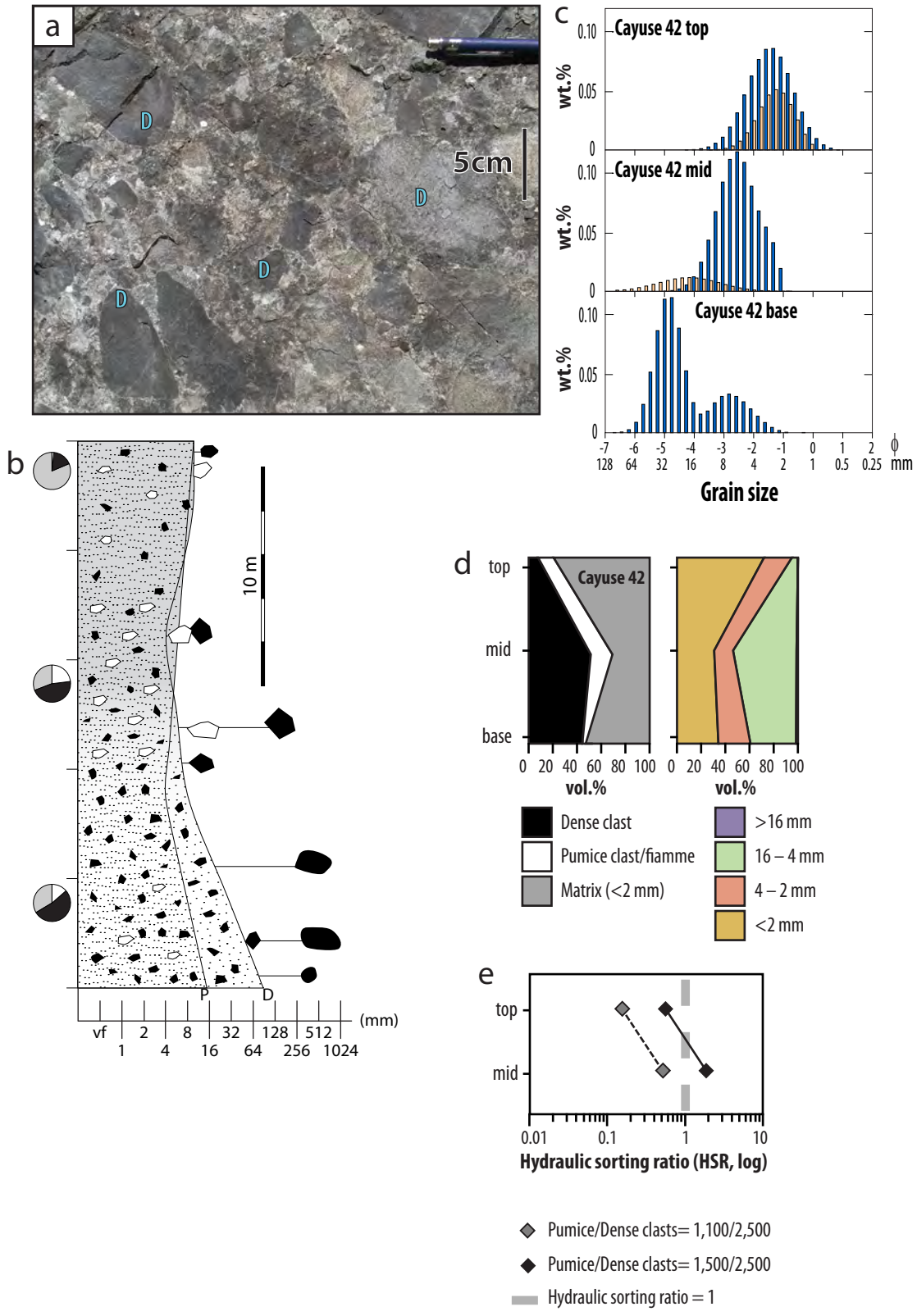

Fig. 3.17 Facies 2 - Fiamme-andesite breccia. **a)** Base of fiamme-andesite breccia (facies 2, unit 42, sample WA-36) with sub-rounded dark grey and brown dense clasts in a grey matrix. This basal facies is very similar to the basal normally graded fiamme-andesite breccia (facies 1); **b)** Typical stratigraphic log of facies 2, unit 42 at Cayuse Pass section; **c)** Grain size distribution (chapter 2) of the three sub-facies in unit 42 at Cayuse Pass. Pumice clasts are absent from basal facies, whereas dense clasts have a nicely developed bimodal distribution. Span in pumice clasts size diminishes from middle to top of facies. Both pumice and dense clasts show normal grading; **d)** Volume of clasts and matrix, and volume per size; **e)** Hydraulic sorting ratio (comparing both the size and density between pumice and dense clasts; chapter 5) is decreasing upwards. Graphic log features and key as in Figures 3.5 and 3.17; chapters 2 and 5 for techniques used for grain size distribution, volume and hydraulic sorting. Dense clast (D).

present. In the top of the unit, the matrix is red-oxidised to dark brown due to a nearby Tatoosh sill.

The lower sub-facies of unit 42 at Cayuse Pass (Figs 3.17b, 3.17c) is clast-supported, contains more than 30 vol.% of clasts coarser than 4 mm and has a bimodal clast size distribution. The facies 2 show normal grading of pumice and dense clasts; the upper part is monomodal and matrix-supported. The hydraulic sorting ratio of facies 2 is similar to 1 in the lower sub-facies, and decreases upwards the stratigraphy (Fig. 3.17e). This indicates a good hydraulic equivalence between pumice and dense clasts in the

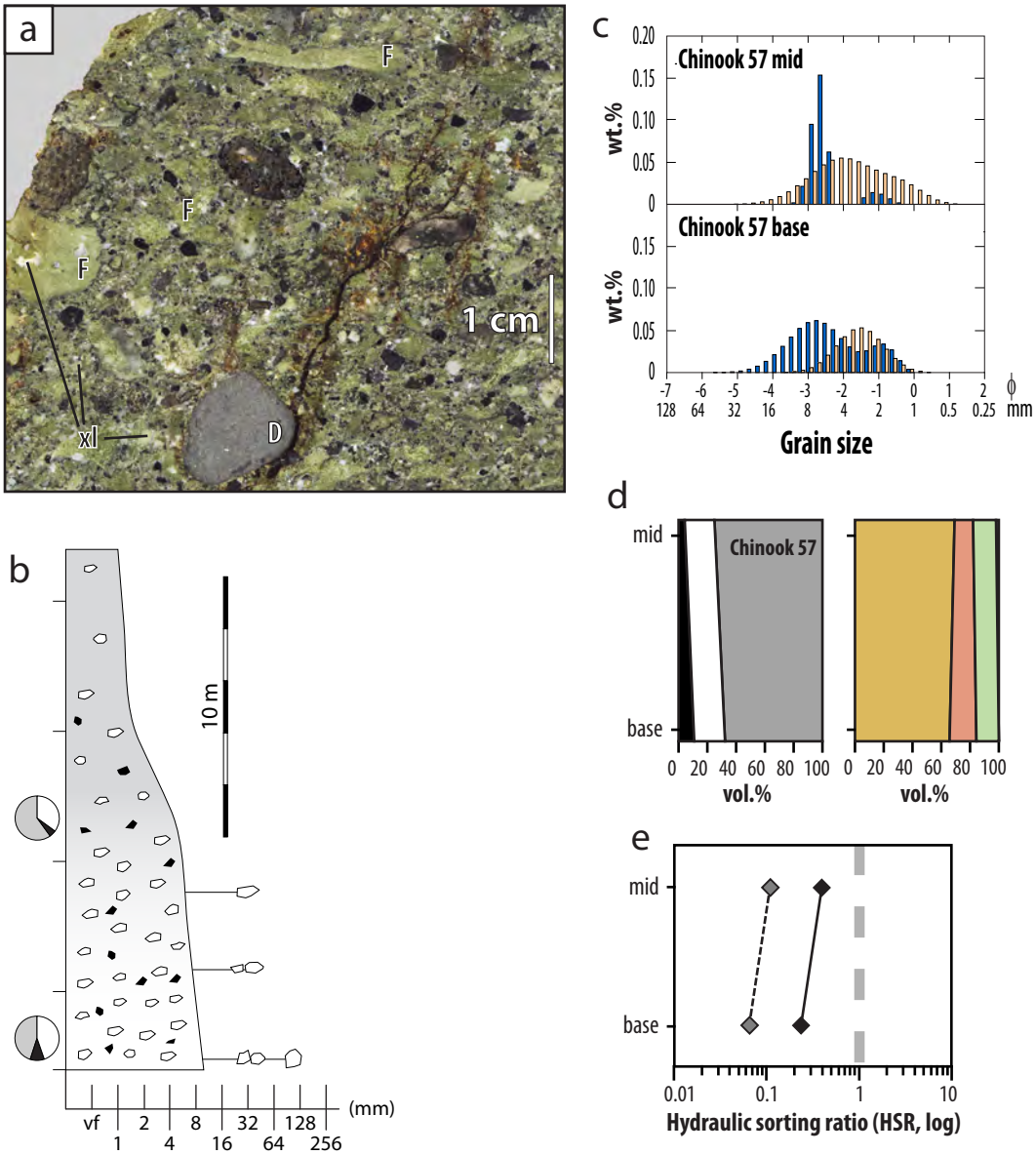

Fig. 3.18 Facies 3 - Normally graded fiamme breccia. **a)** Base of unit 57 (facies 3) at Chinook Pass in the Chinook Pass Member. Abundant fiamme (pale green), minor dense clasts (grey and black) in matrix; **b)** Typical stratigraphic log of facies 3, unit 57 at Chinook Pass; **c)** Grain size distribution (chapter 2) of the basal and middle sub-facies of unit 57 at Chinook Pass. Dense clasts have bimodal distribution, whereas pumice clasts are monomodal. Scattered aspect of the dense clasts distribution is probably due to a too low concentration of dense clasts in the sample; **d)** Volume of clasts and matrix, and volume per size; **e)** Hydraulic sorting ratio (comparing both the size and density between pumice and dense clasts; chapter 5) slightly increases upwards. Graphic log features and key as in Figures 3.5 and 3.17; chapters 2 and 5 for techniques used for grain size distribution, volume and hydraulic sorting. Dense clast (D), fiamme (F) and feldspar crystal (xl).

basal sub-facies, whereas the pumice clasts are too small compared to the dense clasts in the upper sub-facies.

Facies 3 - Normally graded fiamme breccia

The normally graded fiamme breccia facies at Chinook Pass (unit 57; Fig. 3.5) and Cougar Lake (unit 10 of section B; Fig. 3.6) in the Chinook Pass Member occurs in poorly preserved, tabular, 20-m-thick beds and comprises three gradational sub-facies (Fig. 3.18) of similar thickness. The lowest sub-facies is clast-supported and rich in pale-to-dark green fiamme and pumice clasts (>40 vol.%, 10 mm average, max 30 mm), feldspar crystals fragments (5–10 vol.%) and minor sub-rounded dense clasts (<5 vol.%, up to 15 mm). In the middle sub-facies, the fiamme and pumice clast sizes decrease (30 vol.%, 2-3 mm average). The size of dense clasts decreases and their abundance remains similar. The upper sub-facies mostly consists of matrix with a few fiamme and pumice clasts.

The basal and middle sub-facies of unit 57 at Chinook Pass show a weak normal grading and are matrix-supported (Fig. 3.18c). The hydraulic sorting ratio of facies 3 is lower than 1, indicating that dense clasts are too coarse to be in hydraulic equivalence with the pumice clasts (Fig. 3.18e).

Facies 4 - Reversely graded fiamme breccia

This facies occurs at Chinook Pass (units 59 and 61, Chinook Pass Member; Fig. 3.5), in tabular, 40-50-m-thick beds composed of two gradational, matrix-supported sub-facies (Figs 3.19, 3.20). A bed at top of Backbone Ridge (White Pass Member; Fig. 3.9) is tentatively included in this facies. The base (~40 m thick) contains pale-to-dark green fiamme and pumice clasts (40 vol.%, 2–5 mm), free broken feldspar crystals (>10 vol.%), dense clasts (<5 vol.%) and matrix (Fig. 3.19c). The fiamme and pumice clast sizes increase to 10 mm upwards (Fig. 3.19d) and free broken feldspar crystals become more abundant (>15 vol.%). The upper 10 m shows a drastic increase in fiamme and pumice clast sizes (Fig. 3.19e; average 30-40 mm, max 150 mm). Less than 5 vol.% of dense clasts is found throughout the whole bed. The middle part of unit 61 at Chinook Pass is cut by a subhorizontal, 1.5-m-thick Tatoosh sill, whereas the upper part is cut by a very thick (>10 m) Tatoosh sill (Fig. 3.19a).

Unit 61 at Chinook Pass is entirely matrix supported and normally then reversely graded in pumice and dense clasts (Fig. 3.20). Pumice clasts have a bimodal size distribution, whereas dense clasts show a monomodal size distribution (Fig. 3.20b). The hydraulic sorting ratio gradually increases upwards the stratigraphy, from <1 to 1 (Fig. 3.20d). This indicates an increase in hydraulic sorting upwards stratigraphy, and that pumice and dense clasts are at hydraulic equivalence at the top of the unit, whereas dense clasts are relatively too coarse at the base.

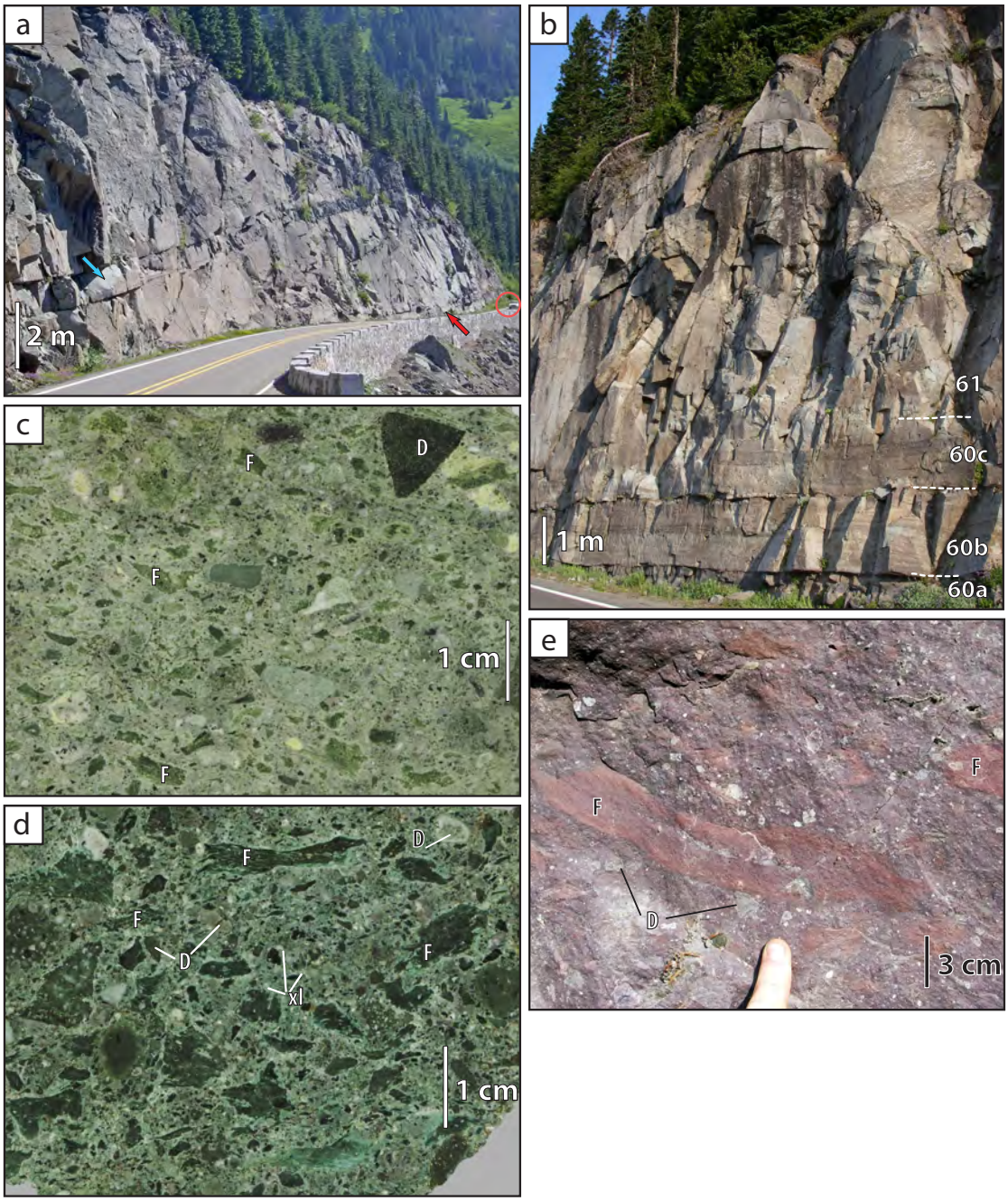

Fig. 3.19 Facies 4 - Reversely graded fiamme breccia, Chinook Pass Member. **a)** Main section at Chinook Pass. Unit 61 (facies 4) is cut by Miocene Tatoosh sill (blue arrow for Miocene intrusions; facies 19). Red arrow points to base of unit 60 and corresponds to viewing position in Figure 3.19b; top of unit 61 is not seen. The red circle shows car for scale; **b)** Units 60a, 60b, 60c (reversely to normally graded pumice breccia, facies 12) and 61 (facies 4) at Chinook Pass; top of unit 61 is not seen. Note the lateral continuity of the thin beds of facies 12 and the knife sharp-contacts; **c)** Middle of unit 61 (facies 4; sample WA-68), with numerous fiamme (dark green) and rare dense clasts (white and dark green) in a pale green matrix; **d)** Middle of unit 61 (facies 4; sample WA-69), with numerous fiamme and pumice clasts (dark green) and rare dense clasts (white and pale green) and free broken feldspar crystals (white) in a green matrix; **e)** Top of unit 61 (facies 4), reddened adjacent to Miocene Tatoosh sill. Large fiamme (red), dense clasts (pale green) in red-purple matrix. Dense clast (D), fiamme (F), and feldspar crystal (xl).

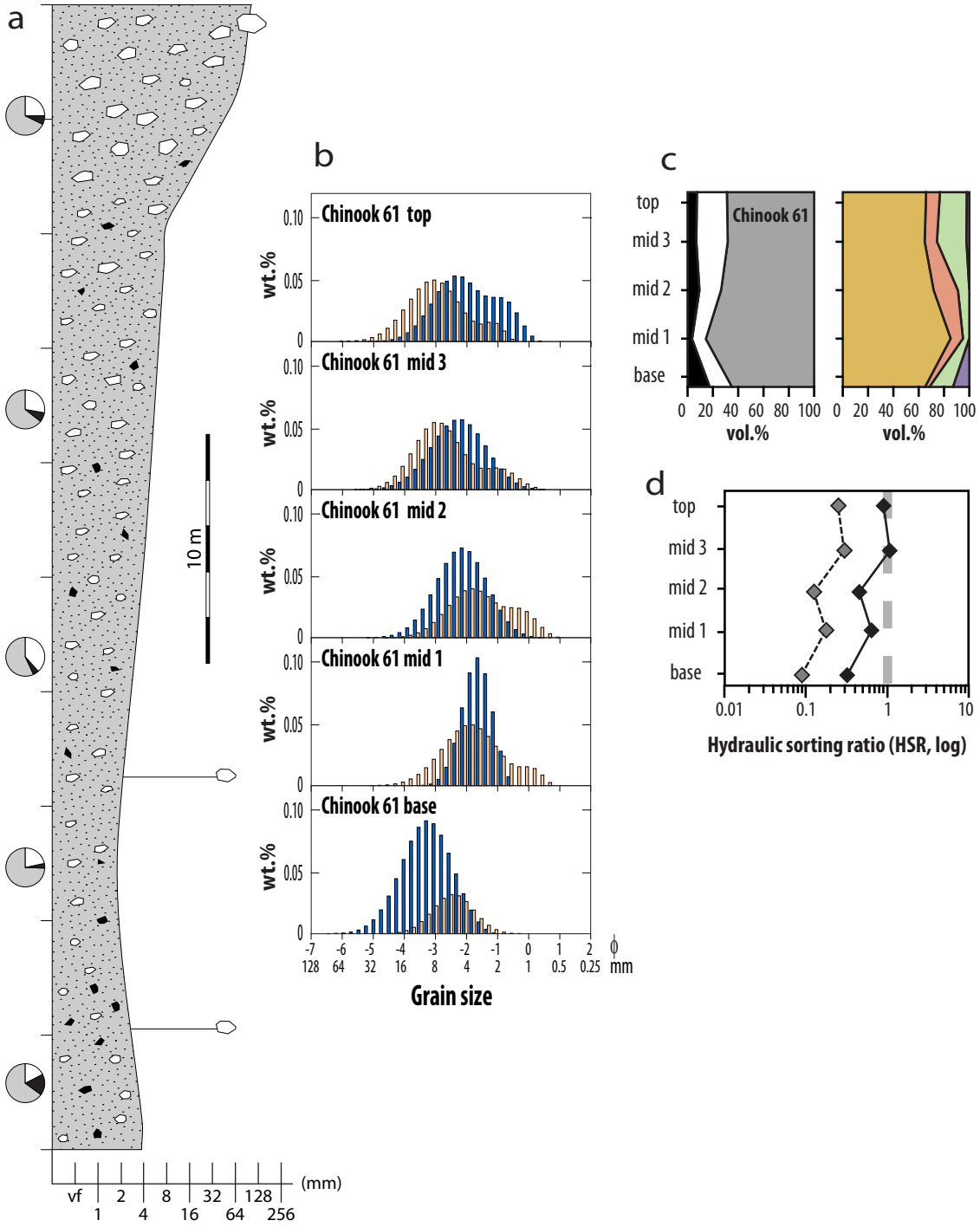

Fig. 3.20 Facies 4 - Reversely graded fiamme breccia, Chinook Pass Member (continuing). **a)** Typical stratigraphic log of the facies, unit 61 at Chinook Pass; **b)** Grain size distribution (chapter 2) of five levels in unit 61 at Chinook Pass. Pumice clasts have mostly a bimodal distribution, in contrast to mostly monomodal distribution of dense clasts. Normal to reverse grading is nicely developed in both pumice and dense clasts distributions; **c)** Volume of clasts and matrix, and volume per size; **d)** Hydraulic sorting ratio (comparing both the size and density between pumice and dense clasts; chapter 5) is small at the base of facies 3 and grades to 1 at top. Graphic log features and key as in Figures 3.5 and 3.17; chapters 2 and 5 for techniques used for grain size distribution, volume and hydraulic sorting.

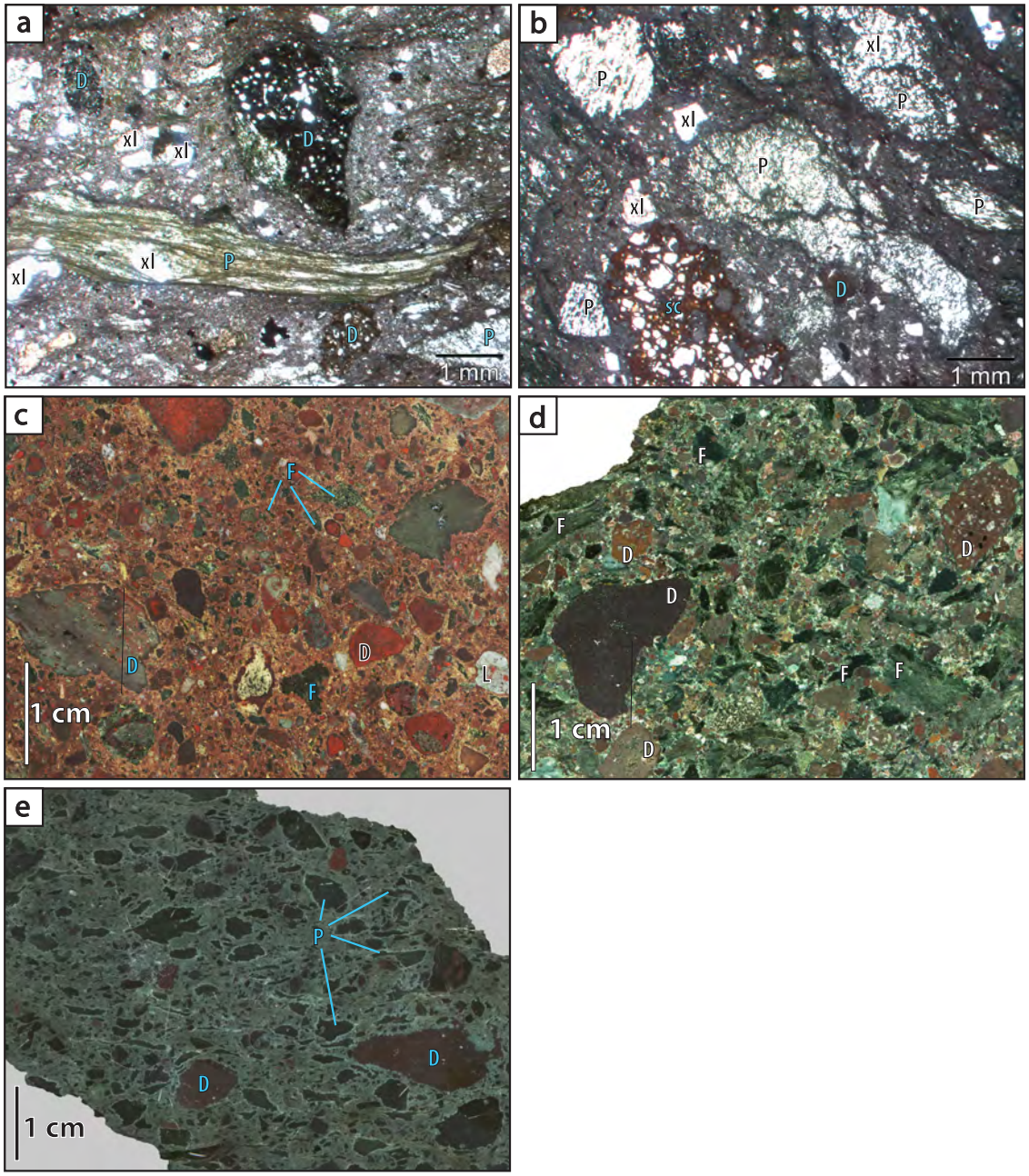

Fig. 3.21 Facies 5 - Graded or massive volcanic breccia; **a)** Tube pumice clasts and dense clasts in a fine (<0.2 mm) matrix in facies 5 in the White Pass section (unit 5, sample WA-98); **b)** Same thin section as a, but transverse orientation to the view in A. Sc, (lower left) mafic scoria clast, sample WA-98; **c)** Facies 5 at Backbone Ridge, strongly red-altered by a Miocene Tatoosh intrusion. Pumice clasts and fiamme are dark green, dense clasts are grey and red, sample WA-60; **d)** Facies 5 at Indian Bar, pumice clasts and fiamme (dark green) and dense clasts (red, purple, orange) and feldspar crystals (white), sample WA-97; **e)** Facies 5 at the base of the Ohanapecosh Formation, at White Pass (unit 5, sample WA-98), dark green fiamme and pumice clasts and red dense clasts in a pale green matrix. Dense clast (D), pumice (P), fiamme (F) and feldspar crystal (xl).

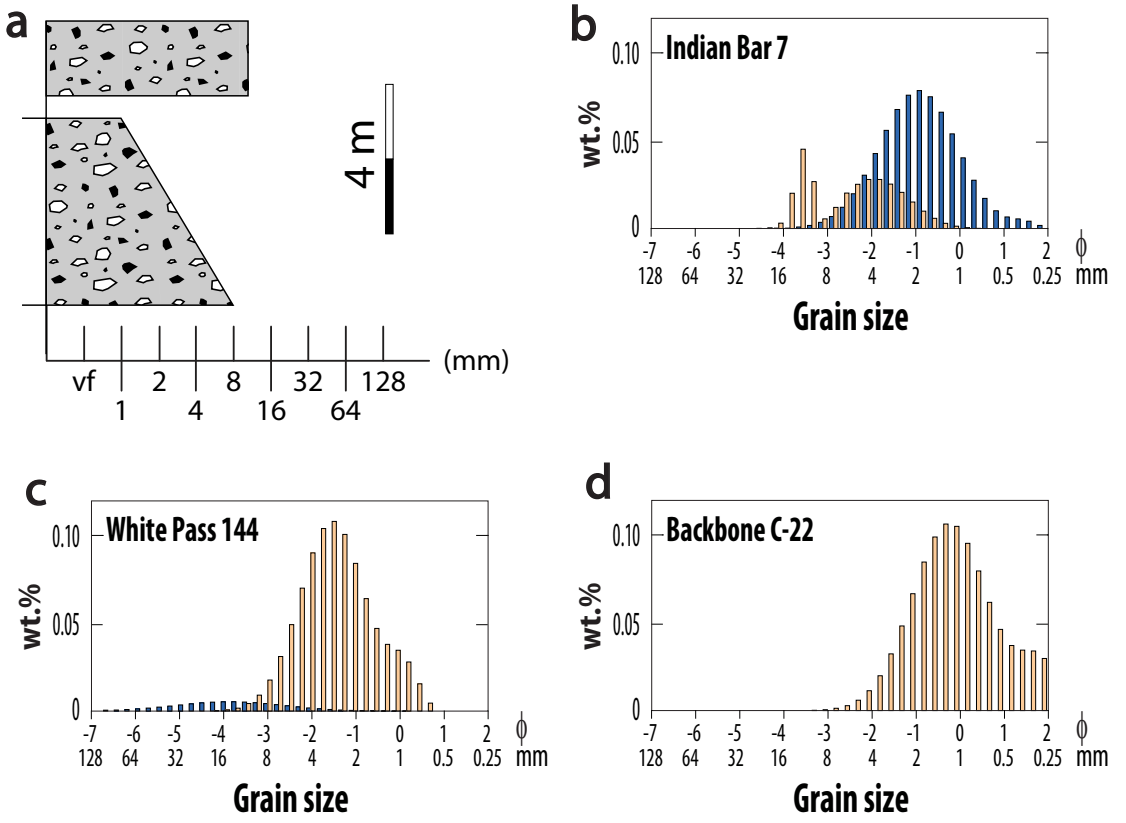

Fig. 3.22 Facies 5 - Graded or massive volcanic breccia (continuing); **a)** Typical stratigraphic log of two beds of facies 5 in the White Pass section (Fig. 3.7); **b)–d)** Three examples of grain size distribution (chapter 2) of facies 5 at various localities in the White Pass member (Figs 3.7, 9). The three samples are distinct in their pumice and dense clasts distributions and span in grain size; d is free of dense clasts. Graphic log features and key as in Figure 3.5.

Facies 5 - Graded or massive volcanic breccia

Beds composed of the normally graded or massive volcanic breccia facies are common at White Pass, Ohanapecosh Campground, Backbone Ridge (White Pass Member; Figs 3.7–3.9), and southern Packwood (Johnson Creek Member; Fig. 3.10) and minor in the lower section of Chinook Pass (Chinook Pass Member; Fig. 3.5). This facies mostly occurs in very thick beds (Fig. 3.21) that are clast-supported or matrix-supported. The beds are rarely thicker than 5 m, but can reach 15 m (southern Packwood). The average grain size decreases from 10 to 4 mm upwards or shows no change (10 mm). The components are green to dark grey fiamme and pumice clasts (30–60 vol.%; Figs 3.22a, 3.22b, 3.22e), very angular dense clasts (10–30 vol.%; Figs 3.21, 3.22c, 3.22d, 3.22e), free broken feldspar crystals (Figs 3.22a, 3.22b) and matrix (20–60 vol.%). The dense clasts are a mixture of red- and dark-grey clasts of probable mafic and intermediate composition.

Examples of this facies that are reversely graded occur at Southern Packwood (Johnson Creek Member; Fig. 3.10) and in rare beds at the top of the Backbone Ridge section. They have the same clasts abundance characteristics as the normally graded and massive beds of this facies, but shows reverse grading. The average dense clasts increase from 2 to 12 mm, whereas fiamme and pumice clasts coarser than 6 mm are rare and can reach 16 mm. The facies is matrix-supported, and the abundance of dense clasts ranges from

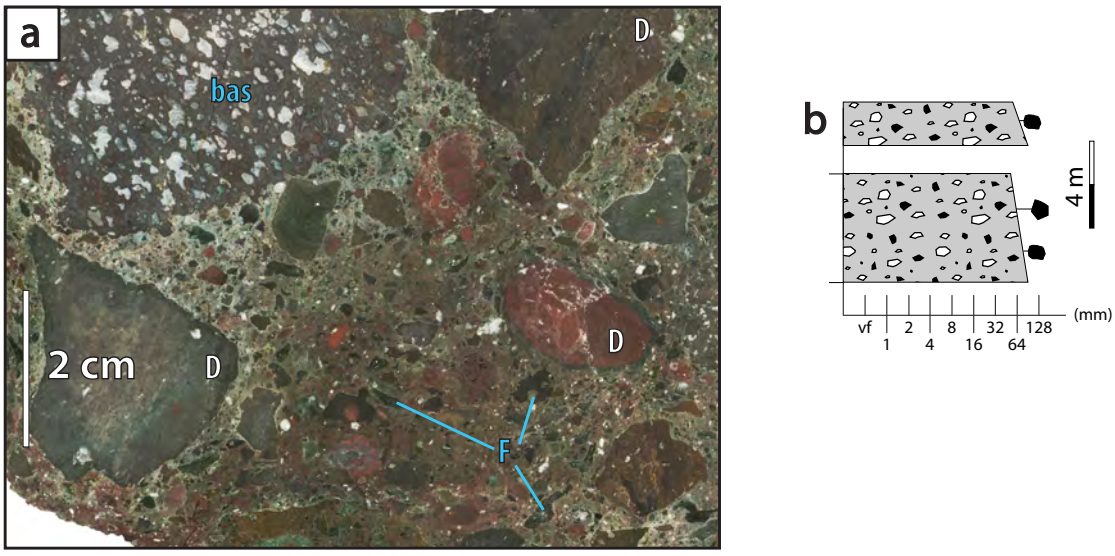

Fig. 3.23 Facies 6 - Coarse volcanic breccia; **a)** Coarse volcanic breccia (facies 7) at White Pass (unit 62), composed of fine pumice clasts and fiamme (black) and dense clasts (red, dark green, brown, vesicular basalt clast), sample WA-07; **b)** Typical stratigraphic log of facies 6. Graphic log features and key as in Figure 3.5. Dense clast (D), fiamme (F), basalt clast (bas).

<1 vol.% to 8 vol.% upwards; pumice clasts range from 5 vol.% to 15 vol.%. Free broken feldspar crystals are less than 10 vol.%.

Facies 6 - Coarse volcanic breccia

This facies occurs in very thick to extremely thick (up to 20 m) beds at White Pass, Ohanapecosh Campground and Backbone Ridge (White Pass Member; Figs 3.7–3.9) and shows slight normal grading in the size of dense clasts (60 to 40 mm; Fig. 3.23b). The clasts are angular to sub-rounded (Fig. 3.23a). Dense clasts (50–70 vol.%), pumice clasts and fiamme (10–20 vol.%), and free broken feldspar crystals together are dominant over matrix (10–25 vol.%). Fiamme are green to dark grey.

Facies 7 - Clast-supported polymictic breccia-conglomerate

This facies was found only at Chinook Pass (unit 58, White Pass Member; Fig. 3.5), and separates two extremely thick beds of normally graded fiamme breccia and reversely graded fiamme breccia (facies 3 and 4, respectively). It is poorly preserved, 3 m thick and normally graded. The major components are sub-rounded to rounded, poorly porphyritic dense clasts (40 mm average, 200 mm max; >60 vol.%); matrix comprises <30 vol.%.

5.2. Very thin to thick beds (0.001–1 m)

Facies 8 - Fine sandstone and mudstone

Laterally extensive, very thin to thick beds of fine sandstone and mudstone facies are

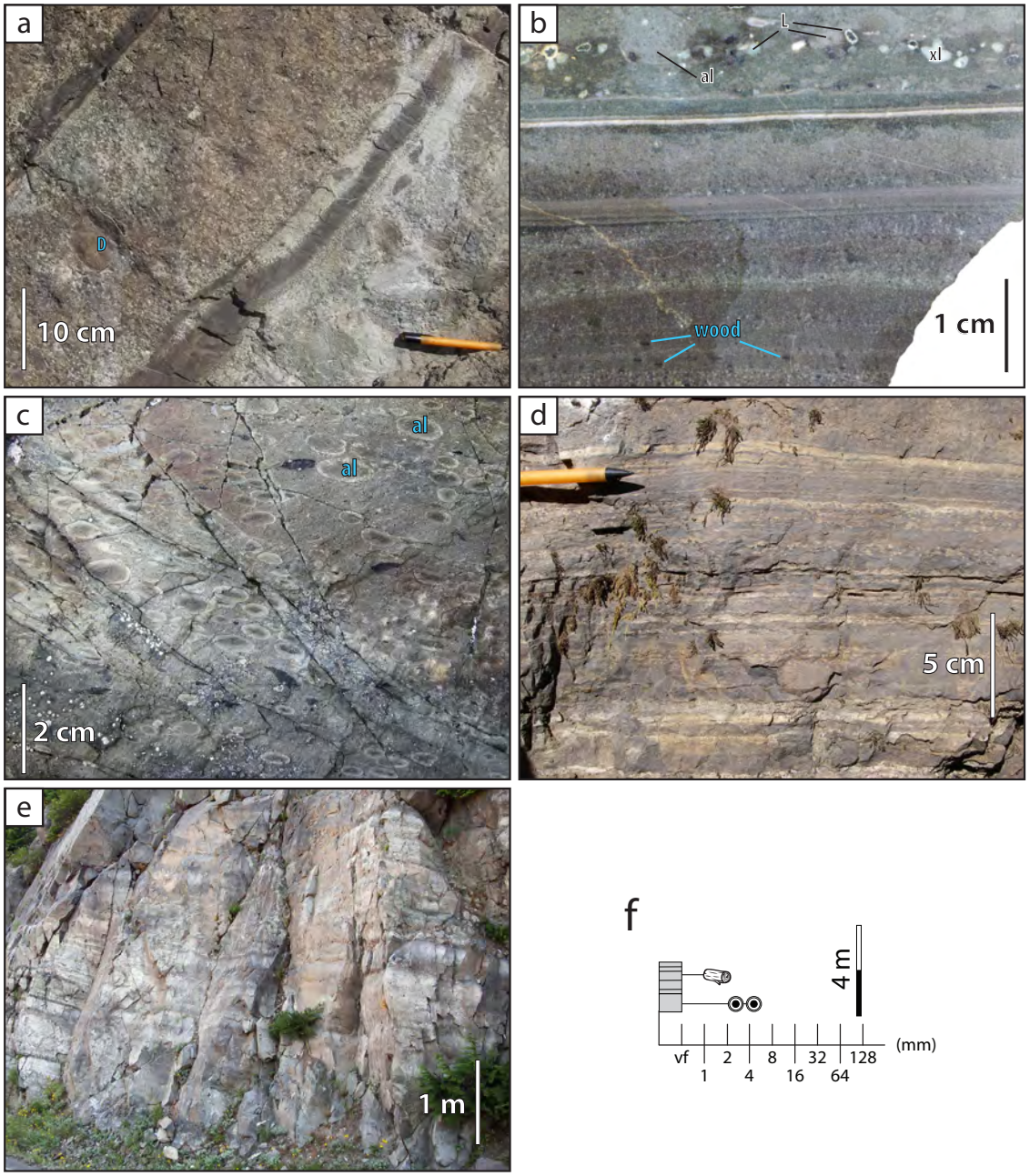

Fig. 3.24 Facies 8 - Fine sandstone and mudstone. **a)** Interbeds of facies 8 (unit 78 of White Pass) interbedded with graded or massive volcanic breccia (facies 5); **b)** Laminated sandstone and mudstone (facies 8, out of section) at Cougar Lake, sample WA-89; **c)** Accretionary lapilli sandstone, in fine sandstone and mudstone (facies 8, unit 12 of log A in the Cougar lake section). Accretionary lapilli are white-rimmed ellipsoids, oriented parallel to the beds); minor black fiamme occur; **d)** Succession of very thin beds and laminae of fine sandstone and mudstone (facies 8, unit D11) at Backbone Ridge; **e)** Succession of parallel-bedded fine sandstone and mudstone (facies 8, out of section) in lower Cayuse Pass; **f)** Typical stratigraphic log of facies 8. Graphic log features and key as in Figure 3.5. Dense clast (D), accretionary lapilli (al), feldspar crystal (xl).

present throughout the Ohanapecosh Formation (Figs 3.4–3.10). The beds commonly occur in m-thick groups separating groups of very thick to extremely thick beds. Fine sandstone and mudstone can be dark grey, purple or pale grey (Fig. 3.24). The beds are laterally continuous and rarely show cm-deep scours and cm-wavelength cross-laminations. Small pieces of wood (<1 cm) as well as rare accretionary lapilli (Figs 3.24b, 3.24c) are present in some examples, especially in the Backbone Ridge section. The largest fossil wood trunk was found in a pale grey unit at lower Cayuse Pass (Chinook Pass Member; Fig. 3.14a). In the southern Packwood region (Johnson Creek Member), fossil leaves are abundant in a >3-m-thick unit of cross-laminated fine feldspathic sandstone (not represented in the stratigraphic log). This unit was interpreted by Winters [1984] to have continental source.

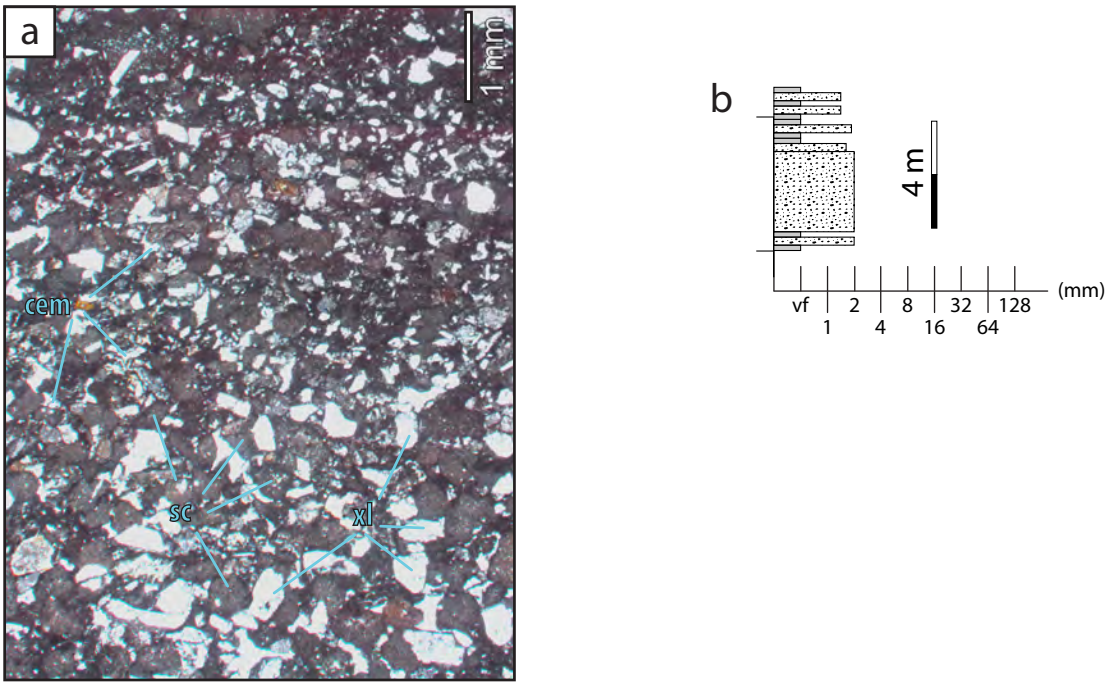

Fig. 3.25 Facies 9 - Fine mafic sandstone. **a)** Scoria clasts and broken feldspar crystals in a normally graded bed of facies 9 at Chinook Pass. Zeolite crystals fill the porosity, sample WA-30; **b)** Typical stratigraphic log of the facies. Graphic log features and key as in Figure 3.5. Scoria (sc), cement (cem) and feldspar crystal (xl).

Facies 9 - Fine mafic sandstone

Thin to very thick beds of relatively well-sorted, fine mafic sandstone are present at White Pass (White Pass Member; Fig. 3.7) and southern Packwood (Johnson Creek Member, Fig. 3.10). The beds are typically massive, though normally graded beds are also present. The sandstone mostly consists of red-oxidised to dark grey, poorly vesicular scoria clasts (>95 vol.%) of probable mafic composition and free broken feldspar crystals (<2 vol.%; Fig. 3.25); fiamme are absent. The cement is composed of zeolites and other secondary minerals. The scoria clasts are made of minor feldspar laths and ferromagnesian phases. The vesicles are ovoid to highly contorted.

Facies 10 - Mafic volcanic breccia

This facies occurs in thin to thick normally graded beds, and is composed of very angular scoria clasts (average 2-4 mm, max 10 mm). It is very abundant in the White Pass and Ohanapecosh Campground sections, and minor in the Backbone Ridge section (White Pass Member; Figs 3.7–3.9). The scoria clasts are red to dark brown (Figs 3.26b, 3.26c), and contain ovoid to highly contorted vesicles. The abundance of feldspar microlites is variable. The matrix makes up 20–95 vol.%, and the clast-supported varieties have monomodal grain size distribution (Fig. 3.26e) and are cemented by white zeolites (Fig. 3.26c). In a cliff close to White Pass (unit 137; Fig. 3.26a), the gently undulating beds

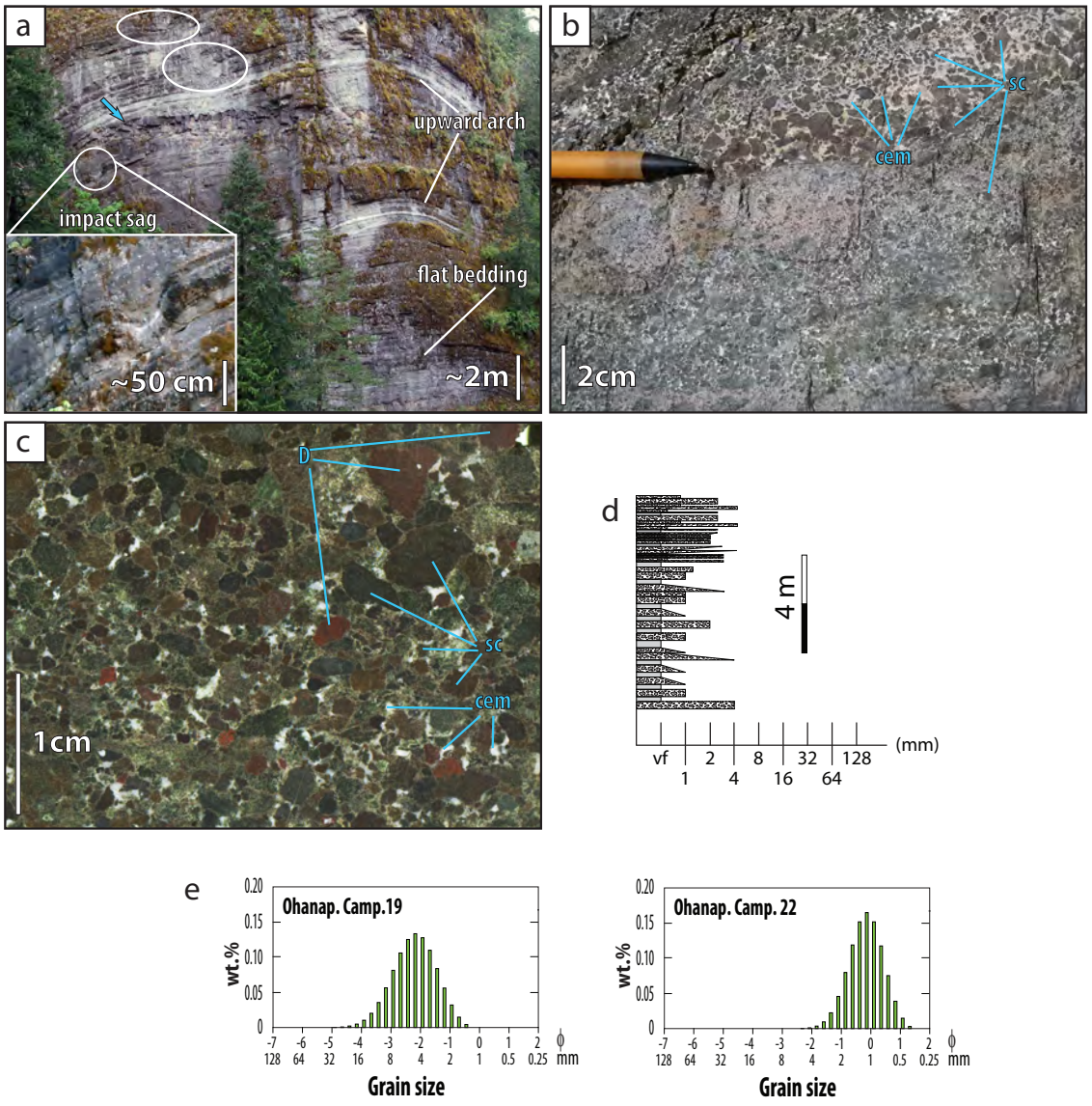

Fig. 3.26 Facies 10 - Mafic volcanic breccia. **a)** Thick section of fine mafic sandstone (facies 9) and mafic volcanic breccia (facies 10, out of section) at White Pass. Note the upward arch in the bedding, interpreted to be primary dip. Cliff face (140-160°) is parallel to the strike of bedding in the Ohanapecosh Formation. White circles for interpreted impact sags, arrow for mafic sill. Inset gives a detailed view of an interpreted impact sag; **b)** Facies 10, (unit 22) in the Ohanapecosh Campground section, normally graded beds of monomictic mafic scoria clasts and pale-cream cement; **c)** Scanned slab of facies 10 (unit 137 in the White Pass section), dark grey and red-oxidised mafic scoria clasts in pale green matrix and white zeolite cement, sample WA-09; **d)** Typical stratigraphic log of the facies 10 in unit 137 at White Pass (Fig. 3.7); **e)** Grain size distribution (chapter 2) of two beds in the Ohanapecosh Campground section (Fig. 3.8). Both samples show a monomodal grain size distribution, probably due to unique fragmentation and transport processes. Graphic log features and key as in Figure 3.5. Scoria (sc), dense clast (D) and cement (cem).

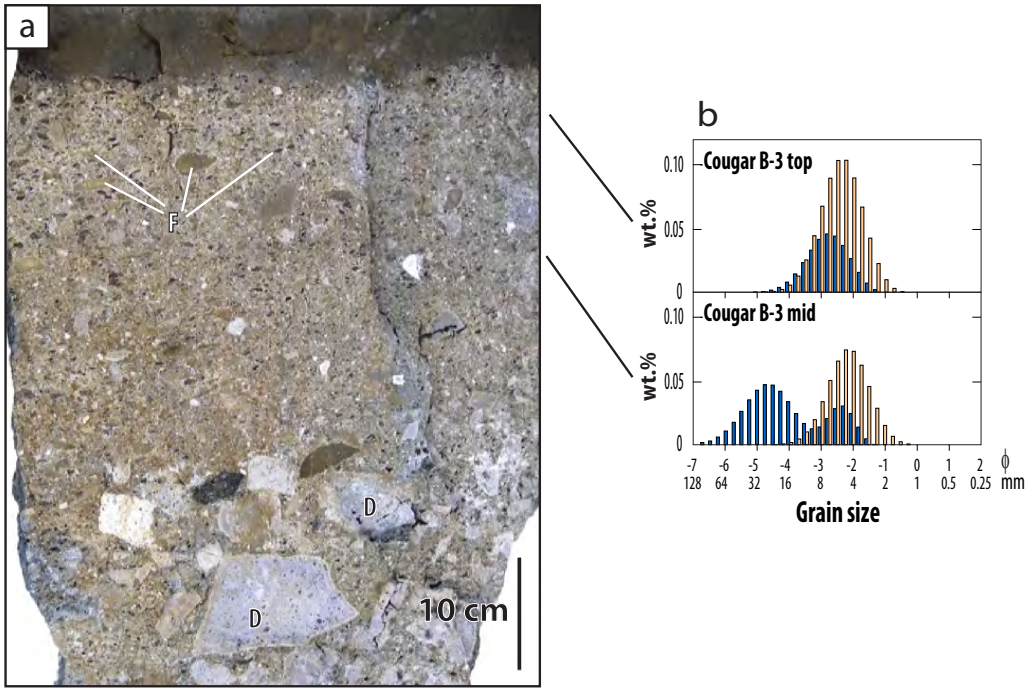

Fig. 3.27 Facies 11 - Normally graded andesite breccia to fiamme breccia. **a)** Normally graded andesite breccia to fiamme breccia (facies 11, out of section) at Cougar Lake. Bed showing strong normal grading; coarse, angular dense clasts (D, white) are concentrated at the base, and overlain by fiamme-rich facies (F, brown and black). The bed ends in, or is followed by mudstone; **b)** Grain size distribution (chapter 2) of the outcrop (Fig. 3.27a) in the fiamme breccia sub-facies. The bimodality in dense clasts disappears upwards, and pumice clasts increase in abundance.

in a 70-100-m-thick succession are discordant to the regional strike. The orientation of beds in the section defines an upward arch. This succession includes scattered <2-m-long depressions in fine-breccia beds that contain 0.5-1 m clasts.

This facies is interbedded with a minor amount of beds of fine sandstone and mudstone (facies 8), and a couple of them show high concentration of accretionary lapilli (Fig. 3.14b). It is unclear if broken accretionary lapilli occur, due to poor rock exposure.

Facies 11 - Normally graded andesite breccia to fiamme breccia

This thick (~1 m), clast-supported facies is present at the top of Chinook Pass (unit 63; Fig. 3.5) and at Cougar Lake (not represented in the stratigraphic log). The facies consists of coarse andesite breccia at the base (up to 40 cm thick), that grades upwards into fiamme breccia (fiamme 10–40 mm long); it is overlain by massive black sandstone to mudstone (Fig. 3.27).

Facies 12 - Reversely to normally graded pumice breccia

This facies occurs in a ~2.5-m-thick interval in the Chinook Pass section (unit 60a–c, Chinook Pass Member; Fig. 3.5) that is laterally extensive over >100 m (Fig. 3.19b). The main part of the facies consists of very thickly bedded pumice breccia chiefly composed of pale yellow to pale brown sub-rounded pumice clasts (average 1 to 10 mm, max 30 mm), with minor fiamme and rare feldspar crystals fragments (<1 mm) and <2 cm,

unbroken and broken, rim-type accretionary lapilli (Figs 3.28, 3.29). Unit 60a is poorly preserved and its base is covered by vegetation. The contact at the base of unit 60b smoothly scours into 20 cm of unit 60a, over 3 m laterally. In units 60b and 60c, there are six main beds that are reversely to normally graded and range from clast-supported to matrix-supported (Fig. 3.28b). The matrix is made of pale yellow to pale brown mudstone of similar colour to the sub-rounded pumice clasts. The mudstone matrix is absent in a few places and inter-clast space is filled with calcite and zeolite cement (Fig. 3.28c). Most units are interrupted with laminae or very thin beds of mudstone (Figs 3.28a, 3.28b, 3.29). The grain size distribution is monomodal (Fig. 3.29b). The main feature of this facies is the upwards continuity in the reverse and normal grading of the pumice clasts in the

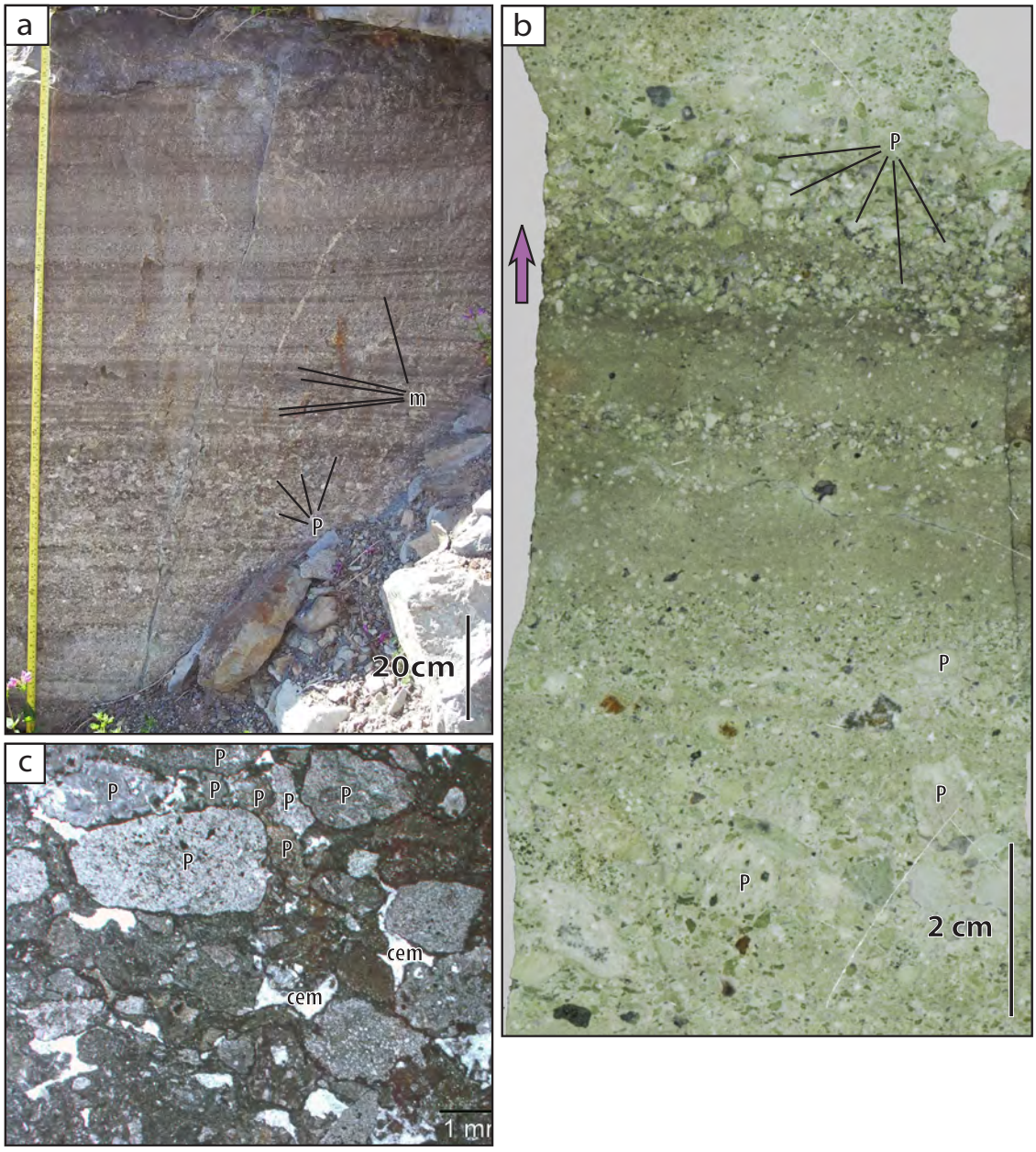

Fig. 3.28 Facies 12 - Reversely to normally graded pumice breccia. **a)** Facies 12 (unit 60b) at Chinook Pass. Note the reverse grading in pale grey pumice clasts in the lower unit, and dark-grey interbeds of mudstone; **b)** Sub-angular pumice clasts and mudstone in reversely to normally graded pumice breccia (facies 12) at Chinook Pass (unit 60). Note the grading in size; sample WA-46; c) Sub-rounded pumice clasts (unit 60b, facies 12, sample WA-46). Zeolite cement fills interstices between pumice clasts. Pumice (P), cement (cem) and mudstone (m).

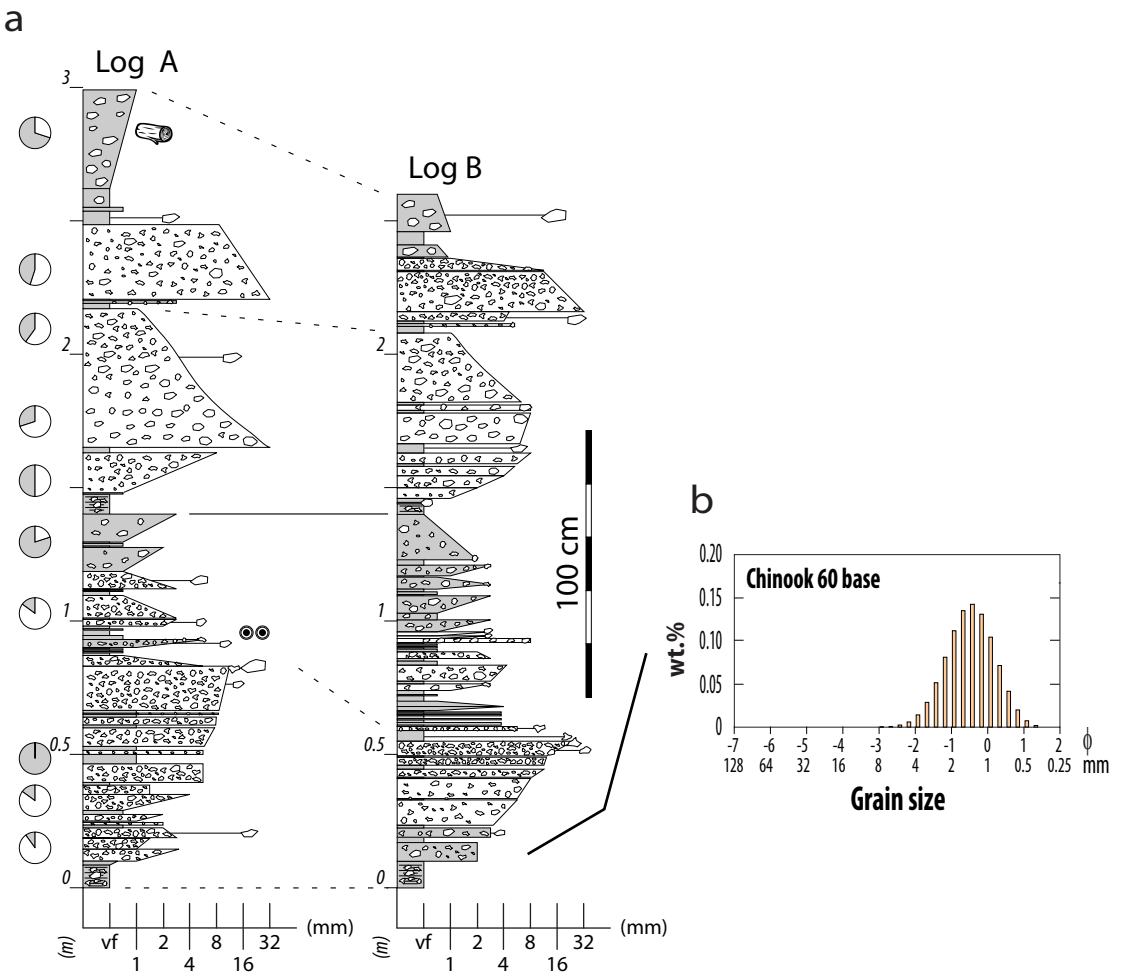

Fig. 3.29 Facies 12 - Reversely to normally graded pumice breccia (continuing). **a)** Two detailed logs of laterally continuous units (60b and 60c) of facies 12 in the Chinook Pass section, in the Chinook Pass Member. Log A is >80 m to the east of log B. The lines show main parts of the two sections that can be traced in the field; **b)** Grain size distribution (chapter 2) at the base of unit 60c. The samples show a monomodal grain size distribution, representing good sorting during suspension settling. Graphic log features and key as in Figure 3.5.

pumice breccia, despite the intercalation of mudstone (Figs 3.28, 3.29). The grading of the pumice breccia is laterally continuous over tens of metres, but the mudstone interlayers vary in thickness laterally and commonly disappear locally. The mudstone at the top of the units contains wood fragments (<2 cm).

Facies 13 - Crystal-rich sandstone

This crystal-rich facies is minor but occurs in thin to medium, massive or normally graded beds throughout the Ohanapecosh Formation particularly at Cayuse Pass (Figs 3.4–3.10). It is commonly composed of broken feldspar crystals (>20 vol.%) and occurs in association with beds of fine sandstone and mudstone (facies 8).

Facies 14 - Poorly porphyritic andesite breccia

Normally graded, medium to very thickly bedded breccia present at Chinook Pass (e.g. unit 51; Chinook Pass Member; Fig. 3.5) and Backbone Ridge (White Pass Member; Fig.

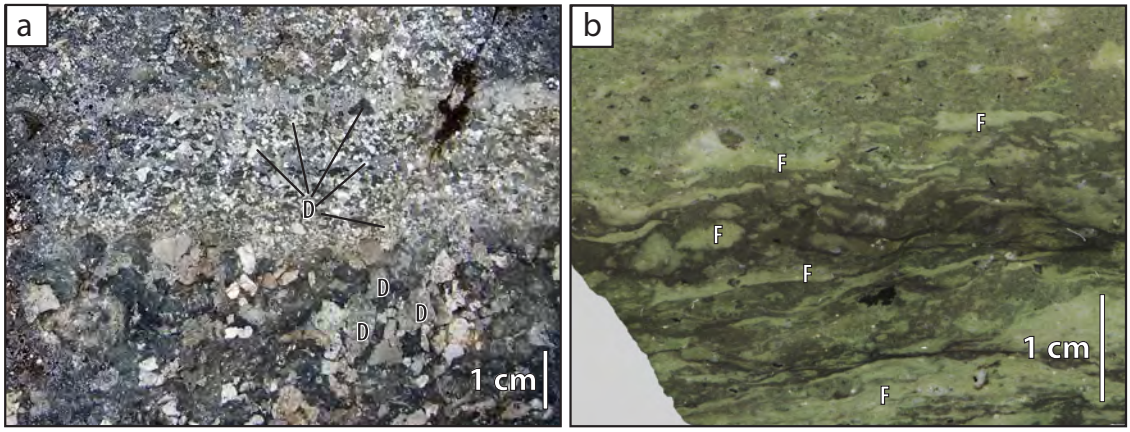

Fig. 3.30 a) Three beds of clast-supported, poorly porphyritic andesite breccia (facies 14, unit 3 in log A in the Cougar Lake section). Poorly porphyritic andesite dense clasts are white in a matrix; **b)** Fiamme sandstone and fiamme mudstone (facies 15) in a thin bed, green fiamme in a black matrix, sample WA-48. Fiamme (F) and dense clast (D).

3.7) is dominated by dense andesite clasts (5–8 mm), minor grey and black dense clasts and rare fiamme of similar size are also present (Fig. 3.30a). The andesitic clasts contain minor feldspar crystals (<10 vol.%). The proportions of matrix and clasts vary from unit to unit.

Facies 15 - Fiamme sandstone and fiamme mudstone

Thinly to thickly bedded, normally or reversely graded fiamme sandstone and fiamme mudstone (Fig. 3.30b) occur at Cougar Lake (Chinook Pass Member; Fig. 3.6), Ohanapecosh Campground and Backbone Ridge (White Pass Member; Figs 3.8, 3.9) and southern Packwood (Johnson Creek Member; Fig. 3.10). Fiamme are supported by matrix. The average fiamme size is 2–4 mm; coarser fiamme (up to 50 mm) are minor. Rare cross laminae, dense clasts and wood occur.

5.3. Coherent facies

Facies 16 - Vesicular basalt

Coherent vesicular basalt occurs in 0.3 to 3-m-thick intervals in the White Pass, Chinook Pass (unit 62) and Cougar Lake sections (Chinook Pass and White Pass Members; Figs 3.5–3.7). The basalt has sharp contacts and is conformable with bedding. Vesicles are ellipsoidal, average 1-2 cm across (Fig. 3.31a) and filled by secondary minerals (zeolites). In unit 62 at Chinook Pass, the size of vesicles increases upwards, and the vesicles occur in bands. Large tortuous cavities up to 10 cm long are common in the Cougar Lake section. No associated brecciated facies is present, except for one, poorly preserved outcrop at White Pass where basalt is overlain by mafic volcanic breccia (facies 10).

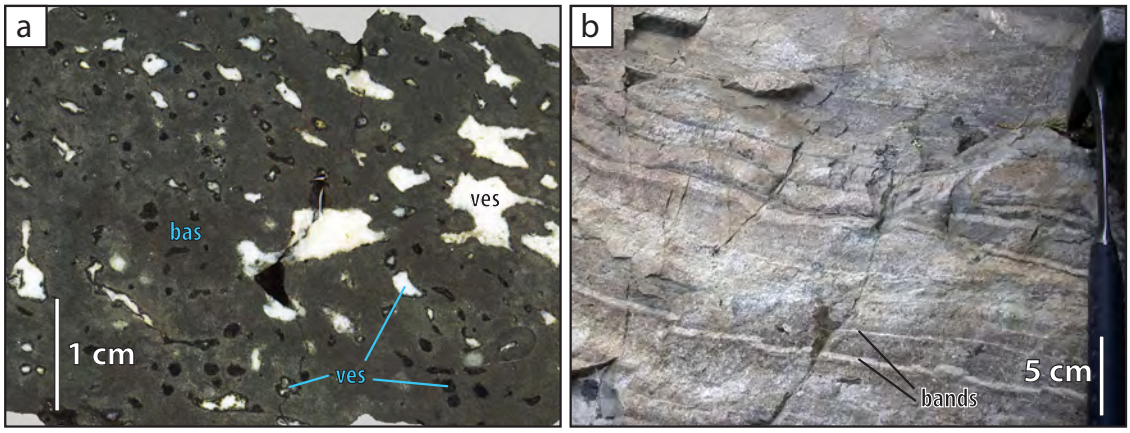

Fig. 3.31 a) Altered, coherent, vesicular basalt (facies 16; unit 105 in the White Pass section, sample WA-08); vesicles are filled with zeolites. Note similarity to vesicular basalt clasts in the coarse volcanic breccia (facies 7) in Figure 3.23a; **b)** Flow banded dacite (facies 17, unit 9 in log B in the Cougar Lake section). White and black bands are mostly regular and parallel; small vertical faults segment the dacite body. Vesicular basalt (bas) and vesicle (ves).

Facies 17 - Flow-banded dacite

Coherent, feldspar-phyric (>20 vol.%, <1 mm), flow-banded dacite (Fig. 3.31b) is intercalated parallel to the bedding in the Ohanapecosh Formation at Cougar Lake (unit 9, Chinook Pass Member; Fig. 3.6). It directly overlies crystal-rich sandstone (facies 13) with a sharp contact. The vertical and horizontal extent of the dacite remains undetermined due to erosion and difficult access, but it is possibly up to 30 m thick and continuous over several hundred metres laterally; the top of the unit is inaccessible. The mineralogy and flow-banded texture distinguish the dacite from the typically massive Tatoosh sills. No flow-banded clasts that could have been derived from this dacite body was found in the Ohanapecosh Formation.

Facies 18 - Miocene intrusions

The Ohanapecosh Formation is intruded by numerous silicic dykes and sills up to several tens of m across. The dykes randomly cut the bedding (Figs 3.3, 3.19a) and are commonly <10 m across. The Ohanapecosh Formation is locally altered at contacts with the largest sills (>>10 m across). The feldspars crystals in the Ohanapecosh Formation are recrystallised and the matrix has a strong reddish colour (e.g. Figs 3.19e, 3.22c). Fiske et al. [1963] related the mineralogy of these intrusions to the Miocene Tatoosh pluton. For clarity, these intrusions are not shown in the stratigraphic logs.

6. INTERPRETATION AND DISCUSSION

The extent (>400 km^2) of the formation and the numerous facies (at least 18) strongly suggest that the origins of the volcanic clasts are numerous, and that the formation is the record of a depocentre supplied by several volcanic edifices over a long (hundred of thousands to millions of years?) period of time.

6.1. Origin and fragmentation mechanisms of clasts in the Ohanapecosh Formation

Pumice clasts and fiamme

Pumice clasts and fiamme are the main clast type in most facies of the Ohanapecosh Formation: normally graded fiamme-andesite breccia (facies 1), fiamme-andesite breccia (facies 2), normally graded fiamme breccia (facies 3), reversely graded fiamme breccia (facies 4), normally graded or massive volcanic breccia (facies 5), coarse volcanic breccia (facies 6), normally graded andesite breccia to fiamme breccia (facies 11), reversely to normally graded pumice breccia (facies 12), and fiamme sandstone and fiamme mudstone (facies 15). They are minor or absent in the other clastic facies.

The high abundance of pumice clasts and fiamme in the Ohanapecosh Formation clastic facies strongly suggests they were produced by explosive eruptions. The grain size of pumice clasts and fiamme is mostly <10 cm, and does not match the coarse size (tens of cm to m) of pumice clasts produced by autoclastic fragmentation of subaqueous pumiceous domes [*Clough et al.*, 1981; *Fiske et al.*, 1998; *Allen et al.*, 2010]. Thus, the pumice clasts and fiamme of the Ohanapecosh Formation are considered to be pyroclasts.

The angularity of the pumice clasts suggests limited clast-to-clast interaction in most facies of the Ohanapecosh Formation during transport to their final resting position. In the reversely to normally graded pumice breccia (facies 12), the sub-rounded pumice clasts suggest moderate abrasion. The original angularity of the fiamme cannot be assessed.

Free broken crystals

The free broken crystals in the Ohanapecosh Formation (mostly feldspar, minor pyroxene and other ferromagnesian phases) match the euhedral phenocryst populations in fiamme, pumice and dense clasts. Thus, they are considered to be pyroclasts derived from the same magmas as the pumice clasts and fiamme. A few very thin to thick beds in the Johnson Creek Member contain abundant non-volcanic feldspar crystals that reflect continental erosion [*Winters*, 1984].

Scoria clasts

The vesicularity of mafic scoria clasts is low to moderate (<40 vol.%). The relatively high abundance of scoria clasts in the clastic facies in the White Pass Member strongly suggests they were produced by explosive eruptions. The grain size of scoria clasts is <10 cm, and does not match the coarse size (tens of cm to m) of autoclastic scoria clasts produced by lavas and domes. The angularity of scoria clasts in facies 9 and 10 indicate minimal clast-to-clast interaction during transport. Thus, most scoria clasts are considered to be pyroclasts.

Accretionary lapilli

Accretionary lapilli are formed by accretion of suspended ash particles in a moist or humid environment [*Schumacher and Schmincke*, 1995]. Suspended ash is the principal constituent of atmospheric or partly atmospheric explosive eruption plumes implying that the source vent was subaerial or in shallow water. Depositional sites can vary widely and accretionary lapilli may be robust enough to withstand sedimentation and resedimentation in water [*Boulter*, 1987].

Accretionary lapilli are present in numerous very thin to thick beds of the Ohanapecosh Formation (facies 8, 10, 12, 13, 15) and intact and broken accretionary lapilli are commonly found together. The accretionary lapilli are apparently absent from all the very thick to extremely thick facies.

Dense clasts

Most dense clasts of the Ohanapecosh Formation contain microlites and phenocrysts that attest to their volcanic origin. Dense clasts are probably of similar compositions to the scoria clasts, pumice clasts and fiamme. Most of the dense clasts are angular, but are also found as sub-rounded to rounded clasts in some facies. Angular dense clasts that occur with abundant pumice clasts or fiamme are possibly pyroclasts. Sub-angular to rounded dense clasts occur in the coarse volcanic breccia (facies 6) and the clast-supported polymictic breccia-conglomerate (facies 7), and at the base of the normally graded fiamme-andesite breccia (facies 1), the fiamme-andesite breccia (facies 2) and the normally graded fiamme breccia (facies 3). The origins of these abraded clasts cannot be resolved but are likely to be complicated and varied. These clasts are derived from coherent facies (e.g. lavas, intrusions) and were abraded prior to and/or during final deposition. The most rounded examples may have been abraded in above wave-base environments, such as rivers or beaches.

Wood

The relatively common occurrence of wood chips and leaves in the very thin to thickly bedded facies (facies 8, 12 and 15) indicates that part of the source areas of these facies

was on land. Wood fragments are apparently absent form the very thick to extremely thickly bedded facies.

6.2. Depositional setting

Poorly preserved fossils ["ostracods, gastropods, and perhaps even Foraminifera"; *Fiske et al.,* 1963] indicate a subaqueous depositional setting for the Ohanapecosh Formation. In addition, the Ohanapecosh Formation includes several very thinly to thickly bedded facies in which beds are planar and laterally continuous, and that lack cross-stratification, erosional surfaces or palæosols. Planar thin beds dominate in the fine sandstone and mudstone (facies 8), mafic volcanic breccia (facies 10), reversely to normally graded pumice breccia (facies 12), crystal-rich sandstone (facies 13), poorly porphyritic andesite breccia (facies 14) and fiamme sandstone and fiamme mudstone (facies 15). These facies are ubiquitous in the Ohanapecosh Formation and strongly constrain the depositional setting of most of the formation to below wave-base.

The very thick to extremely thick beds of the normally graded fiamme-andesite breccia (facies 1), fiamme-andesite breccia (facies 2), normally graded fiamme breccia (facies 3), reversely graded fiamme breccia (facies 4), graded or massive volcanic breccia (facies 5), and coarse volcanic breccia (facies 6), are laterally continuous and tabular. They are commonly graded and they lack internal stratification and cross-beds. Such bed forms are typical of deposits from subaqueous high-concentration density currents [e.g. *Mulder and Alexander*, 2001; *Piper and Normark*, 2009].

The Ohanapecosh Formation was probably deposited in a lake or protected sea embayment because of its setting close to the continental margin [e.g. *McBirney*, 1978; *Johnson*, 1985; *Dickinson*, 2009]. The presence of wood chips and leaves indicates proximity to land. In such a quiet water environment, the wave base could be as little as a few metres depth of water [*Manville*, 2001]. However, the total thickness of the formation suggests a wide, deep basin. Poor rock preservation at the top of the formation may hide facies transitional from below to above wave-base environments

The upper part of the Ohanapecosh became is poorly exposed and the presence or the absence of planar thinly bedded facies is unknown. The overlying Fifes Peak Formation was deposited subaerially [*Fiske et al.,* 1963]. It is possible that shallow water or subaerial setting existed during the last stage of deposition. However, the volume of potentially very shallow to subaerial facies in the Ohanapecosh Formation is minor considered to its total thickness and extent.

6.3 Transport and depositional processes

Water-supported density currents

Most facies of the Ohanapecosh Formation consist of very thick to extremely thick tabular beds with sharp bases that are distinctly graded or massive, as is typical of high concentration density current in general [*Lowe*, 1982; *Mulder and Alexander*, 2001; *Kokelaar et al*., 2007; *Piper and Normark*, 2009; *Sumner et al*., 2009]. Although composed primarily of pyroclasts, all facies in the Ohanapecosh Formation lack textures related to hot state deposition, such as welding, columnar joints and gas segregation pipes [*Cas and Wright*, 1991; *White*, 2000]. These characteristics in combination with the below wave-base subaqueous setting suggest that the Ohanapecosh Formation density currents were water-supported, rather than hot gas supported as in pyroclastic flows s.str. I use the term "subaqueous volcaniclastic density current" for the Ohanapecosh Formation density currents; the term implies the density currents were water-supported, high concentration and composed of volcaniclastic particles and is inclusive of all the triggering mechanisms (eruption-fed versus remobilisation) and source settings (subaerial versus subaqueous). Subaqueous volcaniclastic density currents are a member of a very large group of subaqueous water supported density currents that vary in particle types, particle concentrations and rheology. Because of its viscosity, water allows much better sorting of clasts than air or hot-gas mixture [*Cashman and Fiske*, 1991; *White*, 2000; *White et al*., 2001; *Manville et al*., 2002], thus water-supported volcaniclastic density current deposits are generally better graded than subaerial equivalents [e.g. *Allen and McPhie*, 2009].

Subaqueous density currents

The nomenclature and behaviour of subaqueous density currents is chiefly based on field evidence, laboratory experiments and theoretical hydrodynamic processes [*Lowe*, 1982; *Stow*, 1994; *Mulder and Alexander*, 2001; *Piper and Normark*, 2009; *Sumner et al*., 2009]. The rheology and dynamics of subaqueous density currents are mainly dependent on particle concentrations and grain-grain interactions [*Iverson*, 1997], and viscoplastic properties related to the abundance of clay minerals in the current [*Bagnold*, 1956; *Hampton et al*., 1996]. The behaviour of subaerial density currents cannot be directly exported to subaqueous equivalents, because an unrestricted amount of water can be ingested by subaqueous density currents during transport under water. There have been few observations of natural subaqueous density currents, and the terminology is not consistent [*Mulder and Alexander*, 2001]. In addition, very high particle concentration currents that contain coarse grained clasts are rarely studied [e.g. *Freundt*, 2003; *Allen and Freundt*, 2006; *Kokelaar et al*., 2007; *Allen and McPhie*, 2009]; most rheology studies are based on uniform siliciclastic sand and mud and conventional particle supply rates [e.g. *Shanmugam*, 1997; 2002; *Baas et al*., 2009; *Sumner et al*., 2009]. Subaqueous volcaniclastic

density currents contain a wider range of clast sizes and clast densities (typically 600–900, 1,100–1,500 and 2,500 kg/m^3 for air-filled pumice, waterlogged pumice and dense clasts, respectively; chapter 5) than siliciclastic density currents [e.g. *Houghton and Wilson*, 1989]. This is a major issue in the study of pumice- and dense clast-rich volcaniclastic density currents, because flow rheology depends in part on particle concentration and particle densities [*Julien and Lan*, 1991].

Subaqueous density currents can be described in terms of two major types. Turbidity currents (s.str.) are dilute, non-cohesive and supported by fluid turbulence, whereas subaqueous debris flows [i.e. subaqueous hyperconcentrated density flows; *Mulder and Alexander*, 2001] have a very high sediment concentration (>50 vol.%), particles are supported by matrix strength and they are laminar and behave as a Bingham plastic [*Stow*, 1994; *Mulder and Alexander*, 2001]. Importantly, variation in clast and water concentrations and/or in palæo-topography can generate transformations from one type to the other [*Komar*, 1971; *Hampton*, 1972; *Fisher*, 1983; *Weirich*, 1989; *Sumner et al*., 2009]. In addition, turbidity currents are likely to form at the head and/or over the body of subaqueous debris flows.

The subaqueous density currents transitional between the two end-members are poorly defined, the hydrodynamic threshold conditions debated, and their name vary largely in the literature [*Kneller and Branney*, 1995; *Mulder and Alexander*, 2001 and references therein; *Piper and Normark*, 2009]. For instance, proposed names for subaqueous density currents transitional include concentrated density flow [*Mulder and Alexander*, 2001], weakly, moderately and strongly coherent debris flows [*Marr et al*., 2001; *Ilstad et al*., 2004a], high-density turbulent flow [1982] and sandy debris flow [*Shanmugam*, 1997]. Several authors suggest a continuum between strongly and weakly cohesive subaqueous debris flows [e.g. *Mulder and Alexander*, 2001; *Ilstad et al*., 2004a; *Ilstad et al*., 2004b], but recent experimental studies propose that the spectrum in types of deposits from density currents is restricted to a few categories [*Baas et al*., 2009; *Sumner et al*., 2009], however all these studies did not include coarse-grained volcanic clasts. The spectrum in density currents intermediary between the two end-members is probably restricted to non-Bingham behaviour, are partially turbulent, and mostly sustained by clast-to-clast interaction.

The dominant depositional mechanisms of subaqueous debris flows are vertical accretion and frictional freezing, whereas deposition from non-cohesive density currents involves aggradation by traction and suspension fallout [*Lowe*, 1982]. Subaqueous debris flows may develop hydroplaning at the flow head [*Mohrig et al*., 1998], thus preventing erosion of the substrate [*Mulder and Alexander*, 2001]. On the other hand, turbulent density currents may be erosive [*Mulder and Alexander*, 2001; *Piper and Normark*, 2009]. Turbulence increases sorting and grading of the beds, creating numerous bed forms, whereas cohesive deposits are single-bedded, and massive to only slightly normally graded [e.g. *Mulder and Alexander*, 2001; *Sumner et al*., 2009]. Cohesive density currents are supported

by matrix strength, and produce deposits that are richer in matrix than turbulent density currents.

Subaqueous volcaniclastic density currents in the Ohanapecosh Formation

Lithofacies analysis in the Ohanapecosh Formation remains difficult because the fine-grained (<2 mm) clasts were destroyed during diagenesis, preventing description of the total grain size distribution. The lithofacies suggest that most of clastic facies were produced by high concentration, non-cohesive subaqueous volcaniclastic density currents.

The normally graded fiamme-andesite breccia (facies 1), fiamme-andesite breccia (facies 2), and normally graded fiamme breccia (facies 3) have normally graded, extremely thick (>20 m) beds that are dominated by angular clasts and are matrix-supported in their middle and upper part (or sub-facies). Facies 1 and 2 have a strongly clast-supported basal breccia dominated by angular to sub-rounded dense clasts; facies 3 is less coarse. These characteristics imply depositional processes in subaqueous volcaniclastic density currents that had a degree of turbulence and were not cohesive. Reversely graded fiamme breccia (facies 4) shares most of the characteristics of facies 3. Its reverse grading is probably explained by the lower density of larger pumice clasts present in the upper part of the bed, or delayed waterlogging.

Parts of the beds in graded or massive volcanic breccia (facies 5) are normally graded at their top. However, there are large variations in matrix abundance (20-60 vol.%) depending on the bed, and normal grading is absent or restricted to the upper part of the beds. The flows that generated the massive beds may have been more cohesive. Beds of coarse volcanic breccia (facies 6) are coarser-grained than those of massive volcanic breccia (facies 5) and only weakly graded, and their clasts are angular to sub-rounded. Coarse volcanic breccia (facies 6) suggests deposition from a subaqueous volcaniclastic density current that was more cohesive and less diluted than for facies 5, such as a cohesive type of subaqueous volcaniclastic density current.

Low density turbidity currents

Conventional low density turbidity currents (turbidity currents s.str.) are defined by their high degree of turbulence and lack of cohesion; they can transport a relative low concentration (<10 vol.%) of clasts under water [*Lowe*, 1982; *Mulder and Alexander*, 2001; *Piper and Normark*, 2009]. Their deposits are relatively thin (up to a few m), normally graded, relatively well sorted, chiefly finer than medium sand (≤2 mm), and commonly consist of a regular succession of facies that aggraded progressively [*Bouma*, 1962; *Lowe*, 1982; *Shanmugam*, 2002]. Parts of three fine-grained (mainly <2 mm), and relatively thinly bedded (<30 cm) facies are interpreted to be turbidites: the fine sandstone and mudstone

(facies 8), crystal-rich sandstone (facies 13) and fiamme sandstone and fiamme mudstone (facies 15) may include beds that were deposited from turbidity currents.

Subaqueous suspension settling

Volcanic clasts can settle by vertical motion through the water column. Suspension involves discrete particle fallout with minimum interaction with other particles. Such settling behaviour follows an ideal example of hydraulic sorting [*Rubey*, 1933; *Clift et al*., 1978; *Cashman and Fiske*, 1991; *Manville et al*., 2002; *Burgisser and Gardner*, 2006]. Where abundant particles are put together in water, they may form vertical density currents that can transport clasts up to three orders of magnitude faster than a suspension [*Wiesner et al*., 1995; *Carey*, 1997; *Manville et al*., 1998; *Manville et al*., 2002].

The lateral continuity of pumice clasts in the reversely to normally graded pumice breccia (facies 12; Figs 3.19b, 3.28) at Chinook Pass and the rounded shape of the pumice clasts suggest that settling from pumice rafts formed thin beds in a quiet, below wave-base environment. The successive graded beds suggest a complex system of sedimentation with multiple inputs of pumice clasts into the water body, or multiple wind-driven currents periodically moving pumice rafts. The reverse grading in pumice clasts in facies 12 reflects progressive waterlogging as a function of their size [e.g. *Manville et al*., 1998; *White et al*., 2001; *Manville et al*., 2002], to create deposits that show saturation grading. Pumice lapilli can float for several months [*White et al*., 2001; *Bryan et al*., 2004]. Beds with normal grading indicate that the coarsest particles sank faster than the smaller ones, in a type of sedimentation dominated by hydraulic sorting. Interbeds of mudstone in the reversely to normally graded pumice breccia (facies 12) reflects complex sedimentation of fine-grained clasts contemporaneously with the sinking of the pumice clasts. The fine clast could have been derived from the abrasion of pumice clasts that formed the raft [e.g. *White et al*., 2001], ash from disintegration of pyroclastic flows at the shoreline, or by fallout of ash from atmospheric ash plumes [e.g. *Wetzel*, 2009].

Some beds of fine sandstone and mudstone (facies 8) and fine mafic sandstone (facies 9) are interpreted to be derived from suspension settling by their lateral continuity, regular normal grading and their relatively good sorting.

Other types of density currents

Grain flows are non-Newtonian fluids that are supported by dispersive pressure from grain-to-grain interactions [*Lowe*, 1976; *Mulder and Alexander*, 2001]. They can occur in subaerial and subaqueous environments, require slopes and cannot have extensive run-out distance. They create clast-supported, thin to very thin beds, are typically reversely graded by kinetic sieving, and may have no matrix. They typically deposit on slopes at the angle of repose. In addition, grain flows have the characteristic to transport their

clasts *en masse*, and commonly produce lenticular beds.

Sedimentation of mafic volcanic breccia (facies 10) on the scoria cone was probably mostly generated by subaqueous grain flows. Dilute tractional currents [*Shanmugam et al.*, 1993; *Shanmugam*, 2008] were probably responsible for the cross-laminated beds of fine sandstone and mudstone (facies 8), and the scours between units 60a and 60b of reversely to normally graded pumice breccia (facies 12) in the Chinook Pass section.

6.4. Eruption-fed versus remobilised pyroclasts

Inferring initiation processes that lead to transport in subaqueous density currents from field outcrops is difficult. Piper and Normark [2009] concluded that there is no simple relationship between a type of deposit and its initiating processes. Subaerial explosive eruptions may generate wide range of eruption-fed subaqueous facies [e.g. *Sparks et al.*, 1980; *Yamada*, 1984; *Whitham and Sparks*, 1986; *Whitham*, 1989; *Cas and Wright*, 1991; *Carey et al.*, 1996; *Mandeville et al.*, 1996; *White et al.*, 2001; *Manville et al.*, 2002; *Freundt*, 2003; *Dufek et al.*, 2007]. Pumice-forming, explosive eruptions can also occur in shallow water and up to several hundreds of m below sea level [*Fiske*, 1963; *Kokelaar*, 1983; *Kano*, 2003; *White et al.*, 2003; *Allen and McPhie*, 2009]. Furthermore, subaqueous volcaniclastic density currents can originate from resedimentation of saturated aggregates [*Allen and Freundt*, 2006], or from magmatic-volatile driven, pumice-forming explosive eruptions [*Sparks et al.*, 1980; *Whitham*, 1989; *Carey et al.*, 1996; *Mandeville et al.*, 1996; *Freundt*, 2003; *Allen and Freundt*, 2006; *Trofimovs et al.*, 2006; *Allen et al.*, 2007; *Allen and McPhie*, 2009]. To distinguish between these two fundamental processes is an ongoing challenge [*Fisher and Schmincke*, 1984; *McPhie et al.*, 1993; *White*, 2000; *White et al.*, 2003] and assessing the source and the transport processes associated with subaqueous volcaniclastic density currents is difficult where there is no evidence of hot emplacement [e.g. *Cas and Wright*, 1991].

Pumice clast density

Pumice clast density is mainly controlled by the vesicularity, the density of the glass and phenocrysts and the proportion of waterlogged vesicles [*Whitham and Sparks*, 1986; *Manville et al.*, 1998; *Manville et al.*, 2002; *Allen et al.*, 2008]. Regardless of gas or water-filled, pumice clasts with a vesicularity <60 vol.% will sink because their density is <1,000 kg/m^3 [*White et al.*, 2001]. The presence of pumice clasts in submarine water-supported volcaniclastic density current deposits implies that pumice clasts were denser than water (i.e. density >1,000 kg/m^3). The pumice clasts available for transport in subaqueous volcaniclastic density currents are (1) sufficiently hot on contact with water to ingest water immediately and sink, (2) already sufficiently waterlogged, and/or (3) low-vesicularity types that are denser than water. Andesite compositions may imply lower vesicularities,

i.e. <60 vol.% [e.g. *Whitham*, 1989; *Allen*, 2004].

Hot pumice clasts are quickly waterlogged on contact with water, because vesicles are either largely filled with hot magmatic steam, or create steam on quenching. The condensation of steam draws in water by a vacuum effect associated with the large volume change when steam condenses to liquid water [*Whitham and Sparks*, 1986; *Dufek et al*., 2007; *Allen et al*., 2008]. Thus, pumice clasts in a hot gas-supported pyroclastic density current that reaches the shore may quickly waterlog and create water-supported subaqueous volcaniclastic density currents [*Carey and Sigurdsson*, 1980; *Freundt*, 2003]. The low-concentration ash clouds forming the upper part of the pyroclastic flows and those created by steam explosions at the shoreline continue their course over the water [*Cas and Wright*, 1991; *Carey et al*., 1996; *Freundt*, 2003; *Edmonds and Herd*, 2005; *Dufek et al*., 2007], deposits of which would eventually create pumice rafts, and/or sink by discrete particle fall [*White et al*., 2001; *Manville et al*., 2002] or develop into vertical density currents [*Carey*, 1997; *Manville and Wilson*, 2004].

Waterlogging of cold pumice clasts floating in rafts is also possible but absorbing sufficient water to sink can take up to several months to years [*Whitham and Sparks*, 1986; *Manville et al*., 1998; *White et al*., 2001; *Bryan et al*., 2004], and sub-rounding by clast-to-clast abrasion is expected, as well as clast dispersal.

Facies in the Ohanapecosh Formation

The extreme bed thickness, high abundance of angular pumice clasts and free broken crystals in the normally graded fiamme-andesite breccia (facies 1), fiamme-andesite breccia (facies 2), normally graded fiamme breccia (facies 3) and reversely graded fiamme breccia (facies 4) strongly suggest they were fed directly from voluminous pumice-forming explosive eruptions. In addition, the characteristics of these facies imply transport and deposition by water-supported volcaniclastic density currents. I infer that the bulk of the pumice clasts, that is those that are uncompacted and angular in facies 1–4, were >1,000 kg/m^3, and/or hot on interaction with water, so that they rapidly attained a higher bulk density than water.

The very thick beds of normally graded or massive volcanic breccia (facies 5) and coarse volcanic breccia (facies 6) can have either eruption-fed or remobilised origins. The beds of facies 5 are mostly graded and facies 5 and 6 are non-stratified, contain angular pumice clasts and they are in average less thick and less graded in comparison to facies 1–4. These characteristics can be produced by numerous combinations of volcanic and remobilisation processes. Rounded clasts form most of the very thick (3 m), clast-supported polymictic breccia-conglomerate (facies 7), which suggests resedimentation from an above wave-base environment.

Beds of fine sandstone and mudstone (facies 8) and fine mafic sandstone (facies 9) that show evidence of suspension settling are probably eruption-fed, because fallout from eruption plume is the most likely process to bring a large volume of pyroclasts into a water body [e.g. *Wetzel*, 2009]. Most fine-grained beds of fine sandstone and mudstone (facies 8) probably record distal fallout of volcanic ash, or small-scale remobilisation and non-volcanic (background) activity, with accumulation of plant fossils and other precipitates in the dark mudstone beds.

The mafic volcanic breccia (unit 137 in the White Pass section; facies 10) is inferred to be a remnant of the proximal parts of a scoria cone in shallow water (~<30 m). The scoria cone architecture is inferred from the thickness of the succession, the similar aspect of the beds, and their discordance to the general strike of the White Pass Member. In addition, the scattered depressions containing coarse dense clasts are interpreted as impact sags, and the overall upward charing of the beds reflects a cone-like structure (Fig. 3.26). It is likely that most beds were eruption-fed and deposited by fallout, small-volume volcaniclastic density currents or grain flows directly from the vent. However, slopes on scoria cones are typically unstable and partial remobilisation of loose aggregates over a short distance is probable [e.g. *Sohn et al*., 2008].

The presence of the well sorted sub-rounded pumice clasts and interbedded mudstone in the reversely to normally graded pumice breccia (facies 12) suggests abrasion of pumice lapilli in pumice rafts and subsequent suspension setting of waterlogged pumice lapilli and ash. The accretionary lapilli in facies 12 demonstrate the presence of wet, ash-rich clouds [*Cas and Wright*, 1991]. I interpret facies 12 to be eruption-fed, and to be formed in a two-step process: (1) a pumice-forming subaerial explosive eruption that deposited pumice lapilli and ash onto the water body, forming pumice rafts, and (2) subsequent waterlogging in pumice rafts and settling of the pumice clasts, ash, wood and accretionary lapilli.

Other very thin to thick facies in the Ohanapecosh Formation do not contain sufficient evidence to argue for an eruption-fed origin or otherwise.

6.5. Environment at source

The regional extent (>400 km^2) and duration (~8 million years) of the entire Ohanapecosh Formation [*Tabor et al*., 2000; *Schuster*, 2005], presence of the remnants of at least one scoria cone in the White Pass Member, and the various clast compositions all imply that volcaniclastic sediments were supplied from numerous volcanic edifices [*Fiske*, 1963; *Vance et al*., 1987; this study]. The abundance of pyroclasts in the Ohanapecosh Formation attests of its origin from explosive eruptions. The laterally continuous very thin to thick beds imply deposition in a subaqueous environment. However, the setting of source

vents is difficult to constrain for most facies; both subaerial and subaqueous vents are contenders, and both subaerial and subaqueous vents may have co-existed.

Fine sandstone and mudstone (facies 8) that contain accretionary lapilli indicate water settling derived from products of subaerial explosive eruptions, or explosive eruption columns sufficiently shallow and powerful that they could breach to the water surface. In the White Pass Member, the change of dip in the sequence of mafic volcanic breccia at sections of White Pass (unit 137, facies 10) and Ohanapecosh campground, and numerous beds of mafic volcanic breccia that show upward arch structure (Fig. 3.26a) imply a scoria cone structure. The interbedded beds of fine sandstone and mudstone (facies 8) that include accretionary lapilli constrain the vent of the scoria cone to be subaerial or in shallow water. Reversely to normally graded pumice breccia (facies 12) also contains accretionary lapilli, and is composed of sub-rounded pumice lapilli derived from pumice rafts that are likely to be derived from a subaerial source. The good sorting and relatively high density of scoria clasts (<60 vol.% vesicles; >1,000 kg/m^3) in fine mafic sandstone (facies 9) suggests direct settling from subaerial fallout onto water.

Extremely thick facies

Subaerial explosive eruptions produce deposits that may include accretionary lapilli, rounded clasts derived from abrasion in pyroclastic flows, and clasts with mixed provenance, such as accidental clasts picked-up by pyroclastic density currents. The most efficient way to introduce voluminous pumice clasts, ash and dense clasts to a subaqueous setting is by subaerial pyroclastic flows crossing the shoreline. The typical facies produced by pumice-rich subaerial pyroclastic flows transforming into water-supported volcaniclastic density currents include (1) massive or stratified, poorly sorted pumice lapilli tuff to pumice tuff breccia, containing rounded pumice clasts [e.g. Roseau Ash; *Whitham*, 1989], and (2) well sorted, stratified pumice tuff breccia to pumice lapilli tuff that contains angular pumice clasts, commonly overlying a lithic breccia-conglomerate [e.g. Znp ash *Kurokawa and Tomita*, 1998; *Allen et al*., 2011]. In comparison, subaqueous explosive eruption columns tends to generate relatively well-sorted, fines-poor pumice lapilli-rich facies and angular clasts [e.g. neptunian eruptions; *Allen and McPhie*, 2009].

In the Chinook Pass Member, sub-rounded dense clasts - some with all edges modified - are exclusively restricted to the basal sub-facies of the normally graded fiamme-andesite breccia (facies 1), fiamme-andesite breccia (facies 2), and normally graded fiamme breccia (facies 3) and clast-supported polymictic breccia-conglomerate (facies 7). These sub-rounded clasts may imply more than one history of transport. Sub-rounded dense clasts occur in subaqueous volcaniclastic density current deposits derived from subaqueous explosive eruptions [e.g. Filakopi pumice breccia; *Stewart and McPhie*, 2004] and subaerial pyroclastic density currents that entered water [e.g. *Allen et al*., 2011], thus the origin of the sub-rounded clasts is not restricted to subaerial processes, although it is the most

likely. Abrasion of rounded clasts in subaqueous volcaniclastic density currents that generated facies 1–3 and 7 could occur (1) by recycling in the vent [e.g. *Houghton and Smith*, 1993] (2) during transport, by contact with clasts of similar hardness, and/or (3) by being accidentally picked-up from fluvial, shoreline or deltaic sediments.

In the Chinook Pass section, unit 58 is clast-supported polymictic breccia-conglomerate (facies 7). The polymictic nature, high abundance of rounded dense clasts and the absence of pumice clasts and fiamme suggest resedimentation from an above wave-base environment. Thus, a subaerial source is most likely to have produced the normally graded fiamme breccia (facies 3) and reversely graded fiamme breccia (facies 4), by transformation of pyroclastic flows into water-supported density currents at the shoreline.

Reversely to normally graded pumice breccia (facies 12) occurs in one minor bed (unit 60) in the Chinook Pass section of the Chinook Pass Member. The saturation grading [*White et al.*, 2001] of sub-rounded pumice clasts, lateral continuity and presence of interbeds of mudstone that interrupt the grading, and rare accretionary lapilli and wood suggest sedimentation from pumice rafts, and at least a minor subaerial input. In the Chinook Pass section, unit 60 lies between units 59 and 61 [normally graded fiamme breccia, (facies 3) and reversely graded fiamme breccia (facies 4), respectively]. These two extremely thick beds are interpreted as eruption-fed and deposited from subaqueous volcaniclastic density currents. I interpret this sequence to be genetically related, in which unit 60 records post-eruptive or precursory sedimentation of the climactic eruption that generated unit 59 or 61, respectively. In this case, the implication is that unit 59 (facies 3) and unit 61 (facies 4) are also derived from a subaerial vent.

Some features of the normally graded fiamme-andesite breccia (facies 1), fiamme-andesite breccia (facies 2), normally graded fiamme breccia (facies 3) and reversely graded fiamme breccia (facies 4) deserve particular consideration. The coexistence of angular clasts and abundant matrix (<2 mm), at least in the middle and upper sub-facies, is not expected for either sources of subaerial pyroclastic density currents. The lack of abrasion of pumice and dense clasts in the middle and upper sub-facies of facies 1–4 indicates low clast-to-clast interactions, which could indicate either a transport in a subaqueous environment, or short-distance transport as subaerial pyroclastic flow before entering water. The matrix support indicates poor sorting, and deposition from a type of volcaniclastic density current in which the particle concentration was very high and suppressed turbulence. The abundance of matrix in the middle and upper sub-facies is inconsistent with a neptunian eruption origin [*Allen and McPhie*, 2009].

Therefore, environment at source of eruption-fed facies 1–4 is interpreted to be subaerial, because of their intercalation with facies 7 and 12, the abundance of matrix, and the sub-rounded dense clasts in basal breccia. The facies 1–4 are interpreted to be originated

from subaerial pyroclastic flows that crossed the shoreline, and the angular pumice clasts imply short transport in the abrasive dusty gas-supported transport system. The vent was probably at short distance from shore, preventing abrasion of the pumice clasts. In addition, the abundance of pumice clasts suggests efficient transformation from a gas-supported to water-supported volcaniclastic density current. In this case, it is likely that the sub-rounded dense clasts were accidentally picked-up during transport, such as the shoreline. The abundance of matrix in the facies 1–4 suggests minimum elutriation of the ash [*Freundt*, 2003]. It also implies entry of pyroclastic flows that were not very expanded [e.g. *Cas and Wright*, 1991].

The origins of clasts in the graded or massive volcanic breccia (facies 5) and coarse volcanic breccia (facies 6) remain unsure because this facies contains abundant angular pyroclasts. Because this facies combines both matrix-rich and matrix-poor sub-facies, numerous origins are possible. Overall, beds of facies 5 and 6 are less thick and less graded than facies 1–4, and lack the basal dense clast breccia occurring in facies 1–3. Matrix-poor beds could be related to subaqueous explosive eruptions in which the ash was segregated from the eruption column [e.g. *Allen and McPhie*, 2009]. Both matrix-rich and matrix-poor beds of facies 5 show the same problematic features as those developed for facies 1–4 for presence of angular pumice clasts. However, absence of basal dense clast breccia and diagnostic intercalated facies both precludes a unique origin, and could therefore be related to subaqueous and/or subaerial explosive eruptions or resedimentation of their products.

6.6. Facies architecture

Chinook Pass Member

The Chinook Pass Member comprises volcaniclastic sediments from one main source, because most clasts have similar mineralogy and composition, and beds have been deposited by similar types of volcaniclastic density currents. Most of the thickness of the Chinook Pass Member (more than half of visible sections) consists of extremely thick, tabular and laterally continuous beds (normally graded fiamme-andesite breccia, facies 1; fiamme-andesite breccia, facies 2; normally graded fiamme breccia, facies 3; reversely graded fiamme breccia, facies 4). The extremely thick beds are intercalated with very thin to thick (0.001–1 m), laterally continuous, planar beds that indicate sedimentation in a below wave-base environment. The facies 1–4 are composed primarily of angular pumice clasts of intermediate composition and their extremely thick, unstratified, graded facies suggests deposition from eruption-fed, water-supported volcaniclastic density currents (Fig. 3.32a). The presence of minor intercalated beds, such as clast-supported polymictic breccia-conglomerate (facies 7) and reversely to normally graded pumice breccia (facies 12) have a subaerial signature, and sub-rounded dense clasts in basal breccia of facies

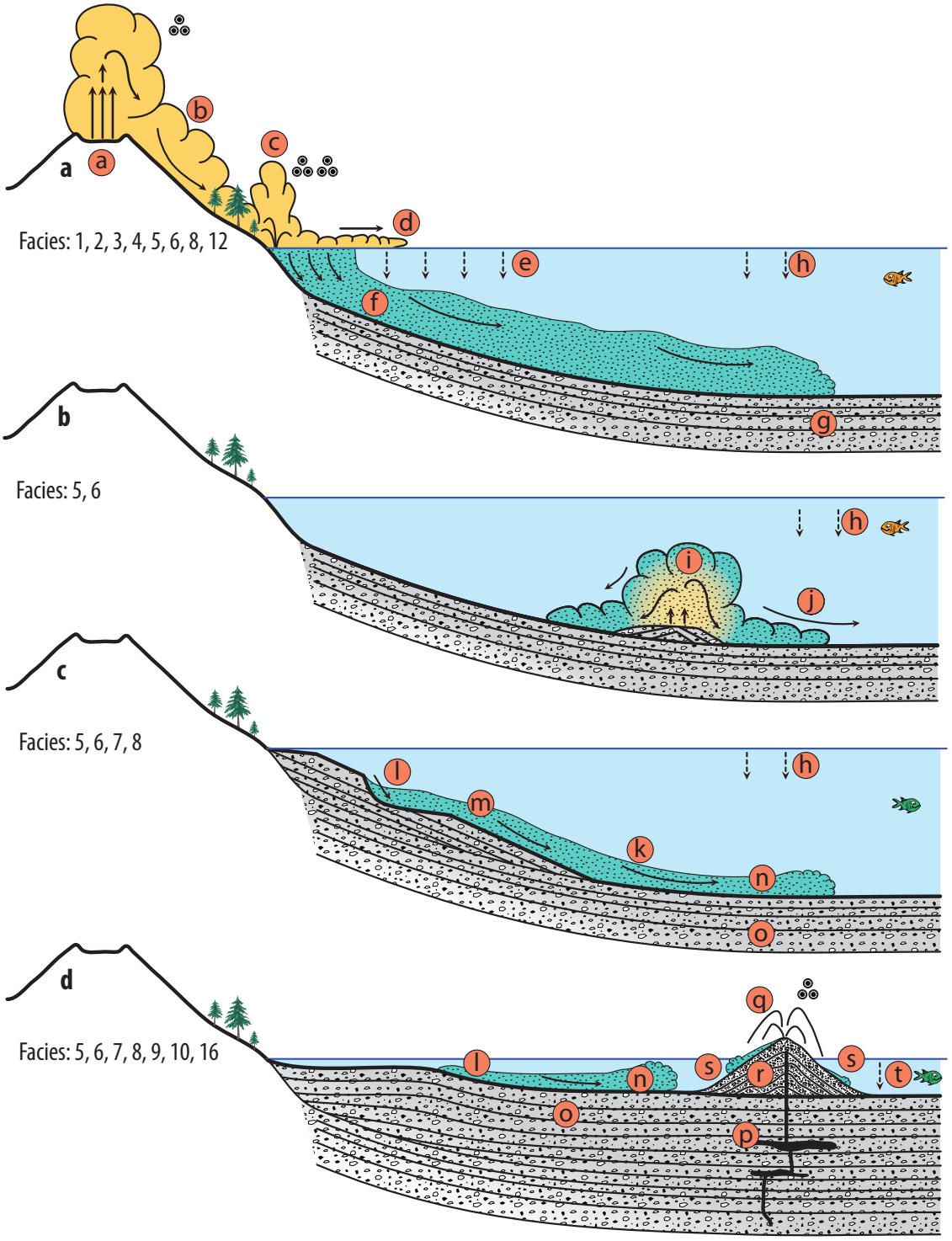

Fig. 3.32 Inferred depositional processes in the Ohanapecosh Formation; no time sequence is implied; **a)** Subaerial magmatic gas-driven, pumice-forming explosive eruption (a) followed by collapse of the eruption column and creation of magmatic gas-supported pyroclastic flow towards water body (b). Coastal steam explosion (c) due to contact of hot pumice with water [e.g. Cas and Wright, 1991; Freundt, 2003; Dufek et al., 2007]. Dilute pyroclastic density current flows over the water body (d). Pumice clasts from dilute pyroclastic density current may stay buoyant and create raft (e), to eventually generate saturation grading in reversely to normally graded pumice breccia (facies 12). Dense part of the pyroclastic flow enters water and transforms into a subaqueous volcaniclastic density current (f) that deposits tabular beds (facies 1, 2, 3, 4, 5, 6, 8) on the basin floor (g). Background sedimentation (h) produces thin beds of fine sandstone and mudstone (facies 8); **b)** Alternative eruption model, with subaqueous explosive pumice-forming eruption on the sea floor. Eruptive column waterlogs (i) and collapses in water-supported volcaniclastic density currents (j) and sediments in tabular beds (facies 5, 6) on basin floor; **c)** Mass-wasting processes (k) remobilise unconsolidated aggregates, creating subaqueous volcaniclastic density currents (l) that forms tabular beds (facies 5, 6, 7, 8) on the basin floor (m). Background sedimentation (h) produces interlayers of thin beds (facies 8); **d)** Same remobilisation process (k) as in b, but in shallower

water. Subaqueous volcaniclastic density currents (k) sediment as tabular beds (facies 5, 6, 7, 8) on the shallow basin floor (n). Shallow intrusions of basalt (o, facies 16) and subaqueous to locally subaerial eruptions (p) build scoria cone of mafic volcanic breccia (q; facies 10) by fallout, suspension, subaerial and subaqueous density currents and remobilisation (r). Scoria cone (q) is discordant with general stratigraphy. Background sedimentation and fallout from eruption column (facies 9) produces interlayers (s) of thin beds (facies 8).

1–3 suggest that the entire sequence of facies 1–4 was sourced from subaerial vents, and derived from subaerial pyroclastic flows that passed the shoreline to transform in water-supported volcaniclastic density currents.

White Pass Member

The White Pass Member collected volcaniclastic sediments from at least two main sources. Most volcaniclastic beds were deposited from subaqueous volcaniclastic density currents generated by subaerial or subaqueous explosive eruptions or remobilisation of unconsolidated aggregates (Fig. 3.32). The major contribution comprises widespread pumiceous volcaniclastic facies of intermediate composition that are very thinly to extremely thickly bedded, planar and laterally continuous (graded or massive volcanic breccia, facies 5; coarse volcanic breccia, facies 6; fine sandstone and mudstone, facies 8). Small-volume, mafic, very thinly to thickly bedded volcaniclastic facies (fine sandstone and mudstone, facies 8; fine mafic sandstone, facies 9; mafic volcanic breccia, facies 10) were generated by weak intrabasinal explosive eruptions and sediment remobilisation, and indicate that one source that was in shallow water or subaerial (Fig. 3.32d).

Strong differences in grain size and average bed thickness occur between sections in the White Pass Member. In modern subaqueous volcaniclastic basins, maximum bed thickness and maximum coarseness occur close to the main transport path and in a medial position relative to the source [e.g. *Trofimovs et al*., 2006; *Gardner*, 2010]. Distal and lateral equivalents are thinner and finer grained. Two settings of deposition in relation to the sediment transport path can be inferred for the White Pass Member. The White Pass section contains the coarsest and thickest beds of the White Pass Member (up to 25 m; coarse volcanic breccia, facies 6). This section is interpreted to record deposition centred on the main sediment transport paths at a medial position compared to the source, in a low-gradient basin. In comparison, beds present in the Ohanapecosh Campground and Backbone Ridge sections are overall thinner and finer grained (fine sandstone and mudstone, facies 8; poorly porphyritic andesite breccia, facies 14; fiamme sandstone and fiamme mudstone, facies 15). Thus, the Ohanapecosh Campground and Backbone Ridge sections were probably situated in a more distal and/or lateral position compared to the main sediment transport path recorded in the White Pass section. Alternatively, the drastic diminution of coarse and very thick deposits may be associated to flow transformation from cohesive to more dilute subaqueous volcaniclastic density currents [e.g. *Komar*, 1971; *Hampton*, 1972; *Fisher*, 1983; *Weirich*, 1989] by change of basin floor morphology or injection of water in the density current [e.g. *Mulder and Alexander*, 2001].

These facies variations suggest a main broad westward direction of sediment transport in the White Pass Member.

The two sections of the White Pass Member from each side of the Ohanapecosh Valley Fault include multiple beds of mafic volcanic breccia (facies 10; Figs 3.11, 3.12). These beds are interpreted to broadly correlate with the mafic scoria-rich facies throughout the White Pass Member. The thick sequence of mafic volcanic breccia containing fine sandstone and mudstone (facies 8) with accretionary lapilli and intrusions of vesicular basalt (facies 16) in the White Pass section indicate proximity to a subaerial to shallow water scoria cone, whereas the thinner sequences of mafic volcanic breccia in the Ohanapecosh Campground and Backbone Ridge sections probably formed at a greater distance from the vent(s).

Johnson Creek Member

The Johnson Creek Member consists of very similar facies to the Backbone Ridge section of the White Pass Member, and is therefore interpreted in a similar way. It is chiefly composed of thin to very thick beds of pumice fragments of intermediate composition (graded or massive volcanic breccia, facies 5; fiamme sandstone and fiamme mudstone, facies 15). These facies probably accumulated in a distal and/or lateral environment with respect to the coarser and thicker facies in the White Pass section. This broad westward direction of sedimentation was proposed by Winters [1984].

Ohanapecosh Formation

The Ohanapecosh Formation provides a good example of the complexity possible in subaqueous volcaniclastic basins associated with volcanoes (Fig. 3.32). The absence of facies entirely derived from shoreline processes [e.g. coarse conglomerates, well sorted pebbly sandstones, etc.; *Allen et al*., 2007] precludes a volcaniclastic apron environment. Most clasts in the Ohanapecosh Formation are angular, which suggests minimum residence in a subaerial or shoreline environment.

The extent and internal variations of the Ohanapecosh Formation indicate deposition of >800 m volcaniclastic sediments in one or several wide basins that could have formed as a far field response to the regional extension further to the northeast during the Eocene [*Johnson*, 1984; *Johnson*, 1985; *Vance et al*., 1987; *Cheney and Hayman*, 2009; *Evans*, 2010]. The three members are close enough (<10 km) to be part of a single, wide basin. However, the lithofacies and alteration pattern of the Chinook Pass Member are different from those in the White Pass Member and Johnson Creek Member, which suggests deposition in two separate basins. The poor exposure between the studied sections precludes a better understanding of the depocentres and their stratigraphic relationships to each other.

The major eruption centres that fed the Ohanapecosh Formation have not been identified, but a broad westward sediment transport is suggested by the facies architecture of the White Pass Member, and partially by the Johnson Creek Member. The flow-banded dacite at Cougar Lake (facies 17) is probably contemporaneous with the Ohanapecosh Formation, and reflects emplacement of an intrabasinal lava or dome. Coherent facies found in the area southeast of Packwood [*Swanson*, 1996; *Swanson et al*., 1997] and at Indian Bar [*Fiske et al*., 1964] were proposed to be remnants of eruption centres associated with the Ohanapecosh Formation. With the exception of the White Pass example (facies 16), it remains unclear whether or not the mafic intrusions are contemporaneous with the Ohanapecosh Formation.

Effect of ash on the coherence of volcaniclastic density currents

Electrostatic properties of clay minerals control the interparticulate forces that induce the subaqueous volcaniclastic density currents to behave with a viscoplastic rheology [*Hampton et al*., 1996; *Ilstad et al*., 2004b]. Clay minerals, the components that conventionally gives their cohesion to debris flows, are likely to be absent from numerous types of volcaniclastic density currents, preventing support mechanism dominated by matrix strength forces. Glass shards [commonly 1–2,000 μm; e.g. *Heiken*, 1974] have a large surface:volume ratio and are known for their electrostatic and capillarity properties, especially in the atmosphere [*Gilbert et al*., 1991; *Schumacher and Schmincke*, 1995; *Textor et al*., 2006]. The role played by clay minerals to create cohesion in debris flows may be taken instead by fine glass shards. Thus, matrix-rich deposits of subaqueous volcaniclastic density currents are likely to be deposited in a fashion including cohesion forces. To the contrary, fines-depleted subaqueous volcaniclastic density currents are more likely to be chiefly governed by granular forces.

7. CONCLUSIONS

The >400 km^2 Ohanapecosh Formation (Washington State, USA) is an Eocene-Oligocene volcaniclastic succession generated by volcanism in the Central Cascades. The formation is >800 m thick. Multiple sources, eruption types, and transport and depositional processes are necessary to explain the extent and diversity of volcaniclastic lithofacies. Tabular, laterally continuous, very thick to extremely thick (1–50 m) and very thin to thick beds (0.001–1 m) and rare presence of fossils suggest sedimentation in a below wave-base lacustrine environment. Lack of coarse-grained conglomerates and other facies including clasts reworking precludes shoreline processes and deposition in a volcanic apron. Therefore, the Ohanapecosh Formation is considered to record deposition in a below wave-base basin.

The Ohanapecosh Formation comprises three members defined by facies association and regional extent. The lithofacies and alteration patterns of White Pass Member and Johnson Creek Member differ strongly from those in Chinook Pass Member, which suggests that they correspond to two depocentres.

In the Chinook Pass Member, four eruption-fed facies that account for ~70% of the preserved section were deposited from eruption-fed, water-supported, subaqueous volcaniclastic density currents. The remaining facies are less thickly bedded and involved remobilisation of pyroclasts and other fragments by less voluminous subaqueous volcaniclastic density currents. It is more likely that the vent was subaerial, because intercalated facies suggest suspension from pumice rafts and resedimentation from above wave-base environments; basal dense clast breccia in three extremely thick facies include coarse sub-rounded dense clasts that were probably incorporated from a shoreline setting. Thus, eruption-fed facies are considered to have been deposited from subaqueous volcaniclastic density currents derived from subaerial pyroclastic flows that entered into water.

In the White Pass Member, a broad westwards transport direction is inferred from variations in thickness and coarseness of the pumice-rich facies. The overall good angularity of the clasts suggests most facies were either resedimented from water-saturated, non-welded pumice-rich pyroclastic deposits, or eruption-fed from subaerial or subaqueous eruptions. Mafic volcanic breccia and vesicular basalt intrusions indicate a local intrabasinal scoria cone.

Variations in grading, bed thickness, matrix content and clast angularity, and overall absence of erosive contacts in the very thick to extremely thick (1–50 m) beds indicate that these facies were deposited by a range of volcaniclastic density currents that range widely in particle concentration, from what were probably of cohesive types of high-concentration density currents to turbidity currents.

4

Effusive-to-explosive transition during an underwater eruption: Dogashima revisited (Japan)

1. INTRODUCTION

On land, active lava domes can be destroyed by open-vent explosive, pumice-forming eruptions [e.g. *Matthews et al.*, 1997; *Sparks*, 1997; *Robertson et al.*, 1998; *Rosi et al.*, 2004; *Martel and Poussineau*, 2007; *Platz et al.*, 2007]. In this chapter, I describe a Pliocene andesitic volcanic succession generated by an effusive-to-explosive eruption in a submarine setting, and I compare the eruption mechanism with equivalent subaerial processes and subaqueous non-explosive dome destruction.

The juvenile components in this succession have a uniform andesitic composition but are strongly bimodal in terms of vesicularity. One population (non-vesicular, coarse, quenched margins) reflects the former presence and destruction of an active lava dome and the other (highly vesicular, fine, ragged) reflects open-vent explosive fragmentation of vesicular magma. I consider the processes known to trigger explosive dome destruction and explore the consequences of these processes operating underwater. The explosive eruption column behaviour is compared to other styles of pumice-forming explosive eruptions. This study is a first step in the recognition of volcaniclastic facies indicative of subaqueous effusive-to-explosive transitions in eruption style.

This study is based on a sequence at Dogashima (Izu Peninsula, Japan) which is particularly well exposed and preserved. The formation was recognized as the product of subaqueous explosive eruptions by Fiske [1969] and Cashman and Fiske [1991] and provided the data (relationships between size and density of clasts) that underpin the widely accepted model for particle fallout from submerged explosive eruption plumes. My facies analysis suggests instead that much of the unit, including the interpreted subaqueous fallout deposit, was deposited from subaqueous, eruption-fed density currents.

This chapter describes the lithofacies of the Dogashima Formation, and focuses on eruption and depositional processes of major eruption-fed units. Interpretation of the eruptive activity is based on data collected in this study, and published thermoremanent magnetic data [*Tamura et al.*, 1991].

1.1. Terminology and methods

The term breccia is non-genetic and describes a clastic deposit composed mostly of angular clasts >2 mm [*Fisher*, 1961]. Fine breccia is used hereafter for breccia with average clast size <10 cm. Finer grained, pumice-rich facies are referred to as pumice sandstone (1/16–2 mm) and shard-rich siltstone (1/256–1/16 mm) without implying genesis. Bed thickness terms follow Ingram [1954]; I have added the term “extremely thick” for beds >10 m thick.

The term "flow" is used as a synonym of "current". Volume percentages of clasts and grain size distribution in volcaniclastic rocks were calculated by image analysis and functional stereology (chapter 2). Geochemical analyses were carried out at the University of Tasmania. Clast composition was determined by X-ray fluorescence (XRF) with a Philips PW1480, whereas crystal analyses were performed on a Cameca 100X electron microprobe.

2. GEOLOGICAL SETTING OF THE DOGASHIMA FORMATION

The Dogashima Formation (Fig. 4.1) is part of the Miocene-early Pliocene volcanogenic Shirahama Group that covers 500 km^2 on the Izu Peninsula, ~130 km southwest of Tokyo, Japan [Appendix D; *Ibaraki*, 1981; *Tamura*, 1994; *Tani et al*., 2011; *Geological Survey of Japan*, 2010]. The Shirahama Group is part of the northern extension of the Izu-Bonin arc, related to the westward subduction of the north-western margin of the Pacific plate under the Philippine plate [*Taylor*, 1992; *Tani et al*., 2011]. The north-western subduction of the Philippine plate under the Eurasian plate (including Japan) has resulted in collision and uplift of the northern segment of the Izu-Bonin arc (including the Shirahama Group) at ~1 Ma [*Huchon and Kitazato*, 1984].

The Shirahama Group spans 5.5–1.7 Ma [UPb; *Tani et al*., 2011], comprises diverse volcanic and subvolcanic facies (lavas, dykes, cryptodomes and volcaniclastic facies). It probably accumulated in a region with complex sea-floor topography, comparable to that of the northern part of the modern arc [e.g. *Yuasa et al*., 1991; *Takahashi and Saito*, 1997]. The Shirahama Group is thought to include the products of at least six scattered and overlapping eruption centres [*Sawamura et al*., 1970; *Kano*, 1983; *Yamada and Sakaguchi*, 1987; *Kano*, 1989]. Gordee [2008] and Geological Survey of Japan [2010] report minor subaerial influence at 11 km south of Dogashima with local beds of charcoal and conglomerates.

The succession is little deformed and virtually unaltered. Most lavas and intrusions range in composition from basaltic andesite to dacite; basalt and rhyolite are rare [*Tamura*, 1994]. The Shirahama Group is derived from a magma that was a mixture of two magma series [*Tamura et al*., 1991]: a tholeiitic series, ranging from basalt to dacite, possibly derived from a single basaltic parent, and a calc-alkaline series, composed of andesite and dacite, derived from a Mg-rich andesite source. Sr/Nd isotopes confirm derivation of the two magma series from a single mantle source and no influence of crustal assimilation [*Tamura and Nakamura*, 1996].

Although detailed information on the environments of eruption and deposition of the Shirahama Group is missing, the widespread presence of numerous planktonic foraminifera species [e.g. *Ibaraki*, 1976; *Ibaraki*, 1981] suggests that an open-marine environment predominated. The abundance of hyaloclastite and pillow lavas throughout the Shirahama Group and in particular, in the Matsuzaki Formation [*Kano*, 1983; 1989;

Tamura, 1990; 1994] also attest to a subaqueous environment. The possible presence of an island in the setting in which the Shirahama Group accumulated near Shimoda and Shirahama towns <20 km southeast of Dogashima is inferred from conglomerates in the late Miocene Asahi Formation and cross-bedded, coastal channel facies, calcarenite and limestone in the early Pliocene Harada Formation [*Matsumoto et al*., 1985]. From rare earth element abundances and mineral assemblages in lavas, Tani et al. [2011] proposed a rear-arc setting for the Shirahama Group, at >20 km from the former and actual Izu-Bonin volcanic front. This distance from the arc is consistent with the Shirahama Group being in an open-marine setting and entirely below wave-base. The absence of subaerially sourced components in the enclosing facies of the Dogashima Formation strongly reinforces a fully submarine environment. I infer that the Dogashima Formation accumulated in an open-marine, below wave-base basin that included seamounts and volcanic islands.

2.1 Previous work

The Dogashima Formation [3-4 Ma K-Ar; *Tamura*, 1994] is 5 to >80 m thick and includes three main subdivisions [*Fiske*, 1969; *Tamura*, 1990; 1994]. A thermo-remanent study at the base of the middle subdivision led Tamura et al. [1991] to interpret that it was a "hot pyroclastic debris flow" deposit, emplaced in a "shallow marine environment". This interpretation was supported by the presence of chilled margins on the andesitic clasts and thermoremanent temperatures of 450°C in clast rims (5 cm width) at deposition. The andesitic breccia is overlain by a 5-m-thick interval of pumice-rich breccia interpreted in part to be a submarine fall deposit from a submerged explosive eruption plume [*Cashman and Fiske*, 1991]. Ratios of sizes of pumice clasts versus dense andesitic clasts are in the range of 5:1 to 10:1 for this part of the breccia. The bimodality in clast sizes was reproduced in experiments and analysed in terms of settling velocities in water. Cashman and Fiske [1991] developed the concept of hydraulic equivalence (i.e. hydraulic sorting; chapter 5), which refers to the ideal situation where the deposit is an accumulation of clasts of different diameter, density and/or shape but with the same terminal fall velocity [*Rubey*, 1933; *Clift et al*., 1978; *Cashman and Fiske*, 1991; *Manville et al*., 2002; *Burgisser and Gardner*, 2006].

3. SETTING OF THE DOGASHIMA FORMATION

The Dogashima Formation extends over >1.5 km^2 of mostly coastal cliff outcrops between Dogashima and Sawada, Izu Peninsula, Japan (Fig. 4.1). Its volume is estimated at $10x10^6$ m^3. The outcrops are well preserved, accessible and stratigraphically continuous and conformable (Fig. 4.2). Numerous joints and faults have a constant northerly strike over the whole area, and overall show little or no displacement. The Dogashima Formation is tilted ~10° eastwards.

The mapped area (Fig. 4.1) is delimited by subvertical faults and intrusions to the north, and by the Matsuzaki Formation to the south [*Tamura*, 1994]. At locality A, the Dogashima Formation overlies the Matsuzaki Formation with an erosive contact (Fig. 4.3a). The Matsuzaki Formation is exposed over ~3 km south of Dogashima town, and mainly consists of coherent andesite and monomictic andesite breccia. Minor units of pumice breccia composed of aphyric pumice clasts, and andesitic fluidal-clast breccia are also present locally.

I refer to the three subdivisions of the Dogashima Formation recognised by Tamura [1990] as Dogashima 1, Dogashima 2 and Dogashima 3 (Fig. 4.2). Dogashima 1 is >15 m thick, mostly exposed in the southern part of the studied area, and composed of multiple, laterally extensive or lenticular, thick graded beds of pumice breccia, cross-bedded pumice breccia and volcanic sandstone and shard-rich siltstone. Dogashima 2 is

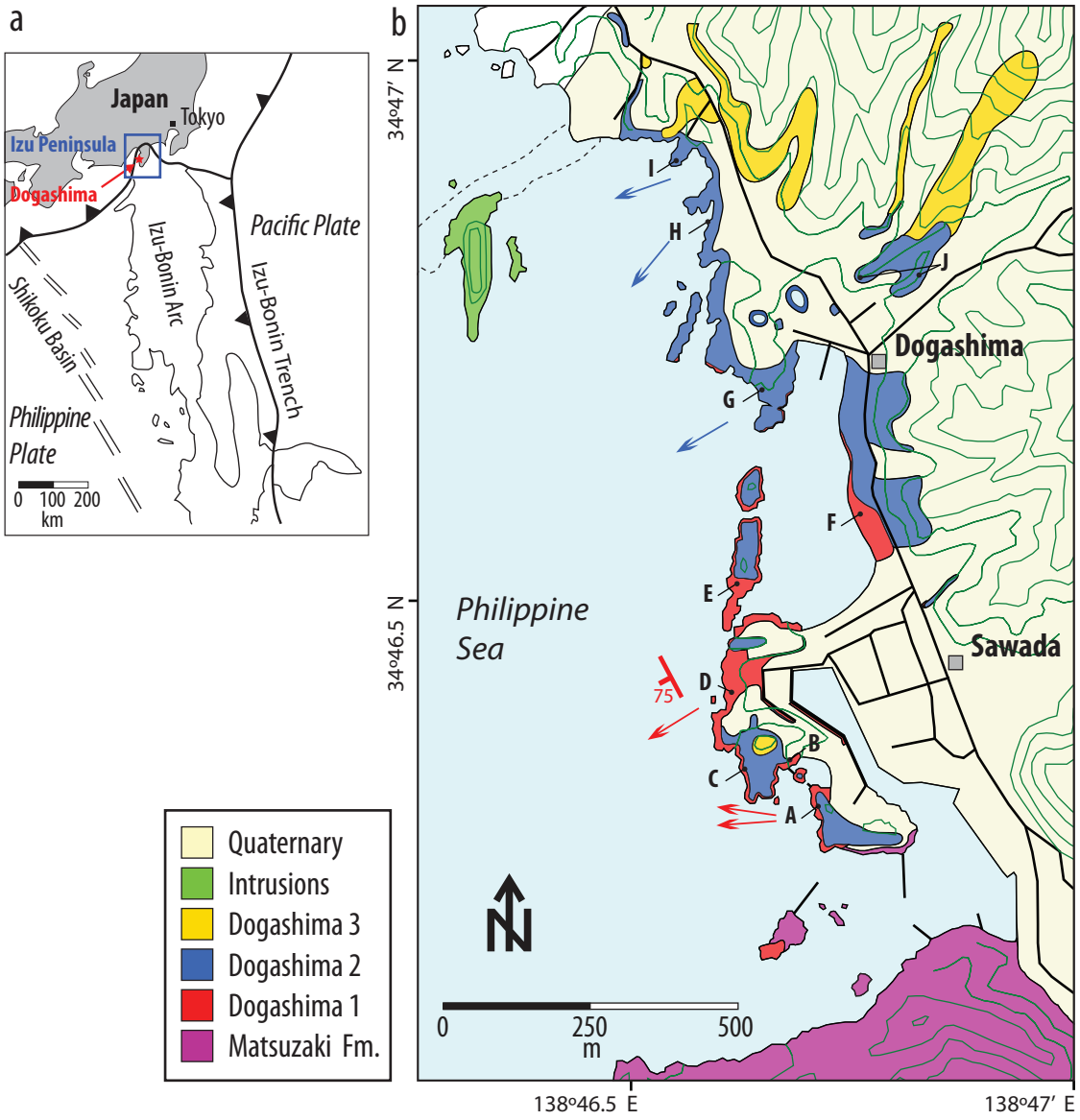

Fig. 4.1 Location and geological maps. **a)** Simplified map of the Izu Peninsula (Japan) and the Izu-Bonin arc. Thin line is the 3,000 mbsl contour; **b)** Local geological map of the Dogashima Formation at Dogashima, Japan; capital letters are studied localities; arrows show palæo-current directions, their colours correspond to the studied unit; dip symbol for syn-sedimentary faults (Table 4.3), thick black lines for roads. On land contour (in green) spacing is 20 m.

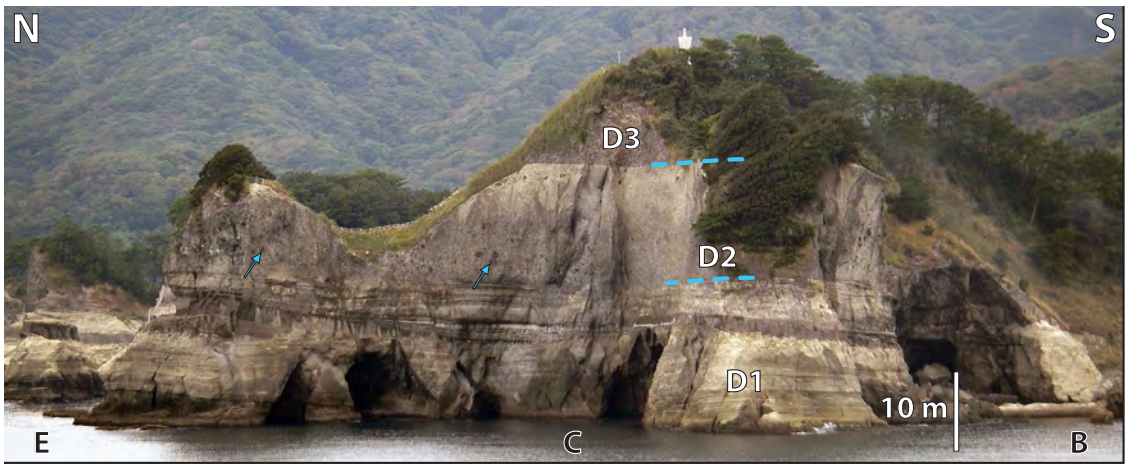

Fig. 4.2 North-south coastal section of the Dogashima Formation at localities B, C and E. The Dogashima Formation is composed of three major subdivisions, Dogashima 1 (D1), Dogashima 2 (D2) and Dogashima 3 (D3). In these sections, D1 is composed of lenticular or tabular, thin to very thick beds, whereas D2 consists of one extremely thick tabular bed that includes coarse clasts of grey andesite (blue arrows) at the base. D3 is massive and overlies D2 with a very sharp contact.

15 to 30 m thick, covers the whole area and is composed of two coarse, andesite breccia units, two pumice breccia units, and multiple beds of planar bedded pumice breccia and cross-bedded pumice breccia-conglomerate. The contact between Dogashima 1 and Dogashima 2 is a disconformity, and Dogashima 2 lies in a palæo-valley eroded into beds of Dogashima 1 between localities A and G. A local palæo-low is visible between localities A and B.

Dogashima 3 is >50 m thick, mostly preserved in the northern part of the area and composed of coarse andesitic breccia. It overlies Dogashima 2 with a knife-sharp, locally disconformable contact. Its upper boundary has not been identified due to vegetation cover and/or erosion.

4. COMPONENTS IN THE DOGASHIMA FORMATION

White pumice clasts

White pumice clasts (Fig. 4.4) with slight yellowish hue are abundant in Dogashima 1 and 2. No distinction in texture and composition could be found between the white pumice clasts of Dogashima 1 and Dogashima 2. They have >60 vol.% vesicles, a uniform phenocryst population and narrow range of composition (62.3–63.5 wt.% SiO_2; Table 4.1). Their compositions plot across the andesite and dacite field boundary. The coarsest pumice clasts (up to 1.50 m) commonly have <10-cm-wide rims locally enhanced by the effects of weathering, and interpreted to result from quenching. Many coarse white pumice (>10 cm) show concave and convex curviplanar shapes, and breadcrust texture is rarely preserved. Vesicle textures are partially preserved everywhere (Fig. 4.4b), although most of the glass has devitrified during diagenesis. The total volume of phenocrysts in white pumice clasts is <40 vol.%. Plagioclase is the most common phenocryst (25-35 vol.%,

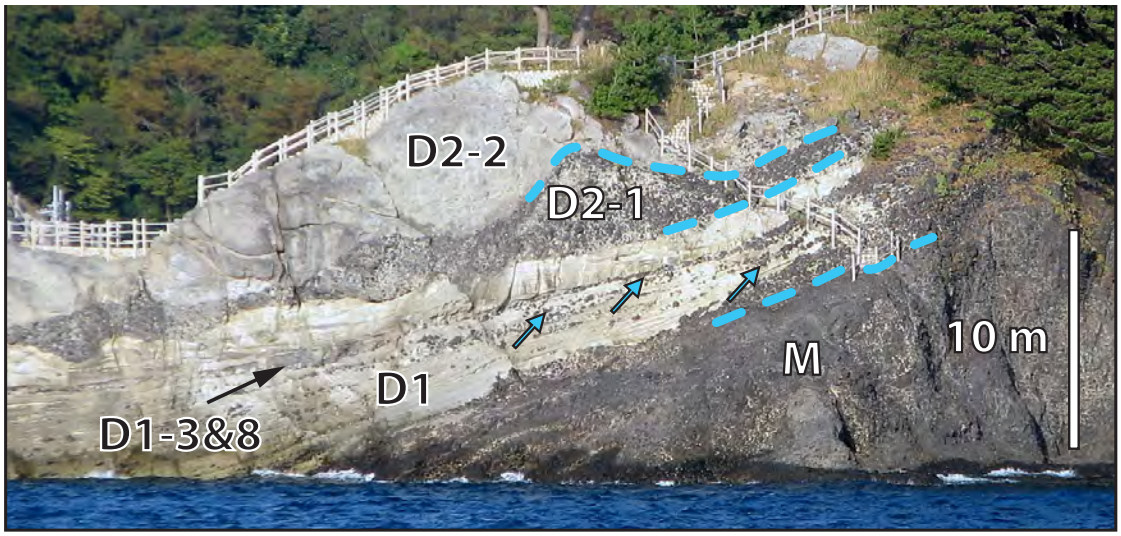

Fig. 4.3 Onlap contact between the Dogashima Formation and the Matsuzaki Formation (M) at locality A. The formations have a regional ~10° tilt eastwards (to the right) but here show primary dip to the west. Dark andesite clasts (blue arrows) of the Matsuzaki Formation are present in the polymictic volcanic breccia beds (D1-3 and D1-8) of Dogashima 1. The basal polymictic volcanic breccia (D2-1) contains dark andesite clasts of the Matsuzaki Formation and is in erosional contact with Dogashima 1. Massive grey andesite breccia (D2-2) has an irregular contact with the basal polymictic volcanic breccia (D2-1); photo courtesy S.M. Gordee.

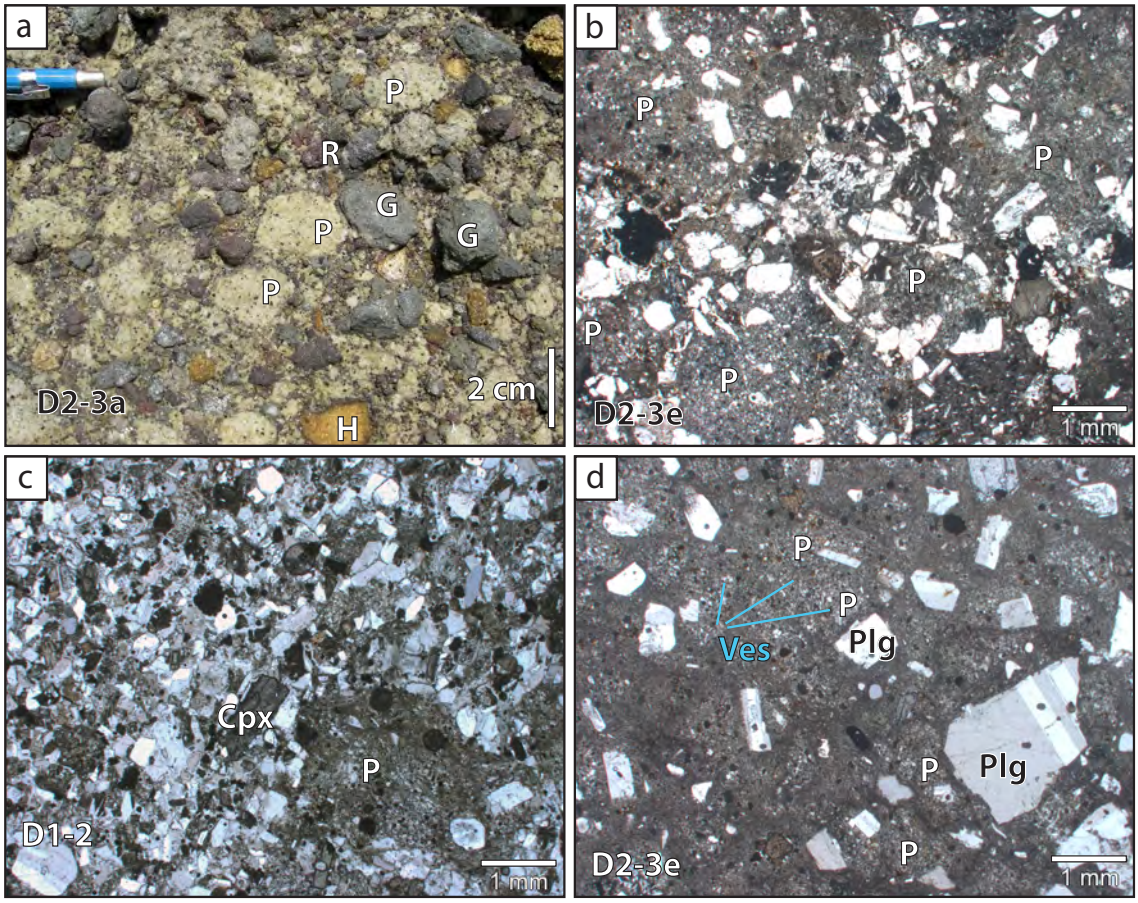

Fig. 4.4 Examples of white pumice clasts. **a)** The white pumice breccia (D2-3a) comprises white pumice clasts (yellowish white, P), grey andesite clasts (grey, G), red andesite clasts (red to purple, R) and hydrothermally altered volcanic clasts (yellow, H), locality G; **b)** White pumice clasts in matrix of free broken crystals, white pumice breccia in unit D2-3-e. Sample IZU-37, crossed nicols; **c)** Free broken crystals [(mainly plagioclase (Plg) and clinopyroxene (cpx)] and white pumice clasts (P), in pumice breccia (D1-2). Sample IZU-12, crossed nicols; **d)** White pumice clasts (P) and plagioclase fragments (Plg) in white pumice breccia in unit D2-3-e. Vesicles (ves) are locally preserved. Sample IZU-37, crossed nicols.

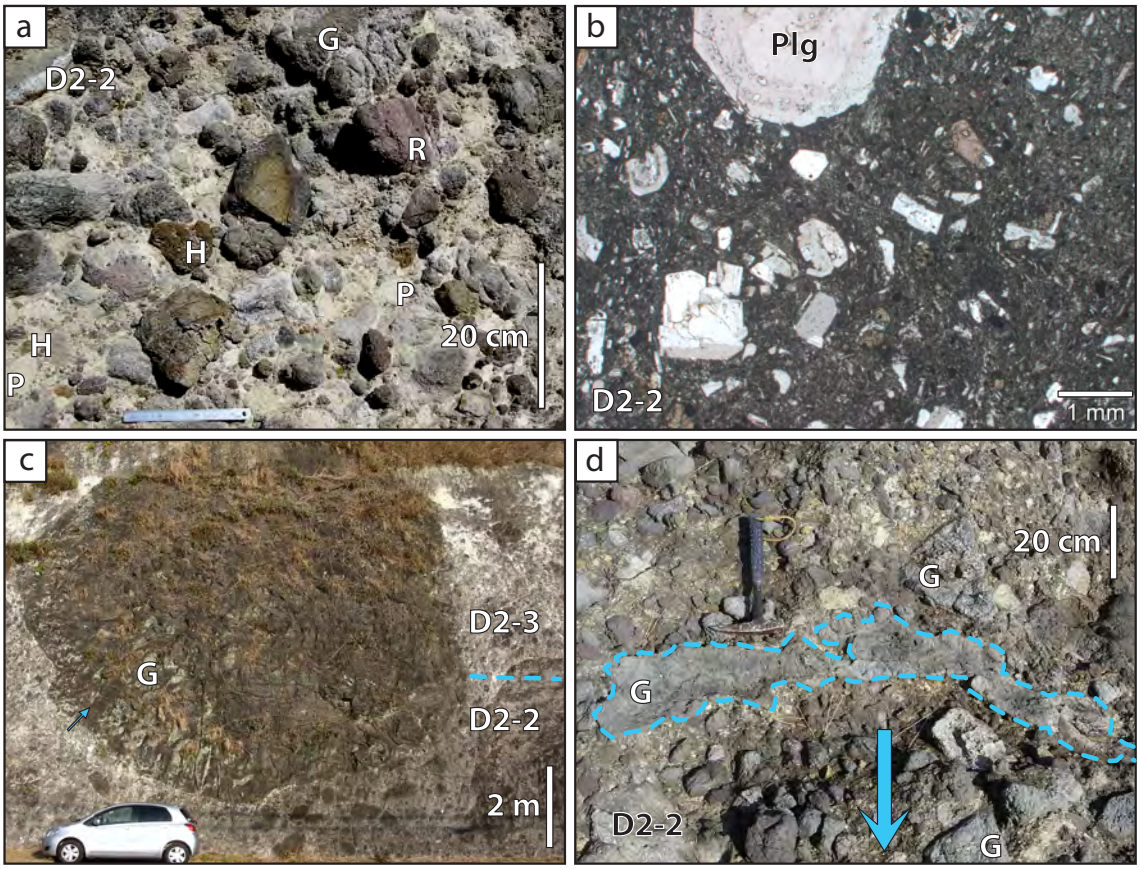

Fig. 4.5 Examples of grey andesite clasts. **a)** The massive grey andesite breccia (unit D2-2), at locality F. Clast types are grey andesite (grey, G), white pumice (white, P), red andesite (red-purple, R) and hydrothermally altered volcanic clasts (yellow to brown, H); **b)** Typical grey andesite clast with trachytic texture and plagioclase phenocryst (Plg) in unit D2-2. Sample IZU-15, crossed nicols; **c)** Locality F, outsize grey andesite clast (G) in the massive grey andesite breccia (D2-2), overlain by white pumice breccia (D2-3). Note the weak columnar joints (blue arrow); **d)** Elongate, irregular grey andesite clast in the massive grey andesite breccia (D2-2), amongst other angular clasts of grey andesite (G), white pumice and red andesite, birds-eye view, arrow indicates inferred flow direction in upper units, locality G.

average <1–1 mm, max 3 mm; An_{48-70}; Appendix D). Phenocrysts are equant and typically broken on one face, and are also found as clusters. Clinopyroxene, orthopyroxene and opaque phases are subordinate (<5 vol.%) and are no more than 0.5 mm in size; quartz phenocrysts are very rare (<0.1 vol.%).

Grey andesite clasts

Grey andesite clasts are grey to dark grey, non-vesicular and andesitic (60.9–61.0 wt.% SiO_2; Figs 4.5a, 4.5b; Table 4.1). They are unaltered and chiefly equant, and present only in Dogashima 2. Coarse clasts (>25 cm) are equant to ovoid, have devitrified quenched rims several cm wide and internal radial joints, and rare fluidally shaped clasts are present (Figs 4.5c, 4.5d). A temperature at deposition of 450 °C was determined for the coarsest of these clasts by Tamura et al. [1991] using thermoremanent magnetisation. These grey andesite clasts contain plagioclase, clinopyroxene, orthopyroxene and opaques phases as phenocrysts (Fig. 4.5b), similar to the white pumice clasts. The phenocryst content of grey andesite clasts (<25 vol.%) is similar to the dense rock equivalent of the white pumice clasts. Plagioclase crystals (15-20 vol.%; An_{49-57}; Appendix D) are equant, euhedral

Sample	Izu-03	Izu-30	Izu-45	Izu-04	Izu-51	Izu-52	Izu-26	Izu-55	Izu-05	Izu-24	Izu-25	Izu42	Izu-08
rock type	White pum.	White pum.	White pum.	Grey and.	Grey and.	Incl. in grey and.	Aphyric pum.	Aphyric pum.	Red and.	White pum.	Grey scoria	Grey and.	Dark and.
bed	D2-3a	D2-3c	D2-6	D2-2	D2-2	D2-2	D2-4b	D2-6	D2-2	D1-2	D1-3	D3	M
SiO_2	63.12	63.47	62.26	60.87	60.98	57.13	71.02	72.29	59.13	62.72	61.90	62.58	58.77
TiO_2	0.54	0.53	0.53	0.71	0.72	0.87	0.20	0.21	0.77	0.53	0.64	0.63	0.74
Al_2O_3	16.40	15.93	16.30	16.58	16.62	17.80	13.70	13.00	17.35	16.61	18.27	16.10	17.40
Fe_2O_3	5.90	5.96	6.29	7.68	7.70	9.62	2.48	2.32	8.59	6.20	7.12	7.12	8.33
MnO	0.14	0.14	0.16	0.17	0.17	0.18	0.14	0.11	0.20	0.15	0.19	0.15	0.18
MgO	2.24	2.38	2.60	2.82	2.77	3.09	1.69	1.49	3.06	2.38	1.52	2.63	3.08
CaO	5.73	5.26	5.54	6.74	6.78	7.17	1.96	2.00	6.97	5.55	5.58	6.29	7.21
Na_2O	4.19	4.40	4.70	3.17	3.05	3.20	6.43	5.84	3.23	4.18	3.58	3.14	3.06
K_2O	1.59	1.81	1.47	1.09	1.02	0.73	2.33	2.72	0.53	1.54	1.07	1.22	1.08
P_2O_5	0.14	0.13	0.14	0.18	0.18	0.19	0.05	0.03	0.18	0.14	0.14	0.14	0.17
LOI (incl. S)	7.33	12.41	7.47	1.94	2.13	3.03	11.19	12.35	1.46	6.25	8.96	0.84	1.67
TOTAL	**99.63**	**99.88**	**99.94**	**100.02**	**100.04**	**100.00**	**99.83**	**99.50**	**99.87**	**99.95**	**100.15**	**99.75**	**100.03**
S	0.02	0.11	0.13	0.01	0.01	0.02	0.24	0.12	0.01	0.04	0.01	0.01	0.02
Ba	159	135	151	137	143	106	161	175	152	151	142	171	129
Ce	17	15	18	16	19	14	23	20	20	20	18	19	15
Cr	1	2	3	2	2	2	3	1	1	2	16	9	3
Cu	19	20	11	17	22	22	17	17	21	28	20	18	17
La	8	6	7	8	7	8	8	8	7	8	6	7	7
Nb	1	1	2	1	2	1	2	2	2	2	2	2	2
Nd	11	9	11	12	14	13	14	13	14	10	11	13	11
Ni	2	5	3	4	2	4	6	4	4	3	10	4	7
Pb	2	2	4	<1.5	3	7	7	6	3	3	2	3	4
Rb	21	22	18	24	28	10	26	39	8	19	9	20	14
Sc	14	9	12	25	26	34	5	5	27	13	27	20	26
Sr	222	183	216	246	252	262	125	122	256	210	220	226	233
V	61	45	57	157	158	187	15	12	138	82	70	138	153
Y	21	20	20	27	25	23	31	37	26	20	25	25	28
Zn	38	42	42	62	63	83	54	56	72	50	84	52	79
Zr	98	87	87	91	93	75	138	133	96	94	84	98	85

Table 4.1 Major and traces compositions analysed by XRF for various clasts of the Dogashima and Matsuzaki Formations. Concentrations recalculated anhydrous. Pumice, pum; andesite, and; inclusion, incl.

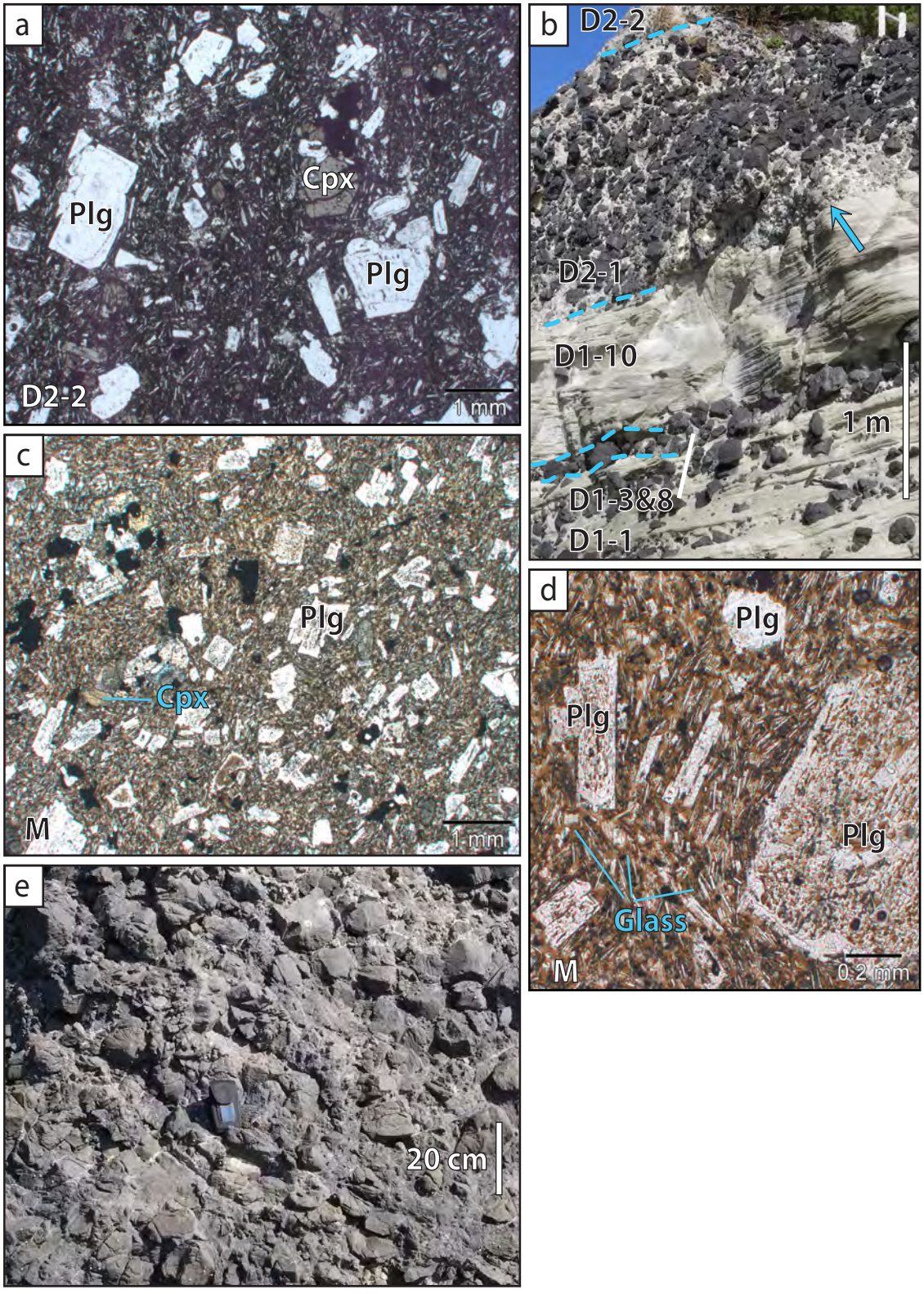

Fig. 4.6 Examples of red andesite and dark andesite clasts **a)** Red andesite clast containing plagioclase (Plg) and clinopyroxene (Cpx) phenocrysts, with trachytic texture in unit D2-2. Sample IZU-05, crossed nicols; **b)** Discordant contact between cross-bedded pumiceous breccia/sandstone (D1-10), and basal polymictic volcanic breccia (D2-1), locality A. This locality is interpreted to be a palæo-high, with beds much thinner than in other localities. Note that presence of dark andesite clasts (the equant-shaped, darkest clasts) is scarce at the base of the basal polymictic volcanic breccia (blue arrow). At this location, a single bed of polymictic volcanic breccia is equivalent to units D1-3 and D1-8; **c)** Dark andesite in Matsuzaki Formation (M). The phenocrysts (plagioclase, Plg; clinopyroxene, Cpx) are finer grained than in grey andesite of the Dogashima Formation (Fig. 4.5b). Sample IZU-08, plane polarized light; **d)** Magnified view on the dark andesite of Matsuzaki Formation (M). Groundmass is glassy (brown colour), and microlites are laths with trachytic texture; plagioclase phenocryst (Plg). Sample IZU-08, plane polarized light; **e)** Dark andesite in Matsuzaki Formation, locality A.

and 2-3 mm long, although clusters are up to 10 mm across. Clinopyroxene (2 mm), orthopyroxene (1 mm) and oxides (1 mm) are subordinate (<5 vol.%), and aggregates composed of these minerals are common. The groundmass has a trachytic texture defined by feldspar microlites. The coarseness of the groundmass is variable; on average, feldspar microlites to microphenocrysts (An_{53-69}; Appendix D) are 0.5 mm long. Scattered, ovoid weakly porphyritic inclusions up to a few cm across have a more mafic composition. One type of inclusion (57.1 wt.% SiO_2; Table 4.1) contains only plagioclase as phenocrysts (2-3 vol.%) in a groundmass of feldspar and subordinate clinopyroxene, orthopyroxene and oxides, whereas a second type contains micro-phenocrysts of plagioclase (50 vol.%) and ferromagnesians phases (10 vol.%) in a very fine-grained groundmass.

Free broken crystals

Crystal fragments and crystals with a veneer of former glass are angular and similar in composition and size to the phenocrysts in adjacent white pumice and grey andesite clasts (Figs 4.4b, 4.5b). Most crystals are plagioclase (An_{51-70}; Appendix D).

Red andesite clasts

The red andesite clasts (Figs 4.4a, 4.5a, 4.6a) are very similar in composition (59.1 wt.% SiO_2; Table 4.1), vesicularity, phenocryst content and plagioclase composition (An_{64-78}; Appendix D) to the grey andesite clasts. They are equant in shape and their maximum size (~30 cm) is much smaller than grey andesite clasts. They occur only in Dogashima 2.

Hydrothermally altered volcanic clasts

These clasts are mostly porphyritic, subrounded and ochre-yellow, brown, dark red, or red (Figs 4.4a, 4.5a). This category includes dense clasts, scoria clasts and clasts of pumice breccia.

Dark andesite clasts

These clasts are poorly vesicular (Figs 4.6c, 4.6d, 4.6e) and slightly lower in SiO_2 than the grey andesite clasts (58.8 wt.% SiO_2; Table 4.1). The phenocryst population is mostly composed of plagioclase (Figs 4.6c, 4.6d) and opaque phases (0.5-1.5 mm; 20 vol.%). Lath-shaped plagioclase micro-phenocrysts (0.1–0.2 mm; >50 vol.%) occur in a brown, glassy groundmass (Fig. 4.6d). These clasts form monomictic breccia in the Matsuzaki Formation (Fig. 4.6e), and occur locally where Dogashima 1 and 2 conformably overlay the Matsuzaki Formation (locality A; Fig. 4.6b).

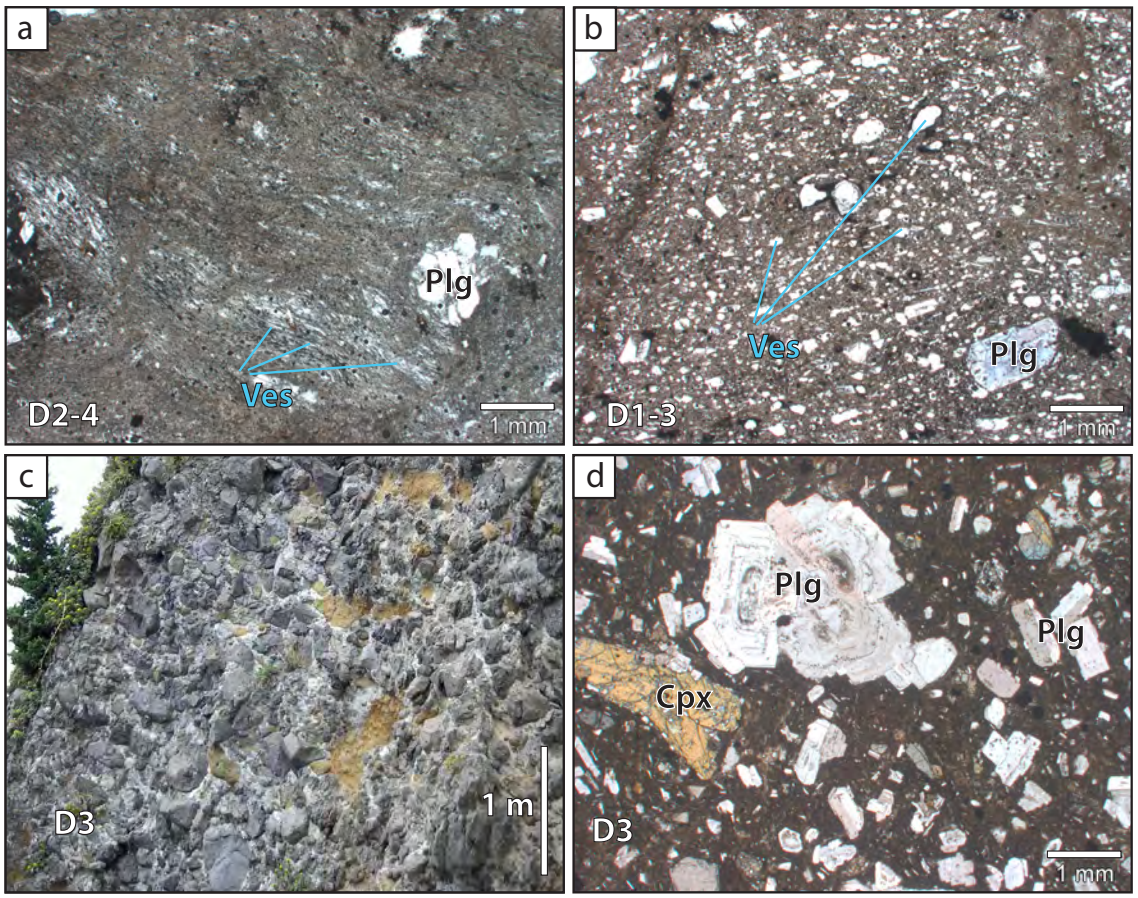

Fig. 4.7 Examples of aphyric pumice, grey scoria and coarsely porphyritic andesite clasts. **a)** Aphyric pumice with very rare plagioclase phenocrysts (Plg) in planar stratified pumice breccia (D2-4). Sample IZU-55, plane polarized light; **b)** Grey scoria in polymictic volcanic breccia (D1-3). Vesicles (Ves) are ellipsoid and minor plagioclase phenocrysts occur in a devitrified groundmass. Sample IZU-25, plane polarized light; **c)** Weakly stratified andesite breccia in Dogashima 3 at locality C, chiefly composed of coarsely porphyritic andesite clasts (grey) and minor hydrothermally altered volcanic clasts (yellow) and white pumice clasts (white). Large yellow-orange domains are actual weathering surfaces; **d)** Coarsely porphyritic andesite clast in Dogashima 3, with plagioclase (Plg) and clinopyroxene (Cpx) phenocrysts (locality I). Sample IZU-42, crossed nicols.

Aphyric pumice clasts

The aphyric pumice clasts have dacitic composition (71.0–72.3 wt.% SiO_2; Table 4.1) and are rare (<1 %). Plagioclase (<1 vol.%) is the only phenocryst present (Fig. 4.7a), and has an average size of 0.1 mm (max 1 mm). Tube vesicles (~60-80 vol.%) are overall much smaller and more elongate than in the white pumice clasts, and the glass is finely devitrified. This almost aphyric pumice type is similar to that found in pumice breccia in the Matsuzaki Formation.

Grey scoria clasts

Grey scoria clasts of andesitic composition (61.90 wt.% SiO_2; Table 4.1) are found only in a specific facies in Dogashima 1. The clasts are pale-grey and are mostly up to 10 cm long. The surfaces of most grey scoria clasts show a fluidal texture that has subsequently been broken into angular pieces. Phenocrysts are minor (<10 vol.%; Fig. 4.7b) and include plagioclase (max 2 mm), clino- and orthopyroxene and rare hornblende. The groundmass

is devitrified. These clasts are moderately vesicular (<50 vol.%) and vesicles are mostly ellipsoidal-shaped and weakly aligned (<0.2 mm, max 3 mm long; Fig. 4.7b). This clast type is closely similar to grey scoria clasts that occur within the fluidal-clast breccia in the underlying Matsuzaki Formation.

Coarsely porphyritic andesite clasts

This clast type makes most of Dogashima 3 (Fig. 4.7c). Phenocrysts (>25 vol.%) are mostly plagioclase (0.5–1 mm; max 10 mm), with minor clinopyroxene, orthopyroxene and opaques (Fig. 4.7d). The phenocryst assemblage and geochemistry give an andesitic composition (62.58 wt.% SiO_2; Table 4.1) that is slightly more evolved than the grey andesite clasts of Dogashima 2. These clasts are very poorly vesicular (<0.5 vol.%). Various types of inclusions are common, and include round-shaped clusters of plagioclase, clinopyroxene and opaque crystals, and poorly porphyritic andesite (<5 vol.% plagioclase and pyroxene crystals). The groundmass is coarse-grained and composed of feldspar and subordinate clinopyroxene, orthopyroxene and opaques.

Matrix

The coarse facies of the Dogashima Formation are mostly clast-supported and matrix-poor. The matrix is mostly sand, and strongly depleted in silt and clay components (<1/16 mm). The matrix in beds of Dogashima 1 and 2 is typically composed of free broken crystals and particles of identical aspect and composition to the clasts (Fig. 4.4b). The exception is the white pumice sandstone matrix that occurs in the weakly stratified andesite breccia of Dogashima 3.

4.1. Composition of clasts in the Dogashima Formation

The bulk compositions of major types of clasts in the Dogashima Formation were determined by XRF (Fig. 4.8; Table 4.1). Most samples of the Dogashima Formation are quartz-normative and have a medium-K composition. Compared to the rest of the Shirahama Group [*Tamura*, 1995], they are transitional between its tholeiitic and calc-alkaline series. Bulk rock compositions match the compositional range of the Shirahama Group (Fig. 4.8a) and the white pumice clasts of Dogashima 2 are very similar in composition to those in Dogashima 1. Vesicular clasts have elevated loss on ignition (LOI; 6-12.5 wt.%; Table 4.1), as well as notable K_2O and Na_2O enrichment compared to dense clasts (LOI ≤3 wt.%). Microprobe analyses of plagioclase phenocrysts in clasts of Dogashima 2, including white pumice clasts, grey andesite clasts and free crystal fragments, and in microlites in the grey andesite clasts, have similar compositions and define a single trend (Fig. 4.9; Appendix D). The plagioclase in the hydrothermally altered andesite clasts is slightly enriched in CaO relative to plagioclase in the grey andesite

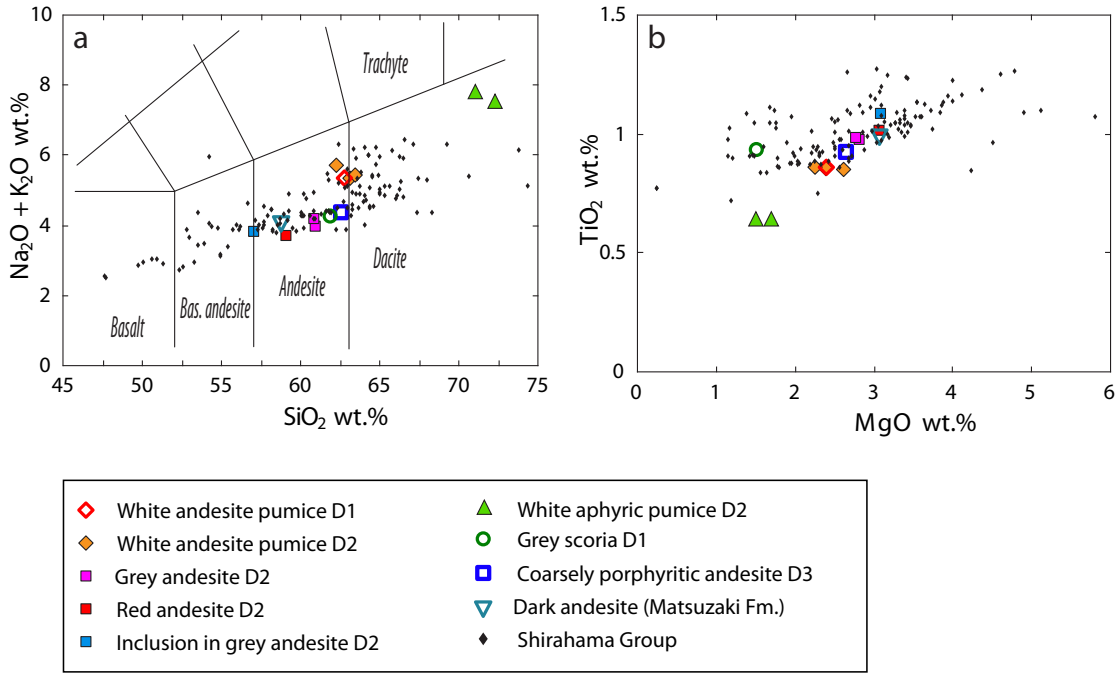

Fig. 4.8 Bulk clast analyses in the Dogashima Formation and Shirahama Group. **a)** Total alkali vs. silica (TAS) diagram for clasts in the Dogashima Formation; compositional fields after Le Bas et al. [1986]; Shirahama Group data from Tamura [1990; 1994; 1995]; **b)** Ti02 vs. Mg0 diagram for clasts in the Dogashima Formation, compared with Shirahama Group analyses [1990; 1994; 1995]. Plotted compositions are recalculated to 100 wt.% anhydrous (Table 1). D1, D2 and D3 for Dogashima 1, Dogashima 2, and Dogashima 3, respectively.

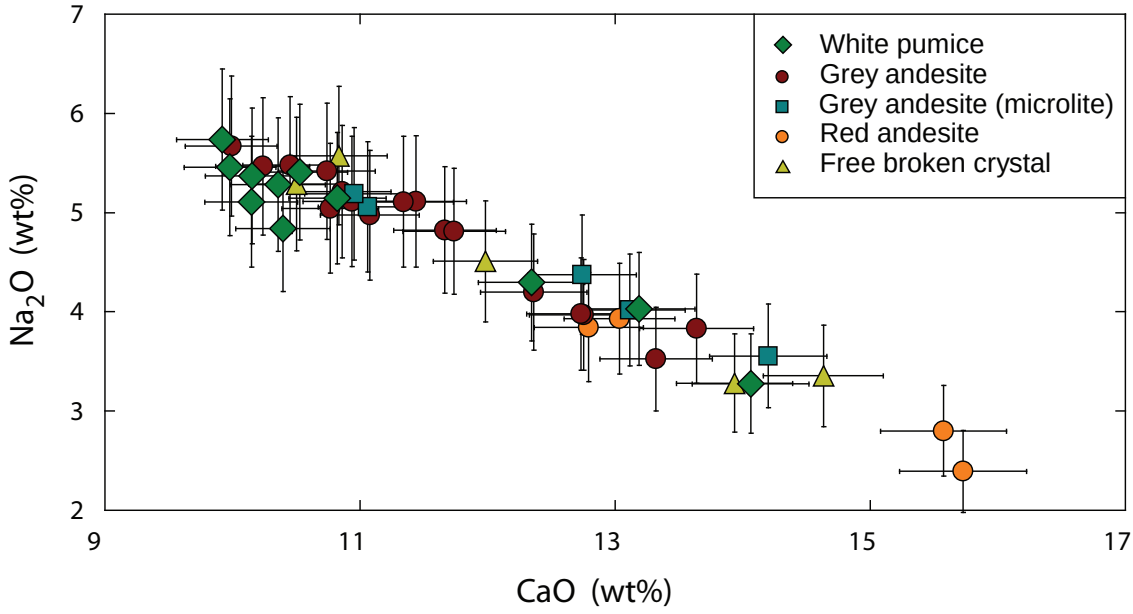

Fig. 4.9 Microprobe analyses of rims and cores of plagioclase crystals in Dogashima 2. Compositions of plagioclase phenocrysts from various origins define a single trend, consistent with a co-magmatic source.

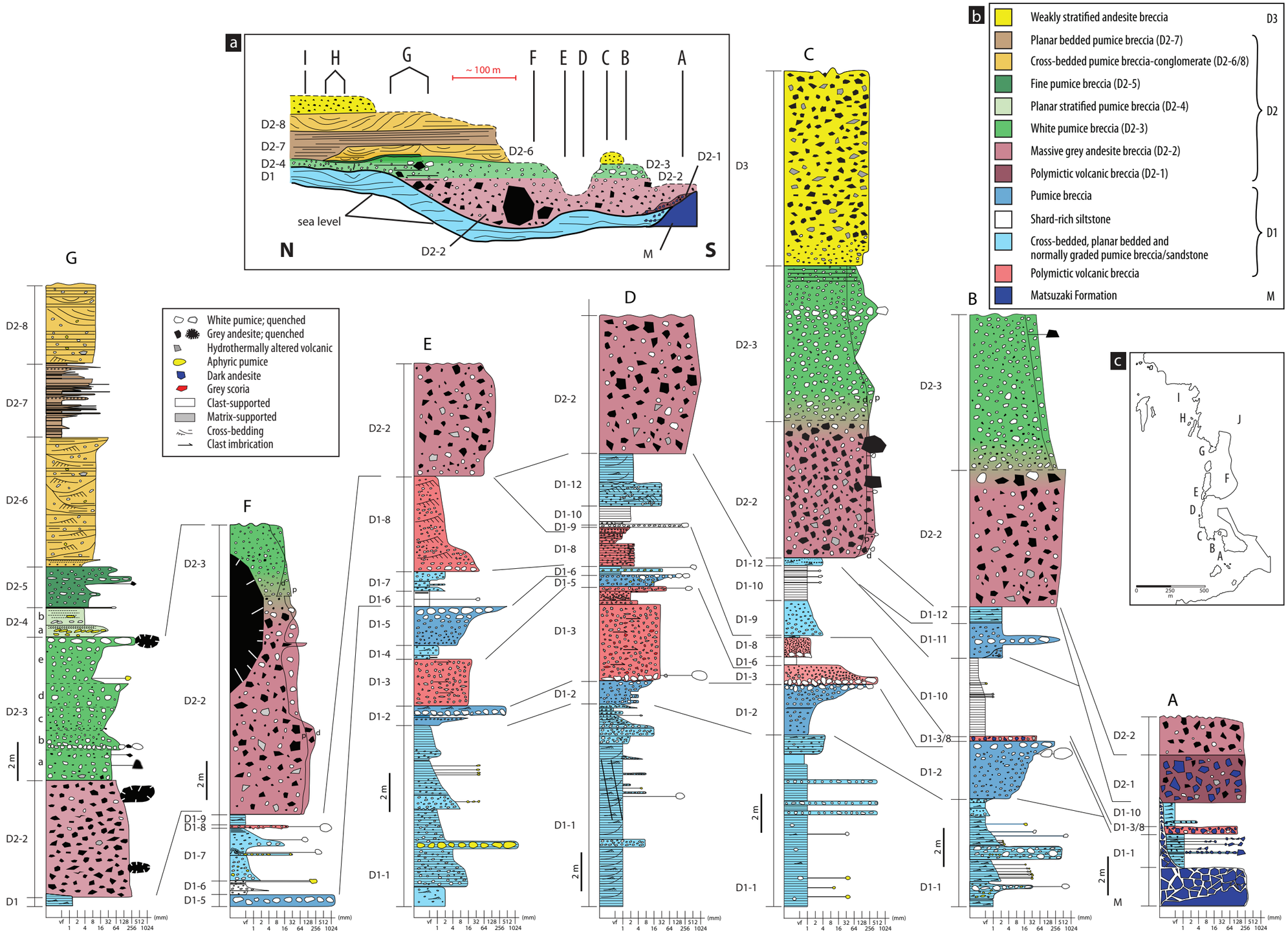

Fig. 4.10 Stratigraphic logs of southern part of the Dogashima Formation (localities A to G), displayed north (left) to south (right). Inset a reconstitutes the original geometry of the Dogashima Formation, and shows Dogashima 2 filling the palæo-valley (localities A to G) that is separated by a palæo-high at localities C, D and E from a secondary palæo-low (between localities A and B) carved in Dogashima 1. Studied localities in capital letters. Inset b shows facies legend, and inset c shows localities on simplified map (Fig. 4.1). All log bases start at sea level. Eastwards tilt of ~10° of the Dogashima Formation with palæo-high at localities C, D and E make more stratigraphy of Dogashima 1 being exposed above sea level, compared to localities A, E, F and G. The base in Dogashima was not found. Note the gradation from massive grey andesite breccia to white pumice breccia at localities B and C (palæo-valley) and the stratification at locality G (rim of the palæo-valley). Basal polymictic volcanic breccia (D2-1) at locality A, and massive grey andesite breccia (D2-2) at localities B to G form the basal part of the palæo-valley eroded in Dogashima 1 and filled by Dogashima 2. D1, D2 and D3 for Dogashima 1, 2, and 3, respectively; M for Matsuzaki Formation, d for dense clast, p for white pumice clast in Dogashima 2. See Tables 4.2 and 4.4 for unit descriptions.

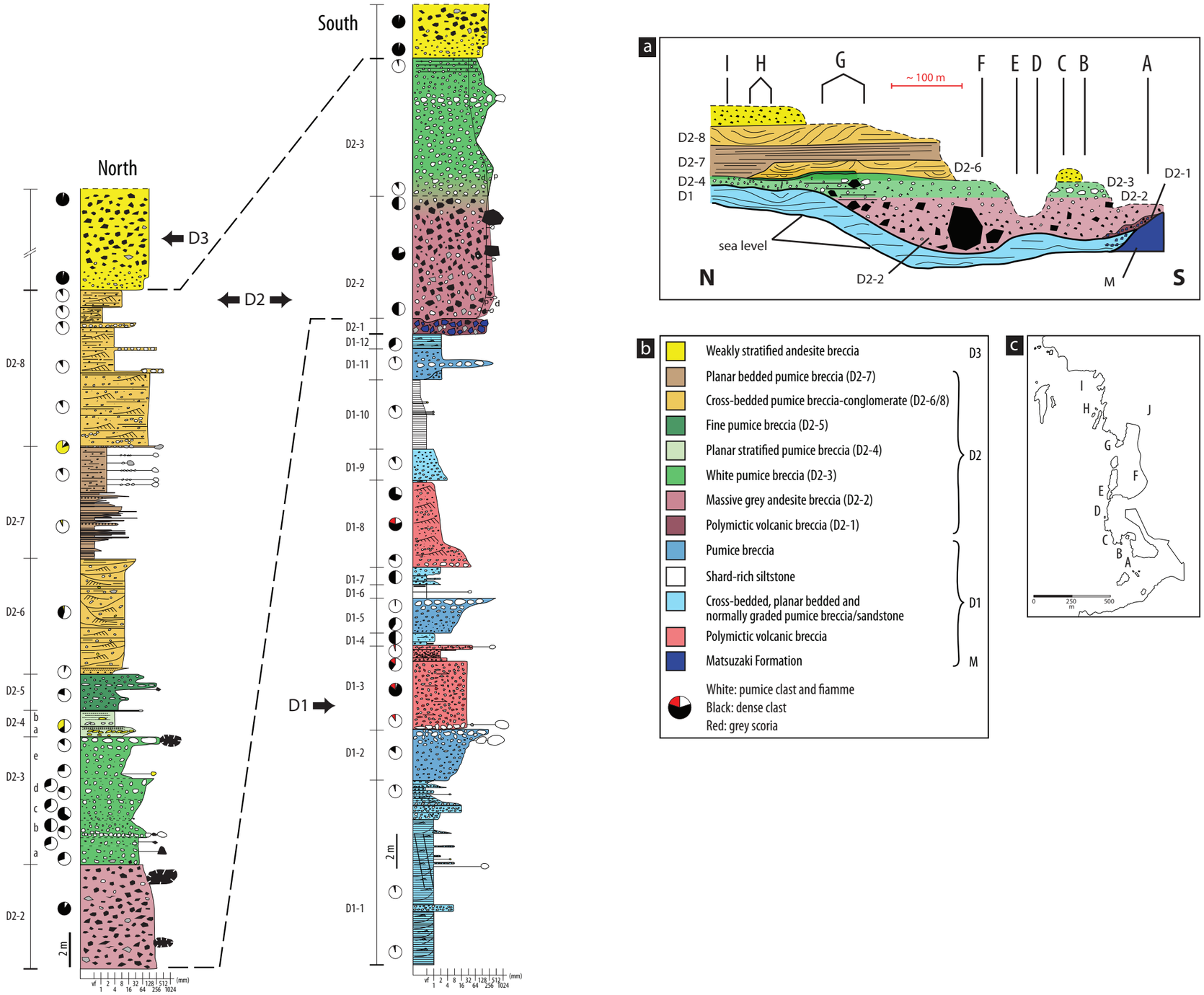

Fig. 4.11 Composite average clast size logs of the Dogashima Formation, showing the main beds to the north (left, G to I) and south (right, A to G). Note the internal stratification in unit 3 in Dogashima 2. Dogashima 3 is at least 50 m thick and the full thickness is not shown here; the top is the modern erosion surface. Pie diagrams represent the volume percent of clasts (>2 mm) estimated in the field. Matrix (<2 mm) is commonly <20 vol.% of the total volume and mostly composed of free broken crystals, and not shown on the pie diagrams. D1, D2 and D3 for Dogashima 1, 2, and 3, respectively; M for Matsuzaki Formation, d for dense clast, p for white pumice clast in Dogashima 2. See Tables 4.2 and 4.4 for unit descriptions.

clasts. In Dogashima 2, there are differences in various major element abundances in the grey andesite and the white pumice (Fig. 4.8; Table 4.1). The red andesite clasts are slightly enriched in FeO but depleted in K_2O compared to the grey andesite clasts, probably due to slight alteration. The plagioclase-phyric andesitic inclusions in grey andesite clasts are tholeiitic and follow the compositional trend of the Dogashima Formation. The dark andesite clasts of Matsuzaki Formation and the coarsely porphyritic andesite clasts from Dogashima 3 match the composition of the grey andesite clasts of Dogashima 2. The grey scoria clasts and aphyric pumice clasts do not match the compositional trend of Dogashima Formation but they do match the trend of the Shirahama Group (Fig. 4.8; Table 4.1), and were probably derived from the Matsuzaki Formation.

5. DOGASHIMA 1

Dogashima 1 is >15 m thick and well represented in the Sawada area (south), where four major facies or facies associations are present (Fig. 4.10; Table 4.2). Its minimum volume is estimated at $2.5x10^6$ m^3. The base of Dogashima 1 is not exposed in the studied area. The units of Dogashima 1 are chiefly laterally continuous, but many are composed of discontinuous, lenticular beds and cut or separated by erosive low-angle contacts (Figs 4.2, 4.3, 4.12). Grey andesite clasts are lacking in Dogashima 1.

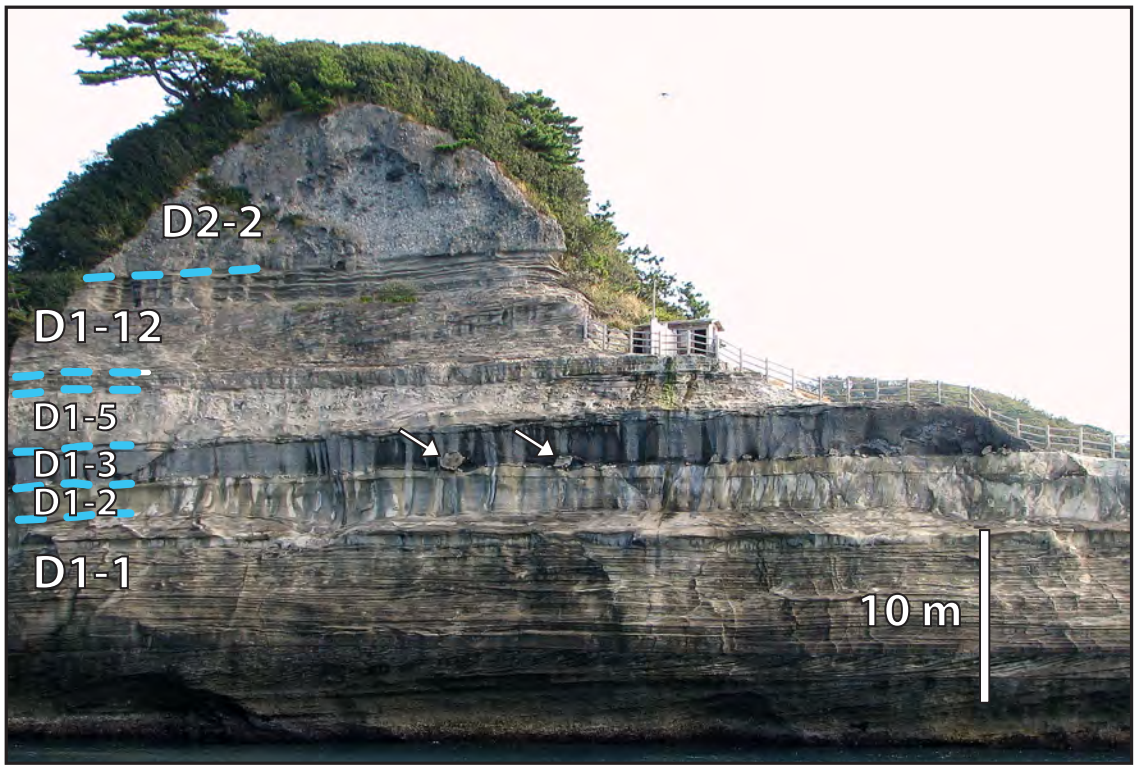

Fig. 4.12 Major tabular units in Dogashima 1 (D1) and Dogashima 2 (D2) at locality D, looking eastwards: pumice breccia (D1-2, D1-5), cross-bedded pumiceous breccia/sandstone (D1-1, D1-12), dark-coloured polymictic volcanic breccia (D1-3), and massive grey andesite breccia (D2-2). Coarse white pumice clasts of pumice breccia D1-2 (white arrows) are present at the base of the polymictic volcanic breccia (D1-3) in Dogashima 1.

Pumice breccia facies (units D1-2, D1-5, D1-11)

The first facies consists of thick to very thick (0.5 to 3 m) beds of pumice breccia (D1-2, D1-5, D1-11; Fig. 4.13; Table 4.2). The beds of pumice breccia are laterally continuous, tabular, massive, and in sharp contact with other units; the top contact is discordant at many localities. It is mainly composed of equant, angular, white pumice clasts (>60 vol.% of the clasts), plagioclase and pyroxene crystal fragments and rare aphyric pumice clasts (<1 vol.%). Most coarse pumice clasts (>10 cm) show both concave and convex curviplanar surfaces and possible remnants of quenched margins and rare breadcrust texture (Fig. 4.13b). This facies has an average grain size of 8–200 mm. The matrix is rich in phenocryst fragments, and can make 20–40 vol.% of the bed; matrix finer grained than sand is absent (Fig. 4.13d).

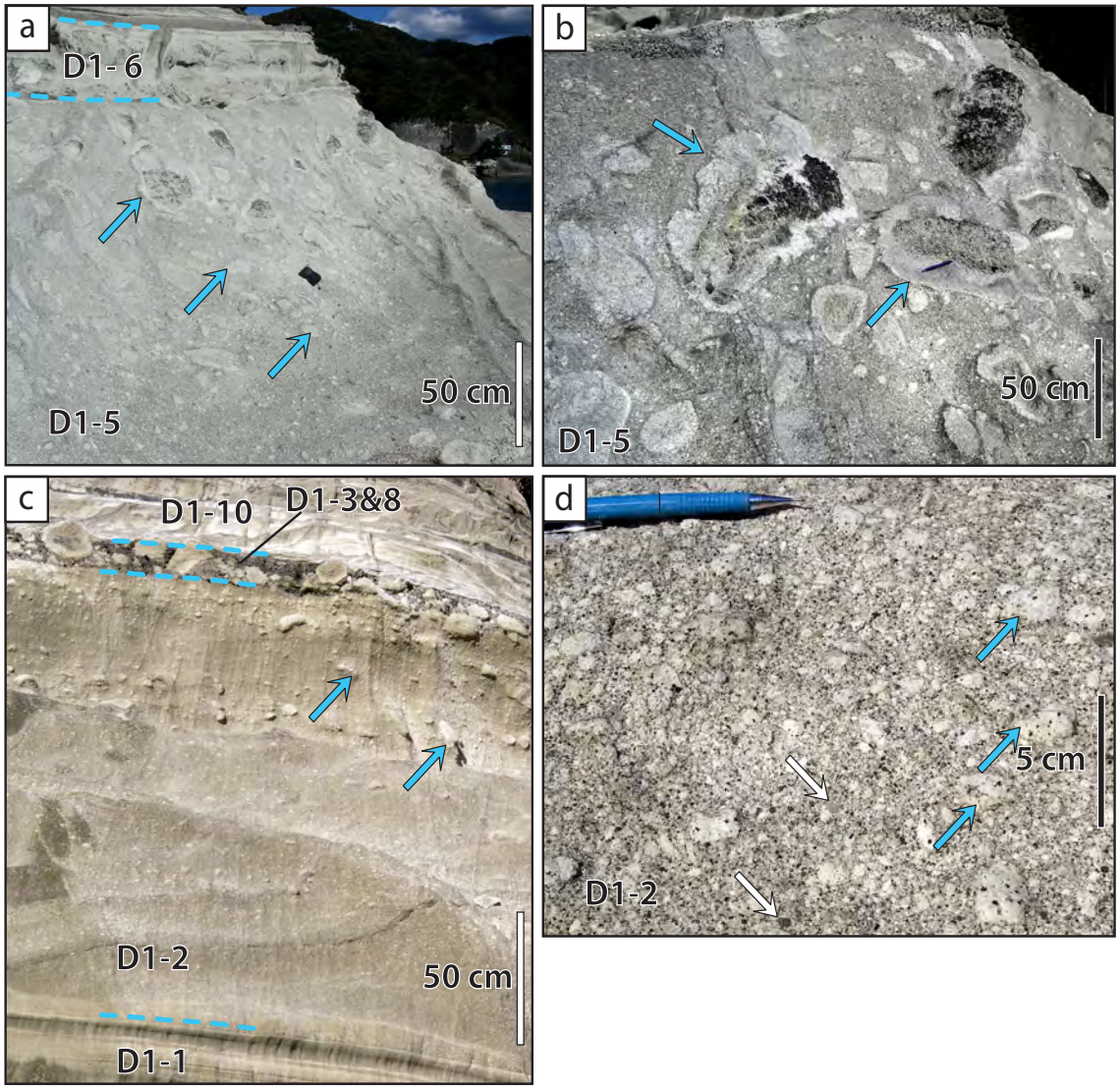

Fig. 4.13 Pumice breccia in Dogashima 1. **a)** Coarse-tail, reversely graded pumice breccia (D1-5), locality E. Note the coarse white pumice clasts (blue arrows), and the regular grading; **b)** Top of the coarse-tail reversely graded pumice breccia (D1-5), locality E. Margins of the coarse white pumice clasts are very irregular, and appear to be differently affected by weathering (blue arrow), and are interpreted to have been quenched. Image has been darkened to increase contrast; **c)** Reversely graded pumice breccia (D1-2), locality B, with white pumice clasts (blue arrow). Unit D1-2 is discordant with overlying polymictic volcanic breccia (D1-3 and D1-8) that includes similar white pumice clasts; **d)** Pumice breccia (D1-2) at locality D, composed of white pumice clasts (blue arrows) with feldspar and pyroxene phenocrysts, free broken crystals and minor hydrothermally altered volcanic clasts (white arrows). Note the low abundance in clasts finer than sand.

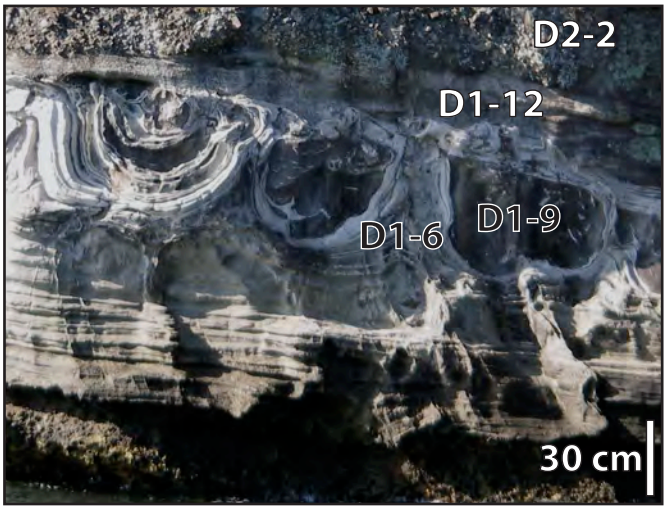

Fig. 4.14 Shard-rich siltstone in Dogashima 1. Ball-and-pillow structure in shard-rich siltstone (D1-6) and polymictic volcanic breccia (D1-9), between localities E and F.

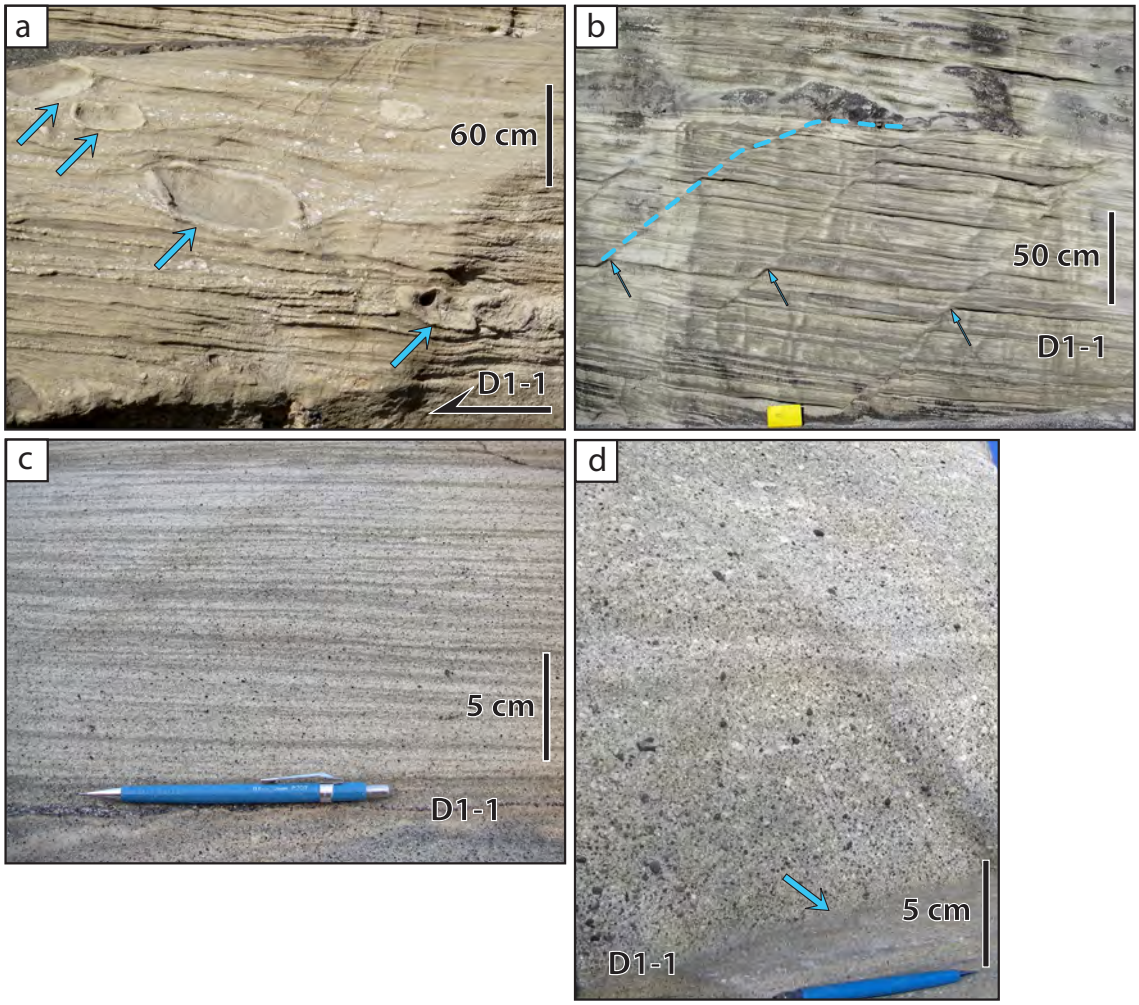

Fig. 4.15 Cross-bedded, planar bedded and normally graded pumice breccia/sandstone in Dogashima 1; beds form >5 m wide lenses. **a)** Cross-bedded pumiceous breccia (D1-1), locality B. Coarse white pumice clasts (up to 80 cm in length, blue arrows) occur in much finer pumice breccia. Margins of the coarse white pumice clasts appear to be differently affected by weathering (blue arrow), and are interpreted to have been quenched; **b)** Syn-sedimentary normal faults (yellow line and yellow arrows) cutting a very thick (>2 m) section of stratified bed in planar bedded pumice breccia (D1-1), locality D; **c)** Laminae of free broken pyroxene crystals and white pumice clasts in a very thick (>2 m), stratified lens of planar-bedded pumiceous breccia (D1-1), locality D; **d)** Normally graded pumice breccia (D1-1) at locality A, composed of white pumice and hydrothermally altered volcanic clasts. Note the small discordance (blue arrow) with underlying pumice sandstone.

Name Bed set abbreviation	Locality	Bed thickness	Major clasts Minor clasts	Textures, structures, Other components	Average grain size Maximum grain size	Initiation and transport processes
DOGASHIMA 1						
Pumice breccia **D1-2, D1-5, D1-11**	B, C, D. E	Thick to very thick	white pumice Free broken crystal, hydrothermally altered volcanic	Reversely or normally graded Can show lense of coarse white pumice clasts and dense clast-rich base	0.2 - 25 cm 120 cm	Subaqueous eruption-fed volcaniclastic density current Derived from subaqueous, pumice-forming explosive eruption
Shard-rich siltstone **D1-6, D1-10**	A, B, C, D, E, F	Thin to medium	Glass shards Coarse white pumice clasts		<0.0063 cm	Subaqueous suspension Derived from subaqueous, pumice-forming explosive eruption
Polymictic volcanic breccia **D1-3, D1-8**	A, B, C, D, E, F	Medium to very thick	Dense Hydrothermally altered volcanic, grey scoria, white pumice	Stratified, normally or reversely graded, or cross bedded Coarse white pumice clasts can occur at base	0.2 - 4 cm 120 cm	Subaqueous volcaniclastic density current and traction current Derived from remobilisation of multiple sources
Cross-bedded, planar bedded and normally graded pumice breccia/ sandstone **D1-1, D1-4, D1-7, D1-9 and D1-12**	A, B C, D, E, F	Thin to thick	White pumice Hydrothermally altered volcanic, free broken crystal, aphyric pumice	Cross-bedded in trough or planar bedded, commonly laminated, or normally graded	<0.2 - 6 cm 150 cm	Traction current and subaqueous volcaniclastic density current Derived from sediment remobilisation process
DOGASHIMA 3						
Weakly stratified andesite breccia **D3**	C, I, J	Extremely thick	Coarsely porphyritic andesite White pumice, hydrothermally altered volcanic	Weakly stratified, with disorganised, weakly stratified pumiceous matrix	20-50 cm 100 cm	Autoclastic fragmentation, or lava or dome collapse Derived from resedimentation of autoclastic facies and delayed settling of pumiceous matrix

Table 4.2 Summary of stratigraphic facies and their interpretation, Dogashima 1 and 3.

Shard-rich siltstone (units D1-6, D1-10)

The shard-rich siltstone facies, units D1-6 and D1-10, overlies other beds at sharp boundaries. It forms intervals 10 cm to 2 m thick that are massive or finely laminated, and show load, liquefaction-convolution (Table 4.2) and ball-and-pillow structures. It is almost exclusively composed of well sorted, partially devitrified glass shards and feldspar fragments (max 0.1 mm); bed D1-6 contains minor <5 mm pumice clasts and rare coarse (up to 40 cm) white pumice clasts are found at locality D. The top contact is commonly an erosion surface with overlying beds of cross-bedded pumiceous breccia/sandstone or polymictic volcanic breccia facies.

Locality	Unit name		Long axis orientation (°)		Number of measures	Inferred flow orientation	Syn-sedimentation faults
			Primary	Secondary		Clast imbrication	Dip/Dip direction
I	Cross-bedded pumice breccia-conglomerate	D2-6	245–265		6		
H	Cross-bedded pumice breccia-conglomerate	D2-6	220		3		
G	Planar stratified pumice breccia	D2-4	235–245		>10	E to W	
G	White pumice breccia	D2-3e	235–245		8		
D	Polymictic volcanic breccia	D1-8				E to W	
D	Polymictic volcanic breccia	D1-3	235–245	225 & 275	18		
D	Cross-bedded pumiceous breccia/sandstone	D1-1			>20		75/210
B	Cross-bedded pumiceous breccia/sandstone	D1-1	265–285	215	7	E to W	

Table 4.3 Bearing (true North) of elongated pumice clasts interpreted to be deposited parallel to flow direction in Dogashima 1 and 2. Flow direction inferred from clast imbrication. Dip direction of syn-sedimentary faults indicate palæo-downslope direction.

Cross-bedded, planar bedded and normally graded pumice breccia/sandstone facies association (units D1-1, D1-4, D1-7, D1-9 and D1-12)

This facies association is composed of cross-bedded, planar bedded (units D1-1, D1-4, D1-7 and D1-12) and normally graded pumice breccia (unit D1-8) (Fig. 4.15; Table 4.2). Beds of these facies are variably graded and thin to very thick (10 cm to >2 m). The cross-bedded, planar bedded and normally graded pumice breccia facies association consists of lenticular sets of trough cross beds with m to 10 m wavelengths and amplitudes up to 2 m (Fig. 4.12). Contacts are sharp between beds within this facies association, as well as with other facies. White pumice and hydrothermally altered clasts are angular to sub-rounded.

The cross beds and planar beds are commonly in low-angle stacks (e.g. unit D1-1; Figs 4.15a, 4.15b, 4.15c). Out-sized white pumice and aphyric pumice clasts (both up to 1.5 m) are spread throughout the beds, or concentrated in single-clast-thick beds (Fig. 4.15a). At

locality B, some elongate white pumice clasts are parallel and have an east-west bearing (Table 4.3). At locality D, numerous subvertical syn-sedimentary normal faults occur in a ~2-m-thick cross-bedded pumice sandstone bed in unit D1-1. The faults dip towards the SE, and have a vertical displacement of <20 cm (Fig. 4.15b; Table 4.3). Scattered dark andesite clasts of Matsuzaki Formation compositions occur in beds in contact with the Matsuzaki Formation at locality A (Figs 4.3, 4.6b).

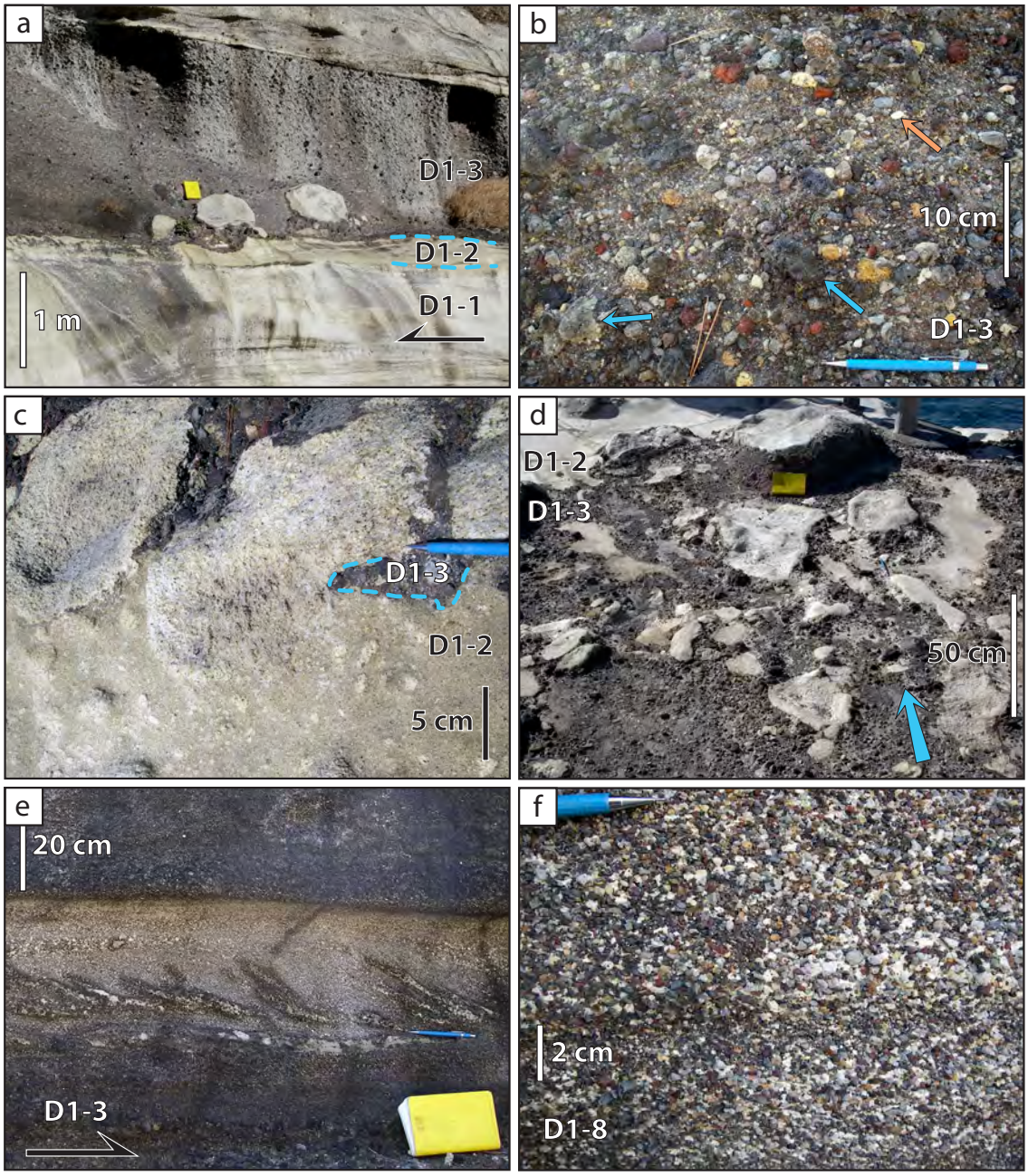

Fig. 4.16 Polymictic volcanic breccia in Dogashima 1. **a)** Polymictic volcanic breccia (D1-3), locality D. The unit contains coarse white pumice clasts (beside notebook); **b)** Polymictic volcanic breccia (D1-3), locality D. Note the coarseness of the facies and the polymictic clast population; grey scoria (blue arrows), white pumice clasts (orange arrow) and numerous hydrothermally altered volcanic clasts; **c)** Highly irregular contact between coarse white pumice clasts of pumice breccia (D1-2) and overlying polymictic volcanic breccia (D1-3); **d)** Elongate coarse white pumice clasts in polymictic volcanic breccia (D1-3), interpreted to define a northeast-southwest palæo-current direction (blue arrow; Table 4.3); **e)** Cross-bedded polymictic volcanic breccia (D1-8), locality D, arrow indicates interpreted current direction; **f)** Polymictic volcanic breccia (D1-8) composed of hydrothermally altered volcanic and white pumice clasts. The beds are very well sorted and weakly stratified.

Normally graded pumice breccia facies (units D1-1 and D1-9) contains white pumice clasts up to 8 mm and minor hydrothermally altered volcanic clasts (Fig. 15d). Their discontinuous occurrence, normal grading and relatively small thickness distinguish them from the pumice breccia facies. Scattered coarse pumice clasts (25 cm) are present in unit D1-1 at locality C and are possibly linked to the same facies.

Polymictic volcanic breccia (units D1-3 and D1-8)

The fourth facies of Dogashima 1 (units D1-3 and D1-8) is polymictic volcanic breccia (Figs 4.6b, 4.16; Table 4.1). This facies occurs in normally to reversely graded, medium to very thick beds (10 cm to 5 m). A variety of hydrothermally altered volcanic clasts occur together, as well as grey scoria, aphyric pumice clasts and dark andesite clasts from the underlying Matsuzaki Formation at locality A (Fig. 4.6b). The facies lacks matrix. This facies forms two units that are stratigraphic markers throughout Dogashima 1 because of their lateral continuity and striking dark colour. The basal contact of each unit is sharp and discordant with underlying beds. Between localities B and C, the units D1-3 and D1-8 become thinner and much coarser 100 m southwards of locality C, and merge together into a single <50-cm-thick coarse bed at 250 m southeastwards of locality C. Units D1-3 and D1-8 have erosional basal contacts with underlying units of Dogashima 1, and pinch out above the Matsuzaki Formation at locality A (Figs 4.3, 4.6b).

The lower unit (unit D1-3) is thicker and coarser than unit D1-8, relatively well sorted and contains abundant white pumice clasts (up to 1 m; Figs 4.16a, 4.15b, 4.15c) at the base, which appear to be derived from the top of the underlying pumice breccia of unit D1-2. These white pumice clasts are elongate and roughly aligned parallel to a northeast-southwest bearing (Fig. 4.15d; Table 4.3). At locality C, unit D1-3 contains three thin cross-bedded and well-sorted beds (Fig. 4.16f) above a very thick bed (Fig. 4.16b). The upper unit (unit D1-8) is rich in rounded white pumice clasts (max 40 cm), shows well-developed clast imbrication, includes planar cross beds (Fig. 4.16e) and is commonly well sorted(Fig. 4.16f).

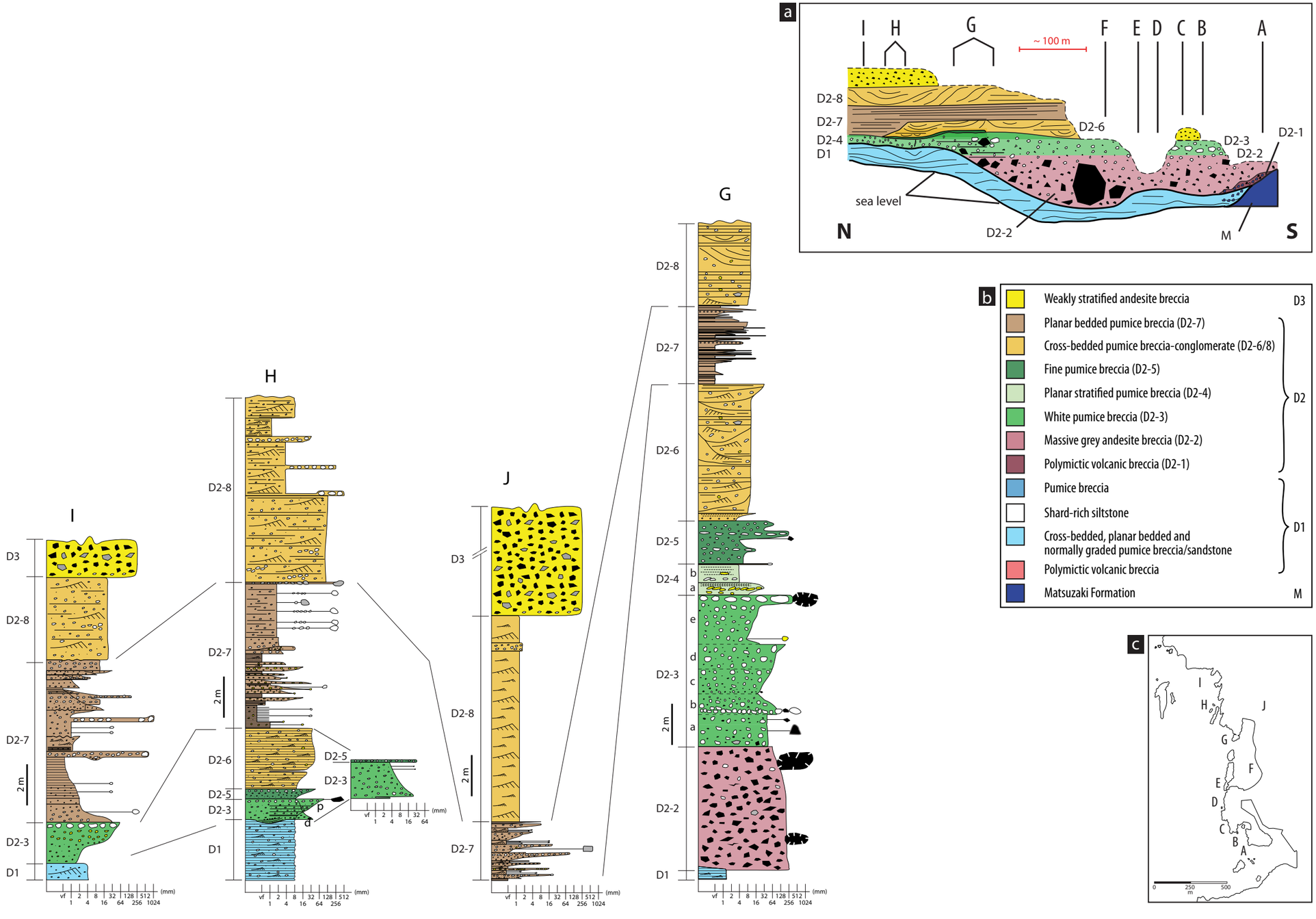

Fig. 4.17 Stratigraphic logs of northern part in Dogashima Formation (localities G to I), displayed north (left) to south (right). Inset a reconstitutes the original inferred geometry of the Dogashima Formation, and shows Dogashima 2 filling the palæo-valley (localities A to G) that is separated by a palæo-high at localities C, D and E from a secondary palæo-low (between localities A and B) carved in Dogashima 1. Studied localities in capital letters. Inset b shows facies legend, and inset c shows localities on simplified map (see Fig. 4.1). Except for log J, all log bases start at sea level. Note the absence of massive grey andesite breccia (D2-2) and the relatively thin (<2 m) white pumice breccia bed (D2-3) in sections I and H. In section G, unit D2-2 is very thick, and unit D2-3 is stratified. D1, D2 and D3 for Dogashima 1, 2, and 3, respectively; d for dense clast, p for white pumice clast in Dogashima 2. See Tables 4.2 and 4.4 for unit descriptions.

Name Bed set abbreviation	Locality	Bed thickness	Major clasts Minor clasts	Textures, structures, Other components	Average grain size Maximum grain size	Initiation and transport processes
DOGASHIMA 2 Planar bedded pumice breccia **D2-7**	G, H, I	Thin to medium thick	White pumice and hydrothermally altered volcanic Free broken crystal, grey andesite, aphyric pumice	Planar bedded, massive, reversely or normally graded, laminated at their top	0.2 - 1 cm 10 cm	Subaqueous suspension Derived from subaqueous, pumice-forming explosive eruption
Cross-bedded pumice breccia-conglomerate **D2-6 and D2-8**	G, H, I	Thin to very thick	Sub-angular to sub-rounded white pumice and hydrothermally altered volcanic Free broken crystal, grey andesite, aphyric pumice	Cross-bedding in trough that can be compound, stratified	0.2 - 3 cm 150 cm	Traction current Derived from sediment remobilisation process
Fine pumice breccia **D2-5**	G, H	Very thick	White pumice and free broken crystal Grey andesite	Randomly stratified, with lenses of coarser andesite pumice clasts Overall reversely graded	0.2 - 6 cm 50 cm	Unsteady type of subaqueous eruption-fed volcaniclastic density current Derived from subaqueous, pumice-forming explosive eruption
Planar stratified pumice breccia **D2-4**	G, H	Medium to thick	White pumice Aphyric white pumice, free broken crystal, grey andesite, hydrothermally altered volcanic	Stratified, reversely to normally graded or massive Laminated at top	0.2 - 5 cm 20 cm	Turbulent type of subaqueous eruption-fed volcaniclastic density current, traction current Derived from wanning phase of subaqueous, pumice-forming explosive eruption or resedimentation processes
White pumice breccia **D2-3**	B, C, F	Very thick	White pumice, grey andesite, free broken crystal Hydrothermally altered volcanic and aphyric pumice	Reversely graded, with coarse lenses of white pumice clasts	0.2 - 60 cm 100 cm	Subaqueous eruption-fed volcaniclastic density current Derived from subaqueous, pumice-forming explosive eruption that destroyed a hot andesitic dome
	G	Very thick	White pumice, grey andesite, free broken crystal Hydrothermally altered volcanic and aphyric pumice, red andesite	Overall reversely graded and stratified, with internal normally or reversely graded beds	0.2 - 60 cm 120 cm	
	G (west), H, I	Medium thick to very thick	White pumice, grey andesite, free broken crystal Hydrothermally altered volcanic and aphyric pumice	Stratified, normally graded Lenses of coarse white pumice clasts at top	0.2 - 1 cm 60 cm	
Massive grey andesite breccia **D2-2**	A, B, C, D, E, F	Very thick	Grey andesite Hydrothermally altered volcanic, red andesite, rounded white pumice	Massive to reversely graded	5 - 50 cm 1,000 cm	
	G	Very thick	Grey andesite Hydrothermally altered volcanic, red andesite, rounded white pumice, fluidal grey andesite	Massive to normally graded, with groups of quenched out-sized andesite clasts	5 - 50 cm 400 cm	
Basal polymictic volcanic breccia **D2-1**	A	Thick to very thick	Dark andesite and grey andesite Hydrothermally altered volcanic, red andesite, white pumice	Massive, scours underlying deposits, in lense	5 - 50 cm 80 cm	Subaqueous eruption-fed volcaniclastic density current Derived from subaqueous, pumice-forming explosive eruption

Table 4.4 Summary of stratigraphic facies and their interpretation, Dogashima 2.

6. DOGASHIMA 2

Dogashima 2 is composed of eight strikingly different stratigraphic units, some of which show strong lateral variations (Figs 4.10, 4.17). The minimum volume of Dogashima 2 is estimated at $5.5x10^6$ m^3. Unit D2-1 is a thick lens of basal polymictic volcanic breccia. The second unit, called hereafter massive grey andesite breccia (D2-2), is limited to localities A to G and overlies Dogashima 1 with a disconformity (Fig. 4.3). The overlying white pumice breccia (unit D2-3) is widespread but changes significantly in thickness and bed form. Planar stratified pumice breccia (unit D2-4) is found at locality G and possibly H. Fine pumice breccia (unit D2-5) occurs at locality G and possibly also at localities H and I. At the top of the succession, two units of cross-bedded pumice breccia-conglomerate (units D2-6 and D2-8) are separated by planar bedded pumice breccia (unit D2-7). These three topmost units are widespread though absent from the southernmost outcrops.

Locality G is the best exposed outcrop of Dogashima 2 (Fig. 4.18), and the middle to upper part of the unit D2-3 was described in Cashman and Fiske [1991] and Tamura et al. [1991]. However, the locality described by Cashman and Fiske [1991] only goes for 20 m laterally and is not representative of most of the volume of Dogashima 2.

Unit D2-1: Basal polymictic volcanic breccia

The basal layer of polymictic volcanic breccia (unit D2-1) is <3 m thick and extends laterally for <10 m at the base of Dogashima 2 at locality A (Fig. 4.3). The lower contact

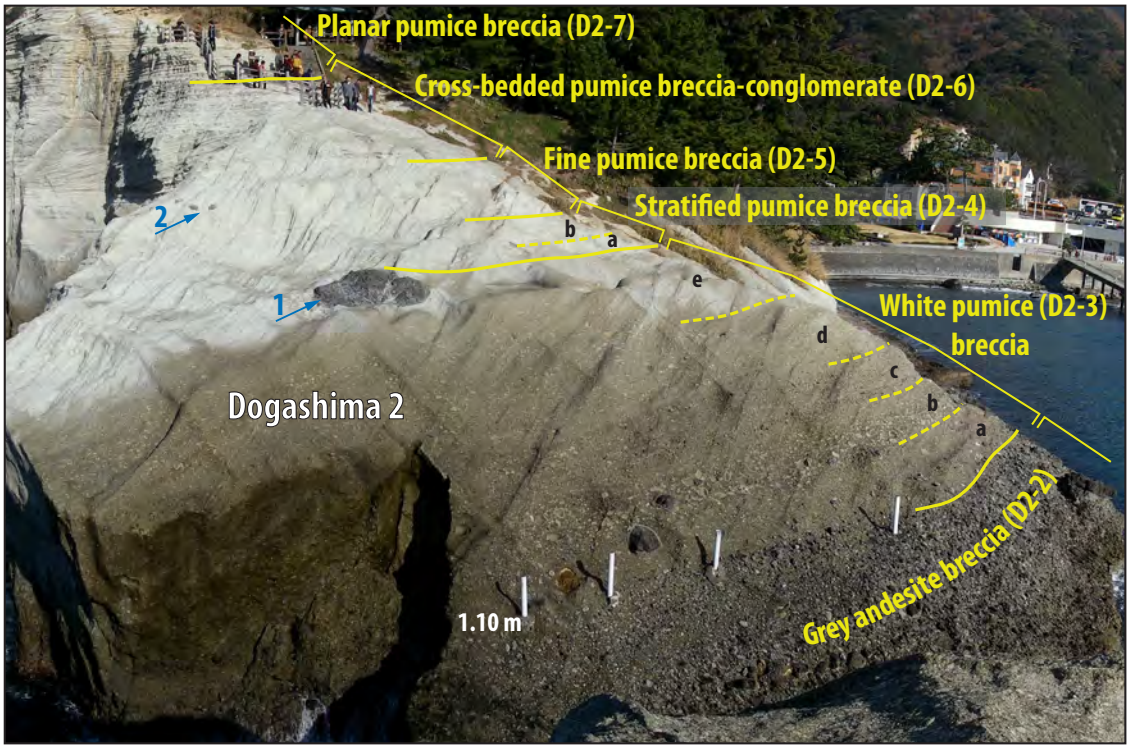

Fig. 4.18 View of Dogashima 2 to the east of locality G. Note the sharp boundary of the massive grey andesite breccia (D2-2) and the white pumice breccia (D2-3), the graded units within the lower beds of the white pumice breccia (especially D2-2a and D2-2b), and the isolated grey andesite clast at the top (arrow 1) and in the fine pumice breccia (D2-5; arrow 2).

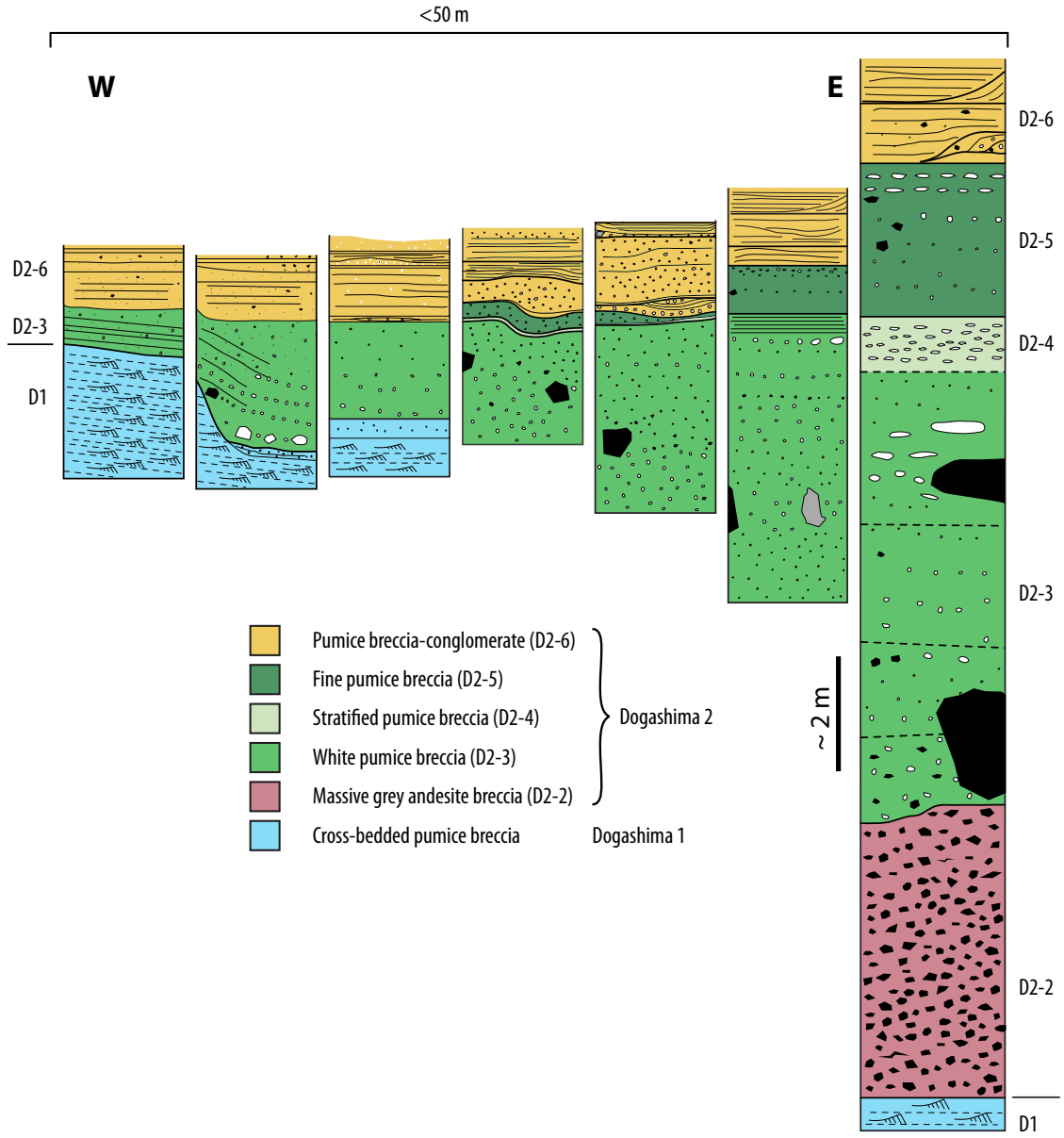

Fig. 4.19 Lateral changes in Dogashima 2 at locality G shown by simplified logs. A medium to thick, stratified bed of white pumice breccia (D2-3) that contains rare grey andesite clasts and hydrothermally altered volcanic clasts occurs in western sections (interpreted overbank facies; left), and overlies Dogashima 1 with a discordant contact. To the east (right), thick beds of massive grey andesite breccia (D2-2) overlie Dogashima 1 with a discordant contact. This lateral section is interpreted to represent the wall of the palæo-valley carved in Dogashima 1. Distance between the logs is ~5 m; top of the vertical section missing.

with underlying Dogashima 1 is an erosion surface and is discordant to bedding; local scours (1 m deep and 2 m wide) occur. It forms a discontinuous, local basal lens below the overlying massive grey andesite breccia (D2-2) unit, and above a local palæo-low lies between localities A and B. The contact with the overlying massive grey andesite breccia is sharp and irregular. The unit is massive, clast-supported, and overall consists of a mixture of dark andesite clasts (0–60 vol.%; Fig. 4.11; Table 4.4) of the underlying Matsuzaki Formation, grey andesite clasts (20-30 vol.%), minor rounded white pumice clasts (<3 vol.%), hydrothermally altered volcanic clasts (<3 vol.%) and broken feldspar crystals. Matrix finer than sand is absent. The proportions of dark andesite clasts changes stratigraphically upwards and is commonly zero in the lowermost 30 cm.

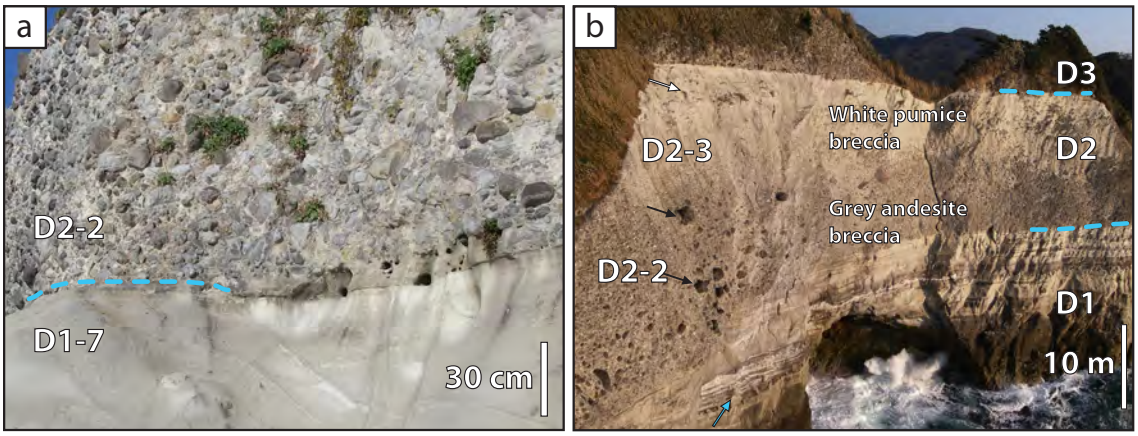

Fig. 4.20 Contacts between Dogashima 1, Dogashima 2 and Dogashima 3. **a)** Sharp basal contact of massive grey andesite breccia (D2-2) on the upper beds of cross-bedded pumice breccia in Dogashima 1, locality E; **b)** Dogashima Formation at locality C. Note sharp contacts between Dogashima 1, Dogashima 2 and Dogashima 3. Black arrows show coarse grey andesite clasts in massive grey andesite breccia (D2-2), white arrow points to lens of coarse white pumice clasts in white pumice breccia in Dogashima 2 (D2-3). Note the gradation from the massive grey andesite breccia to the white pumice breccia in Dogashima 2. Blue arrow points to coarse white pumice clasts in polymictic volcanic breccia of D1.

Unit D2-2: Massive grey andesite breccia

The massive grey andesite breccia (unit D2-2) is up to 7 m thick, massive, or reversely or normally graded and moderately sorted. This bed overlies Dogashima 1 throughout the southern area (localities A–G) and pinches out sharply at outcrop G (Fig. 4.19); it is absent from the northern sector (localities G to I). The minimum volume of the massive grey andesite breccia is $1x10^6$ m^3. A local palæo-low in beds of Dogashima 1 is present between localities A and B. The basal contact of the massive grey andesite breccia is sharp and discordant with Dogashima 1 (Fig. 4.20a) and with the basal polymictic volcanic breccia (D2-1) at locality A, and onlaps the Matsuzaki Formation (Fig. 4.3). The coarseness, dark grey colour and substantial thickness of this breccia make it a good stratigraphic marker in the Dogashima Formation (Figs 4.2, 4.20b). The unit is clast-supported and mostly composed of angular grey andesite clasts (>90 vol.%: Figs 4.5a, 4.11; Table 4.4), some of which have well-preserved fluidal shape (0.1 vol.%; Fig. 4.5d). Outsized grey andesite clasts (up to ~10 m diameter, are typically oblate, with ragged surface and a devitrified quenched rim (Figs 4.5c, 4.21a) and mainly occur in groups in the upper part of the unit at all localities. The thermoremanence of some of the coarse grey andesite clasts at locality F was measured by Tamura et al. [1991], who proposed a temperature of >450°C at deposition. Rounded white pumice clasts (up to 5 vol.%; up to 30 cm) and hydrothermally altered volcanic clasts (<5 vol.%) are found throughout the massive grey andesite breccia. Matrix finer than sand is absent.

Unit D2-3: White pumice breccia

The white pumice breccia (unit D2-3) is 1 to 8 m thick and occurs throughout the mapped extent of the Dogashima Formation, but its texture varies strongly laterally (Figs 4.10, 4.17; Table 4.4). Its minimum volume is estimated at $2.5x10^6$ m^3. To the south, the basal

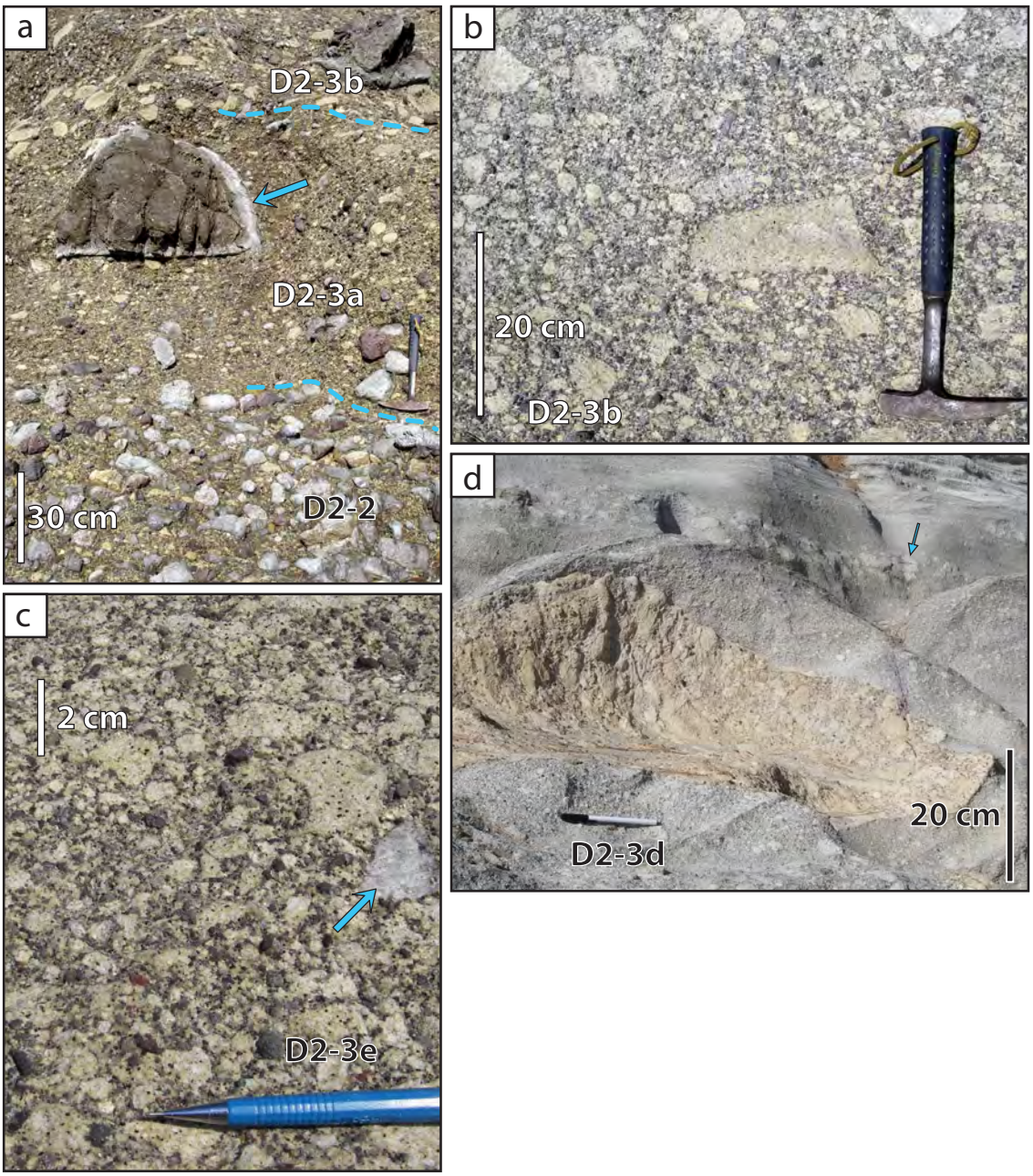

Fig. 4.21 White pumice breccia (D2-2). **a)** Sharp transition from the massive grey andesite breccia (D2-2) to basal beds of the white pumice breccia (D2-3). The grey andesite clast has a quenched rim (blue arrow), locality G; **b)** Coarse, angular white pumice clasts and much smaller grey andesite clasts in white pumice breccia (D2-3b); note the Curviplanar shape of the coarse white pumice clast at centre of the photograph; **c)** Contrasting sizes of white pumice and grey andesite clasts in the upper bed (middle of D2-3f) of the white pumice breccia, reflecting good hydraulic sorting; this part in Dogashima 2 was studied by Cashman and Fiske [1991]. Note the aphyric pumice clast (blue arrow); **d)** Hydrothermally altered clast of pumice breccia in white pumice breccia (D2-3d), locality G. This clast is exceptional in its size and composition. Blue arrow points to coarse white pumice clasts at the top of unit D2-3e.

contact with the massive grey andesite breccia (D2-2) is conformable and varies laterally from very sharp to gradational (Figs 4.17, 4.20b). The transition between these two kinds of contacts occurs over a short distance (<5 m) at locality G (Fig. 4.19). The transition zone is the outcrop detailed in Cashman and Fiske [1991]. Gradational contacts are shown by high concentrations of grey andesite and hydrothermally altered volcanic clasts identical to those found in the massive grey andesite breccia (Fig. 4.20b).

The white pumice breccia is stratified into five well-preserved, thick to very thick (1–2.5 m), graded beds at locality G (Figs 4.16, 4.18). The two lower beds (a, b) are massive or normally graded and rich in grey andesite clasts and hydrothermally altered volcanic clasts (30–50 vol.%; Fig. 4.11). The base of bed D2-3b contains abundant coarse white pumice clasts as well as grey andesite clasts (Fig. 4.21a). The three upper beds (c, d, e) are strongly reversely graded and the abundance of grey andesite clasts diminishes progressively (60 to <20 vol.% upwards; Fig. 4.11). Bed boundaries become less distinct upwards in the unit, and are mostly defined by gradational changes in the size of the white pumice clasts.

The white pumice breccia is clast supported and chiefly composed of white pumice clasts (mostly 70-95 vol.%; up to 70 cm) that are overall coarser (Figs 4.21b, 4.21c) than the dense grey andesite clasts (mostly <30 vol.%; up to 3.5 m). Most coarse pumice clasts (>10 cm) show both concave and convex curviplanar surfaces (Fig. 4.21b) and possible remnants of quenched margins. The clasts less than 2 mm are mostly crystal fragments; matrix finer than sand is absent (Fig. 4.21c). Rare out-sized clasts of grey andesite and hydrothermally altered clasts are also present (Figs 20b, 21a). At locality G, a sub-rounded, >3-m-long hydrothermally altered clast of pumice breccia is present in bed D2-3a, and another one lies in bed D2-3d (Fig. 4.21d). The top of bed D2-3e includes a local concentration of coarse white pumice clasts (up to 30 cm long) surrounding an out-sized grey andesite clast (3.5 m long, Fig. 4.18) that has a quenched rim. The coarsest pumice clasts are elongate and long axes exposed in 2- or 3-dimensions are systematically oriented northeast-southwest (Table 4.3).

Between localities A and F (south), outcrops of white pumice breccia are mostly eroded and of difficult access. At localities B, C and F, the white pumice breccia is massive, very thick to extremely thick (6–10 m) and overall normally graded. At locality C, the white pumice breccia is disrupted by diffuse, coarse (up to 1 m diameter) pumice-rich lenses in the upper part of the unit (Fig. 4.20b), and is stratified in its uppermost part.

On the northern side of locality G, the white pumice breccia and underlying massive grey andesite breccia show striking but gradational changes in facies laterally (Figs 4.11, 4.17, 4.19). The massive grey andesite breccia (unit D2-2) pinches out completely and the white pumice breccia becomes a single, stratified, normally graded bed less than 1 m thick in which a few out-sized grey andesite and hydrothermally altered volcanic clasts are present (Figs 4.19, 4.23).

The white pumice breccia directly overlies Dogashima 1 discordantly at localities H and I (Fig. 4.17). At locality H, the white pumice breccia is represented by a stratified, thickly bedded, normally graded unit and contains a few hydrothermally altered volcanic clasts (up to 30 cm). At locality I, a 1-m-thick reversely graded bed of white pumice breccia overlies Dogashima 1 and is tentatively interpreted as the lateral equivalent of D2-3; it contains out-sized aphyric pumice clasts in the upper part.

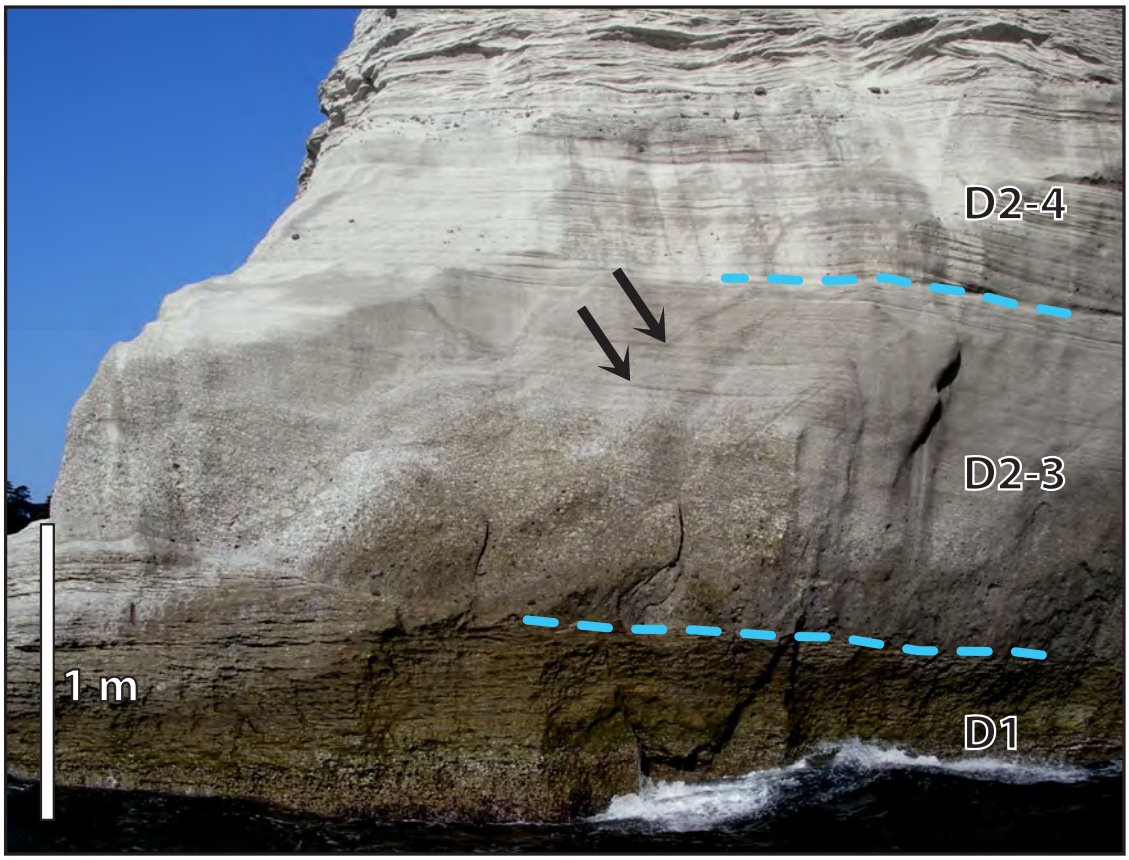

Fig. 4.22 Dogashima 2 at western side of locality G, where the wall of the palæo-valley has been identified. Fine-grained facies of the white pumice breccia (D2-3) and planar stratified pumice breccia (D2-4) overlie a disconformity with Dogashima 1 (D1). Note that unit D2-3 is relatively thin and stratified at the top (arrows), the basal polymictic volcanic breccia (D2-1) and massive grey andesite breccia (D2-2) beds are absent.

Unit D2-4: Planar stratified pumice breccia

The planar stratified pumice breccia (unit D2-4) is only found at locality G, where two thick beds of planar stratified pumice breccia gradationally overlie the white pumice breccia (D2-3). The lower bed has a diffuse contact with unit D2-3 (Fig. 4.23a). Multiple parallel laminations occur in the top 10 cm of each of the two beds. The lower bed (D2-4a) is reversely graded, whereas the upper bed (D2-4b) is slightly normally graded. The planar stratified pumice breccia is clast supported and matrix finer than sand is absent. Aphyric pumice clasts (platy shape, up to 30 mm) are common (up to 35 vol.%; Fig. 4.11; Table 4.4), as well as white pumice clasts (10 mm; up to 15 vol.%) and grey andesite clasts (<5 mm; up to 15 vol.%). Platy aphyric pumice clasts in the lower bed are imbricated and define a down-current palæo-flow direction to the southwest at locality G (Table 4.3).

Unit D2-5: Fine pumice breccia

Fine pumice breccia (unit D2-5) is <3 m thick, and internally diffusely stratified and reversely graded. It occurs at locality G, and is tentatively correlated with a stratified, reversely graded thin bed of fine pumice breccia at locality H (Figs 4.11, 4.17; Table 4.4). Unit D2-5 cannot be found in the southern sections because upper parts of these sections have been eroded. The contacts with unit D2-4 (locality G) and unit D2-3 (locality H) are

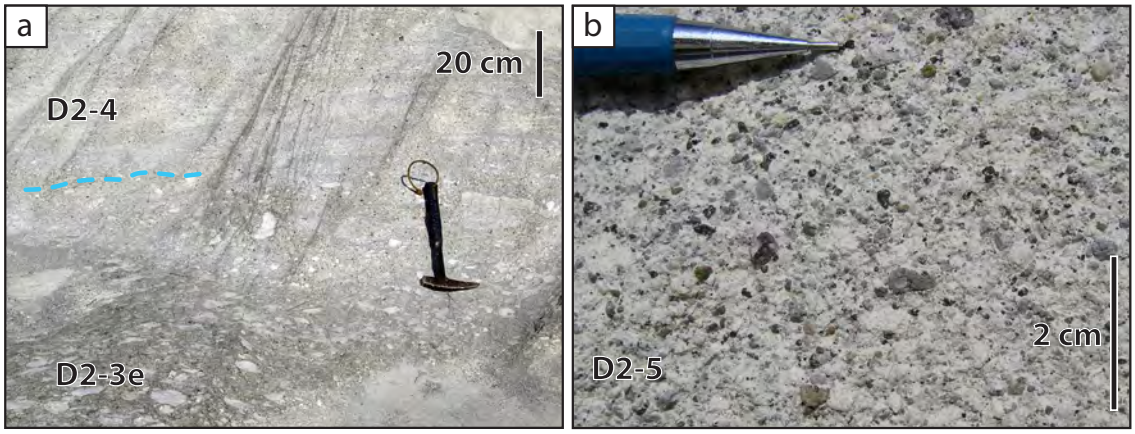

Fig. 4.23 Planar stratified pumice breccia (D2-4) and fine pumice breccia (D2-5). **a)** Diffuse contact between top of white pumice breccia (D2-3e) and planar stratified pumice breccia (D2-4), locality G. Pumice clasts in the foreground are mostly aphyric pumice clasts, whereas white pumice are the coarsest; **b)** White pumice, grey andesite and hydrothermally altered volcanic clasts and free broken crystals in the fine pumice breccia (D2-5) in Dogashima 2, locality G. Note the absence of clasts finer than sand.

sharp and conformable. The fine pumice breccia is clast-supported and mostly consists of white pumice clasts (>80 vol.%, up to 5 cm) and minor amounts of finer grained grey andesite clasts (>10 vol.%, up to 1 cm); matrix finer than sand is absent (Fig. 4.23b). Diffuse lenses of coarse (up to 45 cm) white pumice clasts are common. Rare out-sized grey andesite clasts (<1 vol.%; 6–40 cm) and hydrothermally altered volcanic clasts (<1 vol.%) are present.

Units D2-6 and D2-8: Cross-bedded pumice breccia-conglomerate

The cross-bedded pumice breccia-conglomerate occurs in two thin to very thick, tabular units, D2-6 and D2-8 (Figs 4.16, 4.24a; Table 4.4). Unit D2-6 is present only at localities G and H, whereas unit D2-8 extends through localities G-H-I-J. The basal contacts of both units are sharp and commonly cut across stratification in the beds beneath (units D1-3, D1-5 or D1-8). This facies is composed of lenticular sets of planar and trough cross beds types that have several m wavelengths (Figs 4.24b, 4.24c) and that can be compound [i.e. internally cross-stratified; Figs 4.24d, 4.24e; *McKee and Weir*, 1953; *Allen*, 1963]. Compound cross-beds show opposite palæo-flow directions (Fig. 4.24d).

The units are clast-supported, relatively poorly sorted and mostly composed of sub-angular to sub-rounded white pumice clasts (10–60 vol.%; up to 100 cm), angular grey andesite and angular hydrothermally altered volcanic clasts (10–60 vol.%; up to 30 cm), free broken crystals (up to 20 vol.%), and minor aphyric pumice clasts (Figs 4.11, 4.24c). The volume of fine-grained clasts (<2 mm) is very low (<10 vol.%). At localities H and I, D2-6 contains elongate aphyric pumice clasts that broadly define a northeast-southwest bearing (Table 4.3). This facies is similar to the cross-bedded pumiceous breccia/sandstone in Dogashima 1 (units D1-1, D1-4, D1-7, D1-9 and D1-12), but it much coarser grained (mostly >2 mm) and composed of clasts that are less angular.

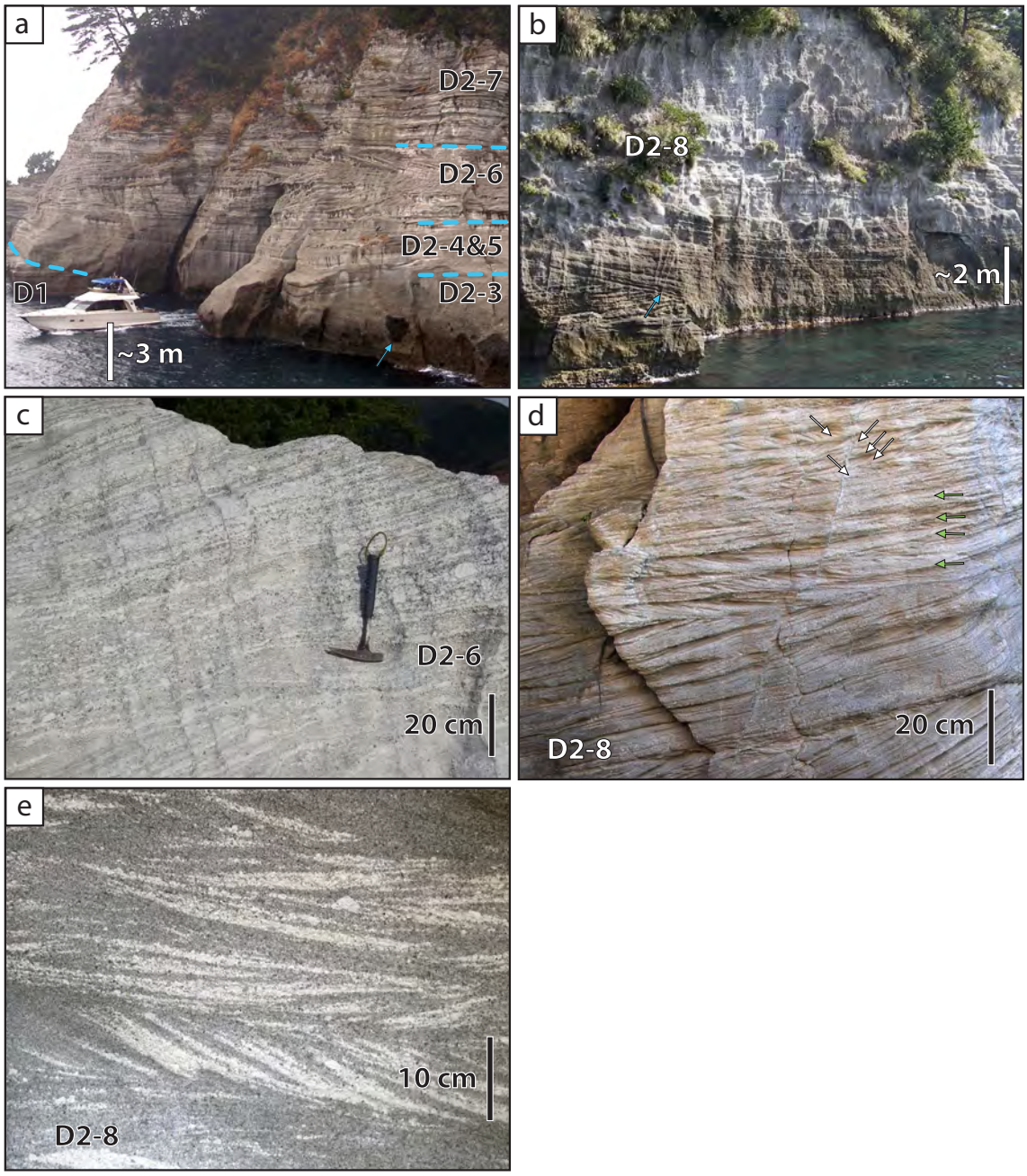

Fig. 4.24 Cross-bedded pumice breccia-conglomerate (D2-6, D2-8). **a)** Transition from the wall of the palæo-valley (right) to overbank setting (left) in Dogashima 2 at northern section of locality G. Dogashima 1 (D1) is overlain by a relatively thin bed of white pumice breccia (D2-3), and by planar stratified pumice breccia and fine pumice breccia (D2-4 and D2-5), cross-bedded pumice breccia-conglomerate (D2-6) and planar bedded pumice breccia (D2-7). Minor grey andesite and hydrothermally altered clasts are present in the white pumice breccia (D2-3, blue arrow); **b)** Large-scale trough cross-beds (blue arrow) in cross-bedded pumice breccia-conglomerate (D2-8) at locality H.; **c)** Cross-beds in the cross-bedded pumice breccia-conglomerate (D2-6), locality G. White pumice clasts are sub-angular to sub-rounded; **d)** Small-scale compound (i.e. internally cross-stratified) cross-beds in cross-bedded pumice breccia-conglomerate (D2-8) at locality I. Green arrows show first order cross-bed, white arrows show second order cross-beds and their orientation; **e)** Small-scale cross-beds composed of white pumice clasts and hydrothermally altered volcanic clasts in D2-8 at locality J in Dogashima 2.

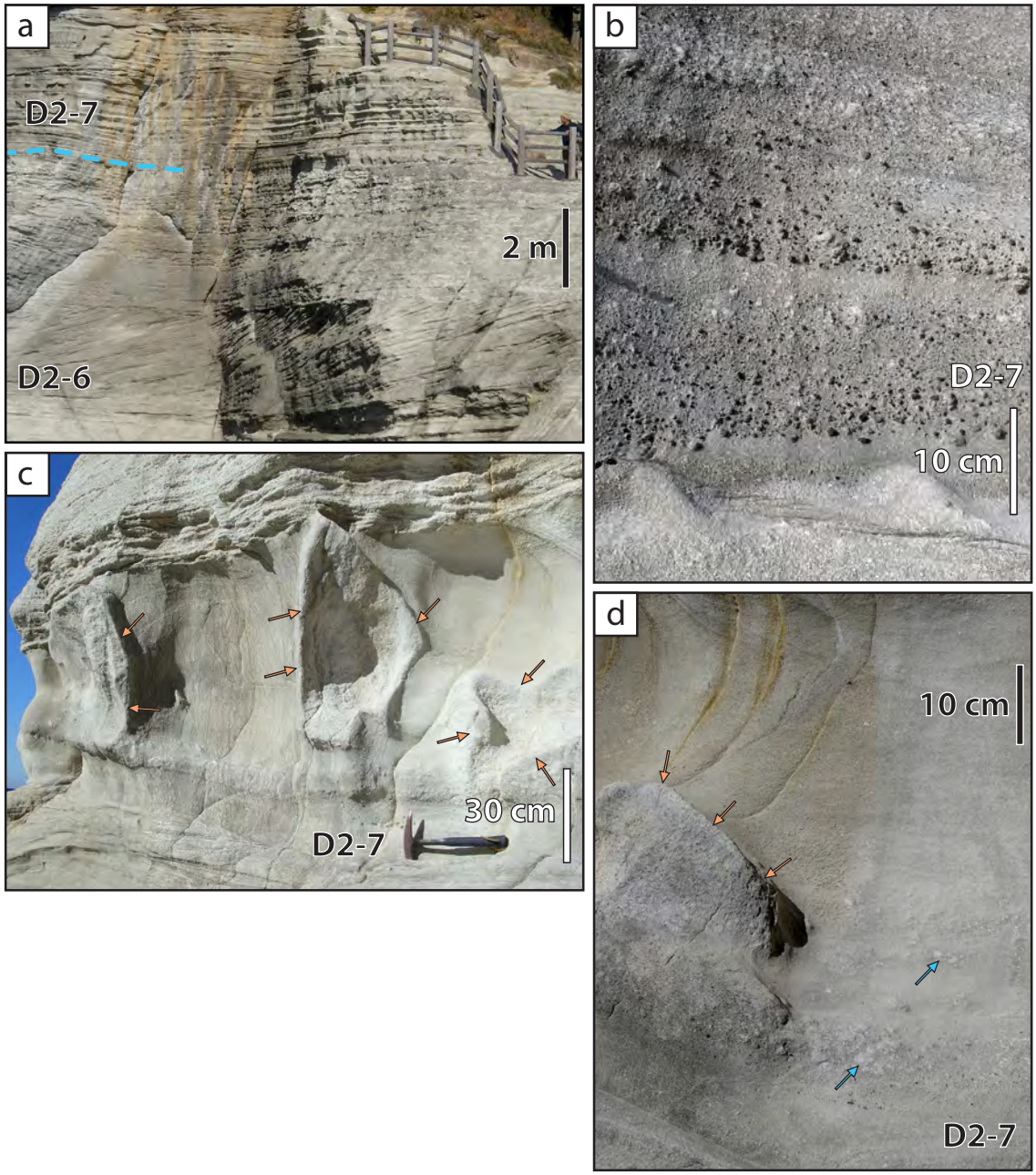

Fig. 4.25 Planar bedded pumice breccia (D2-7). **a)** Planar beds of the planar bedded pumice breccia (D2-7) and large-scale planar and trough cross beds in cross-bedded pumice breccia-conglomerate (D2-6) at locality G; **b)** Normally graded beds in planar bedded pumice breccia (D2-7), locality I. Grey andesite and hydrothermally altered volcanic clasts are abundant at the bases of the beds, whereas white pumice clasts are concentrated at the tops; **c)** Coarse pumice clasts (orange arrows) randomly distributed in a weakly stratified matrix of pumiceous sand, in planar bedded pumice breccia (D2-7), locality I. Note that rim of the white pumice clasts is differently preserved compared to its centre, which is interpreted to result from quenching; **d)** Coarse white pumice clast (orange arrow) and lenses (blue arrows) of finer white pumice clasts in diffusely stratified bed of planar bedded pumice breccia (D2-7) at locality I.

Unit D2-7: Planar bedded pumice breccia

Unit D2-7 consists of tabular to lenticular, very thin to very thick, massive to graded beds of planar bedded pumice breccia (Fig. 4.25a; Table 4.4). Unit D2-7 occurs at localities G, H and I, and internal bed thickness increases northwards. A very thick, normally graded bed of unit D2-7 overlies beds tentatively correlated with unit D2-3 with a sharp contact at locality I, whereas >9 m of units D2-4, D2-5 and D2-6 occur in between at locality G (Figs 4.11, 4.17). At locality H, an erosion surface separates unit D2-7 from beds tentatively correlated with units D2-3 or D2-4, depending on the location. Planar cross beds commonly occur in some beds, and graded beds can be stratified at their top. Normal or reverse grading is present in the very thin to medium beds (Fig. 4.25b). All clasts are smaller than 16 mm, and dominated by aphyric pumice clasts and white pumice clasts, whereas grey andesite clasts and hydrothermally altered volcanic clasts are mostly minor. The planar bedded pumice breccia is overall better sorted and finer grained than the cross-bedded pumice breccia-conglomerate facies (units D2-6 and D2-8).

Strong bimodality occurs in medium to very thick beds at localities H and I; randomly distributed, very coarse white pumice clasts (up to 1 m; Fig. 4.25c) and very rare vesicular, hydrothermally altered volcanic clasts occur in a diffusely stratified matrix mostly composed of white pumice clasts ($^1/_{16}$ mm to 4 mm; >80 vol.%), broken crystals (~10-20 vol.%) and rare grey andesite and hydrothermally altered clasts (<1 vol.%). In addition, diffuse lenses of coarser white andesite and hydrothermally altered clasts (up to 3 cm) occur in the bimodal bed at locality I (Fig. 4.25d).

6.1. Image analysis and functional stereology at locality G

The abundance of clasts versus matrix was documented by image analysis and functional stereology (chapter 2) in various beds of Dogashima 2 at locality G (Fig. 4.26). This data quantifies volume and grain size distribution of pumice and dense clasts, and is used as complement to the facies analysis description. A continuous decrease (50 to <10 vol.%) in dense clasts is seen through the various beds of the section, from the base upwards (Fig. 4.26c), and dense clasts become more abundant again at the top (~20 vol.%). Pumice clasts are almost absent in the basal unit D2-2 and in bed D2-5a, but make 20–30 vol.% of the rock volume in the other beds. The matrix proportion ranges between 50–80 vol.%, and is made of pumice and dense clasts, and crystal fragments (Fig. 4.26c). Multiple analyses were performed on top of bed 3-e, which corresponds to the level discussed in Cashman and Fiske [1991].

The lower part of Dogashima 2 is dominated by coarse dense clasts (Fig. 4.26a). Clasts coarser than 16 mm are only present in units 2, 3 and 5b (Fig. 4.26d). The volume (V_i;

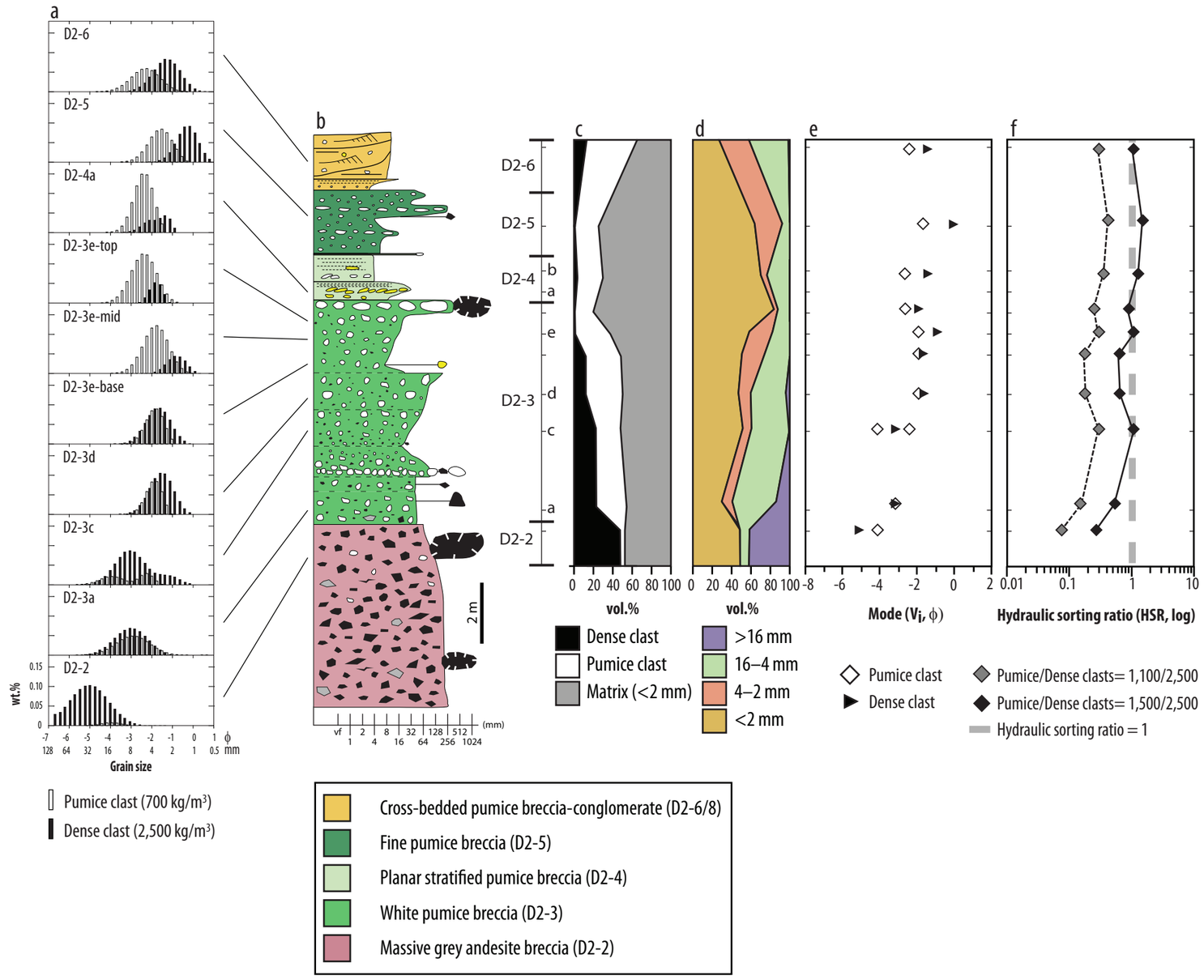

Fig. 4.26 Grain size distribution for white pumice and dense clasts (grey andesite and hydrothermally altered volcanic clasts) at locality G, in Dogashima 2. See chapter 2 for method and chapter 5 for hydraulic sorting ratio (comparing both the size and density between pumice and dense clasts). Note the extreme grain size in D2-2, and the much finer grained dense clasts compared to white pumice clasts in bed D2-3e. Key in Fig. 4.10.

chapter 2) and weight percent (chapter 2) of pumice and dense clasts in Dogashima 2 show normal grading in the lower section (Figs 4.26a, 4.26e), whereas it is narrows between -2 and -3 ϕ in the middle of the section (bed 3-e in particular). In the upper section, the distribution becomes wider (Figs 4.26a, 4.26e). In beds D2-5 and D2-6, most pumice and dense clasts are 4–16 mm diameter (Fig. 4.26d). Pumice clasts have a strong bimodal distribution in bed D2-3c (Fig. 4.26a). The grain size distribution in weight percent shows that pumice clasts are coarser than dense clasts from the middle of bed D2-3e (Fig. 4.26a), which corresponds to good hydraulic sorting (Fig. 4.26f).

7. WEAKLY STRATIFIED ANDESITE BRECCIA OF DOGASHIMA 3

This unit is an extremely thick (>50 m at locality J), clast-supported, weakly stratified to massive, overall monomictic andesite breccia composed of coarsely porphyritic andesite (Figs 4.7c, 4.11; Table 4.2). The contact with the underlying units of Dogashima 2 is knife-sharp (Fig. 4.27). Dogashima 3 occurs at localities C, I and J and its minimum volume is ~2x10^6 m^3. It overlies the white pumice breccia (unit D2-3) of Dogashima 2 at locality C (Fig. 4.10), unit D2-7 of Dogashima 2 at locality J, and unit D2-8 of Dogashima 2 with an erosional contact at locality I (Fig. 4.17). Other road outcrops of this unit occur between localities I and J. The clasts are almost exclusively 20-50 cm (max 1.5 m), equant coarsely porphyritic andesite, that are poorly vesicular (0.5 vol% vesicles), and slightly more enriched in SiO_2 than the grey andesite clasts (62.58 wt.% SiO_2; Fig. 4.8; Table 4.1); their groundmass is microcrystalline (Fig. 4.7d). Rare white pumice and hydrothermally altered volcanic clasts are also present at the base of the bed. Overall, the matrix (<20 vol.%) is composed of white pumiceous sandstone and in places has weak, disorganised stratification. The lowest metre of the unit is finer (average 25 cm). In an outcrop above locality I, Dogashima 3 shows weak sub-horizontal stratification defined by size variation in coarsely porphyritic andesite clasts.

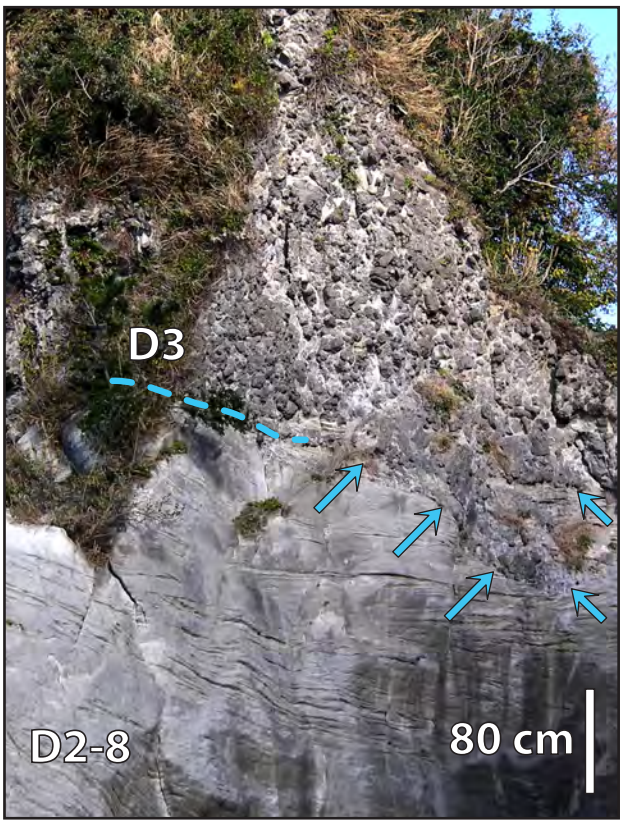

Fig. 4.27 Weakly stratified andesite breccia of Dogashima 3 in erosional contact with underlying cross-bedded pumice breccia-conglomerate (D2-8), locality I. Note the scour (blue arrows) in D2-8.

8. INTERPRETATION OF THE DOGASHIMA FORMATION

8.1 Palæo-bathymetry and palæo-currents

Palæo-bathymetry of the Dogashima Formation

Below wave-base setting in the Dogashima Formation is consistent with the open-marine environment of the Shirahama Group. However, some facies show traction current structures (thin planar beds, cross-beds and clast imbrication) in cross-bedded pumiceous breccia/sandstone in Dogashima 1 (units D1-1, D1-4, D1-7 and D1-12) and cross-bedded pumice breccia-conglomerate in Dogashima 2 (D2-6 and D2-8). These structures could indicate an upper wave-base setting [e.g. *DiMarco and Lowe*, 1989; *Kano*, 1991; *Allen et al*., 1994; *Boggs*, 2006] or part of a fluvial system [e.g. *Reid and Frostick*, 1994; *Mack et al*., 1996; *Manville et al*., 2002]. However, similar structures can be formed where current velocities are higher than in normal below wave-base, e.g. in palæo-canyons, or steep slopes [*Wright*, 2001]. Deep channels and widespread dunes fields surround modern submerged volcanic edifices in the West Mariana Ridge down to 4,000 mbsl [*Gardner*, 2010] and in the South Sandwich volcanic arc [*Leat et al*., 2010], and are associated with erosion of the edifices. Widespread siliciclastic dune fields have been witnessed in several submarine canyons, and origins including tidal forces, internal waves and storm currents have been proposed [*Valentine et al*., 1984; *Shanmugam*, 2008]. For instance, Valentine et al. [1984] observed up-to-3-m-high, 15-m-wavelength active sand dunes formed by down- and up-canyon currents of up to ~1 m/sec at down to >560 mbsl in the Oceanographer Canyon, at the northwest Atlantic continental rise. Alternatively, the traction structures in various units of the Dogashima Formation may be related to medium- to high-energy bottom-currents and/or contourites currents [e.g. *Shanmugam et al*., 1993; *Lee and Ogawa*, 1998; *Stow et al*., 1998; *Martín-Chivelet et al*., 2008; *Shanmugam*, 2008; *Stow and Faugères*, 2008; *Stow et al*., 2008]. Also, water-saturated, highly vesicular pumice clasts are prone to be re-entrained [*Manville et al*., 1998; *Manville et al*., 2002], because of their low specific gravity [~1.3; *Allen et al*., 2008]. The preferred interpretation is that the entire Dogashima Formation was deposited in a below wave-base region where strong currents occurred.

Palæo-current directions

Minor beds show elongate pumice clasts that show parallel orientation and/or imbrication, which is interpreted as palæo-current orientation and directions [Table 4.3; *Kennett*, 1982]. These units include the cross-bedded pumiceous breccia/sandstone (units D1-1, D1-4, D1-7 and D1-12), and the polymictic volcanic breccia in Dogashima 1 (units D1-3 and D1-8), as well as the top of the white pumice breccia (D2-3), planar stratified pumice breccia (D2-4) and cross-bedded pumice breccia-conglomerate (D2-6 and D2-8) in Dogashima 2. These orientations and directions are remarkably similar and are interpreted to indicate

an overall northeast to southwest palæo-current direction (Fig. 4.1), and, at locality B an east-west orientation. Syn-depositional faults at locality D suggest the same palæo-slope orientation, and a downslope direction towards the southwest.

Palæo-valley

Between the southern localities A and G, the internal architecture of Dogashima 2 preserves evidence for deposition in a sea-floor palæo-valley (Figs 4.10, 4.17). The palæo-valley was eroded into beds of Dogashima 1 between localities A to G, and is interpreted to coincide with especially thick sections of the massive grey andesite breccia (unit D2-2) in gradational contact with the overlying white pumice breccia (unit D2-3, localities B, C and F). Farther north, the white pumice breccia is very thin (<1 m), finer grained and commonly stratified, and coarse grey andesite clasts and the massive grey andesite breccia (unit D2-2) are absent, indicating a probable overbank setting. Between the palæo-valley and the northern overbank, in the northern part of locality G, the massive grey andesite breccia (unit D2-2) pinches out, and both the white pumice breccia and the fine pumice breccia (unit D2-5) units are thin and stratified. The southern wall of the palæo-valley is not exposed although at locality A, Dogashima 1 pinches out and the massive grey andesite breccia is thinner where it onlaps the Matsuzaki Formation (Fig. 4.3), possibly indicating proximity to the southern valley wall.

The palæo-valley between localities A and G includes two topographic lows. The main palæo-low occurs at localities E, F and the western part of G, and a less pronounced, ~5-m-deep palæo-low occur between localities A and B. A palæo-high is present between the two palæo-lows, over localities C, D and E, where Dogashima 1 is 15–25 m thicker than at localities A, F and G (Fig. 4.10). However, the difference in thickness is exaggerated by a general tilt of ~10° towards the east of the whole Dogashima Formation. The palæo-valley was more than 600 m wide and up to 15 m deep, and was filled by units of Dogashima 2 (Fig. 4.17).

The base of both polymictic volcanic breccia beds (D1-3 and D1-8) show sharp, discordant surfaces with underlying beds that indicate erosion and filling of small palæo-lows. These features are interpreted to be associated with strong erosion or mass wasting by small-scale collapse of the substrate [e.g. *Wright et al.*, 2008].

The out-sized (up to 10 m) grey andesite clasts in the massive grey andesite breccia (D2-2) can only be transported as bed load over steep slopes, suggesting a relatively proximal facies. No steep palæo-slope is preserved in the coastal section, but the out-sized clasts indicate that such a slope must have been nearby.

8.2. Source of clasts in the Dogashima Formation

The very similar mineral assemblage, and bulk rock and plagioclase compositions of the grey andesite, red andesite and the white pumice clasts strongly suggest they are co-magmatic.

White pumice clasts are ubiquitous throughout the Dogashima Formation, and are the dominant clast type in most beds. The abundance of angular, white pumice clasts smaller than 10-20 cm, and of free broken feldspar crystals of similar composition (An_{51-70}) to the feldspar phenocrysts in the pumice (An_{48-70}) suggest that explosive disruption of hot, vesicular magma produced these clasts. Curviplanar surfaces and remnants of quenched margins in most coarse pumice clasts (>10 cm) in pumice breccia of Dogashima 1 (units D1-2, D1-5, D1-11), and white pumice breccia of Dogashima 2 (unit D2-3) suggest breakage along thermal contraction cracks, implying that quenching contributed to magma fragmentation [e.g. *Allen and McPhie*, 2009].

The grey andesite clasts (60.9–61.0 wt.% SiO_2) that comprise up to 90 vol.% of the massive grey andesite breccia (unit D2-2) occur in the same beds as the white pumice clasts, and some coarser clasts show quenched margins. The grey andesite clasts are interpreted to come from an active lava, dome, crypto-dome or intrusion because of their temperature [*Tamura et al*., 1991], and of the presence of quenched margins, rare fluidal shape, coarseness, porphyritic texture, and absence of vesicles. It is probable that the grey andesite clasts were formed by fragmentation from multiple origins, including magmatic and steam explosions, quenching and gravitational collapse. Magmatic fragmentation is suggested by the presence of white pumice pyroclasts in massive grey andesite breccia (unit D2-2) and overlying white pumice breccia (unit D2-3). Unstable lava dome are prone to collapse from gravitational forces, and steam explosions are likely to occur in subaqueous domes at shallow depth [e.g. *Reynolds and Best*, 1976; *Fiske et al*., 1998]. Quench fragmentation could only be effective on the surfaces of the hot grey andesite lava that were put in contact with water, by exogenous lava extrusion and/or deep fracturation of the lava body. Thus, fragmentation by quenching is likely to have occurred, but remained probably secondary because only the coarse clasts show quenched rims. Thus, grey andesite clasts are interpreted to have, at least, a partial pyroclastic origin, probably associated with the magmatic gas-driven fragmentation of the white pumice clasts.

The hydrothermally altered volcanic clasts (dense clasts, scoria clasts and clasts of pumice breccia) and red andesite clasts occur in minor quantities overall and their presence (or absence) does not strongly affect the facies characteristics. Their small volume and thorough mixing with white pumice clasts suggests that they could also be pyroclasts, but not juvenile. An alternative is that they were incorporated from the substrate by the density currents of the Dogashima Formation.

Aphyric pumice clasts found in minor quantities in the Dogashima Formation and

grey scoria fragments in the polymictic volcanic breccia of Dogashima 1 match the components in the aphyric pumice-rich and fluidal clast breccia units, respectively, in the Matsuzaki Formation. They are considered to be accidental components in the Dogashima Formation and likely to have been sourced from the Matsuzaki Formation. The dark andesite clasts in the basal polymictic volcanic breccia (unit D2-1) are identical to those in monomictic breccia of the Matsuzaki Formation, and they are also regarded as accidental clasts.

The weakly stratified andesite breccia of Dogashima 3 contains coarsely porphyritic andesite clasts that have coarser and more abundant feldspar phenocrysts than in the andesitic clasts in Dogashima 1 and 2. The coarsely porphyritic andesite clasts are interpreted to be derived from an andesite lava or dome that is not preserved. The weakly stratified andesite breccia is mostly monomictic, its clasts are equant-shaped and the matrix is from another origin. This suggests auto-brecciation of an andesite lava dome. The andesite breccia is extremely thick and weakly stratified to massive. An origin by sector collapse is preferred because numerous pulses of steam explosions would produce stratified breccia.

8.3. Transport and depositional processes

The transport and depositional processes that produced the Dogashima Formation can be inferred on the basis of facies characteristics. In this section, five main modes of subaqueous transport and deposition are considered: subaqueous high-concentration volcaniclastic density current, rolling, saltation and sliding, volcaniclastic turbidity current, traction current, and suspension settling. Examples of units thought to belong to each mode are discussed. Most facies were deposited from high-concentration density currents. These currents were probably cohesionless, because clay and silt matrix is almost absent everywhere [*Lowe*, 1982; *Mulder and Alexander*, 2001].

Subaqueous high-concentration volcaniclastic density current deposits

The beds of basal polymictic volcanic breccia (D2-1), the massive grey andesite breccia (D2-2), the white pumice breccia (D2-3) and the fine pumice breccia (D2-5) in Dogashima 2, and the pumice breccia (units D1-2, D1-5, D1-11) and the basal bed of polymictic volcanic breccia (base of unit D1-3) of Dogashima 1 are mostly very thick, tabular, massive, and commonly normally graded. Discordant basal contacts with underlying units suggest they overlie erosion surfaces. They display relatively good sorting of clasts of different density, clasts are angular and sandy matrix is present. This collection of features indicates deposition from mostly cohesionless high-concentration density currents. This transport mode is part of the family of "high-density turbidity currents" of Lowe [1982] for density currents of siliciclastic compositions. Similar density currents have also be

named "high-density turbulent flows" by Postma et al. [1988], and "concentrated density flows" by Mulder and Alexander [2001]. This transport mode is here referred to as a subaqueous volcaniclastic density current.

D2-1 to D2-3

The complete gradation between units D2-2 (massive grey andesite breccia) and D2-3 (white pumice breccia) of Dogashima 2 in the palæo-valley sections (locations B, C and F) suggests that a single, cohesionless density current deposited the two main beds by (1) imperfect density segregation where dense, grey andesite clasts were preferentially concentrated at the base of the current, whereas vesicular, white pumice clasts remained at the top, and (2) a change in clast composition, from mainly dense andesite clasts to mainly white pumice clasts, during continuous aggradation.

The absence of well-developed stratification in the massive grey andesite breccia (D2-2) and white pumice breccia (D2-3) in the palæo-valley sections (locations B, C and F) indicates that the clast concentration was high enough to suppress turbulent segregation [e.g. *Kokelaar et al.*, 2007]. In contrast, the sharp contact at locality G between units D2-2 and D2-3, the presence of at least five beds in unit D2-3 that are mostly well graded, and the unusually good hydraulic sorting (comparing both the size and density between pumice and dense clasts; chapter 5) at the top of unit D2-3 [Fig. 4.26f; hydraulic sorting ratio close to 1; *Cashman and Fiske*, 1991] indicate local current unsteadiness, and an increase in turbulence and expansion, possibly induced by current interaction with the wall of the palæo-valley (less than 10 m away laterally), in the same manner as in the flow transformations at a hydraulic jump [e.g. *Komar*, 1971; *Fisher*, 1983; *Weirich*, 1988].

The increase in pumice clast size in the white pumice breccia (unit D2-3) at localities C and G (Fig. 4.26) suggests a temporary and local increase in the size of clasts in the density current [*Kneller and Branney*, 1995] and/or flow surge [*Lowe*, 1982; *Mulder and Alexander*, 2001]. The strong preferential orientation of the coarse white pumice clasts at the top of unit D2-3-e at locality G is interpreted to reflect syn-depositional shear in the depositional boundary layer [e.g. *Branney and Kokelaar*, 2002].

Coarse grey andesite clasts occur in groups in the middle and upper part of the massive grey andesite breccia (D2-2) at all localities, and define a coarse-tail reverse grading that can be explained by various processes of size segregation, including grain flow [e.g. *Sohn and Chough*, 1993], traction carpet [e.g. *Sohn*, 1997], temporal increase in the size of clasts during progressive aggradation [e.g. *Kneller and Branney*, 1995; *Branney and Kokelaar*, 2002], increase in current velocity ["flow surge", e.g. *Lowe*, 1982; *Mulder and Alexander*, 2001], and "gliding" of out-sized clasts between a basal laminar inertia-flow and an upper turbulent flow [e.g. *Postma et al.*, 1988]. Such a "gliding" mechanism is enhanced by flow confinement in canyons or channels [*Postma et al.*, 1988].

The discontinuous, local lens of basal polymictic volcanic breccia in Dogashima 2 (unit D2-1) has a very similar facies to the overlying massive grey andesite breccia (unit D2-2), except for the larger concentration of dark andesite clasts. The basal contact with Dogashima 1 follows the general geometry of the palæo-valley in which Dogashima 2 lies. Unit D2-1 is interpreted to be derived from strong local erosion of the substrate and remobilisation of dark andesite clasts of the Matsuzaki monomictic breccia by shearing at the base of the continuous subaqueous volcaniclastic density current that generated D2-2. The presence of white pumice and grey andesite clasts in unit 1 strongly indicates that it was deposited from the same current as D2-2. The formation of a separate unit (D2-1) containing a large amount of angular dark andesite clasts suggests that incorporation of these accidental clasts by the D2-2 density current was brief, and that they were probably transported over a short distance (m to tens of m). The presence of coarse, rounded white pumice clasts in the basal polymictic volcanic breccia (D2-1) and massive grey andesite breccia (D2-2) suggests that these delicate clasts were abraded in the bed load of the subaqueous volcaniclastic density current.

D2-4 and D2-5

At locality G, the internal stratification and clast imbrication in the planar stratified pumice breccia (unit D2-4) indicate the development of traction, or turbulence and unsteadiness, all of which are usually associated with lower clast concentration [e.g. *Lowe*, 1982; *Mulder and Alexander*, 2001]. This unit may have been deposited from the tail or waning phase of the current that deposited unit D2-3. The poorly stratified structure of the fine pumice breccia (unit D2-5) probably indicates unsteadiness in a subaqueous volcaniclastic density current. Because of its similarity and stratigraphic proximity to units D2-3 and D2-4, it may represent a secondary pulse of the subaqueous volcaniclastic density current that deposited units D2-3 and D2-4, or part of minor secondary volcanic events.

Dogashima 1

In Dogashima 1, the tabular, graded or massive beds of pumice breccia (units D1-2, D1-5, D1-11) and lower bed of polymictic volcanic breccia D1-3 are broadly similar to the white pumice breccia (D2-3) and the grey andesite breccia (D2-2) of Dogashima 2, respectively. The occurrence of these similar facies in Dogashima 1 indicates that similar pumice- and dense clasts-rich volcaniclastic density currents were operating during accumulation of Dogashima 1. The coarse-tail reverse grading in the D1-11 pumice breccia is probably related to an increase in clast size during aggradation.

Rolling, saltation and sliding

The extreme coarseness of the massive grey andesite breccia (unit D2-2) suggests transport of the coarsest, densest clasts by rolling, saltation and sliding on the bed base and deposition when the momentum of the clasts decreased. Such coarse dense clasts cannot be suspended in density currents. Instead, they roll, saltate or slide down steep slopes and have a short distance of run-out [e.g. *Sohn and Chough*, 1993]. The coarse dark andesite clasts in cross-bedded pumiceous breccia/sandstone beds of Dogashima 1 at locality A could also have been transported in a bed load following a local rock fall from the underlying Matsuzaki Formation.

Volcaniclastic turbidity current deposit

The overall lateral continuity, internal grading, relatively fine grain size, as well as medium bed thickness of many beds of unit D2-7 in Dogashima 2 are features consistent with deposition from intermittent volcaniclastic turbidity currents [e.g. *Lowe*, 1982; *Normark and Piper*, 1991; *Shanmugam*, 2002; *Mulder et al*., 2003].

Traction current deposits

The planar and trough cross-beds of cross-bedded and planar bedded pumiceous breccia/sandstone (Dogashima 1), cross-bedded pumice breccia-conglomerate (units D2-6 and D2-8, Dogashima 2) and few beds in polymictic volcanic breccia (units D1-3 and D1-8, Dogashima 1) show strong erosive surfaces that indicate high-energy, semi-continuous tractional currents, and formation and erosion of dune fields [e.g. *Shanmugam*, 2008]. In addition, these beds contain sub-rounded white pumice clasts that suggest clast-clast interaction in tractional currents.

Suspension settling deposits

There are two types of units that probably involved vertical settling of particles suspended in the water column. The strongly bimodal grain size of pumice clasts in some of the tabular, laterally extensive beds of unit D2-7 at locality H and I suggests delayed waterlogging of coarse pumice clasts conjointly with slow sinking of finer-grained clasts [*White et al*., 2001; *Stewart and McPhie*, 2004; *Allen and McPhie*, 2009]. The laterally extensive shard-rich siltstone of Dogashima 1 (unit D1-6 and D1-10) and the interstitial fine-grained (<2 mm) pumice clasts in Dogashima 3 show well sorted, laminated facies composed of glass shards and free broken feldspar crystals, and minor pumice clasts that were probably all pyroclasts. These facies are also likely to have been deposited vertically in the water column, and at slow settling velocities.

8.4. Eruption-fed vs. remobilised facies

Explosive, pumice-forming eruption-fed facies deposited under water can be differentiated from products of remobilisation by various criteria, including 1) a high volume of pyroclasts deposited in a short period of time, forming very thick beds that are laterally continuous, 2) massive to graded beds that overall lack internal stratifications, 3) dominated by one type of angular, juvenile pyroclasts, 4) abundance of crystal fragments of same composition than the phenocrysts in the juvenile pyroclasts, 5) lack of matrix, 6) coarse clasts that have a similar thermoremanent signature. In contrast, inferred remobilised facies show characteristics of deposition under more dilute and turbulent flow conditions, and are developed in thin to very thick beds that are more stratified, in which traction structures (cross beds, planar beds) are common, and they are well sorted with respect to size and density of clasts. In addition, remobilised facies are more polymictic and are more likely to contain rounded clasts from clast-to-clast interactions. However, these characteristics are sometimes insufficient to infer the initiating processes (chapter 6).

Eruption-fed facies

Very thick, tabular, massive to graded, and laterally continuous beds of clast-supported, pumice-dominated breccia with a feldspar crystal-rich matrix are considered to be deposits from subaqueous, explosive eruption-fed density currents. In Dogashima 2, units D2-1 to D2-5 are considered to be deposits from subaqueous explosive eruption-fed density currents. Abundance of hot-deposited clasts [*Tamura et al.*, 1991] in grey andesite breccia (D2-2), and its overall gradational contact with the overlying pumice-dominated white pumice breccia (D2-3) are additional evidence for these beds to have been deposited by subaqueous, eruption-fed density currents. The normal distribution by density through units D2-1 to D2-3 is similar to the products of neptunian eruptions [*Allen and McPhie*, 2009]. A neptunian eruption is a type of fully submerged, magmatic volatile-driven, sustained explosive eruption that produces massive to weakly graded, matrix-poor, pumice-dominated breccia overlying a neptunian lithic breccia, and that can be overlain by coarse pumice clasts and shard-rich suspension deposit [*Allen and McPhie*, 2009]. However, the abundance of dense clasts, some of them partially hot at deposition in D2-1 (0-60 vol.%), D2-2 (>90 vol.%) and D2-3 (up to 30 vol. %), distinguish this succession from the ideal neptunian model.

Planar stratified pumice breccia (D2-4) is considered to be deposited from a dilute eruption-fed density current, because it is in gradational contact with the underlying white pumice breccia (D2-3). Unit D2-5 of Dogashima 2 has similar facies characteristics to the white pumice breccia (D2-3), but is finer and thinner. This unit is considered as the product of a second, less violent magmatic volatile-driven explosive eruption, and was deposited from unsteady, eruption-fed, subaqueous density currents. The absence

of basal breccia may imply lower incorporation of dense clasts at the vent, or that these dense clasts were deposited elsewhere.

Pumice breccia in Dogashima 1 (D1-2, D1-5, D1-11) are similar to the white pumice breccia (D2-3) in Dogashima 2, and are also interpreted as deposits from explosive eruption-fed density currents. They are overall finer and thinner and do not have a basal dense clast breccia, but have good lateral continuity on coastal outcrops, are graded and non-stratified, and commonly contain coarse pumice clasts that show quench margins and rare breadcrust texture.

Glass shards and coarse pumice clasts facies are interpreted to be explosive eruption-fed and derived from suspension settling associated to subaqueous explosive eruptions. The diffusely stratified, fine-grained (<2 mm) shard-rich and pumiceous beds in units D1-6, D1-10 and D2-7 that can contain randomly distributed, very coarse white pumice clasts (up to 1 m) are interpreted to be explosive eruption-fed suspension settled deposits. Suspension (vertical settling) deposits from neptunian eruptions may be bimodal and consist of ash and giant pumice clasts [*Allen and McPhie*, 2009]. Ash and coarse pumice clasts from neptunian eruptions are not entrained in the collapsing eruption column, and settle by vertical suspension or in vertical density currents. Coarse pumice clasts derived from subaqueous explosive eruptions may be initially buoyant, thus having delayed waterlogging compared to fully waterlogged pumice lapilli [*Allen and McPhie*, 2009]. The bimodal bed in D2-7 could be related to the explosive eruption that formed units D2-1 to D2-5. The presence of unit D2-6 and beds of D2-7 underlying the bimodal beds of unit D2-7 indicate a time break between deposition from the density currents (D2-1 to D2-5) and deposition from suspension deposits (D2-7). Clasts in suspension are likely to be quickly dispersed by marine currents, and be deposited elsewhere. Thus, presence of unit D2-7 at the same site as the density current deposits D2-1 to D2-5 suggests that deposition of the entire Dogashima 2 sequence was relatively rapid. Alternatively, D2-7 could be related to another subaqueous explosive eruption that did not deposit a thick density current sequence at Dogashima, or that was not preserved.

Remobilised facies

Small volume, laterally discontinuous, thin to thick, cross bedded or planar bedded, relatively well sorted and polymictic facies that may contain rounded clasts are interpreted to be products of subaqueous sediment remobilisation. The pumice breccia-conglomerate (D2-6 and D2-8) and cross-bedded, planar bedded and normally graded pumice breccia/sandstone facies (D1-1, D1-4, D1-7 and D1-12) share most of these characteristics, and are considered to be remobilised facies. These beds are interpreted to be produced by semi-continuous remobilisation of pyroclasts by marine currents and/or gravitational mass-wasting, forming low-amplitude dune fields at Dogashima. The few cross-beds that show opposite palæo-flow directions in unit D2-8 suggest complex sedimentation from

up- and down-slope currents [*Valentine et al.*, 1984], possibly related to water movement associated with tides, and/or reflected currents associated with the channel setting.

Resedimented autoclastic facies

The very coarse, overall monomictic, weakly stratified andesite breccia of Dogashima 3 is interpreted to be a proximal deposit from autoclastic fragmentation, or from post-eruptive collapse from an unknown coarsely porphyritic andesite lava or dome that is not exposed or not preserved. The disorganised, weakly stratified pumiceous sandstone matrix of the weakly stratified andesite breccia of Dogashima 3 is interpreted as deposited after the andesite clasts, from multiple settlings of pumice sand, remobilized by marine currents filtering through the interstices between the clasts in the unconsolidated breccia [e.g. *Gifkins et al.*, 2002].

9. DISCUSSION

Dogashima 1 and 2 provide evidence of cyclic eruptive activity that included gas-rich magma erupted explosively under water (pumice breccia facies D1-2, D1-5, D1-11, D2-3 and D2-5), and extrusion and degassing of gas-poor magma on the sea floor (D2-1, D2-2 and D3). In particular, the units D2-1 to D2-3 show evidence of an effusive-to-explosive transition. In this section, the eruption dynamics and possible causes of changes from effusive to explosive behaviour are discussed, drawing in part on information about similar transitions and cycles in subaerial settings. The volcaniclastic sequence at Dogashima is compared to subaerial analogues and to other dense clast-rich subaqueous facies.

9.1. Eruption style and column dynamic

The explosive eruption-fed, pumice-rich density currents deposits of Dogashima (D2-3, as well as D2-5, D1-2, D1-5 and D1-11) are similar in all being dominated by highly-vesicular (>60 vol.% vesicles) white pumice clasts in a crystal-rich matrix. These characteristics constrain that magmatic-volatile-driven explosions were the dominant type of fragmentation to produce these units. Transition from a hot-gas interstitial fluid to water interstitial fluid is constrained by the abundance of highly-vesicular pumice clasts that would have floated if filled by gas. It was proposed that hot pumice lapilli erupted under water quickly quench and waterlog [*Allen et al.*, 2008], thus eruption column are probably short lived. The good hydraulic sorting ratio between white pumice clasts and dense clasts matches deposition of waterlogged pumice clasts from water-supported currents, indicating that the interstitial fluid was either cool or warm water.

Large amount of dense clasts in the sequence D2-1 to D2-3, and mostly continuous

grading in white pumice and grey andesite clasts between units D2-2 and D2-3 suggests continuous deposition from a single volcaniclastic density current composed of juvenile pumice clasts and hot-dome-derived [*Tamura et al.*, 1991] dense clasts. The abundance in grey andesite clasts implies powerful brecciation of a lava dome at the vent, and incorporation of dome fragments in the bed load of the density current. Rapid pumice waterlogging and eruption column collapse are attested by the continuity between D2-2 and D2-3, preventing a delay between depositions of the white pumice clasts derived from the column collapse and the grey andesite clasts derived from dome destruction, which would have resulted in two separate density currents, forming two separate beds.

Dense clasts are almost absent in the three pumice breccia units of Dogashima 1 and in D2-5, whereas grey andesite is the dominant type of clast in the breccia units D2-1 and D2-2, and occur together with hydrothermally altered volcanic clasts in the white pumice breccia (D2-3). Moderate amount of hydrothermally altered volcanic clasts could be vent derived and suggest that conduit erosion accompanied the explosive disruption of the dome. Absence of dome-related clasts in the three pumice breccia of Dogashima 1 suggests that no dome was present at the vent when these units were formed, or that the dense clasts were deposited elsewhere.

With the exception of the shard-rich siltstone facies, the very low abundance of shards in eruption-fed beds of the Dogashima Formation could be due to a combination of factors such as: reduced explosivity of below wave-base, explosive eruptions compared to their subaerial homologues; reduced production of fine particles due to minimum clast-clast interactions; elutriation during transport in water-supported, volcaniclastic density currents; and/or deposition of fine particles elsewhere than in the studied area.

9.2. Eruption history at Dogashima

Phase 1: Precursory explosive activity (Dogashima 1)

The sequence composed of units D1-2, D1-5 and D1-11 records deposition from subaqueous explosive eruption-fed density currents. These units are separated by remobilised facies (units D1-1, D1-3, D1-4, D1-7, D1-8, D1-9, D1-12) that imply that the explosive activity was intermittent. The mineralogy and composition of pumice clasts and feldspar crystals of Dogashima 1 and 2 suggest they are co-magmatic, and probably coming from the same volcano. In addition, the conformable bedding and apparent uniform palæo-slope and flow direction of Dogashima 1 and 2 strongly suggest they were erupted from a vent in a similar location or from the same volcano. The eruption-fed units in Dogashima 1 are thinner than in Dogashima 2, which suggests smaller magnitude eruptions, and they show no evidence of an associated dome. Thus, Dogashima 1 is interpreted to record precursory explosive volcanic activity to the climactic eruption recorded by Dogashima 2.

Phase 2: Effusive eruption (Dogashima 2)

The volume (~1x10^6 m^3) of the hot grey andesite clasts in D2-1 and D2-2 indicate the presence of a dome or crypto-dome that was partially destroyed (Fig. 4.28). The grey andesite clasts have a less evolved composition than the white pumice clasts but a similar mineralogy, and probably come from closely related magmas at the same volcano. Thermoremanent magnetisation of the grey andesite clasts [*Tamura et al.*, 1991], and their quenched rims indicate that some of the grey andesite clasts in D2-2 were deposited while still hot. Tamura et al. [1991] concluded that the out-sized clasts of D2-2 were deposited less than 1 hour after their brecciation, and their external rims (5 cm width) were at 450-500°C at deposition. The maximum temperature retained in the interior of the large grey andesite clasts is unknown, but presumably somewhat hotter. The presence of rare fluidal grey

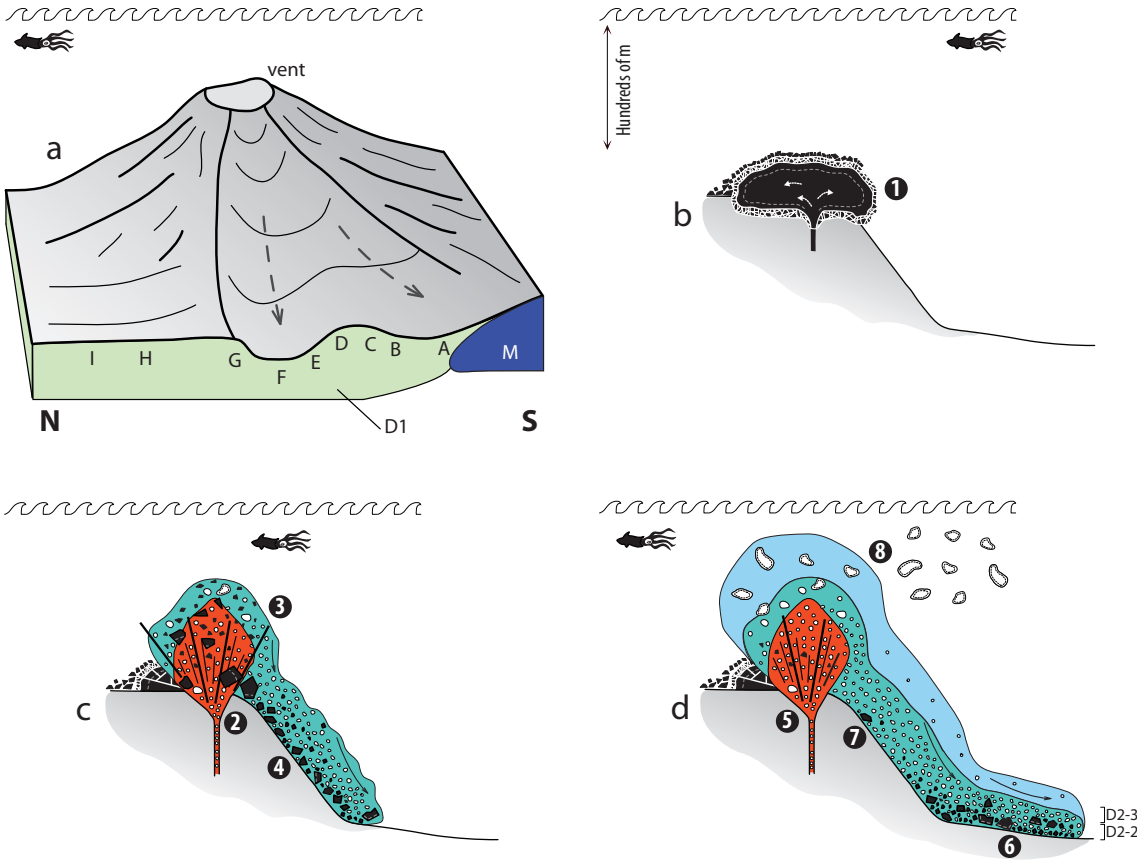

Fig. 4.28 Model for the origin of Dogashima 2, involving destruction of a subaqueous dome by a magmatic volatile-driven explosive eruption; the vertical scale of the volcanic edifice is strongly exaggerated. **a)** Geometry of the palæo-valley just before deposition of Dogashima 2, N-S section. Palæo-valley (sections A–G) and overbank facies (sections H–I) at a lower elevation than the vent, carved in Dogashima 1 (green). Palæo-valley is centred on localities E, F and G, palæo-high at C, D and E, and palæo-low between A and B. Matsuzaki Formation (M, blue) forms a palæo-high to the south; **b)** Effusive subaqueous eruption (1), producing an andesitic lava dome with quench-fractured hyaloclastite carapace; **c)** Destruction of the hot dome (2) by a magmatic volatile-driven explosive eruption. Dense hot dome fragments (3) fall out rapidly. The eruption column collapses, producing (4) a water-supported, subaqueous volcaniclastic density current of grey andesite dome clasts and white pumice clasts (units D2-1 and D2-2); **d)** Fewer dome clasts are available to be entrained in the collapsing explosion column (5) and vesicular pumice clasts become the dominant clast type (unit D2-3). Dense dome clasts are concentrated near the base of the water-supported density current (6). Very coarse grey andesite clasts (7) dislodged from the dome slide and roll downslope and sediment at top of unit D2-3e. Waning stage (D2-4), secondary explosion (D2-5) and pumice remobilisation (D2-6 and D2-8) not mentioned in cartoon. Coarse pumice clasts are temporarily buoyant (8) and deposited from suspension later (unit D2-7). Red for explosive jet sustained by magmatic gases; aqua for water-supported region containing a high concentration of coarse waterlogged white pumice and grey andesite clasts; pale blue for water-supported region with a lower concentration of finer grained pumice clasts.

andesite clasts in unit D2-2 suggests that some clasts were derived from still molten andesite.

The grey andesite clasts in Dogashima 2 are dense, non-vesicular and massive (i.e. no flow bands). Subaqueous, silicic domes and crypto-domes commonly have a poorly vesicular core and a rim that is flow banded and/or pumiceous [e.g. *Goto and McPhie*, 1998; *Gifkins et al.*, 2002; *Stewart and McPhie*, 2003; *Goto and Tsuchiya*, 2004; *Allen et al.*, 2010]. However, the volume of flow-banded and vesicular facies can be minor in comparison to the core [*Goto and Tsuchiya*, 2004], especially in volatile-poor magmas. The absence of such textures in the grey andesite clasts in Dogashima 2 could be explained by it having a low volatile content. Another possibility would involve derivation from an intrusion sufficiently deep to prevent vesiculation. If the grey andesite clasts were derived from such intrusion, a large volume of non-juvenile clasts representing the cover ought to be present. However, <5 vol.% of hydrothermally altered volcanic clasts occur in D2-2 suggesting that a deep intrusive source is unlikely. Therefore, I favour the model that a gas-poor, andesitic magma was extruded as lava dome on the same volcano that generated pumice breccia in Dogashima 1 and 2, and was subsequently destroyed while still hot (Fig. 4.28).

Phase 3: Explosive pumice-forming eruption (Dogashima 2)

Units D2-3 to D2-5 are dominantly composed of vesicular pumice clasts and free broken crystals suggesting that the explosive eruption began magmatic volatile-driven, but produced water-supported volcaniclastic density currents composed of dense grey andesite clasts and waterlogged white pumice clasts. The clast componentry in D2-2 imply that the density current was first over-loaded by hot dense grey andesite clasts, but the gradual increase of white pumice clasts in D2-3 indicates that the clast supply changed to be dominated by white pumice clasts. Presence of the planar stratified pumice breccia (D2-4) gradually overlying D2-3 probably indicates a decrease of activity during the eruption, with deposition of more dilute density currents, which attests of a waning phase in the density current. The fine pumice breccia (D2-5) is thinner and finer than D2-3, which suggests, together with its diffuse stratification, a similar type of eruption than D2-3, but weaker, thus generating unsteady density currents.

Phase 4: Resedimentation and suspension settling

The units of cross-bedded pumice breccia-conglomerate (D2-6 and D2-8) are interpreted to record remobilisation of pyroclasts deposited below wave-base by strong currents in a palæo-channel during a period of repose or weakly explosive volcanic activity.

A laterally continuous bed of planar bedded pumice breccia (D2-7) shows evidence of post-eruption settling of coarse white pumice clasts, here interpreted as delayed waterlogging of initially buoyant highly vesicular pumice clasts [e.g. *Allen and McPhie*,

2009] that were erupted at the same time as white pumice clasts of D2-3. The presence of water settled beds related to the D2-3 eruption interbedded with resedimented facies suggest that beds D2-6 to D2-8 were deposited relatively quickly after deposition of the D2-1 to D2-5 sequence.

Phase 5: Effusive eruption (Dogashima 3)

The disintegration of a new lava dome is suggested by presence of the more crystal-rich, weakly stratified andesite breccia of Dogashima 3, which corresponds to a renewal of effusive activity, probably from the same volcano where Dogashima 1 and 2 erupted. However, there is no time constraint between Dogashima 2 and Dogashima 3 eruptions. The absence of evidence for explosive eruptions associated with dome growth suggests that the magma was volatile-poor, such as during the effusion of the grey andesite dome in Dogashima 2.

9.3. Effusive-to-explosive transitions

I propose that the dramatic shift in the clast vesicularity between units D2-2 and D2-3 indicates that dome-forming effusive activity was followed by underwater, open-vent magmatic volatile-driven explosive activity (Fig. 4.28). I infer that the explosive, pumice-forming activity destroyed a still-hot andesitic dome (or lava), and dome fragments were incorporated by the eruption-fed, subaqueous volcaniclastic density currents that formed units D2-1 to D2-5. This shift in eruption style is referred to as an effusive-to-explosive transition.

The discordant contact between Dogashima 1 and 2, and the formation of the palæo-valley in the beds of Dogashima 1 between localities A and G implies that a significant erosional event occurred between the precursory phase and phases D2-1 to D2-3. Growth and degassing of the grey andesite dome of Dogashima 2 presumably occurred during this time. Here, I describe the processes that may have led to the destruction of the still-hot grey andesite dome by a pumice-forming explosive eruption, generating the D2-1 to D2-3 succession at Dogashima.

9.3.1. Subaerial effusive-to-explosive transitions

Subaerial effusion of highly viscous lava domes is widely regarded to occur in an open magmatic system, in which passive degassing proceeds during residence in a shallow reservoir and ascent in the conduit, thereby preventing explosive degassing [*Eichelberger et al*., 1986; *Jaupart and Allègre*, 1991; *Eichelberger*, 1995; *Villemant and Boudon*, 1998; *Okumura et al*., 2009]. However, several studies have shown that a hot subaerial dome can be destroyed by magmatic volatile-driven pumice-forming explosive eruptions. Such

effusive-to-explosive transitions in eruption processes have been attributed to a number of circumstances (scenarios).

(1) Spatial variations in crystallinity and volatile content of the magma within the conduit are thought to control shifts between effusive (volatile-poor) and explosive (volatile-rich) activity during an eruption. This widely recognized mechanism is proposed for the unwitnessed AD 1655 eruption at Taranaki [New Zealand; *Platz et al.*, 2007] and for the 1997 eruption at Bezymianny [Kamchatka, Russia; *Belousov et al.*, 2002], after an initial dome collapse. In Dogashima 2, the composition of the white pumice clasts is slightly more evolved than that of the grey andesite clasts, whereas the mineralogy and range in feldspar composition are similar. However, the absence of clasts with vesicularities intermediate between the two extremes suggests that this mechanism was not the primary one.

(2) Sudden catastrophic decompression of the magma chamber may occur in response to gravitational instabilities, a vulcanian eruption, or (crypto-)dome collapse [e.g. *Sparks*, 1997; *Alidibirov and Dingwell*, 2000; *Mason et al.*, 2006; *Alatorre-Ibargüengoitia et al.*, 2010]. Examples include the climactic eruption of Mount St Helens in 1980 in the USA [*Christiansen and Peterson*, 1981; *Cashman*, 1988; *Hoblitt and Harmon*, 1993], the 1956 and 1997 eruptions at Bezymianny [Kamchatka, Russia; *Belousov et al.*, 2002; *Neill et al.*, 2010], the 17 September 1996 eruption of Soufriere Hills [Montserrat, West Indies; *Robertson et al.*, 1998], the climactic eruption of Pinatubo in 1991 [Philippines; *Wolfe and Hoblitt*, 1996], and the eruption of Lascar in 1993 [Chile; *Matthews et al.*, 1997]. The 1913 eruption at Colima is tentatively added to this list [Mexico; *Luhr and Carmichael*, 1990; *Saucedo et al.*, 2010], however the dome was erupted a decade earlier, but its core was probably still hot. The eruption of Bezymianny in 1997 involved initial gravitational collapse of an active dome triggered by vulcanian eruptions, that rapidly shifted to explosive, dense-pumice-forming with the arrival of a more evolved, volatile-rich magma batch [scenario 1; *Belousov et al.*, 2002]. The massive grey andesite breccia (D2-2) in Dogashima 2 was generated by disintegration of an active dome, but the primary cause, gravitational collapse or destruction by an explosive eruption, cannot be assessed. This scenario is highly likely, considering the volume of dome clasts in D2-2 (~$1x10^6$ m^3).

(3) The magma chamber may become over-pressured by a low magma flow rate in the conduit, eventually triggering an explosive eruption [*Woods and Koyaguchi*, 1994]. Martel et al. [2007] inferred this mechanism for unwitnessed eruptions P1 (650 BP), P3 (2010 BP) and P4 (2440 BP) at Mt Pelée (Martinique, Antilles). Scandone and Malone [1985] proposed a similar process for three post-climactic eruptions at Mount St Helens (USA) in 1980. This circumstance is applicable to Dogashima 2, considering the cyclic effusive and explosive activity recorded in Dogashima 1, Dogashima 2, and Dogashima 3. In addition, the uniformly low vesicularity of the dome-derived clasts implies plenty of time for passive out-gassing.

(4) Frictional shearing of highly crystalline magma along the margins of the conduit, accompanied by phenocryst fragmentation and resorption, may increase the mass flux by lowering the magma viscosity, allowing faster ascent of the magma [*Rosi et al*., 2004]. This process is proposed [*Rosi et al*., 2004] to have acted at Pinatubo (Philippines) in 1991 and in the 800 BP eruption at Quilotoa (Ecuador). This circumstance is unlikely to have happened in Dogashima 2, because the grey andesite and white pumice clasts have only moderate crystallinity and the phenocrysts and free broken crystals are consistently euhedral.

Therefore, facies analysis in Dogashima 2 suggest that the units D2-2 and D2-3 are derived from an effusive-to-explosive transition, associated with either gravitational dome collapse and/or destruction by an explosive eruption (scenario 2), or low magma flow rate in the conduit that caused magma chamber overpressure (scenario 3).

9.3.2. Comparison of subaerial and subaqueous effusive-to-explosive eruptions

Products of subaerial effusive-to-explosive eruptions

The typical subaerial products of pumice-forming explosive eruptions that destroy a hot dome (Fig. 4.29d) are composed of juvenile pumice and denser hot-dome-derived clasts [e.g. *Hoblitt and Harmon*, 1993; *Wolfe and Hoblitt*, 1996; *Robertson et al*., 1998; *Martel et al*., 2000; *Wilson*, 2001; *Belousov et al*., 2002; 2004; *Platz et al*., 2007; *Neill et al*., 2010; *Saucedo et al*., 2010]. Pyroclasts are dispersed by a variety of density currents (dense-clast-rich block-and-ash flows, pumiceous pyroclastic flows, surges) and by fallout. Dome fragments and juvenile pumice clasts are typically deposited together. However, a delay between the initial dome destruction by collapse and the pumice-forming eruption may produce separate beds. The main product of this process is an overall matrix-supported breccia. Block-and-ash flows and pyroclastic surges may be generated by precursory dome collapse and generate dome-derived, monomictic breccia supported in an ash and fine-ash matrix. Pumice-rich fallout deposits may be deposited before, during and after the main eruptive event, and may contain dome-related clasts. The top of the sequence may be reworked or consist of a laminated ash fall deposit of regional extent. Accretionary lapilli are likely to be found in any part of the sequence produced by the subaerial eruption column.

Products of subaqueous effusive-to-explosive eruptions

The facies in Dogashima 2 demonstrate that products of underwater hot dome destruction can be distinguished from the equivalent subaerial facies (Fig. 4.29). The products typical of subaqueous dome-explosive transition include a very thick basal breccia composed of dome clasts overlain by very thick, graded, clast-supported pumice breccia with a shards-depleted, crystal-rich matrix. The deposits are likely to be relatively well hydraulically sorted [e.g. *Cashman and Fiske*, 1991], because of the greater density and viscosity of water

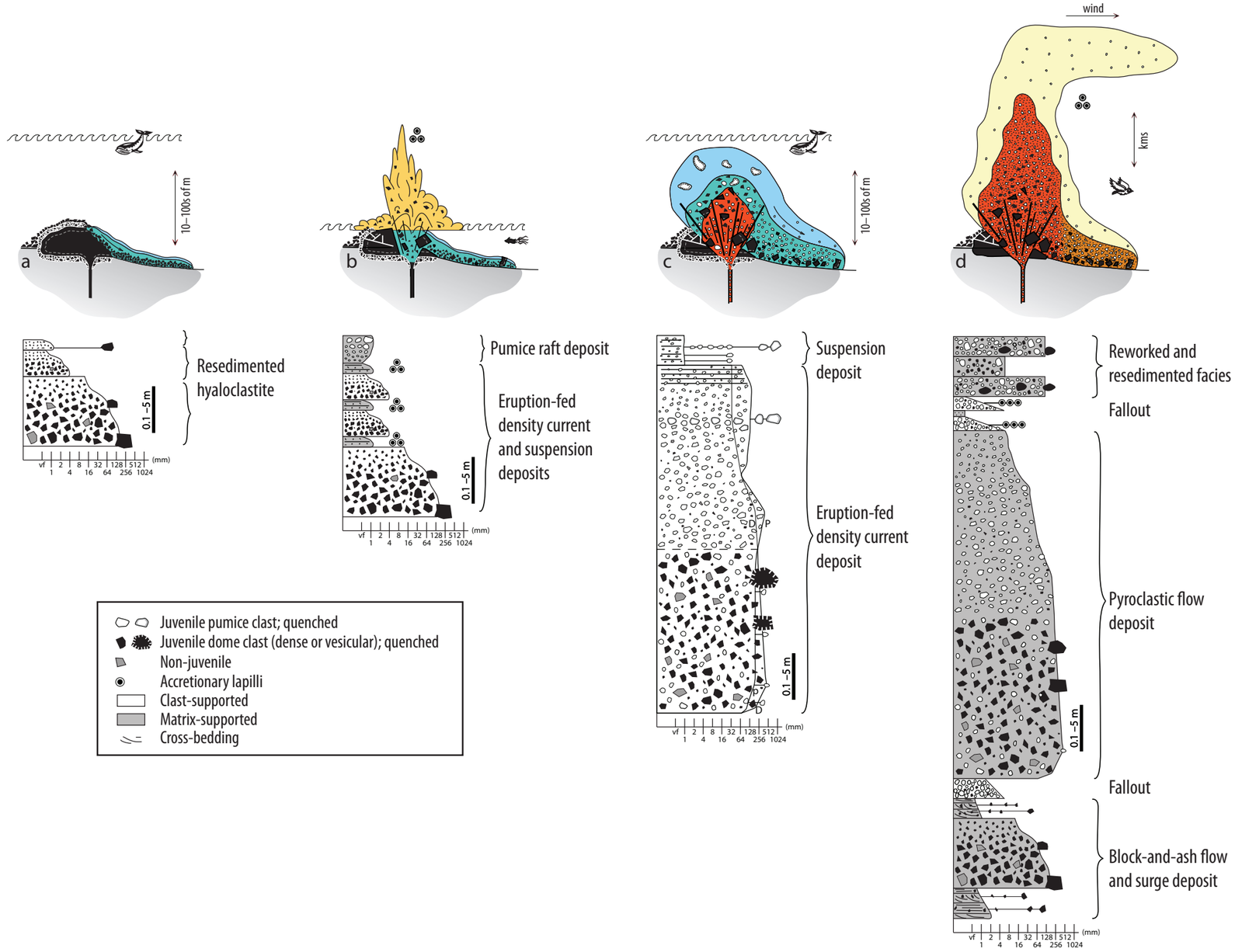

Fig. 4.29 Comparison of dome destruction processes. **a)** Non-explosive destruction of a subaqueous hot dome. Transport of dome clasts in grain flows, rock fall and avalanches (green) and minor dilute density currents (pale blue). Minor rock falls or grain flows can occur. Modified after Gifkins et al. [2002] and McPhie et al. [1993]; **b)** Explosive destruction of an active shallow-water dome. The dome-derived clasts (vesicular or dense) are intensely fragmented by phreatomagmatic explosions, and entrained in subaqueous volcaniclastic density currents that deposit clast-supported dome-derived clast breccia. Settling from suspension of ash in the subaqueous plume, and from subaerial fallout and dilute density currents deposit interbedded ash layers that contain glassy ash, crystal fragments and accretionary lapilli. Delayed vertical settling by waterlogging of pumice dome-derived clasts produce reversely graded, suspension settling deposits; **c)** Destruction of a hot, subaqueous lava dome by a magmatic volatile-driven, pumice–forming explosive eruption. A magmatic gas-supported, pumice-rich explosive eruption column (red) collapses into a water-supported, subaqueous volcaniclastic density current (green); dilute density current in pale blue. Rock fall of dome clasts can occur. This process forms an overall normally graded, clast-supported, coarse, density sorted breccia that may have a finer, laminated top. A suspension deposit may occur above the graded breccia. Coarse dome clasts and coarse pumice clasts have quenched margins; **d)** Destruction of a hot, subaerial lava dome by a magmatic volatile-driven, pumice-forming explosive (plinian or sub-plinian) eruption [e.g. Scandone and Malone, 1985; Wolfe and Hoblitt, 1996; Matthews et al., 1997; Robertson et al., 1998; Belousov et al., 2002; Rosi et al., 2004; Martel and Poussineau, 2007; Platz et al., 2007; Saucedo et al., 2010]. Dome clasts are entrained in the magmatic gas-supported, pumice-rich explosive eruption column (red) that may collapse into pyroclastic density currents (orange); dilute density current in yellow. Cartoons: Red for explosive jet sustained by magmatic gases; yellow for dilute, hot air and magmatic gas-sustained region, aqua for water-supported region containing a high concentration of coarse water-logged juvenile pumice clasts; pale-blue for water-supported region with a lower concentration of finer grained pumice clasts. Pumice clasts, p; dome-related clasts, d.

compared with air and the cohesionless nature of high-concentration density currents (chapter 3, chapter 5). The coarsest dome-derived and pumice clasts have quenched rims, contraction cracks and curviplanar surfaces reflecting brittle fragmentation at contact of hot clasts with water.

Comparison with products of shallow-water phreatomagmatic destruction of domes

Entry of water into the deep structure of a hot subaerial dome can fragment magma by quenching, and/or by flashing to steam and producing phreatomagmatic and phreatic explosions that can cause its collapse [e.g. *Elsworth et al.*, 2004; *Matthews and Barclay*, 2004; *Taron et al.*, 2007; *Hicks et al.*, 2010]. Dome destruction by phreatomagmatic eruptions at shallow water depths has been witnessed [*Reynolds and Best*, 1976; *Reynolds et al.*, 1980; *Fiske et al.*, 1998; *Maeno and Taniguchi*, 2006]. Therefore, parameters such as hydrostatic pressure and the high heat capacity of external water can be expected to play important roles in the potential destruction of active underwater domes. Hydrostatic pressure influences magma vesiculation and (magmatic and external) steam expansion, and therefore, potential explosive fragmentation [*White*, 2000; *Head and Wilson*, 2003]. Confining pressure from increase of water depth dramatically reduces the volume of steam produced in hydrovolcanic explosions [*Head and Wilson*, 2003]. Water has a high heat capacity and is very effective in cooling hot magma and condensing magmatic gases [*Allen et al.*, 2008]. The presence of water may favour collapse of the hot dome by build-up of steam overpressure at its margins, and creation of thermal contraction cracks deep in the structure of the dome, by quenching of the hot lava.

On the basis of witnessed eruptions [*Reynolds and Best*, 1976; *Reynolds et al.*, 1980; *Fiske et al.*, 1998; *Maeno and Taniguchi*, 2006], I infer that the subaqueous deposits derived from shallow-water phreatomagmatic eruptions that destroy a hot dome should include multiple clast-supported beds of dome-derived breccia. Interbedded suspension settled deposits from subaqueous plume and subaerial fallout onto the water surface and from dilute density currents that flow over water are also likely to occur [*Sohn and Yoon*, 2010] if the eruptions are shallow and powerful enough to generate subaerial plume. Such suspension deposits are likely to include glassy ash, crystal fragments and accretionary lapilli (Fig. 4-29b). The pumice clasts that cool in air may not immediately waterlog in contact with water, and create rafts. Delayed waterlogging of buoyant pumiceous dome components may generate reversely graded settling deposits composed of sub-rounded to rounded pumice clasts that were abraded in pumice rafts [chapter 3; *White et al.*, 2001].

9.3.3. Comparisons of explosive and non-explosive destruction of submarine domes

Autoclastic fragmentation of subaqueous domes generates in-situ and resedimented hyaloclastite (Fig. 4.29a) that is much smaller than the dome itself, and composed of massive to stratified, clast-supported, overall monomictic breccia. It is composed of clasts that span from dense to pumiceous but dense dominate usually, and clasts are glassy or have glassy margins [*Pichler*, 1965; *Horikoshi*, 1969; *Horikoshi and Sato*, 1970; *Kato et al*., 1971; *Yamazaki et al*., 1973; *Yamagishi*, 1987; *McPhie et al*., 1993; *Kano*, 1996; *Busby et al*., 2003]. Such deposits may extend up to several hundreds of metres away laterally from the original extrusion.

The D2-D3 sequence in Dogashima 2 differs from the products of autoclastic fragmentation in that it is mostly composed of various types of lapilli-size clasts. The relatively fine grain size, abundance of highly vesicular pumice, and lack of clasts transitional between the dense grey andesite and the white pumice clasts, in the white pumice breccia are best accounted for by a pumice-rich, subaqueous explosive eruption. In addition, the grey andesite clasts are not glassy, although the coarsest clasts have margins that were formerly glassy. Curviplanar surfaces on coarse pumice clasts in D2-3 indicate that quenching contributed to the fragmentation of these clasts. The beds of pumice breccia in Dogashima 1 indicate that pumice-forming, precursory explosive activity occurred.

9.3.4. Recognition of products from dome destroyed by an explosive eruption

The presence of a growing lava dome prior to or during an explosive eruption could be difficult to recognize in the associated deposits, for several reasons including: (1) In the absence of palæo-temperature data, fragments of an old inactive dome [e.g. *Shepherd and Aspinall*, 1982; *Swanson and Kienle*, 1988; *Macías et al*., 1998; *Paterson et al*., 2009] may be indistinguishable from fragments of an active dome; (2) Dome-derived clasts could be easily missed in the deposits if the dome was relatively small; (3) Proximal facies that potentially contain coarse dome fragments have very small volumes (<<1 km^3) and limited extents (<100s m) and are generally not well preserved in the rock record; (4) Poorly vesicular juvenile clasts that have been identified as "dense pumice" in many facies descriptions could, in some instances, belong to the vesicular facies of a lava dome. (5) Juvenile clasts in the products of effusive-to-explosive transitions can be uniform in composition [e.g. *Martel et al*., 2000] or vary [e.g. *Pallister et al*., 1996; *Platz et al*., 2007], and making such an eruption process difficult to identify. Therefore, it could be that many subaerial and subaqueous explosive eruptions begin with effusive activity in the form of a shallow intrusion or a dome, as proposed for Dogashima 2.

9.4. The Dogashima "fallout layer"

Cashman and Fiske [1991] interpreted the white pumice breccia at locality G (beds D2-3d and D2-3e in this study) to be "fallout" from the buoyant umbrella of a "subaqueous eruption plume", drawing attention in particular to the good hydraulic sorting (chapter 5) between white pumice and dense clasts. However, my detailed facies analysis of all exposures of Dogashima 2 has provided evidence that D2-3 and in fact almost all of Dogashima 2 involved final transport as sea-floor-hugging density currents.

The hydraulically sorted part of the white pumice breccia (beds D2-3d and D2-3e) at locality G is <4 m thick, stratified, reversely graded in white pumice clasts and can be traced for no more than 20 m laterally. It pinches out where the entire D2-1 to D2-5 succession thins to a 1-m-thick, stratified bed, almost exclusively composed of pumice lapilli and feldspar crystal fragments. The palæo-valley facies of unit D2-3 is very thick, tabular, massive, and contains minor lenses of coarse pumice clasts. It grades continuously downward into the underlying massive grey andesite breccia (D2-2) and the local polymictic volcanic breccia (D2-1) that rests on an erosional surface. This facies association (D2-1 to D2-3) also shows strong density segregation of the dense clasts and forms a much thicker deposit in topographic lows, implying a final transport as a high-concentration density current.

The peculiar locality G occurs on the rim of a palæo-valley that lies between localities A and G. This uneven palæo-topographic feature may have locally caused current unsteadiness and flow expansion that increased its turbulence, in a similar way to a hydraulic jump [e.g. *Komar*, 1971; *Fisher*, 1983; *Weirich*, 1988], resulting in local stratification and good hydraulic sorting [*Cashman and Fiske*, 1991].

Allen et al. [2008] demonstrated that the waterlogging of hot pumice lapilli that are filled with magmatic gases happens rapidly within the eruption jet during underwater magmatic volatile-driven explosive eruptions from vents deeper than ~200 m. Hence, underwater eruption columns are prone to collapse as these waterlogged pumice clasts are negatively buoyant, and also because the gas (magmatic steam) driving the jet cools and condenses. The pumice lapilli are then transported in water-supported density currents over large distances from vent. Hence, subaqueous pumice-rich eruption columns may produce buoyant, laterally spreading umbrella plumes [Cashman and Fiske, 1991], but these plumes are composed almost exclusively of clasts with slow settling velocities, such as glass shards and buoyant, hot large pumice clasts [Allen and McPhie, 2009]. Coarse subaqueous fall deposits are very hard to preserve due to the pumice being easily remobilised [Manville et al., 1998; Manville et al., 2002]. Subaqueous fall deposits should mimic some of the major characteristics of fall deposits from subaerial explosive eruption columns [e.g. Pyle, 1989], including non-erosive lower contacts, lateral continuity over substantial distances, and systematic thickness and grain size changes with distance

from source. None of these characteristics are displayed by either the "fallout layer" (D2-3d, D2-3e) or by the gradationally enclosing D2-1 to D2-3 succession.

10. CONCLUSIONS

The Pliocene Dogashima Formation (Izu Peninsula, Japan) is composed of three volcaniclastic sequences erupted and deposited under water. Dogashima 1 is mostly composed of pumice breccia, cross-bedded and planar-bedded pumiceous breccia/sandstone and polymictic volcanic breccia that show sharp and erosive bed contacts. The base of Dogashima 2 is dominated by a very thick, clast-supported massive grey andesite breccia composed of andesite clasts with quenched margins, exceptional coarseness and rare fluidal shapes. It is gradationally overlain by a very thick, clast-supported white pumice breccia chiefly composed of white pumice clasts. The white pumice breccia becomes better sorted and stratified in proximity to the wall of a paleo-valley, and is much thinner, stratified and finer grained in overbank facies, whereas the massive grey andesite breccia is confined to a paleo-valley eroded to beds of Dogashima 1. The top of Dogashima 2 is dominated by very thick cross-bedded pumice breccia-conglomerate and planar bedded pumice breccia. Top of the sequence is in erosive contact with weakly stratified andesite breccia of Dogashima 3.

Similar mineralogy and bulk rock and feldspar composition in white pumice, grey andesite clasts and free broken crystals in Dogashima 1 and 2 suggests they were co-magmatic and erupted from the same vent. Dogashima 2 is interpreted to record explosive destruction of a subaqueous hot lava dome by a magmatic volatile-driven explosive eruption, generating eruption-fed, subaqueous volcaniclastic density currents. Coarse pumice clasts and ash in overlying planar bedded pumice breccia suggest delayed suspension settling. This sequence demonstrates that lava or dome effusion on the sea floor can, like in subaerial analogues, dramatically switch to an open-vent, pumice-forming, magmatic volatile-driven explosive activity.

A cyclic behaviour of effusive and explosive eruptions in the Dogashima Formation is suggested by pumice-rich breccia of Dogashima 1 interpreted as precursory explosive activity, hot dome destruction by a subaqueous explosive eruption in Dogashima 2, and monomictic andesite breccia in Dogashima 3 that suggests dome-building episode. Abundance of cross-bedded facies in the Dogashima Formation in a pelagic, below wave-base regional setting suggests below wave-base resedimentation of pumiceous aggregates by bottom currents and mass-wasting processes.

5

Image analysis and grain size stereology on rocks: Application to subaqueous volcaniclastic facies and characterisation of deposition processes

1. INTRODUCTION

Interpretation of detrital sediments in terms of mechanisms of transport and deposition has been a constant focus in geology [*Friedman*, 1962; *Kuno et al.*, 1964; *Passega*, 1964; *Buller and McManus*, 1973; *Garzanti et al.*, 2009]. Visher [1969] and Glaister [1974] proposed a classification of multi-modal distributions based on the segmentation pattern of cumulative grain size distribution curves. Their method was designed to discriminate three major types of transport (traction, saltation, suspension), but could be applied only to certain types of detrital sediments [*Sengupta et al.*, 1991], and has not been tested for volcaniclastic deposits. The values of median diameter and standard deviation of grain diameter are by far the most widely used parameters to identify similar clast populations as a first step in determining the fragmentation and the transport of volcaniclastic deposits [*Murai*, 1961; *Walker*, 1971; 1983; 1984].

Grain size characteristics of pyroclastic deposits are an important attribute in physical models of subaerial explosive volcanic eruptions [e.g. *Walker*, 1971; *Sparks et al.*, 1973; *Sparks*, 1976; *Walker*, 1983; 1984; *Wilson and Walker*, 1985; *Carey*, 1991; *Bonadonna and Houghton*, 2005; *Dufek and Bergantz*, 2007; *Macedonio et al.*, 2008; *Volentik et al.*, 2010]. However, it has not been possible to apply these physical models to lithified and/or welded deposits from such eruptions, although these rocks are far more abundant than unconsolidated deposits.

In this chapter, the grain size distribution of numerous volcaniclastic rocks is statistically reconstructed by image analysis and functional stereology, using photographs of outcrops and scans of rock slabs (chapter 2). I explore grain size characteristics in terms of modal grain size distribution, median and standard deviation parameters to infer transport and depositional processes. In addition, the degree of hydraulic sorting between pumice and dense clasts is discussed in relation to transport and depositional processes.

2. SAMPLES

2.1. Sample collection

Image analysis and functional stereology were performed on a selection of 85 volcaniclastic samples of different origins and from several localities (Digital appendix). Most samples belong to formations discussed in the previous chapters, i.e. the Dogashima Formation (Izu Peninsula, Japan; chapter 4) and the Ohanapecosh Formation (Washington State, USA; chapter 3). Additional samples were collected in the Manukau Sub-Group [Northland, New Zealand; Appendix E; *Allen et al.*, 2007] and in the Sierra la Primavera caldera [Jalisco State, Mexico; *Clough et al.*, 1981]. The grain size data are based on images that are a combination of up to three nested datasets from outcrop photographs and rock

slab scans taken at different magnifications (chapter 2), for a total of 165 images.

Results of facies analysis (chapters 3 and 4) are used to test whether proportional volume and grain size distribution of coarse clasts is indicator of transport and depositional processes in subaqueous volcaniclastic deposits. From the dataset at disposition, three general subaqueous volcaniclastic facies could be identified on the basis of bed thickness, degree of sorting and abundance of matrix. These facies include (Table 5.1) two very thick to extremely thick, massive or graded facies that can be divided into (MR-thick) matrix-rich (>50 vol.%) and (MP-thick) matrix-poor (<50 vol.%) types, and a (MP-thin) thin to thick (< 1 m), clast-supported, well sorted and matrix-poor facies.

The abundance of matrix is used to discriminate between facies MR-thick and MP-thick, because the abundance of fine-grained particles may reflect eruption, transport and depositional processes (chapters 3 and 4). However, graded beds are difficult to classify, because textural characteristics such as grain size and volume of clast types and matrix vary through the stratigraphy, by definition (Figs 5.1, 5.2). In this chapter, beds are considered matrix-rich for their overall abundance of matrix, but they can contain matrix-poor sub-facies (generally dense clast basal breccia) that are clast-supported.

The beds included in the matrix-rich, very thick to extremely thick, massive or graded facies (MR-thick) were sampled in the Ohanapecosh Formation (facies 1, 2, 3, 4, 5; chapter 3). Typical examples comprise graded beds 57 and 61 in the Chinook Pass section, and beds 40 and 42 in the Cayuse Pass section (Chinook Pass Member). These five facies in the Ohanapecosh Formation were interpreted as deposits from eruption-fed and resedimented subaqueous volcaniclastic density currents, and most likely to be related to subaerial pyroclastic flows that entered water. The matrix-poor, very thick to extremely thick, massive or graded facies (MP-thick) occur in the Dogashima Formation (chapter 4). The most typical example is the bed of grey andesite breccia (D2-2) overlain by white pumice breccia (D2-3) in Dogashima 2. These clast-supported facies were interpreted to have been deposited from subaqueous volcaniclastic density currents derived from collapse of a subaqueous explosive column. Finally, the matrix-poor, thin to thick, clast-supported, well sorted facies (MP-thin) is exemplified by beds of normally graded pumice lapillistone at Bethells Beach and Pillow Lava Bay in the Manukau Sub-Group, New Zealand (Appendix E). The samples from Sierra La Primavera caldera are also

Facies	Number of samples	Facies characteristics	Formation/Sub-Group
MR-thick	46	Matrix-rich, very thick to extremely thick, massive or graded	Ohanapecosh, Dogashima, Manukau
MP-thick	25	Matrix-poor, very thick to extremely thick, matrix or graded	Dogashima 1 and 2
MP-thin	14	Matrix-poor, thin to thick, clast-supported, well sorted	Ohanapecosh, Manukau, Primavera caldera

Table 5.1 Facies of volcaniclastic rocks analysed by functional stereology

included in this third facies, although they are extremely thickly bedded. This facies was interpreted as deposited from suspension settling.

2.2. Terminology

The clast types in the samples analysed are grouped into two main categories for simplicity: (1) Pumice clasts, which contain ~60–80 vol.% vesicles and are intermediate (Dogashima, Ohanapecosh) to silicic (Manukau) in composition. Some of the pumice clasts have been compacted to form fiamme. "Deflattening" of the fiamme (Appendix B) could not be done because the fiamme and pumice clasts coexist in some facies and the original pumice clast vesicularity is unknown. Fiamme only occur in some beds of the Ohanapecosh Formation. The density of waterlogged pumice clasts is assumed to have been approximately 1,100 to 1,500 kg/m^3. (2) Dense clasts, which are non-vesicular and include basalt, andesite and hydrothermally altered clasts (chapters 3 and 4). Their density is assumed to have been 2,500 kg/m^3.

Clastic rocks may contain one or multiple types of clasts, matrix, interstitial pore space and cement. Matrix refers to the finer grained clasts that surround the coarse clasts [e.g. *Boggs*, 2006]. Matrix can have the same composition and be part of the same modal population as the main coarse clasts, or form secondary, finer grained modes. The original texture of fine grained particles, typically <2 to <0.25 mm (<-1 to <2 ϕ) in clastic rocks, is commonly destroyed or poorly preserved. Two mm is a critical boundary that separates sand from gravel, sandstone from breccia or conglomerate, ash from lapilli, and tuff from breccia or lapillistone in pyroclastic deposits [*McPhie et al.*, 1993; *Blott and Pye*, 2001; *Boggs*, 2006], thus it is appropriate to use 2 mm as a cut-off value in this study. All particles <2 mm are called matrix, even though cement might also be present. Cement is a post-depositional, chemical and/or biochemical precipitate that may partly or completely fill the porosity left between particles that constitute the sediment (matrix and/or clasts). In a rare case (Manukau Sub-Group), cement could be separated from matrix, and this sample is clearly mentioned.

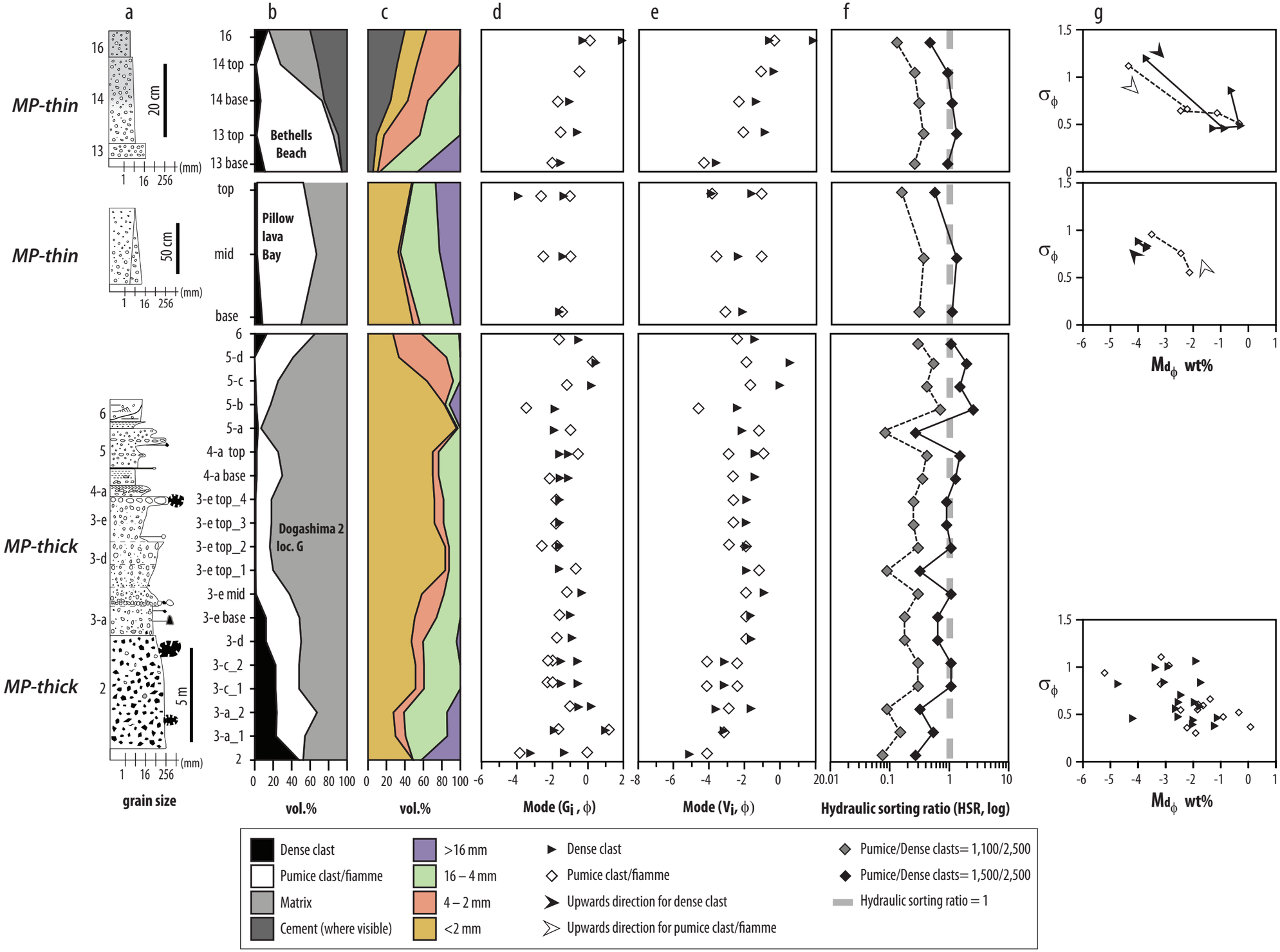

Fig. 5.1 Image analysis and functional stereology on graded beds in the Dogashima Formation and the Manukau Sub-Group. **a)** Stratigraphic logs from field estimates; **b)** Clast, matrix and cement volume percent from image analysis; **c)** Volume percent of various clast size groups and cement, extracted from functional stereology; **d)** Modal grain size distribution density (G_i) from functional stereology; **e)** Modal volume per phi (V_i) from functional stereology; **f)** Hydraulic sorting ratio (comparing both the size and density between pumice and dense clasts) at two waterlogging ratios; **g)** Standard deviation versus median values for samples from locations progressively up stratigraphy.

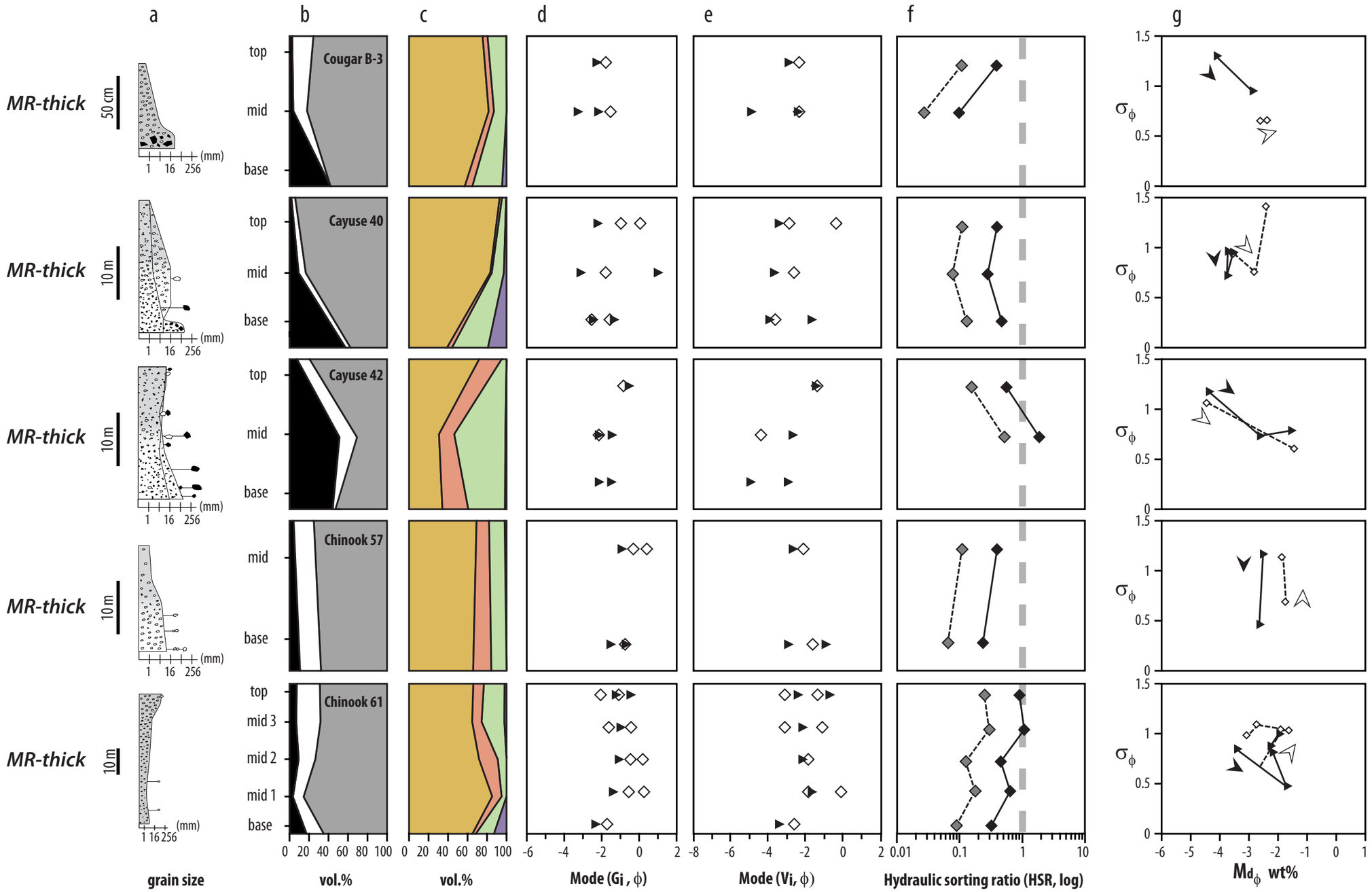

Fig. 5.2 Image analysis and functional stereology on graded beds in the Ohanapecosh Formation. **a)** Stratigraphic logs from field estimates; **b)** Clast, matrix and cement volume percent from image analysis; **c)** Volume percent of various clast size groups and cement, extracted from functional stereology; **d)** Modal grain size distribution density (G_i) from functional stereology; **e)** Modal volume per phi (V_i) from functional stereology; **f)** Hydraulic sorting ratio (comparing both the size and density between pumice and dense clasts) between pumice and dense clasts at two waterlogging ratios; **g)** Standard deviation versus median values for samples from locations progressively up stratigraphy. See Figure 5.1 for legend.

3.QUANTIFICATIONOFTEXTURALCHARACTERISTICSINGRADEDVOLCANICLASTIC BEDS

3.1 Clast volume in graded beds

Stratigraphic logs are commonly based on visual estimates in the field that reproduce the main textural characteristics and approximate grain size. The image analysis method (chapter 2) quantifies clast and matrix volumes. As example of the image analysis method, Figures 5.1 and 5.2 show typical graded facies from the Ohanapecosh Formation (chapter 3), the Dogashima Formation (chapter 4) and the Manukau Sub-Group (Appendix E).

Data extracted from image analysis give a large choice of parameters to characterise and classify clastic aggregates. In contrast to object size distribution, a volume is proportional to its area on a representative cross section [*Reid*, 1955]. This relationship permits the direct quantification of the abundance of separate clast types and porosity from image analysis. Parameters such as the volumes of matrix and cement in various samples can be quantified. Volumes in clastic rocks are approximated by:

$$A_{Tot} \cong V_{Tot} \cong V_{Matrix} + V_{Cement} + V_{Pum\_coarse} + V_{Dense\_coarse} \qquad (5\text{-}1)$$

where A_{Tot} is the total area of the sample, V_{Tot} is the total volume of the sample, V_{Cement} is the total volume of the porosity and cement (where identifiable) from image analysis, V_{Matrix} is the total volume of the matrix (<2 mm), and V_{Pum_coarse} and V_{Dense_coarse} are the volumes of pumice and dense clasts coarser than 2 mm, respectively.

The volume of pumice and dense clasts (>2 mm) over matrix and cement (<2 mm) reflects the bulk rock composition, and is indicator of the degree of sorting. A large proportion of samples (Fig. 5.3) is dominated by matrix (>50 vol.%) and depleted in dense clasts (<20 vol.%). The presence of cement or porosity instead of matrix indicates poor packing of clasts [*Jerram et al*., 1996] and corresponds to relatively good sorting. Thus, the volumes of matrix and cement in a deposit can be used as proxies for the degree of coarse tail sorting, providing that cement can be distinguished from matrix.

The studied samples of matrix-poor, thin to thick, clast-supported, well sorted facies (MP-thin) are chiefly composed of pumice clasts (Fig. 5.3) and their content of matrix (and cement) is variable. Numerous samples of matrix-poor, very thick to extremely thick, massive to graded facies (MP-thick) have a matrix-rich signature (Fig. 5.3), because they are the fine-grained sub-facies of overall matrix-poor beds (e.g. Dogashima; Fig. 5.1). The matrix-rich, very thick to extremely thick, massive or graded facies (MR-thick) has overall the highest abundance of dense clasts, and commonly contains a basal dense clast breccia sub-facies that is depleted in matrix (e.g. bed Cayuse 40; Fig. 5.2)

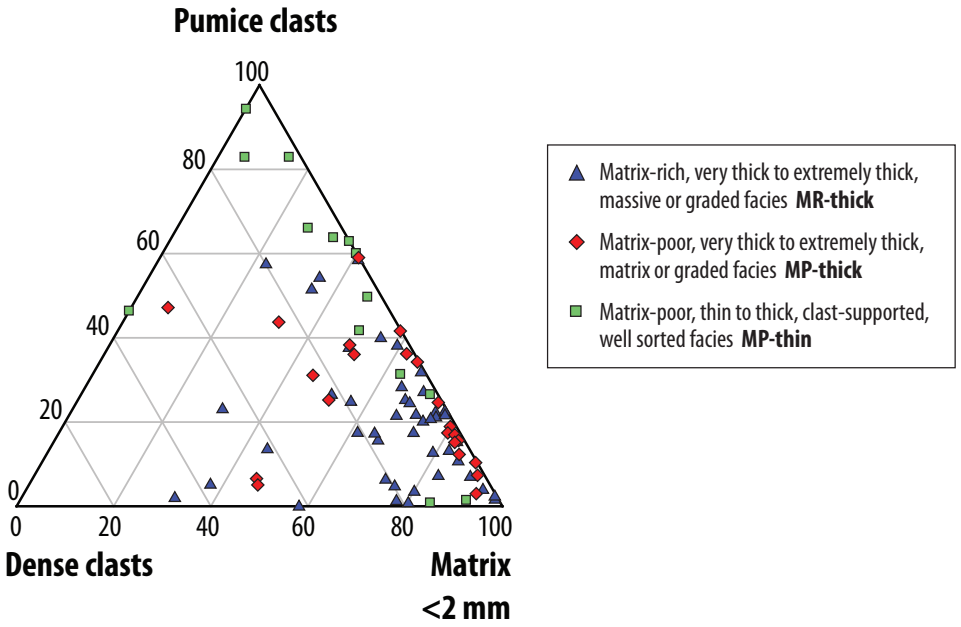

Fig. 5.3 Triangular diagram of proportional volumetric abundance of matrix, pumice clasts and dense clasts in a variety of pumice rich volcaniclastic deposits, determined by image analysis.

3.2. Grain size distribution in graded beds

Conventional quantitative grain size distributions can only be assessed for unconsolidated samples [e.g. *Walker*, 1971; *Folk*, 1980]. The functional stereology technique (chapter 2) allows calculation of the grain size distribution for clastic rocks. Examples of the method outputs for the Ohanapecosh Formation, the Dogashima Formation and the Manukau Sub-Group are presented in Figures 5.1 and 5.2.

The output from functional stereology gives the grain size distribution density (G_i) in $m^3\phi^{-3}$, calculated as average clast diameters. From G_i, the volume of clasts in m^3 per ϕ (V_i) can be calculated (chapter 2). The G_i and V_i show variations in grain size in graded beds (Figs 5.1d, 5.1e, 5.2d, 5.2e). Modal values of coarse (i.e. >2 mm) pumice and dense clasts can be extracted from functional stereology distribution densities. The modal grain size distribution density G_i and volume V_i show variations in grain size in the stratigraphy (Figs 5.1d, 5.1e, 5.2d, 5.2e). The modal distribution of V_i represents the statistically most likely abundant grain sizes, thus this measure relates closely to a physical aspect of the clastic rock. Overall, the grading in V_i, determined from outcrop photographs and rock slabs scans, consistently follows the field estimates summarized as logs (Figs 5.1, 5.2). In the studied samples, both pumice and dense clasts commonly contain bimodal distributions in their coarse (>2 mm) clast populations. Here, only modal V_i is discussed, because it is easier to represent and compare volumes than distribution densities. Uncertainties remain for the fiamme size distribution in some beds of the Ohanapecosh Formation, because modal diameter may appear smaller than the original size of the pumice clasts (Appendix B).

3.2.1 Statistical measurements

The median M_ϕ and standard deviation σ_ϕ of grain size distributions are good indicators of transport and depositional processes for subaerial pyroclastic facies [*Murai*, 1961; *Walker*, 1971; 1983; 1984]. Exact quantification of grain size and sorting values by median and standard deviation is theoretically restricted to monomodal distributions [*Folk*, 1980]. However, median and standard deviation are commonly used on multimodal populations, because they give an estimate of the grain size population characteristics, and allow broad classification.

V_i is proportional to weight percent, assuming the density of each clast type (pumice versus dense clasts) is homogeneous. Hence, the weight percent of pumice clast and dense clast populations can be approximated by multiplying the density and V_i of each clast type (chapter 2; Fig. 5.4). Combination of weight percent datasets for pumice clasts and dense clasts gives the total clast weight percent (chapter 2; Fig. 5.4c) used in M_ϕ and σ_ϕ. For comparison with datasets on subaerial pyroclastic deposits [*Walker*, 1983], the density of dense and pumice clasts is arbitrarily set at 2,500 and 700 kg/m^3, respectively.

Significant values such as modes, D_{16}, D_{50} (i.e. median, M_ϕ), D_{84}, and standard deviation σ_ϕ (i.e. sorting) were extracted from G_i, V_i and weight percent distributions with *Gradistat*

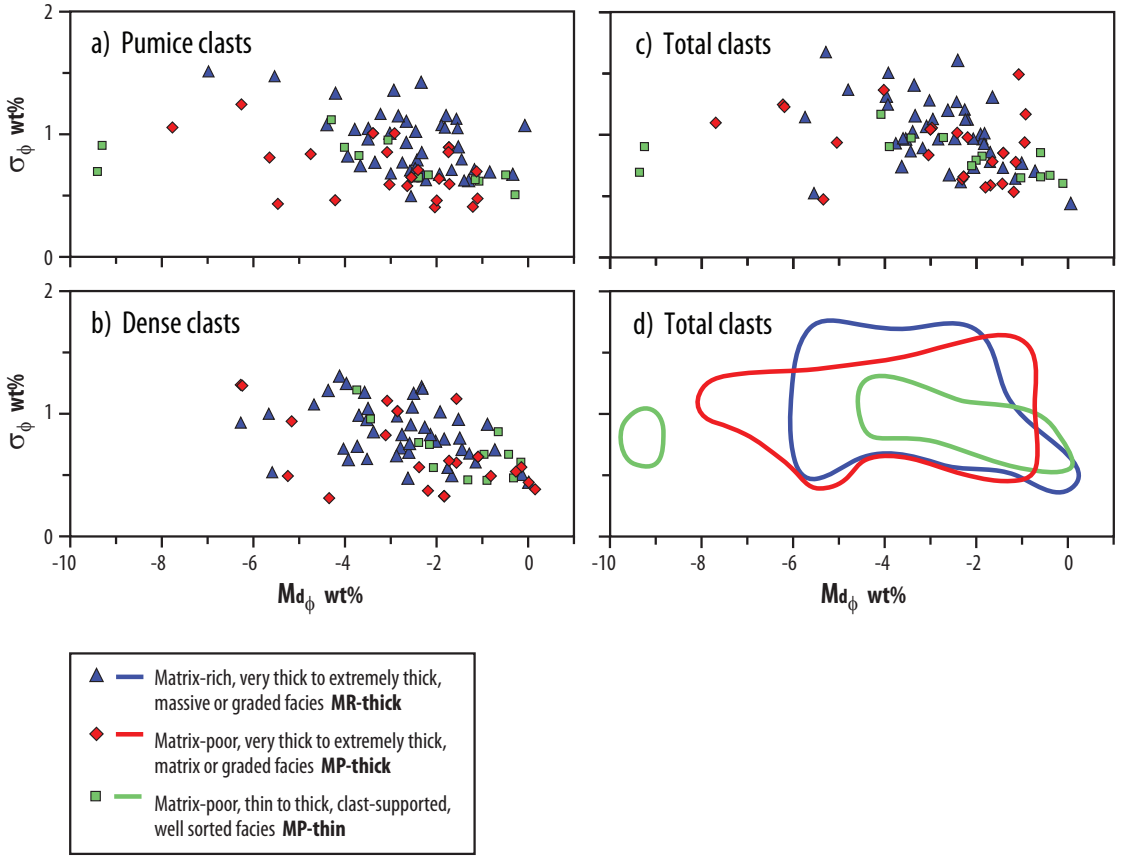

Fig. 5.4 Standard deviation versus median of weight percent of a variety of pumice-rich volcaniclastic deposits. **a)** Pumice clasts with fixed density of 700 kg/m^3; **b)** Dense clasts with fixed density of 2,500 kg/m^3; **c)** Total clasts by combination of pumice and dense clasts datasets; d) Contour of the total clasts datasets from c).

[*Blott and Pye*, 2001], using the graphical measures of Folk and Ward [1957]. Graphical measures are preferred to values from methods of moments, which give too much importance to the tails of the distribution [*Folk*, 1980].

Statistical measurements were calculated for particles >2 mm only, to prevent any disparity between matrix-poor and matrix-rich facies. The exclusion of matrix (<2 mm) in these calculations shifts the median and standard deviation to overall lower values, which means samples appear to be coarser and better sorted than they are (Figs 5.1g, 5.2g). Changes in the median upwards through the stratigraphy reflect the grading, whereas the standard deviation indicates the degree of sorting.

3.2.2. Functional stereology on subaqueous volcaniclastic rocks

The weight percent dataset of various types of subaqueous volcaniclastic deposits overlap and do not show major variations on the standard deviation versus median plot (Fig. 5.4). The extreme coarseness of pumice clasts (>5 m) in matrix-poor, thin to thick, clast-supported, well sorted facies (MP-thin) in the Sierra La Primavera caldera gives extreme median values of ~-9.5 ϕ. Examples of this facies do not show standard deviation values higher than 1.2, whereas this parameter reaches 1.6 in both of the very thick to extremely thick facies.

I compare the value of standard deviation versus median from functional stereology of volcaniclastic rocks with data from sieving of subaerial unconsolidated pyroclastic deposits (Fig. 5.5). The exclusion of the matrix data in this study (weight percent data ranges -12 to -1 ϕ) results in bias to relatively coarse and well-sorted values (Fig. 5.5 a–d), compared to total grain size populations determined by Walker [1983], who sieved pyroclastic deposits between -5 to 5 ϕ. The subaqueous volcaniclastic rocks dataset overlaps with subaerial plinian fall and fines-depleted pyroclastic flow fields of Walker [1983], which indicates good sorting and relatively coarse populations. Because the original raw data from Walker [1983] is unpublished, I use the sieving data of the ignimbrite units D and E of the Kos Plateau Tuff [KPT; *Allen et al*., 1999] as an approximation of pyroclastic flow deposit. The total weight percent data (-6 to +5 ϕ) of KPT ignimbrites fits in the well-sorted end of the pyroclastic flow field in the standard deviation versus median plot of Walker [1983], whereas the coarse-grained (-6 to -1 ϕ) data matches the functional stereology field for matrix-rich, very thick to extremely thick, massive or graded facies (MR-thick; Fig. 5.5e).

The overlap between coarse grained weight percent data of subaerial ignimbrite of KPT and matrix-rich, very thick to extremely thick, massive or graded facies (MR-thick) confirms that functional stereology data matches results from the sieving technique. Median and standard deviation of coarse clasts in subaqueous volcaniclastic deposits totally overlap, and it is difficult to distinguish between subaqueous deposits that are

well sorted (matrix poor) or not (matrix rich). This contrast to subaerial pyroclastic flow and fallout deposits, which occupy two distinct fields [Fig. 5.5; *Walker*, 1971; *Walker*, 1983]. However, matrix-poor, thin to thick, clast-supported, well sorted facies (MP-thin) have a much narrower extent in standard deviation. The overlap of the data for subaqueous volcaniclastic facies implies that the coarse clasts in all types of water-lain deposits presented in this study were efficiently sorted during transport; such sorting by motion in a fluid is named hydraulic sorting.

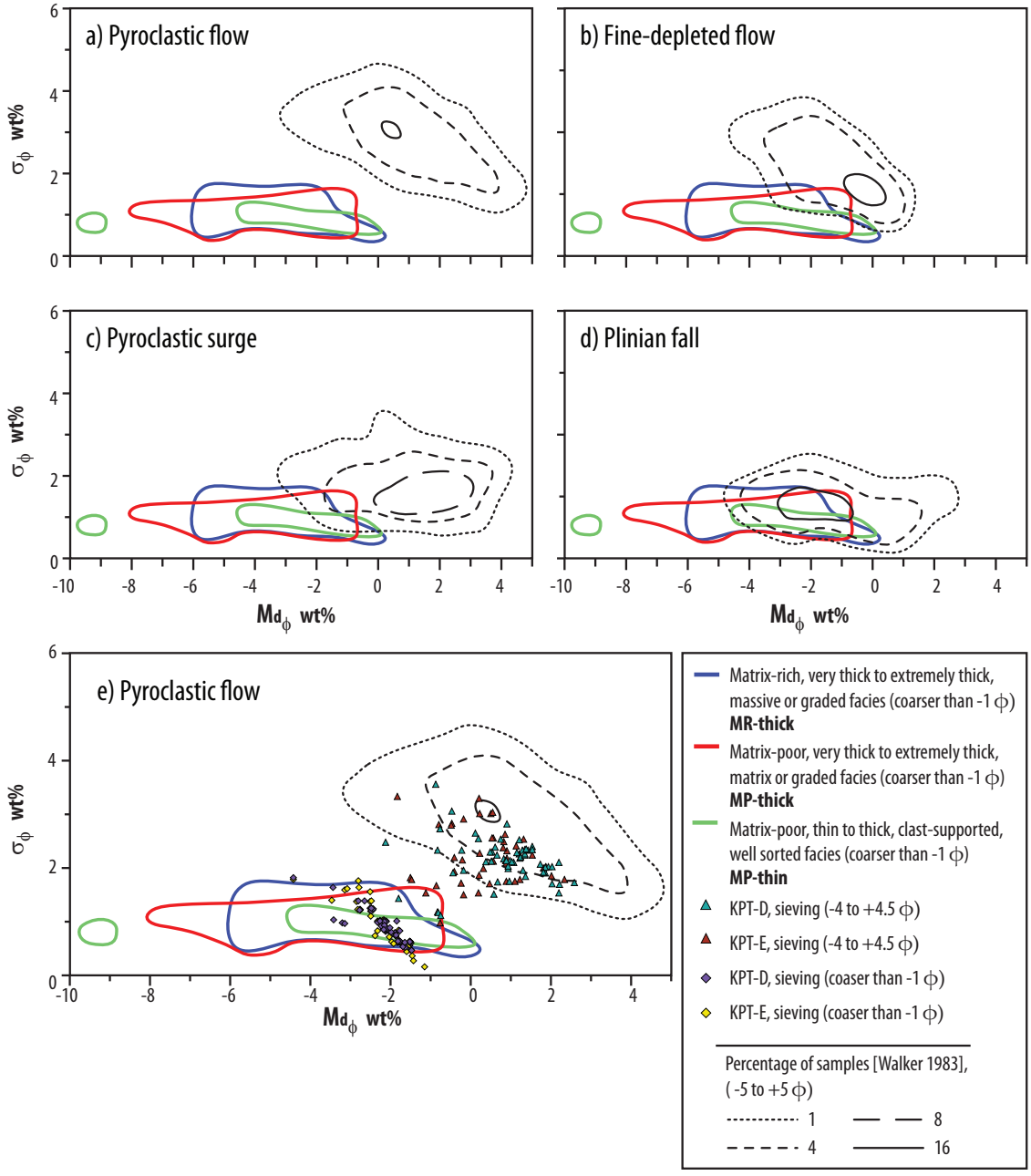

Fig. 5.5 Median versus standard deviation from functional stereology (this study) and sieving data. **a)–d)** Coarse clast sizes (<-1 φ; >2 mm) of subaqueous volcaniclastic rocks are compared with total clast sizes by sieving of four types of unconsolidated subaerial pyroclastic deposits; **e)** Sieving and functional stereology data with different minimum cut offs. Sieving data of units D and E (ignimbrite) of the Kos Plateau Tuff [KPT; Allen et al., 1999] match well-sorted part of Walker's [1983] subaerial pyroclastic flow field. Coarse-grained sieving data D and E of KPT match fine-grained functional stereology data of subaqueous volcaniclastic deposits when both minimum cut-off at -1 φ.

3.3. Hydraulic equivalence and hydraulic sorting

3.3.1 Hydraulic equivalence in subaqueous volcaniclastic deposits

Hydraulic equivalence is the condition where particles of different size and density have similar terminal velocity when in motion in a continuous fluid [*Rubey*, 1933; *Clift et al.*, 1978; *Cashman and Fiske*, 1991; *Manville et al.*, 2002; *Burgisser and Gardner*, 2006]. For instance, a large and low-density pumice clast falling in a fluid will have a terminal velocity equivalent to a smaller and denser clast. The terminal velocity of particles in a fluid is widely covered in the engineering and sedimentology literature [e.g. *Clift et al.*, 1978; *Komar and Reimers*, 1978; *Sallenger*, 1979; *Komar et al.*, 1984; *Cashman and Fiske*, 1991; *Crowe et al.*, 1998; *Manville et al.*, 2002; *Burgisser and Gardner*, 2006]. Although the grain size distribution of a clastic deposit reflects the physical diameter of clasts, it does not give much information on its mode of deposition. Hydraulic sorting reflects whether or not constituents of a clastic aggregate were deposited under hydraulic equivalence, implying steady terminal velocity.

The hydrodynamic properties of natural particles depend on multiple factors related to the particle, such as density, size, shape (~aspect ratio), surface roughness, as well as the type of ambient fluid (air, steam or seawater) and interactions with other particles [*Manville et al.*, 2002; *Burgisser and Gardner*, 2006]. The bulk density of pumice clasts depends on the volume, type and density of the fluid that fills the porosity [*Manville et al.*, 1998; *White et al.*, 2001; *Manville et al.*, 2002]. The degree of waterlogging is defined by the relative abundance of liquid water versus gas in the pore space of a pumice clast.

One way to produce well-hydraulically sorted natural deposits is by the vertical fall of discrete grains at their terminal velocity (suspension settling). The type of fluid has great importance. From the equations of Clift [1978], Cashman and Fiske [1991] proposed a hydraulic equivalence ratio of 5–10 to 1 for the diameters of waterlogged pumice clasts (1,100-1,300 kg/m^3) versus dense clasts (2,500 kg/m^3) during free fall in seawater. A ratio of 2–3 to 1 characterises grain diameters of pumice clasts versus dense clasts in free fall in air. This difference indicates that water is a better "sorting agent" than air [e.g. *Cashman and Fiske*, 1991; *Manville et al.*, 2002]. The range in these ratios reflects variation in clast densities, in particular the vesicularity and degree of waterlogging of the pumice clasts, as well as discrepancies from grain shape [*Clift et al.*, 1978; *Komar and Reimers*, 1978; *Cashman and Fiske*, 1991] and bulk interaction with other particles. In addition, where particles are in large concentrations, vertical density currents may form and travel 1 to 3 orders of magnitude faster than discrete particles settling from suspension [*Wiesner et al.*, 1995; *Carey*, 1997; *Manville and Wilson*, 2004].

In this chapter, I follow the general equation of terminal velocity (U_T) [e.g. *Clift et al.*, 1978]:

$$U_T = \frac{4\Delta\rho d^2 g}{3\rho\mu C_D \mathrm{Re}} \qquad (5\text{-}2)$$

where $\Delta\rho$ is the difference in density between the clast and the fluid, ρ is the fluid density (kg/m^3), g is the acceleration due to gravity (m/s^2), d is the particle diameter (m), μ is the water viscosity (Pa·s), C_D the drag coefficient and *Re* the Reynolds number.

Relatively large particles (>2 mm) correspond to the range 750 < *Re* < 3.5x10^3 where C_D

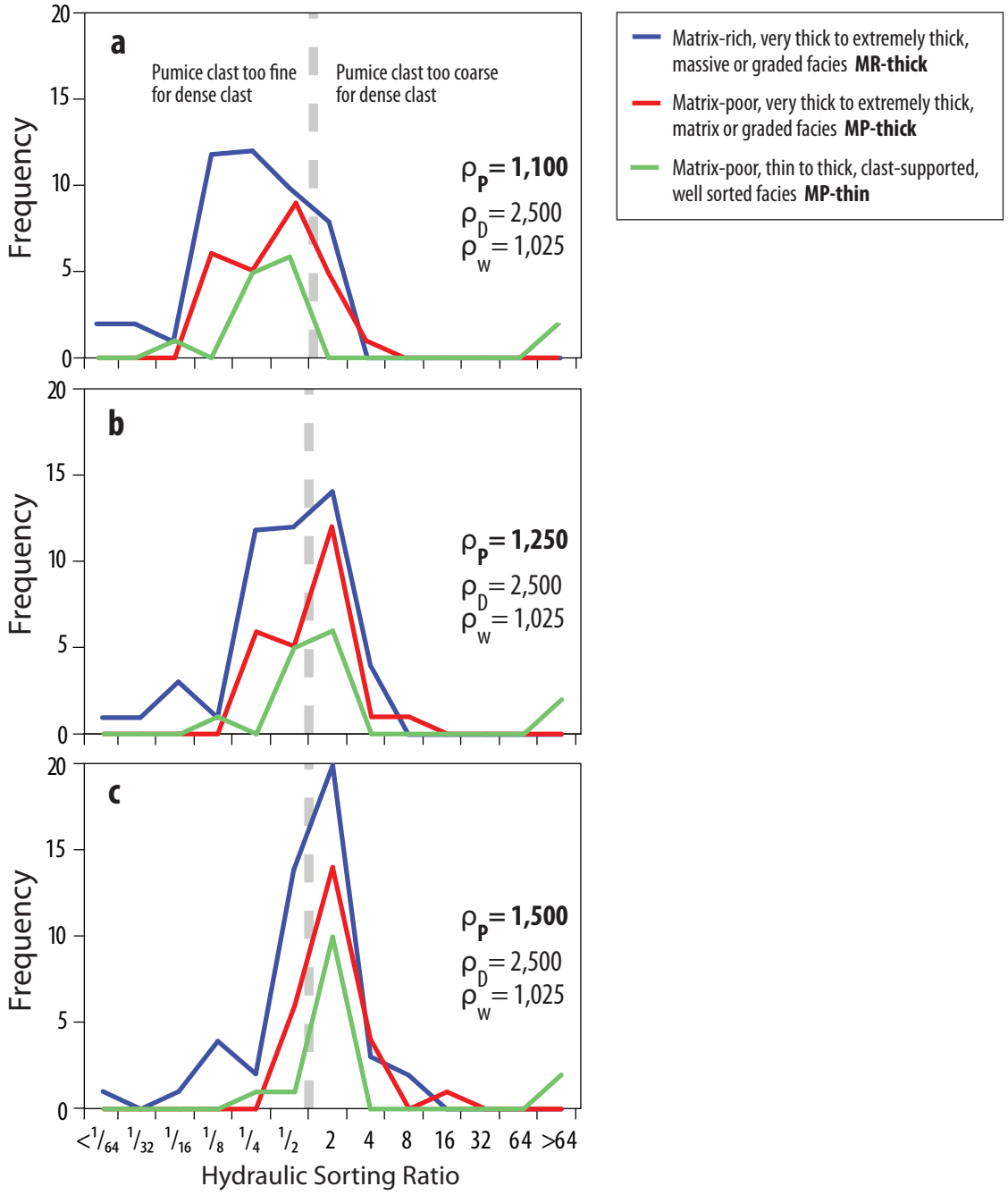

Fig. 5.6 Frequency histogram of hydraulic sorting ratio between pumice and dense clasts. Pumice clast density varies as a function of vesicularity and waterlogging ratios. Densities (kg/m^3) of pumice clasts, ρ_P; density of dense clasts, ρ_D; density of seawater, ρ_W.

can be approximated as 0.45 [*Clift et al.*, 1978; *Crowe et al.*, 1998; *Burgisser and Gardner*, 2006]. Following the approach of Burgisser and Gardner [2006], the hydraulic sorting between pumice clasts and dense clasts that were deposited together (i.e. at same level in stratigraphy) in water can be evaluated by their respective diameter. Most modes of sedimentation in air, including fallout from a suspended-load during progressive aggradation, suspension from discrete vertical fallout, saltation, and saltation and packed rolling have similar hydraulic behaviour, and can be approximated by [*Burgisser and Gardner*, 2006]:

$$\rho_{Dense}\, d_{Dense} \cong \rho_{Pum}\, d_{Pum} \qquad \text{, for Re } >10^3 \qquad (5\text{-}3)$$

In contrast, transport in a traction carpet includes rolling and shear stress, that induce a weaker hydraulic sorting [*Burgisser and Gardner*, 2006]; this type of transport is not considered here.

For transport in water, the water density is not negligible, and I modify the equation (5-3) into:

$$\frac{\rho_{Dense} - \rho_{Fluid}}{\rho_{Dense}} d_{Dense} \cong \frac{\rho_{Pum} - \rho_{Fluid}}{\rho_{Pum}} d_{Pum} \qquad \text{, for Re } >10^3 \qquad (5\text{-}4)$$

where ρ_{Dense} is the density of dense clasts (~2,500 kg/m^3), ρ_{Pum} is the density of waterlogged pumice clasts (~1,100–1,500 kg/m^3, which corresponds to 60–90 vol.% vesicles), ρ_{Fluid} is the ambient fluid density (1,025 kg/m^3) and d_{Pum} and d_{Dense} are the diameters of pumice clasts and dense clasts, respectively. Equations (5-3) and (5-4) are valid only for relatively high Reynolds numbers (Re>10^3) that correspond to waterlogged pumice clasts larger than 5–8 mm (depending on their vesicularity) and dense clasts larger than 3 mm. This minimum grain size is compatible with most of the grain size populations studied in the natural examples.

3.3.2. Hydraulic sorting ratio in subaqueous volcaniclastic deposits

The hydraulic sorting ratio (HSR) assesses whether the grain sizes of pumice and dense clasts in natural samples are consistent with them being hydraulically sorted. Following equation (5-4), the hydraulic sorting ratio corresponds to:

$$HSR = \frac{\rho_{Pum} - \rho_{Fluid}}{\rho_{Pum}} d_{Pum} \Big/ \frac{\rho_{Dense} - \rho_{Fluid}}{\rho_{Dense}} d_{Dense} \qquad \text{, for Re } >10^3 \qquad (5\text{-}5)$$

A deposit is hydraulically sorted if the hydraulic sorting ratio equals 1. Values less than 1 indicate that the dense clasts are too coarse to be hydraulically equivalent to pumice clasts in the same sample. Inversely, values higher than 1 imply that the dense clasts are too small to be in hydraulic equivalence with the pumice clasts. The clast diameters d_{Pum} and d_{Dense} are approximated by the value of the modes, or of the most voluminous (main) mode of each clast type in multimodal distributions. The value of the main mode is preferred to the median, because the mode reflects the most abundant clast size, whereas

the median is strongly dependant on the matrix cut-off size. Because the original pumice clasts vesicularity and degree of waterlogging are not known, extreme values were tested; at one extreme, waterlogged pumice clasts at 1,100 kg/m^3 (poorly vesicular and poorly waterlogged, or highly vesicular and poorly waterlogged) and 1,500 kg/m^3 (highly vesicular and mostly waterlogged, or poorly vesicular). Dense clasts density is fixed to 2,500 kg/m^3. Thus, the ratio of the equation (5-5) shows the effect of hydraulic sorting on clast populations [*Manville et al.*, 2002; *Burgisser and Gardner*, 2006], instead of the classical sorting based on the diameter of the particles only (i.e. physical sorting).

3.3.3. Interpretation of hydraulic sorting in graded subaqueous volcaniclastic rocks

The hydraulic sorting ratios in the selected successions of the Manukau Sub-Group (Fig. 5.1) are consistently very close to 1 for pumice clasts at 1,500 kg/m^3. The top of the Bethells Beach outcrop has a hydraulic sorting ratio less than 1, contains abundant matrix and cement, and only minor pumice clasts (>2 mm).

In the upper part of the succession of Dogashima 2 (i.e. above bed D2-3a), pumice clasts at ~1,500 kg/m^3 are well hydraulically sorted with dense clasts (hydraulic sorting ratio ~1). In particular, bed 3-e in Dogashima 2 shows good hydraulic sorting. This bed was interpreted as fallout from a submarine eruption column by Cashman and Fiske [1991]. However, the depositional processes that produced the well-hydraulically sorted bed 3-e in Dogashima 2 cannot be reduced to a single possibility, because vertical settling and subaqueous density currents would both produce aggregates with similar hydraulic sorting [equation (5-3); *Burgisser and Gardner*, 2006]. Reappraisal of the Dogashima Formation (chapter 4) concluded that this bed was deposited from a locally well-sorted, subaqueous pyroclastic density current related to the collapse of a submerged magmatic-volatile-driven explosive eruption column.

The hydraulic sorting ratios of beds in the Ohanapecosh Formation are overall less than 1, which indicates that the dense clasts are too coarse compared to the pumice clasts to be in hydraulic equivalence with them. The exception is the top of bed 61 in the Chinook Pass section, where pumice clasts are much coarser than the dense clasts. The poor hydraulic sorting in the Ohanapecosh Formation suggests transport processes in which clasts were not efficiently sorted by water, such as in cohesive types of high-concentration subaqueous volcaniclastic density currents (chapter 3). Part of this low hydraulic sorting ratio may be imputed to flattening of pumice clasts into fiamme, and decreased the apparent clast size. However, the ratio of hydraulic sorting is too low to be exclusively caused by post-depositional compaction (Appendix B).

The hydraulic sorting ratios in the grey andesite breccia (D2-2, Dogashima), the basal dense clast breccia of unit 40 at Chinook Pass, the base of unit Cougar B-3 (Ohanapecosh Formation) and the lower section of fine pumice breccia (D2-5a, Dogashima) are very

low, because dense clasts are much coarser than pumice clasts. These basal breccia were probably deposited from a current in which the hydraulic sorting is much lower, such by rolling, sliding and saltation in a traction carpet [*Burgisser and Gardner*, 2006], that can develop in the lower part of density currents [e.g. *Sohn*, 1997] and generates clast-supported basal sub-facies (Figs 5.1, 5.2).

3.3.4. Hydraulic sorting ratio of pumiceous clastic rocks

The hydraulic sorting ratio is evaluated for the three volcaniclastic facies of this study (Table 5.1), following equation (5-5). For poorly waterlogged, highly vesicular pumice clasts (1,100 kg/m^3), the hydraulic sorting ratio with dense clasts is overall smaller than 1, which indicates that the pumice clasts are too small to be in good hydraulic equivalence to coexisting dense clasts (Fig. 5.6a). With increasing pumice clast densities (1,250–1,500 kg/m^3), the amount of samples that are hydraulically sorted (i.e. hydraulic sorting ratio close to 1) increases dramatically (Figs 5.6b, 5.6c). With pumice clasts at 1,250 kg/m^3, all waterlain deposits have hydraulic sorting ratios that are close to being ideally hydraulically sorted, with the exception of the matrix-rich, very thick to extremely thick, massive or graded facies (MR-thick). Fully waterlogged, highly vesicular pumice clasts (1,500 kg/m^3) have good hydraulic equivalence to dense clasts at 2,500 kg/m^3 in most samples tested. However, compared with the dense clasts, the pumice clasts are chiefly too small to be hydraulically sorted (HSR <1) in the matrix-rich, very thick to extremely thick, massive or graded facies (MR-thick; Fig. 5.6c). The opposite occurs in the two matrix-poor facies (MP-thick, MP-thin), where pumice clasts are chiefly too coarse compared to the dense clasts (HSR >1). A HSR>1 indicates that the pumice clasts are too coarse to be in good hydraulic equivalence to coexisting dense clasts. Such a ratio can be achieved if the pumice clasts are less dense than expected, indicating a high vesicularity and/or only partial waterlogging.

4. DISCUSSION

4.1. Applications of functional stereology

The quantification of grain size distributions of volcaniclastic facies is greatly extended by using combined techniques of image analysis and functional stereology. Clast types and their relative volume can be determined by image analysis for any clastic deposit, unconsolidated or not, on the condition that the image shows an even surface (chapter 2). Volumetric and coarse-tail grading can be assessed by taking several samples at various levels in the same bed. From data extracted by image analysis, the grain size distribution of each clast type and total clasts can be determined by functional stereology.

The limitation of the technique to grain sizes coarser than 2 mm arises from state of preservation of the samples. For instance, the grain size distribution of welded ignimbrites that contain well preserved matrix shards could ideally be calculated following the functional stereology approach, assuming the clast shapes can be simplified to a common geometry [*Sahagian and Proussevitch*, 1998].

The modes of V_i give an accurate description of the volumetric grain distribution of a clast population. Modes correspond to physical characteristics of aggregates - the most common grain sizes in a population - that are easier to represent than the median. Extraction of modes from consolidated samples allows quantification of textural features such as coarse-tail grading (Figs 5.1d, 5.2d). Multiple modes in the grain size distribution of a clastic sample may record a complex history of fragmentation and/or transport [*Wohletz et al*., 1989].

4.2. Implications for transport and depositional processes

Image analysis and functional stereology on diverse volcaniclastic rocks allow better quantification of their texture. However, classification of depositional processes remains complex, because the grain size distribution of the matrix cannot be determined in the studied samples, due to poor preservation of the fine grains. The hydraulic sorting of particles in a volcaniclastic rock can be estimated by modification of the equation of Burgisser and Gardner [2006] into equation (5-4), which is applicable to waterlain deposits.

Most coarse-grained fractions (>2 mm) of waterlain pumiceous volcaniclastic deposits show a similar grain size distribution signature, and types of deposits cannot be distinguished on the standard deviation versus median diagram (Fig. 5.5). In addition, the hydraulic sorting ratio is similar for matrix-poor and matrix-rich facies. In contrast, the low hydraulic sorting ratios in basal dense-clasts-rich breccias of subaqueous volcaniclastic density currents and their interpretation facies suggest deposition from a traction carpet that developed at the base of the main density current. These characteristics imply that clasts are hydraulically sorted as long as turbulent segregation is efficient to sort clasts hydraulically, and that the terminal velocity of the clasts is steady. In addition, hydraulic equivalence in a deposit only applies if settling was the main mechanism of deposition, implying the grain size distribution of the clasts that were deposited corresponds to the grain size distribution of the clasts in motion.

All studied waterlain pumiceous volcaniclastic deposits occupy a different field on standard deviation versus median than subaerial pyroclastic flow deposits. This effect is due to the much lower cut-off (+5 ϕ; $^1/_{32}$ mm) in sieved data used by Walker [1983] compared to the cut-off used in this study (-1 ϕ; 2 mm), because the coarse grained

fraction (-6 to -1 ϕ) of the sieving data of the KPT overlap the field of coarse (>2 mm) matrix-rich, very thick to extremely thick, massive or graded facies (MR-thick).

The measurement of hydraulic sorting can help in the interpretation of the eruption environment. In the various subaqueous deposits examined, a better hydraulic equivalence is found between the main modes of pumice and dense clasts if pumice density spans 1,250–1,500 kg/m^3 than 1,100 kg/m^3. This relationship suggests efficient waterlogging of the pumice clasts before their deposition in water, and/or that these pumice clasts were originally denser than water. This inference is of critical importance in assessing the origin of pumice clasts deposited subaqueously. Hot pumice clasts are efficiently waterlogged when quenched on contact with water [*Whitham and Sparks*, 1986; *Allen et al.*, 2008], and can be deposited under water from subaqueous volcaniclastic density currents derived from subaerial pyroclastic flows that entered water [*Whitham and Sparks*, 1986; *Freundt*, 2003], or from subaqueous explosive eruptions [e.g. neptunian; *Allen and McPhie*, 2009]. Waterlogging of cold air-filled pumice clasts can require months [e.g. *Whitham and Sparks*, 1986]. For any pumice clast density, part of the matrix-rich, very thick to extremely thick, massive or graded facies (MR-thick) shows a lower hydraulic sorting ratio than for the matrix-poor deposits. This relationship also suggests that high clast concentrations reduce the efficiency of hydraulic sorting because water is less abundant, which reduces turbulent segregation [e.g. *Kokelaar et al.*, 2007]. The abundance of fine-grained glass shards might favour cohesive behaviour of volcaniclastic density currents (chapter 3) in the same manner that clay particles increase the cohesiveness of non-volcanic density currents [*Hampton et al.*, 1996; *Ilstad et al.*, 2004].

4.3. Grain size distribution in the literature

The statistical values of median diameter and standard deviation of sieved samples have been used to discriminate the mode of emplacement of unconsolidated subaerial pyroclastic deposits [*Moore*, 1934; *Murai*, 1961; *Walker*, 1971; *Walker and Croasdale*, 1971; *Walker*, 1983; 1984], without considering their multi-modal distributions. Importantly, such statistical parameters are meaningful only for monomodal distributions [*Folk*, 1980]. Moreover, modern techniques [e.g. laser diffraction; *Evans et al.*, 2009] identify finer-grained sizes than sieving, and minimum sieving grain size cut-off remains undefined. To compare median and standard deviation of grain populations from dataset at different cut-off and/or from different techniques introduces a flaw, because the total range in grain size is not the same. Secondary modes are common in pyroclastic deposits [e.g. *Wohletz et al.*, 1989; *Orsi et al.*, 1992], and reflect poor sorting and diverse origins of fragmentation and/or transport [*Wohletz et al.*, 1989]. Both juvenile and non-juvenile clast populations can be responsible for secondary modes in the total grain size distribution [*Walker*, 1972; 1983; *Wohletz et al.*, 1989; *Carey and Houghton*, 2010].

4.4. Comparison of sieving and functional stereology

Direct comparison of weight percent data from sieving and functional stereology is possible, but the limits of detection - especially for the fine-grained clasts - should be identical. To compare sieving and functional stereology outputs in graphs of standard deviation versus median of Walker [1983] is difficult, because particles <2 mm could not be retrieved from the clastic rocks of this study. In addition, Walker's [1983] complete sieving dataset is not published, which precludes comparison of the coarse tails of his grain size distributions with my dataset. However, application of the units D and E of the KPT ignimbrites as a proxy for pyroclastic flow deposits match the field of matrix-rich, very thick to extremely thick, massive or graded facies (MR-thick).

Many of the samples analysed by functional stereology - as well as Walker's [e.g. *Walker and Croasdale*, 1971] - contain two modes of coarse clasts (>2 mm) and it is likely that the matrix also included one or more modes per sample. Consequently, the median and standard deviation of the grain size distributions of the studied subaqueous volcaniclastic samples can only be compared qualitatively with unconsolidated subaerial equivalents.

5. CONCLUSIONS

The application of image analysis and functional stereology to clastic rocks enables determination of textural features that conventional sieving methods are unable to retrieve on consolidated samples, such as clast and matrix volume, and grain size distribution. Matrix abundance, and coarse (>2 mm) clasts volume, modes, median and standard deviation were extracted from the grain size distribution of Tertiary pumiceous volcaniclastic rocks deposited in subaqueous environment.

All waterlain pumiceous volcaniclastic deposits occupy one field on standard deviation versus median diagrams, and the types of transport and depositional processes cannot be discriminated by grain size distribution itself. With similar minimum cut-off (>2 mm), the sieving dataset of units D and E of the KPT ignimbrites overlap the functional stereology data of matrix-rich, very thick to extremely thick, massive or graded facies (MR-thick) on the standard deviation versus median plot, attesting the validity of this new method.

High clast concentration reduces efficient hydraulic sorting, as demonstrated by the matrix-rich facies (MR-thick) which are overall slightly less hydraulically sorted than the matrix-poor facies (MP-thick, MP-thin). The high degree of hydraulic sorting of pumice and dense clasts in all studied waterlain pumiceous deposits implies that the pumice clasts were dense at deposition, thus mostly waterlogged and/or initially poorly vesicular.

6

Synthesis

1. INTRODUCTION

There is a wide range of sedimentological processes associated with transport and deposition of large volumes of pyroclastics produced by explosive eruptions. The timeframes considered in this thesis are such that the described successions are instantaneous from a geological point of view; however time constraints between the members of the Ohanapecosh Formation remain difficult to establish. Nevertheless, it is clear that some facies correlate directly with an eruption whereas others do not.

On the basis of data collected in this thesis, I discuss the facies characteristics associated with eruption-fed, resedimented and reworking processes. This discussion is chiefly limited to processes that lead to deposition below wave-base, and that involve intermediate to silicic, pumice-forming explosive eruptions. In this context, distinguishing between eruptions at vents on land versus those under water is imperative.

2. PUMICE-FORMING EXPLOSIVE ERUPTIONS

Intermediate to silicic explosive eruptions can include numerous eruptive pulses (seconds to hours), each of which is capable of forcing a sedimentation event. These types of eruptions typically have durations of minutes to days and disperse their products over tens to thousands of km^2. [*Walker*, 1973; *Newhall and Self*, 1982; *Allen and McPhie*, 2009]. The pyroclasts are dominantly highly vesicular pumice. In cases that involve porphyritic magma, these eruptions produce free broken crystals with same composition as phenocrysts in juvenile pumice clasts. Although these eruptions have durations that are geologically very brief, they are long enough to allow interplay of volcanic and other surface processes. These surface processes may lead to sedimentation and reworking of the primary facies.

3. SYN-ERUPTIVE AND POST-ERUPTIVE FACIES

Eruption-fed facies are strictly contemporaneous with an eruption. In contrast, resedimented and reworked facies may also occur at the same time as discharge from the vent, i.e. being syn-eruptive, and/or during breaks between eruptive phases, i.e. being post-eruptive. The subaqueous records of subaerial and subaqueous pumice-forming explosive eruptions are likely to include eruption-fed, syn-eruptive resedimented and post-eruptive resedimented facies. Subaerial pumice-forming explosive eruptions might also produce syn- and post-eruptive reworked facies in subaqueous successions.

4. ERUPTION-FED PYROCLASTIC FACIES IN SUBAQUEOUS VOLCANIC SUCCESSIONS

In subaqueous environment, it is difficult to determine whether a facies is eruption-fed pyroclastic or not, because the source vent can be subaerial or subaqueous. In addition, subaqueous eruption-fed facies may be emplaced cold, which is a big contrast to density currents generated by subaerial explosive eruptions. In below wave-base settings, the principal transport and depositional processes are water-supported volcaniclastic density currents and settling from suspension.

4.1. Subaqueous eruption-fed pyroclastic facies from submarine sources

As a result of rapid cooling and reduced explosivity due to confining pressure at a subaqueous vent, subaqueous magmatic volatile-driven eruption columns are likely to collapse [*Allen et al*., 2008; *Allen and McPhie*, 2009] and produce seafloor-hugging, water-supported density currents composed primarily of pumice lapilli. Only ash and giant pumice clasts are likely to remain buoyant and form rising warm-water plumes; these pyroclasts subsequently settle from suspension.

Destruction of a subaqueous active lava dome by a subaqueous pumice-forming explosive eruption is exemplified in Dogashima 2 (chapter 4). The massive grey andesite breccia (D2-2) contains coarse grey andesite clasts that were hot when deposited [chapter 4; *Tamura et al*., 1991]. Hence, this unit (D2-2) and the gradationally overlying white pumice breccia (D2-3) provide an excellent example of eruption-fed density current facies associated with a subaqueous pumice-forming explosive eruption.

In the Dogashima Formation, eruption-fed facies deposited from subaqueous volcaniclastic density currents are all clast-supported, and dominated by angular or ragged, highly vesicular pyroclasts of uniform composition. Widespread, thick, and graded or massive bed forms indicate rapid aggradation from high-concentration density currents that may originate from a sustained source. For example, Dogashima 2 shows valley-filling behaviour with the massive grey andesite breccia (D2-2), but pumice-rich overbank facies (white pumice breccia, D2-3) is extensive laterally. In the white pumice breccia (D2-3), pumice lapilli are relatively well hydraulically sorted [e.g. chapter 5; *Manville et al*., 2002] with dense clasts. The deposits tend to be coarse grained (lapilli) and matrix-poor, because ash is effectively elutriated during transport in the column and in the density currents [*Allen et al*., 2008; *Allen and McPhie*, 2009] and clast abrasion is reduced by the presence of water as the interstitial fluid. However, coarse juvenile pumice clasts present in unit D2-2 show abrasion during transport in a dense-clast-dominated bed load. Coarse basal dense-clast breccia, such as in bed D2-2, is likely to occur only at relatively proximal locations with regard to the source, as coarse dense clasts are rapidly de-coupled from

the eruption column and from density currents. Because of their relatively close distance from source, such clasts may be still hot at deposition [chapter 4; *Tamura et al.*, 1991]. Juvenile pumice and dense clasts with quenched rims and internal curviplanar fractures are expected to occur, especially if these are coarse grained [*Allen and McPhie*, 2009]. Such clasts types were found in all eruption-fed breccia in Dogashima (pumice breccia D1-2, D1-5 and D1-10; massive grey andesite breccia, D2-2; white pumice breccia, D2-3; planar pumice breccia, D2-7).

Some beds in the planar bedded breccia (D2-7) of Dogashima 2 consists of fines-depleted facies deposited by suspension settling that contain coarse (>1 m) pumice clasts. Suspension beds are entirely composed of pumice clasts, or are well hydraulically sorted [e.g. chapter 5; *Manville et al.*, 2002], because the process of suspension settling allows steady interaction of clasts with the ambient fluid.

4.2. Subaqueous facies derived from subaerial pyroclastic flows

When subaerial pyroclastic flows reach the shoreline, they can transform into water-supported debris flows [e.g. *Carey and Sigurdsson*, 1980; *Sparks et al.*, 1980; *Whitham*, 1989], or water-supported volcaniclastic density currents [e.g. *Freundt*, 2003; *Trofimovs et al.*, 2006] or remain as hot gas-supported pyroclastic flows [*Mandeville et al.*, 1994; *Mandeville et al.*, 1996]. In many cases, contact of hot clasts with water is likely to produce steam explosions [*Freundt*, 2003; *Dufek et al.*, 2007] and hot pumice clasts immersed in water will quench and waterlog [*Whitham and Sparks*, 1986; *Freundt*, 2003]. Because of their relatively low density, dilute pyroclastic density currents cannot enter water, and will continue to flow over water [*Mandeville et al.*, 1996; *Hart et al.*, 2004] and may create pumice lapilli rafts; tsunami may be generated at shoreline [*Mandeville et al.*, 1996; *Freundt*, 2003].

Facies inferred to be deposits from subaqueous density currents fed by subaerial pyroclastic flows are commonly extremely thick, graded or massive, but can be stratified [*Cas*, 1983; *Yamada*, 1984; *Whitham*, 1989; *Cas and Wright*, 1991; *Allen and McPhie*, 2009; *Allen et al.*, 2011]. Their components can comprise clasts or fossils typical from above wave-base settings. In addition, regional context and correlations allow identification of the environment at source. Rarely, combination of historic records and sampling give proofs of a subaerial vent [e.g. *Mandeville et al.*, 1996].

In the Chinook Pass Member (Ohanapecosh Formation; chapter 3), presence of accretionary lapilli, wood and rounded clasts in a few beds (facies 7 and 12) intercalated with extremely thick beds (facies 1–4) is critical for determination of the origin of the entire volcaniclastic succession. A bed of clast-supported polymictic breccia-conglomerate (facies 7) underlies extremely thick facies 1–4, and is dominated by rounded dense clasts, which suggests a subaerial source. Subaerial fallout onto water is a source of ash that commonly forms

widespread, thin, well sorted and graded layers on the sea floor [*Wetzel*, 2009]. Pumice lapilli and blocks that cool in air will form rafts rather than immediately settle to the seafloor, such exemplified by the saturation grading in the reversely to normally graded pumice breccia (facies 12) in the Ohanapecosh Formation. Such facies are likely to be eruption-fed but they can also be post-eruptive, because pumice can take months to waterlog [*Whitham*, 1989; *White et al*., 2001; *Bryan et al*., 2004]. In addition, the presence of accretionary lapilli in facies 12 suggests an eruption-fed origin, whereas wood and accretionary lapilli emphasises a subaerial source. Thus, this facies is considered eruption-fed and originated from above wave-base environment.

Presence of components from subaerial origin at the base and in the middle of the Chinook Pass Member strongly suggests a subaerial origin for the entire volcaniclastic succession. In addition, the facies 12 is interpreted as eruption-fed, and its presence between two extremely thick facies strongly suggests the underlying bed to be eruption-fed. Because facies 1–4 share similar characteristics (e.g. extreme thickness, pumice-dominated), it is likely that they are all eruption-fed, even though they might not contain accretionary lapilli and wood. Rounded dense clasts in the basal breccia of eruption-fed facies 1, 2 and 3 may have been abraded in an above wave-base environments, and probably incorporated from a shoreline setting by pyroclastic flows.

Pumice clasts are likely to be rounded during transport in a subaerial pyroclastic flow [*Walker*, 1981; *Dufek and Manga*, 2008]. However, this mechanical abrasion necessitates some distance from the vent to the shoreline to be effective. Eruption-fed facies in the Ohanapecosh Formation contain angular pumice clasts, which suggest that the distance from vent(s) to shoreline was relatively small. Subaqueous volcaniclastic density currents derived from subaerial pyroclastic flows are commonly depleted in fines [*Cas*, 1983; *Whitham*, 1989; *Cas and Wright*, 1991; *Allen et al*., 2011], whereas apparently matrix-rich (<2 mm) facies are dominant in the eruption-fed facies 1–4 in the Ohanapecosh Formation (chapter 3). However, the fine-grained components in the rocks of the Ohanapecosh Formation have been destroyed by diagenesis and the original grain size distribution of the particles <2 mm is not known, thus these facies could be relatively fines-poor, despite a matrix-supported aspect.

Origin of the beds in graded or massive volcanic breccia (facies 5) and coarse volcanic breccia (facies 6) remains difficult to establish, because these two facies contain a wide range of bed types. For instance, facies 5 comprises clast-supported to matrix-supported beds, and abundance of dense clasts varies. Presence of minor sub-rounded dense clasts in facies 6 suggests a subaerial origin. However, clast are overall angular in facies 5 and 6, which suggests a short transport in subaerial environment, or a subaqueous origin.

The hydraulic sorting ratios of the coarse (>2 mm) components of the Ohanapecosh Formation facies 1–4 do not show a large difference compared to products of subaqueous

explosive eruptions (chapter 5). However, hydraulic sorting ratios between pumice and dense coarse (>2 mm) clasts in facies 1–4 of the Ohanapecosh Formation seem to be slightly lower (i.e. pumice clasts too fine compared to dense clasts) compared to facies of the subaqueously erupted Dogashima Formation (chapter 5), indicating a less efficient hydraulic sorting in coarse clasts for volcaniclastic density currents fed from subaerial pyroclastic flows.

5. RESEDIMENTED PYROCLASTIC FACIES IN SUBAQUEOUS VOLCANIC SUCCESSIONS

During and following large explosive eruptions, large volumes of volcanic clasts are typically not stable where deposited on subaerial and subaqueous slopes or in channels [e.g. *Cas et al.*, 1990; *Smith and Lowe*, 1991; *Wolfe and Hoblitt*, 1996; *Wright*, 2001; *Wright et al.*, 2008; *Gardner*, 2010; *Leat et al.*, 2010]. Gravitational re-equilibration of newly deposited, non-welded pyroclasts results in resedimentation in depocentres, such as below wave-base basins [e.g. *Moore et al.*, 1994; *Wright*, 2001; *Gardner*, 2010]. Resedimentation does not necessarily involve clast reworking, especially underwater where clast abrasion is reduced by the presence of water as the interstitial fluid.

Remobilisation of pyroclasts can be initiated by earthquakes, mass-wasting, fluidisation, or dewatering [e.g. *Normark and Piper*, 1991; *Stow*, 1994; *Piper et al.*, 1999; *Boggs*, 2006; *Piper and Normark*, 2009], as well as by erosion during storms [*Smith and Lowe*, 1991] or by currents in subaqueous canyons [e.g. *Wright and Black*, 1981; *Wright et al.*, 2008]. Mass-wasting events can remobilise large volumes of pyroclasts over very short (tens of m) to very long distances [>200 km; e.g. *Moore et al.*, 1994]. The expected volume and thickness of deposits depend on the type, size, and duration of the remobilisation event, and of the environment of initiation and deposition [e.g. *Smith and Lowe*, 1991; *Piper et al.*, 1999], thus resedimented deposits comprise a wide range of facies.

A first order reasonable expectation for resedimentation processes in pumice-dominated volcanic settings is that these will occur in close association with eruption-fed facies, because low-density waterlogged pumice clasts [1,300 kg/m3; *Allen et al.*, 2008] are easily resedimented [*Manville et al.*, 2002]. The same complication as for eruption-fed facies exists, because subaqueous resedimented facies can come from subaerial or subaqueous sources. In addition, multiple cycles of resedimentation may have occurred. However, presence of pumice clasts implies they were previously waterlogged [>1,000 kg/m^3; *Allen and Freundt*, 2006], thus implying resedimentation from unconsolidated subaqueous aggregates, or that pumice clasts have been originally denser than water. Characteristics of resedimented facies may reflect lower volumes and dilute transport systems, thus include thinner units and tractional bed forms.

Resedimented pyroclastic facies from subaerial source may be characterised by presence of components typical from above wave-base environment, such as rounded dense clasts, above wave-base fossils, wood and accretionary lapilli. In the Ohanapecosh Formation (chapter 3), the relative small thickness of clast-supported polymictic breccia-conglomerate (facies 7), despite containing coarse dense clasts, matches a resedimented origin. The abundance of sub-rounded to rounded dense clasts in this facies reflects abrasion in above wave-base environment.

Some beds of the coarse volcanic breccia (facies 6) may have a resedimented origin. Coarse, sub-rounded dense clasts in this facies suggest they were abraded in an above wave-base environment. However, this facies, as well as graded or massive volcanic breccia (facies 5), are dominated by pumice clasts that needed to be hot or initially dense to be waterlogged [*Whitham and Sparks*, 1986; *Cas and Wright*, 1991]. Sedimentation from waterlogging of pumice lapilli in rafts cannot be considered for these facies, because dense clasts are present and randomly distributed throughout the beds. It seems unlikely that all the pumice clasts were poorly vesicular throughout the dozens of beds of facies 5 and 6 in the White Pass Member in the Ohanapecosh Formation. Therefore, the resedimented beds of facies 5 and 6 that contain pumice and sub-rounded dense clasts are probably derived from resedimentation of subaqueous volcaniclastic density current deposits that were initially derived from subaerial pyroclastic flows.

In the Dogashima Formation (chapter 4), resedimented beds from subaqueous source are thinner, well graded, commonly cross- or planar-bedded, and overall better sorted and more polymictic than eruption-fed facies. These facies include beds of cross-bedded, planar bedded and normally graded pumice breccia/sandstone (D1-1, D1-4, D1-7, D1-9 and D1-12), polymictic volcanic breccia (D1-3 and D1-8), cross-bedded pumice breccia-conglomerate (D2-6 and D2-8), planar bedded pumice breccia (D2-7) and possibly planar stratified pumice breccia (D2-4). Deposits from resedimentation of subaqueous pyroclastic aggregates may be very similar to primary eruption-fed deposits, depending on the distance travelled, the transport process, and the initiation event. In the Ohanapecosh Formation (chapter 3), preservation and lateral extent of the beds of graded or massive volcanic breccia (facies 5) and coarse volcanic breccia (facies 6) does not allow distinguishing deposits from resedimented or eruption-fed processes under water.

6. REWORKED PYROCLASTIC FACIES IN SUBAQUEOUS VOLCANIC SUCCESSIONS

Reworking of volcanic clasts designates a process that modifies the surface of the clasts. Volcanic clast abrasion is mostly effective on delicate pumice clasts, but long-term abrasion can also transform the shape of dense clasts. Above wave-base settings, such as fluvial and coastal environments, are the most adapted for clast reworking.

However, reworking can be important in below wave-base successions if the reworked facies are subsequently resedimented, and where deep-water currents operate, such as in submarine canyons [e.g. *Stow et al*., 2002; *Martín-Chivelet et al*., 2008; *Shanmugam*, 2008]. Remobilisation by traction currents from clear water currents or dilute density currents is likely to affect only surface deposits, but occur over considerable areas and can rework large volumes of pyroclasts [*Martín-Chivelet et al*., 2008; *Stow et al*., 2008]. Deposits from traction currents produce very different facies compared to deposits from eruption-fed volcaniclastic density currents. Semi-continuous traction currents commonly form thin stratified units that are likely to be planar- or cross-bedded, and form dune fields at least at several hundreds of m deep [*Valentine et al*., 1984; *Stow et al*., 1998; *Shanmugam*, 2008; *Stow et al*., 2008], and are likely to be pumice-dominated. Volcaniclastic facies can record transport histories that comprise both resedimentation and reworking processes, and a blend of both is likely in most cases. Abraded shape of a reworked pyroclast will be preserved during eventual subsequent resedimentation. In the Dogashima Formation, sub-rounded white pumice clasts that occur in beds of cross-bedded pumice breccia-conglomerate (D2-6 and D2-8) are interpreted to have been reworked and deposited from semi-continuous traction currents in a below wave-base canyon environment.

In Dogashima 2, the bed of massive grey andesite breccia (D2-2) contains juvenile pumice clasts that are rounded, whereas the same type of pumice clasts are angular in the overlying beds D2-3 to D2-5. The rounded juvenile pumice clasts in bed D2-2 are interpreted to have been abraded by coarser and denser clasts during transport in the bed load of the eruption-fed subaqueous volcaniclastic density current that deposited the main volcaniclastic succession of Dogashima 2. Relatively low content of dense clasts higher in the sequence (D2-3 to D2-5) suggests that pumice clast abrasion is more efficient in the dense-clast dominated part of high-concentration density currents. Abrasion was minimal in the pumice-dominated part of the density current, because of reduced clast-to-clast interactions and lower clast momentum.

In the Ohanapecosh Formation (chapter 3), the angularity of the pumice clasts in graded or massive volcanic breccia (facies 5) and coarse volcanic breccia (facies 6) suggests a short transport in subaerial environment, because pumice clasts are likely to be reworked in most eruption-fed or resedimentation processes in above wave-base environment [*Walker*, 1981; *Smith and Lowe*, 1991; *Dufek and Manga*, 2008]. Sub-rounded dense clasts in facies 1–3, 6 and 7 suggest reworking history in above wave-base setting before their final deposition. The sub-rounded pumice lapilli and the vitric matrix in eruption-fed reversely to normally graded pumice breccia (facies 12) suggest reworking by clast-to-clast interaction of cold pumice lapilli in rafts, and their eventual waterlogging by suspension settling.

7. AMBIGUOUS CASES

Criteria used to recognise eruption-fed versus other pyroclastic facies may be impossible to apply if the preservation state of the facies, the lateral and vertical extent of exposures, and presence of other units for facies correlations are inadequate. In addition, the lack of offshore samples, witnessed events and analogue experiments means that only a few types of subaqueous volcanic eruptions have been described, and eruption and transport processes under water remain poorly understood, thus the full range of facies is unknown. Generally, the origin of a facies is difficult to determine without information on its relationships with other facies in the succession; lateral facies continuity and extent, and the nature of contacts are critical characteristics.

The local thickness of a volcaniclastic deposit cannot give information on the dimensions of the entire succession [e.g. *Riedel et al.*, 2001]. Facies characteristics can be strongly controlled by local topography. For example, the best preserved outcrops of Dogashima 2 (chapter 4) are in a palæo-valley setting, and the overbank setting consists of facies with markedly different characteristics (number of beds, thickness and grain size). In addition, the distal facies related to a voluminous explosive eruption can be very similar to the proximal facies from a small-scale event. Interpretation of the succession of Dogashima 2 would have been challenging without the palæo-valley facies. In the overbank setting of Dogashima 2, the entire eruption is represented by 1 m of stratified pumice breccia. Thus, the regional extent of a succession is needed to fully assess its origin.

A major problem studying volcaniclastic successions is the identification of clasts that are juvenile, especially where pumice or scoria clasts are altered and/or compacted into fiamme. Juvenile and accidental pumice clasts can be very similar in shape, size and composition, which may lead to difficulties in interpreting the primary nature of the deposit. However, pumice clast morphology is irreversibly destroyed once compacted to fiamme. Compaction of pumice clasts increases the difficulty of interpreting the numerous beds in the Ohanapecosh Formation (chapter 3).

8. SIGNIFICANCE OF BREAKS AND NON-VOLCANIC FACIES

Post-eruptive processes are commonly dominant through time, thus it is likely that subaqueous volcaniclastic successions will include, or be dominated by intercalated units derived from resedimentation and reworking processes, as well as continental (non-volcanic) sediment input, and background sedimentation. In addition, the slower sedimentation rates will allow bioturbation [e.g. *Stow et al.*, 2002]. A break in deposition of eruption-fed pyroclastic clasts or presence of interbedded non-volcanic facies can be difficult to interpret, because they may indicate a break in explosive volcanic activity, modification of particle distribution patterns, or starvation of a basin by formation of new sedimentation paths. In addition, climactic explosive eruptions, or syn- or post- eruption

sector collapses can starve a basin by filling valleys and creating new catchment areas, and sending eruption products elsewhere. Such processes are likely to involve a longer timeframe than in the examples considered previously.

The volcano may start an effusive period, and no longer supply voluminous clasts. Dome-building episodes in the Dogashima Formation probably occurred after the deposition of the last eruption-fed bed (D1-10) of Dogashima 1, and after the climactic eruption of Dogashima 2 (D2-1 to D2-5). Thus, resedimented facies of D1-11 and D2-6 and D2-8 can either be considered post-eruptive or syn-eruptive, because they occurred during a break in explosive volcanic activity, but probably during effusive eruptions, which later produced the massive grey andesite breccia (D2-2) and the weakly stratified andesite breccia (D3).

Water currents can erode substantial sediment thickness over hundreds of square kilometres [*Stow et al*., 1998; *Wright*, 2001; *Martín-Chivelet et al*., 2008; *Stow et al*., 2008], and obliterate thin beds critical for the reconstruction of a volcaniclastic sequence. For example, the erosive contact between Dogashima 1 and Dogashima 2 does not give information on the time span between the depositions of the two successions. In the Ohanapecosh Formation, many beds of fine sandstone to mudstone (facies 8) are probably related to dilute density currents and suspension settling from products of explosive eruptions, resedimentation events, and/or non-volcanic sedimentation, indicated by presence of wood and leaves and some darker beds that may contain organic material.

Further significance of interbedded non-volcanic facies is twofold. Input of non-volcanic components may be the best constraint on the depositional setting of a succession dominated by pyroclastic facies, and non-volcanic interbeds can be used to argue for post-eruptive (versus syn-eruptive) associations. Post-eruptive pyroclastic associations comprise resedimented pyroclastic facies, reworked pyroclastic facies and non-volcanic facies. In contrast, syn-eruptive pyroclastic associations contain eruption-fed pyroclastic facies and resedimented pyroclastic facies, but reworked and non-volcanic facies are not expected.

In the Ohanapecosh Formation (chapter 3), most of the succession in the Chinook Pass Member is interpreted to be a syn-eruptive association, whereas abundance of interbedded thin beds in the White Pass Member implies long-term deposition, and probably involves both syn-eruptive and post-eruptive processes. In the Dogashima Formation (chapter 4), the succession of resedimented and reworked pyroclastic facies interbedded with eruption-fed pyroclastic facies suggests syn- and post-eruptive processes. However, part of the resedimented and reworked pyroclastic facies were probably deposited at Dogashima during dome growth at the vent, thus can be considered syn-eruptive as well.

References

Alatorre-Ibargüengoitia M.A., Scheu B., Dingwell D.B., Delgado-Granados H., Taddeucci J. (2010), Energy consumption by magmatic fragmentation and pyroclast ejection during Vulcanian eruptions, *Earth Planet. Sci. Lett.*, *291*, 60-69, doi:10.1016/j.epsl.2009.12.051.

Alidibirov M., Dingwell D.B. (2000), Three fragmentation mechanisms for highly viscous magma under rapid decompression, *J. Volcanol. Geotherm. Res.*, *100*, 413-421.

Allen J.R.L. (1963), The classification of cross-stratified units, with notes on their origin, *Sedimentology*, *2*, 93-114.

Allen J.R.L., Friend P.F., Lloyd A., Wells H. (1994), Morphodynamics of intertidal dunes: a year-long study at Lifeboat Station Bank, Wells-next-the-Sea, Eastern England, *Philos. Trans. R. Soc., A*, *347*, 291-344.

Allen S.R., Stadlbauer E., Keller J. (1999), Stratigraphy of the Kos Plateau Tuff: Product of a major Quaternary explosive rhyolitic eruption in the eastern Aegean, Greece, *Int. J. Earth Sci.*, *88*, 132-156.

Allen S.R., McPhie J. (2000), Water-settling and resedimentation of submarine rhyolitic pumice at Yali, eastern Aegean, Greece, *J. Volcanol. Geotherm. Res.*, *95*, 285-307.

Allen S.R., Stewart A.L. (2003), Products of explosive subaqueous felsic eruptions based on examples from the Hellenic island arc, Greece, in *Explosive Subaqueous Volcanism*, *Geophysical Monograph*, vol. 140, edited by J.D.L. White, et al., p. 285-298, AGU, Washington, D.C.

Allen S.R. (2004a), Complex spatter- and pumice-rich pyroclastic deposits from an andesitic caldera-forming eruption: The Siwi pyroclastic sequence, Tanna, Vanuatu, *Bull. Volcanol.*, *67*, 27-41.

Allen S.R. (2004b), The Parnell Grit beds revisited: Are they all the products of sector collapse of western subaerial volcanoes of the Northland Volcanic Arc?, *N. Z. J. Geol. Geophys.*, *47*, 509-524.

Allen S.R., Freundt A. (2006), Resedimentation of cold pumiceous ignimbrite into water: Facies transformations simulated in flume experiments, *Sedimentology*, *53*, 717-734.

Allen S.R., Hayward B.W., Mathews E. (2007), A facies model for a submarine volcaniclastic apron: The Miocene Manukau Subgroup, New Zealand, *Geol. Soc. Am. Bull.*, *119*, 725-742.

Allen S.R., Fiske R.S., Cashman K.V. (2008), Quenching of steam-charged pumice; implications for submarine pyroclastic volcanism, *Earth Planet. Sci. Lett.*, *274*, 40-49, doi:10.1016/j.epsl.2008.06.050.

Allen S.R., McPhie J. (2009), Products of neptunian eruptions, *Geology*, *37*, 639-642.

Allen S.R., Fiske R.S., Tamura Y. (2010), Effects of water depth on pumice formation in submarine domes at Sumisu, Izu-Bonin Arc, western Pacific, *Geology*, *38*, 391-394, doi:10.1130/G30500.1.

Allen S.R., Freundt A., Kurokawa K. (2011), Characteristics of submarine pumice-rich gravity flow deposits sourced from explosive disintegration of subaerial pyroclastic flows at the shoreline: field and experimental assessment, paper presented at XXV IUGG Conference, Melbourne.

Armstrong R.L., Ward P. (1991), Evolving geographic patterns of Cenozoic magmatism in the North American Cordillera: the temporal and spatial association of magmatism and metamorphic core complexes, *J. Geophys. Res.*, *96*, 13201-13224, doi:10.1029/91JB00412.

Baas J.H., Best J.L., Peakall J., Wang M. (2009), A phase diagram for turbulent, transitional, and laminar clay suspension flows, *J. Sediment. Res.*, *79*, 162-183.

Bagnold R.A. (1956), The flow of cohesionless grains in fluids, *Philos. Trans. R. Soc., A*, *249*, 235-297.

Bates R.G., Beck M.E., Jr., Burmester R.F. (1981), Tectonic rotations in the Cascade Range of southern Washington, *Geology*, *9*, 184-189.

Batiza R., Fornari D.J., Vanko D.A., Lonsdale P. (1984), Craters, calderas, and hyaloclastites on young Pacific seamounts, *J. Geophys. Res.*, *89*, 8371-8390, doi:10.1029/JB089iB10p08371.

Beck M.E. (1986), Model for Late Mesozoic-Early Tertiary tectonics of coastal California and western Mexico and speculations on the origin of the San Andreas fault (USA), *Tectonics*, *5*, 49-64.

Belousov A., Voight B., Belousova M., Petukhin A. (2002), Pyroclastic surges and flows from the 8-10 May 1997 explosive eruption of Bezymianny volcano, Kamchatka, Russia, *Bull. Volcanol.*, *64*, 455-471, doi:10.1007/s00445-002-0222-5.

Blakely R.J., Wells R.E., Weaver C.S., Johnson S.Y. (2002), Location, structure, and seismicity of the Seattle fault zone, Washington: Evidence from aeromagnetic anomalies, geologic mapping, and seismic-reflection data, *Geol. Soc. Am. Bull.*, *114*, 169-177.

Blott S.J., Pye K. (2001), Gradistat: A grain size distribution and statistics package for the analysis of unconsolidated sediments, *Earth Surf. Processes Landforms*, *26*, 1237-1248.

Boggs S. (2006), Principles of Sedimentology and Stratigraphy, 4th ed., 784 pp., Pearson Prentice Hall, Upper Saddle River.

Bonadonna C., Houghton B.F. (2005), Total grain-size distribution and volume of tephra-fall deposits, *Bull. Volcanol.*, *67*, 441-456.

Bonini W.E., Hughes D.W., Danes Z.F. (1974), Complete bouguer gravity anomaly map of Washington, Washington Department of Natural Resources Division of Geology and Earth Resources Olympia WA, United States (USA).

Boulter C.A. (1987), Subaqueous deposition of accretionary lapilli: significance for palaeoenvironmental interpretations in Archaean greenstone belts, *Precambrian Res.*, *34*, 231-246.

Bouma A.H. (1962), Sedimentology of some flysch deposits; a graphic approach to facies interpretation, 168 pp., Elsevier, Amsterdam.

Branney M.J., Kokelaar P. (2002), Pyroclastic density currents and the sedimentation of ignimbrites, 143 pp., Geological Society (London).

Bryan S.E., Cook A., Evans J.P., Colls P.W., Wells M.G., Lawrence M.G., Jell J.S., Greig A., Leslie R. (2004), Pumice rafting and faunal dispersion during 2001-2002 in the Southwest Pacific: Record of a dacitic submarine explosive eruption from Tonga, *Earth Planet. Sci. Lett.*, *227*, 135-154.

Bull K.F., McPhie J. (2007), Fiamme textures in volcanic successions: Flaming issues of definition and interpretation, *J. Volcanol. Geotherm. Res.*, *164*, 205-216.

Buller A.T., McManus J. (1973), The quartile-deviation/median-diameter relationships of glacial deposits, *Sediment. Geol.*, *10*, 135-146.

Burgisser A., Gardner J.E. (2006), Using hydraulic equivalences to discriminate transport processes of volcanic flows, *Geology*, *34*, 157-160, doi:10.1130/G21942.1.

Busby C.J., Kessel L.G., Schulz K.J., Foose M.P., Slack J.F. (2003), Volcanic setting of the Ordovician Bald Mountain massive sulfide deposits, northern Maine, in *Economic Geology Monographs*, vol. 11, edited, p. 210-244.

Capaccioni B., Valentini L., Rocchi M.B.L., Nappi G., Sarocchi D. (1997), Image analysis and circular statistics for shape-fabric analysis: Applications to lithified ignimbrites, *Bull. Volcanol.*, *58*, 501-514.

Carey R.J., Houghton B.F. (2010), "Inheritance"; an influence on the particle size of pyroclastic deposits, *Geology*, *38*, 347-350.

Carey S., Sigurdsson H., Mandeville C., Bronto S. (1996), Pyroclastic flows and surges over water: An example from the 1883 Krakatau eruption, *Bull. Volcanol.*, *57*, 493-511.

Carey S. (1997), Influence of convective sedimentation on the formation of widespread tephra fall layers in the deep sea, *Geology*, *25*, 839-842.

Carey S.N., Sigurdsson H. (1980), The Roseau ash: deep-sea tephra deposits from a major eruption on Dominica, Lesser Antilles arc, *J. Volcanol. Geotherm. Res.*, *7*, 67-86.

Carey S.N. (1991), Transport and deposition of tephra by pyroclastic flows and surges, in *Sedimentation in volcanic settings*, edited by R.V. Fisher, G.A. Smith, p. 39-57, SEPM, Tulsa; Special Publication, 45.

Cas R.A.F. (1983), Submarine 'crystal tuffs': their origin using a Lower Devonian example from southeastern Australia, *Geol. Mag.*, *120*, 471-486.

Cas R.A.F., Wright J.V. (1987), Volcanic successions, modern and ancient; a geological approach to processes, products and successions, 528 pp., Allen & Unwin, London, United Kingdom (GBR).

Cas R.A.F., Allen R.L., Bull S.W., Clifford B.A., Wright J.V. (1990), Subaqueous, rhyolitic dome-top tuff cones: a model based on the Devonian Bunga Beds, southeastern Australia and a modern analogue, *Bull. Volcanol.*, *52*, 159-174.

Cas R.A.F., Wright J.V. (1991), Subaqueous pyroclastic flows and ignimbrites: an assessment, *Bull. Volcanol.*, *53*, 357-380.

Cashman K.V. (1988), Crystallization of Mount St. Helens 1980-1986 dacite: A quantitative textural approach, *Bull. Volcanol.*, *50*, 194-209, doi:10.1007/BF01079682.

Cashman K.V., Fiske R.S. (1991), Fallout of pyroclastic debris from submarine volcanic eruptions, *Science*, *253*, 275-280, doi:10.1126/science.253.5017.275.

Castro J.M., Cashman K.V., Manga M. (2003), A technique for measuring 3D crystal-size distributions of prismatic microlites in obsidian, *Am. Mineral.*, *88*, 1230-

1240.

Chadwick J.W.W., Cashman K.V., Embley R.W., Matsumoto H., Dziak R.P., de Ronde C.E.J., Lau T.K., Deardorff N.D., Merle S.G. (2008), Direct video and hydrophone observations of submarine explosive eruptions at NW Rota-1 volcano, Mariana arc, *J. Geophys. Res., [Solid Earth Planets]*, *113*, B08S10, doi:10.1029/2007JB005215.

Cheney E.S., Hayman N.W. (2009), The Chiwaukum Structural Low; Cenozoic shortening of the central Cascade Range, Washington State, USA, *Geol. Soc. Am. Bull.*, *121*, 1135-1153.

Christiansen R.L., Peterson D.W. (1981), The 1980 eruptions of Mount St. Helens, Washington. Chronology of the 1980 eruptive activity, *U.S. Geol. Surv. Prof. Pap.*, *1250*, 17-30.

Clift R., Grace J.R., Weber M.E. (1978), Bubbles, drops, and particles, 2005 ed., 381 pp., Dover Publications, Mineola, NY, USA.

Clough B.J., Wright J.V., Walker G.P.L. (1981), An unusual bed of giant pumice in Mexico, *Nature*, *289*, 49-50.

Cole J.W. (1986), Distribution and tectonic setting of late Cenozoic volcanism in New Zealand, *Bull. - R. Soc. N. Z.*, *23*, 7-20.

Crandell D.R. (1976), The geologic story of Mount Rainier, U.S. Geol. Surv. Bull., 43 pp, U.S. Geological Survey, Reston.

Crowe C., Sommerfield M., Tsuji Y. (1998), Multiphase flows with droplets and particles, 496 pp., CRC Press, Boca Ration, Flordia.

Davey F.J. (1974), Magnetic anomalies off the west coast of Northland, New Zealand, *J. R. Soc. N. Z.*, *4*, 203-216.

Degruyter W., Burgisser A., Bachmann O., Malaspinas O., Gualda G.A.R., Baker D.R., Polacci M. (2010), Synchrotron X-ray microtomography and lattice Boltzmann simulations of gas flow through volcanic pumices, *6*, 470-481.

Dickinson W.R. (2009), Anatomy and global context of the North American Cordillera, in *Memoirs of the Geological Society of America*, vol. 204, edited, p. 1-29.

DiMarco M.J., Lowe D.R. (1989), Shallow-water volcaniclastic deposition in the Early Archean Panorama Formation, Warrawoona Group, eastern Pilbara Block, Western Australia, *Sediment. Geol.*, *64*, 43-63.

Downey W.S., Lentz D.R. (2006), Igneous rock associations 6. Modelling of deep submarine pyroclastic volcanism: A review and new results, *Geosci Canada*, *33*, 5-19.

Dufek J., Bergantz G.W. (2007), Dynamics and deposits generated by the Kos Plateau Tuff eruption: Controls of basal particle loss on pyroclastic flow transport, *Geochem., Geophys., Geosyst.*, *8*, Q12007, doi:10.1029/2007GC001741.

Dufek J., Manga M., Staedter M. (2007), Littoral blasts: Pumice-water heat transfer and the conditions for steam explosions when pyroclastic flows enter the ocean, *J. Geophys. Res., [Solid Earth Planets]*, *112*, B11201, doi:10.1029/2006JB004910.

Dufek J., Manga M. (2008), In situ production of ash in pyroclastic flows, *J. Geophys. Res., [Solid Earth Planets]*, *113*, B09207, doi:10.1029/2007JB005555.

Duncan R.A. (1982), A captured island chain in the Coast Range of Oregon and Washington, *J. Geophys. Res., [Solid Earth Planets]*, *87*, 10827-10837, doi:10.1029/JB087iB13p10827.

Duncan R.A., Kulm L.D. (1989), Plate tectonic evolution of the Cascades arc-subduction complex, in *The eastern Pacific Ocean and Hawaii*, edited by E.L. Winterer, et al., p. 413-438, Geol. Soc. Am., Denver.

Edmonds M., Herd R.A. (2005), Inland-directed base surge generated by the explosive interaction of pyroclastic flows and seawater at Soufrière Hills volcano, Montserrat, *Geology*, *33*, 245-248.

Eichelberger J.C., Carrigan C.R., Westrich H.R., Price R.H. (1986), Non-explosive silicic volcanism, *Nature*, *323*, 598-602, doi:10.1038/323598a0.

Eichelberger J.C. (1995), Silicic volcanism: ascent of viscous magmas from crustal reservoirs, *Annu. Rev. Earth Planet. Sci.*, *23*, 41-63.

Ellingson J.A. (1972), The rocks and structure of the White Pass area, Washington, *Northwest Science*, *46*, 9-24.

Elsworth D., Voight B., Thompson G., Young S.R. (2004), Thermal-hydrologic mechanism for rainfall-triggered collapse of lava domes, *Geology*, *32*, 969-972, doi:10.1130/G20730.1.

Evans J.E. (2010), The Chiwaukum Structural Low: Cenozoic shortening of the central Cascade Range, Washington State, USA: Comment, *Geol. Soc. Am. Bull.*, *122*, 2097-2102.

Evans J.R., Huntoon J.E., Rose W.I., Varley N.R., Stevenson J.A. (2009), Particle sizes of andesitic ash fallout from vertical eruptions and co-pyroclastic flow clouds, Volcán de Colima, Mexico, *Geology*, *37*, 935-938.

Evarts R.C., Ashley R.P., Smith J.G. (1987), Geology of the Mount St. Helens area: record of discontinuous volcanic and plutonic activity in the Cascade arc of southern Washington (USA), *J. Geophys. Res.*, *92*, 10155-10169, doi:10.1029/JB092iB10p10155.

Fernlund J.M.R. (1998), The effect of particle form on sieve analysis: a test by image analysis, *Eng. Geol. (Amsterdam, Neth.)*, *50*, 111-124.

Fisher R.V. (1961a), Stratigraphy of the Ashford area, southern Cascades, Washington, *Geol. Soc. Am. Bull.*, *72*, 1395-1407.

Fisher R.V. (1961b), Proposed classification of volcaniclastic sediments and rocks, *Geol. Soc. Am. Bull.*, *72*, 1409-1414.

Fisher R.V. (1983), Flow transformations in sediment gravity flows, *Geology*, *11*, 273-274.

Fisher R.V., Schmincke H.-U. (1984), Pyroclastic rocks, 472 pp., Springer-Verlag, Berlin, Federal Republic of Germany (DEU).

Fiske R.S. (1963), Subaqueous pyroclastic flows in the Ohanapecosh Formation, Washington, *Geol. Soc. Am. Bull.*, *74*, 391-406.

Fiske R.S., Hopson C.A., Waters A.C. (1963), Geology of Mount Rainier National Park, Washington, *U.S. Geol. Surv. Prof. Pap.*, *444*, 93.

Fiske R.S., Hopson C.A., Waters A.C. (1964), Geologic map and section of Mount

Rainier National Park, Washington.

Fiske R.S., Matsuda T. (1964), Submarine equivalents of ash flows Tokiwa Formation Japan, *Am. J. Sci.*, *262*, 76-106.

Fiske R.S. (1969), Recognition and significance of pumice in marine pyroclastic rocks, *Geol. Soc. Am. Bull.*, *80*, 1-8.

Fiske R.S., Cashman K.V., Shibata A., Watanabe K. (1998), Tephra dispersal from Myojinsho, Japan, during its shallow submarine eruption of 1952-1953, *Bull. Volcanol.*, *59*, 262-275, doi:10.1007/s004450050190.

Folk R.L., Ward W.C. (1957), Brazos River bar [Texas]; a study in the significance of grain size parameters, *J. Sediment. Petrol.*, *27*, 3-26.

Folk R.L. (1980), Petrology of sedimentary rocks, Edition: 2. First edition published in 1974 ed., 184 pp., Hemphill Publ. Co., Austin.

Freundt A. (1999), The formation of high-grade ignimbrites, Part II. A pyroclastic suspension current model with implications also for low-grade ignimbrites, *Bull. Volcanol.*, *60*, 545-567.

Freundt A. (2003), Entrance of hot pyroclastic flows into the sea: Experimental observations, *Bull. Volcanol.*, *65*, 144-164.

Freundt A., Strauch W., Kutterolf S., Schmincke H.U. (2007), Volcanogenic tsunamis in lakes: Examples from Nicaragua and general implications, *Pure Appl. Geophys.*, *164*, 527-545.

Friedman G.M. (1962), On sorting, sorting coefficients, and the lognormality of the grain-size distribution of sandstones, *J. Geol.*, *70*, 737-753.

Frizzell V.A., Jr., Tabor R.W., Booth D.B., Ort K.M., Waitt R.B., Jr. (1984), Preliminary geologic map of the Snoqualmie Pass 1:100,000 Quadrangle, Washington, 43 p., 41 sheet pp, U. S. Geological Survey, Reston, VA, United States (USA).

Gard L.M., Jr. (1968), Bedrock geology of the Lake Tapps Quadrangle, Pierce County, Washington, B1-B33 pp, U. S. Geological Survey, Reston.

Gardner J.V. (2010), The West Mariana Ridge, western Pacific Ocean: Geomorphology and processes from new multibeam data, *Geol. Soc. Am. Bull.*, *122*, 1378-1388, doi:10.1130/B30149.1.

Garzanti E., Andò S., Vezzoli G. (2009), Grain-size dependence of sediment composition and environmental bias in provenance studies, *Earth Planet. Sci. Lett.*, *277*, 422-432.

Geological Survey of Japan, AIST (Ed.), 2010. Seamless digital geological map of Japan 1:200, 000, Feb 1, 2010 version. Research Information Database DB084. Geol. Surv. Jpn. AIST.

Gifkins C.C., McPhie J., Allen R.L. (2002), Pumiceous rhyolitic peperite in ancient submarine volcanic successions, *J. Volcanol. Geotherm. Res.*, *114*, 181-203, doi:10.1016/S0377-0273(01)00284-0.

Gilbert J.S., Lane S.J., Sparks R.S.J., Koyaguchi T. (1991), Charge Measurements on Particle Fallout from a Volcanic Plume, *Nature*, *349*, 598-600.

Glaister R.P., Nelson H.W. (1974), Grain-size distributions, an aid in facies

identification, *Bull. Can. Pet. Geol.*, *22*, 203-240.

Gordee S.M., McPhie J., Allen S.R. (2008), Facies mapping of volcanic and sedimentary facies of a partly extrusive submarine cryptodome, Mio-Pliocene Shirahama Group, Izu Peninsula, Japan, paper presented at IAVCEI General Assembly, Iceland.

Goto Y., McPhie J. (1998), Endogenous growth of a Miocene submarine dacite cryptodome, Rebun Island, Hokkaido, Japan, *J. Volcanol. Geotherm. Res.*, *84*, 273-286, doi:10.1016/S0377-0273(98)00040-7.

Goto Y., Tsuchiya N. (2004), Morphology and growth style of a Miocene submarine dacite lava dome at Atsumi, northeast Japan, *J. Volcanol. Geotherm. Res.*, *134*, 255-275, doi:10.1016/j.jvolgeores.2004.03.015.

Gualda G.A.R., Baker D.R., Polacci M. (2010), Advances in 3D imaging and analysis of geomaterials, *6*, 468-523.

Hammond P.E. (1979), A tectonic model for evolution of the Cascade Range, in *Pacific Coast Paleogeography Symposium, no.3*, edited by J.M. Armentrout, et al., p. 219-237, Pacific Section, Society of Economic Paleontologists and Mineralogists.

Hammond P.E. (2005), Geologic map of the Timberwolf Mountain 7.5 minute Quadrangle, Yakima County, Washington, Washington State Department of Natural Resources, division of Geology and Earth Resources

Hampton M.A. (1972), The role of subaqueous debris flow in generating turbidity currents, *J. Sediment. Petrol.*, *42*, 775-793.

Hampton M.A., Lee H.J., Locat J. (1996), Submarine landslides, *Rev. Geophys.*, *34*, 33-59, doi:10.1029/95rg03287.

Hart K., Carey S., Sigurdsson H., Sparks R.S.J., Robertson R.E.A. (2004), Discharge of pyroclastic flows into the sea during the 1996-1998 eruptions of the Soufrière Hills volcano, Montserrat, *Bull. Volcanol.*, *66*, 599-614.

Hatherton T., Davey F.J., Hunt T.M. (1979), Geophysical anomalies and igneous bodies off the west coast, North Island, *J. R. Soc. N. Z.*, *9*, 13-28.

Hayward B.W. (1976a), Lower Miocene stratigraphy and structure of the Waitakere Ranges and the Waitakere Group (new), *N. Z. J. Geol. Geophys.*, *19*, 871-895.

Hayward B.W. (1976b), Lower Miocene geology and sedimentary history of the Muriwai-Te Waharoa coastline, North Auckland, New Zealand, *N. Z. J. Geol. Geophys.*, *19*, 639-662.

Hayward B.W. (1976c), Lower Miocene Geology and Sedimentary History of Muriwai-Te Waharoa Coastline, North-Auckland, New-Zealand, *N. Z. J. Geol. Geophys.*, *19*, 639-662.

Hayward B.W. (1977), Miocene volcanic centres of the Waitakere Ranges, North Auckland, New Zealand., *J. R. Soc. N. Z.*, *7*, 123-141.

Hayward B.W. (1979), Eruptive history of the early to mid Miocene Waitakere volcanic arc, and palaeogeography of the Waitemata Basin, northern New Zealand, *J. R. Soc. N. Z.*, *9*, 297-320.

Hayward B.W. (1983), Waitakere, N.Z. Geol. Surv. Lower Hutt New Zealand (NZL).

Hayward B.W. (1993), The tempestuous 10 million year life of a double arc and intra-arc basin; New Zealand's Northland Basin in the early Miocene, *Sedimentary Basins of the World*, *2*, 113-142.

Hayward B.W., Black P.M., Smith I.E.M., Ballance P.F., Itaya T., Doi M., Takagi M., Bergman S., Adams C.J., Herzer R.H., Robertson D.J. (2001), K-Ar ages of early Miocene arc-type volcanoes in Northern New Zealand, *N. Z. J. Geol. Geophys.*, *44*, 285-311.

Head J.W., Wilson L. (2003), Deep submarine pyroclastic eruptions: Theory and predicted landforms and deposits, *J. Volcanol. Geotherm. Res.*, *121*, 155-193.

Heiken G. (1974), An atlas of volcanic ash, 101 pp., Smithsonian Institution, Washington, DC, United States (USA).

Hicks P.D., Matthews A.J., Cooker M.J. (2010), Triggering of a volcanic dome collapse by rainwater infiltration, *J. Geophys. Res.*, *115*, B09212, doi:10.1029/2009JB006831.

Higgins M.D. (2000), Measurement of crystal size distributions, *Am. Mineral.*, *85*, 1105-1116.

Hildreth W. (2007), Quaternary magmatism in the Cascades; geologic perspectives, *U.S. Geol. Surv. Prof. Pap.*, *P 1744*, 125.

Hoblitt R.P., Harmon R.S. (1993), Bimodal density distribution of cryptodome dacite from the 1980 eruption of Mount St. Helens, Washington, *Bull. Volcanol.*, *55*, 421-437, doi:10.1007/BF00302002.

Horikoshi E. (1969), Volcanic activity related to the formation of the Kuroko-type deposits in the Kosaka district, Japan, *Miner. Deposita*, *4*, 321-345, doi:10.1007/BF00207161.

Horikoshi E., Sato T. (1970), Volcanic Activity and Ore Deposition in the Kosaka Mine, in *Volcanism and ore genesis*, edited, p. 181-195, Univ. Tokyo Press, Tokyo.

Houghton B.F., Wilson C.J.N. (1989), A vesicularity index for pyroclastic deposits, *Bull. Volcanol.*, *51*, 451-462.

Houghton B.F., Smith R.T. (1993), Recycling of magmatic clasts during explosive eruptions: estimating the true juvenile content of phreatomagmatic volcanic deposits, *Bull. Volcanol.*, *55*, 414-420.

Huchon P., Kitazato H. (1984), Collision of the Izu Block with central Japan during the Quaternary and geological evolution of the Ashigara area, *110*, 201-210.

Ibaraki M. (1976), Notes on planktonic foraminifera from the Harada Formation, Shirahama Group, southern Izu Peninsula, *Geoscience Reports of Shizuoka University*, *2*, 1-7.

Ibaraki M. (1981), Geologic ages of "Lepidocyclina" and Miogypsina horizons in Japan as determined by planktonic foraminifera, paper presented at IGCP-114; International workshop on Pacific Neogene biostratigraphy; 6th international working group meeting, Osaka, Japan, Nov. 25-29, 1981, Osaka Mus. Nat. Hist., Osaka, Japan (JPN).

Ilstad T., Elverhoi A., Issler D., Marr J.G. (2004a), Subaqueous debris flow behaviour and its dependence on the sand/clay ratio: a laboratory study using particle tracking, *Mar. Geol.*, *213*, 415-438.

Ilstad T., Marr J.G., Elverhoi A., Harbitz C.B. (2004b), Laboratory studies of subaqueous debris flows by measurements of pore-fluid pressure and total stress, *Mar. Geol.*, *213*, 403-414.

Ingram (1954a), Terminology for the thickness of stratification and parting units in sedimentary rocks, *Geol. Soc. Am. Bull.*, *86*, 937-938.

Ingram R.L. (1954b), Terminology for the thickness of stratification and parting units in sedimentary rocks, *Geol. Soc. Am. Bull.*, *65*, 937-938.

Iverson R.M. (1997), The physics of debris flows, *Rev. Geophys.*, *35*, 245-296, doi:10.1029/97rg00426.

Jaupart C., Allègre C.J. (1991), Gas content, eruption rate and instabilities of eruption regime in silicic volcanoes, *Earth Planet. Sci. Lett.*, *102*, 413-429, doi:10.1016/0012-821X(91)90032-D.

Jerram D.A., Cheadle M.J., Hunter R.H., Elliott M.T. (1996), The spatial distribution of grains and crystals in rocks, *Contrib. Mineral. Petrol.*, *125*, 60-74.

Jerram D.A., Davidson J.P. (2007), Frontiers in textural and microgeochemical analysis, *Elements*, *3*, 235-238.

Jerram D.A., Davis G.R., Mock A., Charrier A., Marsh B.D. (2010), Quantifying 3D crystal populations, packing and layering in shallow intrusions; a case study from the Basement Sill, Dry Valleys, Antarctica, *Geosphere*, *6*, 537-548.

Johnson S.Y. (1985), Eocene strike-slip faulting and nonmarine basin formation in Washington, in *Strike-slip deformation, basin formation, and sedimentation*, vol. 37, edited by K.T. Biddle, N. Christie-Blick, p. 283-302, SEPM, Tulsa; Special Publication.

Johnson T.C. (1984), Sedimentation in large lakes (chemical processes), *Annu. Rev. Earth Planet. Sci.*, *12*, 179-204.

Julien P.Y., Lan Y. (1991), Rheology of hyperconcentrations, *J. Hydr. Eng.*, *117*, 346-353.

Jutzeler M., Schmincke H.U., Sumita M. (2010), The incrementally zoned Miocene Ayagaures ignimbrite (Gran Canaria, Canary Islands), *J. Volcanol. Geotherm. Res.*, *196*, 1-19, doi:10.1016/j.jvolgeores.2010.07.002.

Kano K.-I. (1983), Structures of submarine andesitic volcano - an example in the Neogene Shirahama group in the southern part of the Izu Peninsula, Japan, *Geoscience Reports of Shizuoka University*, *8*, 9-37.

Kano K.-I. (1989), Interactions between andesitic magma and poorly consolidated sediments: examples in the Neogene Shirahama Group, South Izu, Japan, *J. Volcanol. Geotherm. Res.*, *37*, 59-75.

Kano K. (1991), Volcaniclastic sedimentation in a shallow-water marginal basin: the Early Miocene Koura Formation, SW Japan, *Sediment. Geol.*, *74*, 309-321.

Kano K., Orton G.J., Kano T. (1994), A hot Miocene subaqueous scoria-flow deposit in the Shimane Peninsula, SW Japan, *J. Volcanol. Geotherm. Res.*, *60*, 1-14.

Kano K. (1996), A Miocene coarse volcaniclastic mass-flow deposit in the Shimane Peninsula, SW Japan: Product of a deep submarine eruption?, *Bull. Volcanol.*, *58*, 131-143, doi:10.1007/s004450050131.

Kano K., Yamamoto T., Ono K. (1996), Subaqueous eruption and emplacement of the Shinjima Pumice, Shinjima (Moeshima) Island, Kagoshima Bay, SW Japan, *J. Volcanol. Geotherm. Res.*, *71*, 187-206.

Kano K. (2003), Subaqueous pumice eruptions and their products; a review, in *Explosive Subaqueous Volcanism*, *Geophysical Monograph*, vol. 140, edited by J.D.L. White, et al., p. 213-230, AGU, Washington, D.C.

Karatson D., Sztano O., Telbisz T. (2002), Preferred clast orientation in volcaniclastic mass-flow deposits; application of a new photo-statistical method, *J. Sediment. Res.*, *72*, 823-835.

Kato I., Muroi I., Yamazaki T., Abe M. (1971), Subaqueous pyroclastic flow deposits in the Upper Donzurubo Formation, Nijo-san District, Osaka, Japan, *Chishitsugaku Zasshi = Journal of the Geological Society of Japan*, *77*, 193-206.

Kato Y. (1987), Woody pumice generated with submarine eruption, *Chishitsugaku Zasshi = Journal of the Geological Society of Japan*, *93*, 11-20.

Kellerhals R., Shaw J., Arora V.K. (1975), On grain size from thin sections, *J. Geol.*, *83*, 79-96.

Kennedy S.K., Meloy T.P., Durney T.E. (1985), Sieve data - size and shape information, *J. Sediment. Petrol.*, *55*, 356-360.

Kennett J.P. (1982), Marine Geology, Prentice-Hall, Engelwood Cliff, New Jersey.

Kervyn M., Boone M.N., van Wyk de Vries B., Lebas E., Cnudde V., Fontijn K., Jacobs P., Gualda G.A.R., Baker D.R., Polacci M. (2010), 3D imaging of volcano gravitational deformation by computerized X-ray micro-tomography, *6*, 482-498.

Ketcham R.A., Slottke D.T., Sharp J.M., Jr., Gualda G.A.R., Baker D.R., Polacci M. (2010), Three-dimensional measurement of fractures in heterogeneous materials using high-resolution X-ray computed tomography, *6*, 499-514.

Kneller B.C., Branney M.J. (1995), Sustained high-density turbidity currents and the deposition of thick massive sands, *Sedimentology*, *42*, 607-616.

Kobberger G., Schmincke H.U. (1999), Deposition of rheomorphic ignimbrite D (Mogán Formation), Gran Canaria, Canary Islands, Spain, *Bull. Volcanol.*, *60*, 465-485.

Kokelaar B.P. (1983), The mechanism of Surtseyan volcanism, *J. Geol. Soc. (London, U. K.)*, *140*, 939-944.

Kokelaar P., Raine P., Branney M.J. (2007), Incursion of a large-volume, spatter-bearing pyroclastic density current into a caldera lake: Pavey Ark ignimbrite, Scafell caldera, England, *Bull. Volcanol.*, *70*, 23-54, doi:10.1007/s00445-007-0118-5.

Komar P.D. (1971), Hydraulic jumps in turbidity currents, *Geol. Soc. Am. Bull.*, *82*, 1477-1487.

Komar P.D., Reimers C.E. (1978), Grain shape effects on settling rates, *J. Geol.*, *86*, 193-209.

Komar P.D., Baba J., Cui B. (1984), Grain-size analyses of mica within sediments and the hydraulic equivalence of mica and quartz (Capistrano Formation, California), *J. Sediment. Petrol.*, *54*, 1379-1391.

Krumbein W.C. (1936), Application of logarithmic moments to size-frequency distributions of sediments, *J. Sediment. Petrol.*, *6*, 35-47.

Kuno H., Ishikawa T., Taneda S., Yagi K., Yamasaki M. (1964), Sorting of pumice and lithic fragments as a key to eruptive and emplacement mechanism, *Recent Progress of Natural Sciences in Japan = Nihon Shizen Kagaku Shuho*, *35*, 223-238.

Kurokawa K., Tomita Y. (1998), The Znp-Ohta ash; an early Pliocene widespread subaqueous tephra deposit in central Japan, *Chishitsugaku Zasshi = Journal of the Geological Society of Japan*, *104*, 558-561.

Le Bas M.J., Le Maitre R.W., Streckeisen A., Zanettin B. (1986), A chemical classification of volcanic rocks based on the total alkali-silica diagram, *J. Petrol.*, *27*, 745-750, doi:10.1093/petrology/27.3.745

Leat P.T., Tate A.J., Tappin D.R., Day S.J., Owen M.J. (2010), Growth and mass wasting of volcanic centers in the northern South Sandwich arc, South Atlantic, revealed by new multibeam mapping, *Mar. Geol.*, *275*, 110-126.

Lee I.T., Ogawa Y. (1998), Bottom-current deposits in the Miocene-Pliocene Misaki Formation, Izu forearc area, Japan, *Isl. Arc*, *7*, 315-329.

Legros F., Druitt T.H. (2000), On the emplacement of ignimbrite in shallow-marine environments, *J. Volcanol. Geotherm. Res.*, *95*, 9-22.

Lowe D.R. (1976), Grain flow and grain flow deposits, *J. Sediment. Petrol.*, *46*, 188-199.

Lowe D.R. (1982), Sediment gravity flows: II. Depositional models with special reference to the deposits of high-density turbidity currents, *J. Sediment. Petrol.*, *52*, 279-297.

Luhr J.F., Carmichael I.S.E. (1990), Petrological monitoring of cyclical eruptive activity at Volcán Colima, Mexico, *J. Volcanol. Geotherm. Res.*, *42*, 235-260.

Macedonio G., Costa A., Folch A. (2008), Ash fallout scenarios at Vesuvius: Numerical simulations and implications for hazard assessment, *J. Volcanol. Geotherm. Res.*, *178*, 366-377.

Macías J.L., Espíndola J.M., Bursik M., Sheridan M.F. (1998), Development of lithic-breccias in the 1982 pyroclastic flow deposits of El Chichón Volcano, Mexico, *J. Volcanol. Geotherm. Res.*, *83*, 173-196.

Mack G.H., McIntosh W.C., Leeder M.R., Monger H.C. (1996), Plio-Pleistocene pumice floods in the ancestral Rio Grande, southern Rio Grande rift, USA, *Sediment. Geol.*, *103*, 1-8.

Maeno F., Taniguchi H. (2006), Silicic lava dome growth in the 1934-1935 Showa Iwo-jima eruption, Kikai caldera, south of Kyushu, Japan, *Bull. Volcanol.*, *68*, 673-688, doi:10.1007/s00445-005-0042-5.

Mandeville C.W., Carey S., Sigurdsson H., King J. (1994), Paleomagnetic evidence for high-temperature emplacement of the 1883 subaqueous pyroclastic flows from Krakatau volcano, Indonesia, *J. Geophys. Res.*, *99*, 9487-9504, doi:10.1029/94JB00239.

Mandeville C.W., Carey S., Sigurdsson H. (1996), Sedimentology of the Krakatau 1883 submarine pyroclastic deposits, *Bull. Volcanol.*, *57*, 512-529.

Manville V., White J.D.L., Houghton B.F., Wilson C.J.N. (1998), The saturation

behaviour of pumice and some sedimentological implications, *Sediment. Geol.*, *119*, 5-16.

Manville V. (2001), Sedimentology and history of Lake Reporoa; an ephemeral supra-ignimbrite lake, Taupo volcanic zone, New Zealand, in *Volcaniclastic sedimentation in lacustrine settings*, vol. 30, edited by S.P.o.t.I.A.o. Sedimentologists, p. 109-140.

Manville V., Segschneider B., White J.D.L. (2002), Hydrodynamic behaviour of Taupo 1800a pumice: Implications for the sedimentology of remobilized pyroclasts, *Sedimentology*, *49*, 955-976.

Manville V., Wilson C.J.N. (2004), Vertical density currents: A review of their potential role in the deposition and interpretation of deep-sea ash layers, *J. Geol. Soc. (London, U. K.)*, *161*, 947-958, doi:10.1144/0016-764903-067.

Marr J.G., Harff P.A., Shanmugam G., Parker G. (2001), Experiments on subaqueous sandy gravity flows: The role of clay and water content in flow dynamics and depositional structures, *Geol. Soc. Am. Bull.*, *113*, 1377-1386, doi:10.1130/0016-7606(2001)113<1377:eossgf>2.0.co;2.

Martel C., Bourdier J.L., Pichavant M., Traineau H. (2000), Textures, water content and degassing of silicic andesites from recent plinian and dome-forming eruptions at Mount Pelée volcano (Martinique, Lesser Antilles arc), *J. Volcanol. Geotherm. Res.*, *96*, 191-206, doi:10.1016/S0377-0273(99)00147-X.

Martel C., Poussineau S. (2007), Diversity of eruptive styles inferred from the microlites of Mt Pelée andesite (Martinique, Lesser Antilles), *J. Volcanol. Geotherm. Res.*, *166*, 233-254, doi:10.1016/j.jvolgeores.2007.08.003.

Martín-Chivelet J., Fregenal-Martínez M.A., Chacón B. (2008), Traction structures in contourites, in *Contourites*, *Developments in Sedimentology*, vol. 60, edited by M. Rebesco, A. Camerlenghi, p. 159-182, Elsevier Science, Amsterdam, Netherlands.

Mason R.M., Starostin A.B., Melnik O.E., Sparks R.S.J. (2006), From Vulcanian explosions to sustained explosive eruptions: The role of diffusive mass transfer in conduit flow dynamics, *J. Volcanol. Geotherm. Res.*, *153*, 148-165, doi:10.1016/j.jvolgeores.2005.08.011.

Matsumoto R., Katayama T., Iijima A. (1985), Geology, igneous activity, and hydrothermal alteration in the Shimoda district, southern part of Izu Peninsula, central Japan, *J. Geol. Soc. Jap.*, *91*, 43-63.

Matthews A.J., Barclay J. (2004), A thermodynamical model for rainfall-triggered volcanic dome collapse, *Geophys. Res. Lett.*, *31*, L05614, doi:10.1029/2003GL019310.

Matthews S.J., Gardeweg M.C., Sparks R.S.J. (1997), The 1984 to 1996 cyclic activity of Lascar Volcano, northern Chile; cycles of dome growth, dome subsidence, degassing and explosive eruptions, *Bull. Volcanol.*, *59*, 72-82, doi:10.1007/s004450050176.

McBirney A.R. (1978), Volcanic evolution of the Cascade Range, *Annu. Rev. Earth Planet. Sci.*, *6*, 437-456.

McKee E.D., Weir G.W. (1953), Terminology for stratification and crosstratification in sedimentary rocks, *Geol. Soc. Am. Bull.*, *64*, 381-389.

McPhie J., Doyle M., Allen R. (1993), Volcanic Textures, 198 pp., ARC- Centre of Excellence in Ore Deposits University of Tasmania.

McPhie J., Allen R.L. (2003), Submarine, silicic, syn-eruptive pyroclastic units in the Mount Read Volcanics, western Tasmania; influence of vent setting and proximity on lithofacies characteristics, in *Explosive Subaqueous Volcanism*, *Geophysical Monograph*, vol. 140, edited by J.D.L. White, et al., p. 245-258, AGU, Washington, D.C.

Meiburg E., Kneller B. (2010), Turbidity currents and their deposits, *Annu. Rev. Fluid Mech.*, *42*, 135-156.

Middleton G.V. (1993), Sediment deposition from turbidity currents, *Annu. Rev. Earth Planet. Sci.*, *21*, 89-114.

Mock A., Jerram D.A. (2005), Crystal size distributions (CSD) in three dimensions: Insights from the 3D reconstruction of a highly porphyritic rhyolite, *J. Petrol.*, *46*, 1525-1541.

Mohrig D., Whipple K.X., Hondzo M., Ellis C., Parker G. (1998), Hydroplaning of subaqueous debris flows, *Geol. Soc. Am. Bull.*, *110*, 387-394.

Moore B.N. (1934), Deposits of possible nuée ardente origin in the Crater Lake region, Oregon, *J. Geol.*, *42*, 358-375.

Moore J.G., Normark W.R., Holcomb R.T. (1994), Giant Hawaiian landslides, *Annu. Rev. Earth Planet. Sci.*, *22*, 119-144.

Mulder T., Alexander J. (2001), The physical character of subaqueous sedimentary density flow and their deposits, *Sedimentology*, *48*, 269-299, doi:10.1046/j.1365-3091.2001.00360.x.

Mulder T., Syvitski J.P.M., Migeon S., Faugères J.C., Savoye B. (2003), Marine hyperpycnal flows: Initiation, behaviorand related deposits. A review, *Mar. Pet. Geol.*, *20*, 861-882, doi:10.1016/j.marpetgeo.2003.01.003.

Murai I. (1961), A study of the textural characteristics of pyroclastic flow deposits in Japan, *Bulletin of the Earthquake Research Institute*, *39*, 133-248.

Neill O.K., Hammer J.E., Izbekov P.E., Belousova M.G., Belousov A.B., Clarke A.B., Voight B. (2010), Influence of pre-eruptive degassing and crystallization on the juvenile products of laterally directed volcanic explosions, *J. Volcanol. Geotherm. Res.*, doi:10.1016/j.jvolgeores.2010.09.011.

Newhall C.G., Self S. (1982), The volcanic explosivity index (VEI): an estimate of explosive magnitude for historical volcanism, *J. Geophys. Res.*, *87*, 123-1238, doi:10.1029/JC087iC02p01231.

Normark W.R., Piper D.J.W. (1991), Initiation processes and flow evolution of turbidity currents: implications for the depositional record, in *From shoreline to abyss: contributions in marine geology in honor of Francis Parker Shepard*, vol. 46, edited by R.H. Osborne, p. 207-230, SEPM, Tulsa; Special Publication.

Okumura S., Nakamura M., Takeuchi S., Tsuchiyama A., Nakano T., Uesugi K. (2009), Magma deformation may induce non-explosive volcanism via degassing through bubble networks, *Earth Planet. Sci. Lett.*, *281*, 267-274, doi:10.1016/j.epsl.2009.02.036.

Orsi G., Gallo G., Heiken G., Wohletz K., Yu E., Bonani G. (1992), A comprehensive

study of pumice formation and dispersal: the Cretaio Tephra of Ischia (Italy), *J. Volcanol. Geotherm. Res.*, *53*, 329-354.

Pallister J.S., Hoblitt R.P., Meeker G.P., Knight R.J., Siems D.F. (1996), Magma mixing at Mount Pinatubo; petrographic and chemical evidence from the 1991 deposits, in *Fire and mud; eruptions and lahars of Mount Pinatubo, Philippines*, edited by C.G. Newhall, R.S. Punongbayan, p. 457-511, Philippine Institute of Volcanology and Seismology and University of Washington.

Passega R. (1964), Grain size representation by CM patterns as a geologic tool, *J. Sediment. Petrol.*, *34*, 830-847.

Paterson G.A., Roberts A.P., Mac Niocaill C., Muxworthy A.R., Gurioli L., Viramonté J.G., Navarro C., Weider S. (2009), Paleomagnetic determination of emplacement temperatures of pyroclastic deposits: an under-utilized tool, *Bull. Volcanol.*, 1-22, doi:10.1007/s00445-009-0324-4.

Pichler H. (1965), Acid hyaloclastites, *Bull. Volcanol.*, *28*, 293-310, doi:10.1007/BF02596934.

Piper D.J.W., Cochonat P., Morrison M.L. (1999), The sequence of events around the epicentre of the 1929 Grand Banks earthquake: Initiation of debris flows and turbidity current inferred from sidescan sonar, *Sedimentology*, *46*, 79-97.

Piper D.J.W., Normark W.R. (2009), Processes that initiate turbidity currents and their influence on turbidites; a marine geology perspective, *J. Sediment. Res.*, *79*, 347-362.

Platz T., Cronin S.J., Cashman K.V., Stewart R.B., Smith I.E.M. (2007), Transition from effusive to explosive phases in andesite eruptions - A case-study from the AD1655 eruption of Mt. Taranaki, New Zealand, *J. Volcanol. Geotherm. Res.*, *161*, 15-34, doi:10.1016/j.jvolgeores.2006.11.005.

Postma G., Nemec W., Kleinspehn K.L. (1988), Large floating clasts in turbidites: a mechanism for their emplacement, *Sediment. Geol.*, *58*, 47-61.

Proussevitch A.A., Sahagian D.L. (2001), Recognition and separation of discrete objects within complex 3D voxelized structures, *Comput. Geosci.*, *27*, 441-454.

Proussevitch A.A., Sahagian D.L., Carlson W.D. (2007a), Statistical analysis of bubble and crystal size distributions: Application to Colorado Plateau basalts, *J. Volcanol. Geotherm. Res.*, *164*, 112-126.

Proussevitch A.A., Sahagian D.L., Tsentalovich E.P. (2007b), Statistical analysis of bubble and crystal size distributions: Formulations and procedures, *J. Volcanol. Geotherm. Res.*, *164*, 95-111.

Pyle D.M. (1989), The thickness, volume and grainsize of tephra fall deposits, *Bull. Volcanol.*, *51*, 1-15.

Quane S.L., Russell J.K. (2005), Ranking welding intensity in pyroclastic deposits, *Bull. Volcanol.*, *67*, 129-143.

Reid I., Frostick L.E. (1994), Fluvial sediment transport and deposition, in *Sediment transport and depositional processes*, edited by K. Pye, p. 89-155, Blackwell Scientific Publications, Edinburgh.

Reid W.P. (1955), Distribution of sizes of spheres in a solid from a study of slices of the solid, *J. Math. Phys.*, *34*, 95-102.

Reiners P.W., Ehlers T.A., Garver J.I., Mitchell S.G., Montgomery D.R., Vance J.A., Nicolescu S. (2002), Late Miocene exhumation and uplift of the Washington Cascade Range, *Geology*, *30*, 767-770.

Reynolds M.A., Best J.G. (1976), Summary of the 1953-57 eruption of Tuluman volcano, Papua New Guinea., in *Volcanism in Australasia*, edited by R.W. Johnson, p. 287-296, Elsevier, Amsterdam.

Reynolds M.A., Best J.G., Johnson R.W. (1980), 1953-57 eruption of Tuluman Volcano; rhyolitic volcanic activity in the northern Bismarck Sea., 44 pp., Geological Survey of Papua New Guinea, Port Moresby.

Riedel J.L., Pringle P.T., Schuster R.L. (2001), Deposition of Mount Mazama tephra in a landslide-dammed lake on the upper Skagit River, Washington, USA, in *Volcaniclastic sedimentation in lacustrine settings*, vol. 30, edited by S.P.o.t.I.A.o. Sedimentologists, p. 285-298.

Robertson R., Cole P., Sparks R.S.J., Harford C., Lejeune A.M., McGuire W.J., Miller A.D., Murphy M.D., Norton G., Stevens N.F., Young S.R. (1998), The explosive eruption of Soufriere Hills Volcano, Montserrat, West Indies, 17 September, 1996, *Geophys. Res. Lett.*, *25*, 3429-3432, doi:10.1029/98GL01442.

Rosi M., Landi P., Polacci M., Di Muro A., Zandomeneghi D. (2004), Role of conduit shear on ascent of the crystal-rich magma feeding the 800-year-B.P. Plinian eruption of Quilotoa Volcano (Ecuador), *Bull. Volcanol.*, *66*, 307-321, doi:10.1007/s00445-003-0312-z.

Rubey W.W. (1933), The size distribution of heavy minerals within a water-laid sandstone, *J. Sediment. Petrol.*, *3*, 3-29.

Sahagian D.L., Maus J.E. (1994), Basalt vesicularity as a measure of atmospheric pressure and palaeoelevation, *Nature*, *372*, 449-451.

Sahagian D.L., Proussevitch A.A. (1998), 3D particle size distributions from 2D observations: Stereology for natural applications, *J. Volcanol. Geotherm. Res.*, *84*, 173-196.

Sahu B.K. (1965), Theory of sieving, *J. Sediment. Petrol.*, *35*, 750-753.

Sallenger A.H. (1979), Inverse grading and hydraulic equivalence in grain flow deposits, *J. Sediment. Petrol.*, *49*, 553-562.

Saucedo R., MacÃas J.L., Gavilanes J.C., Arce J.L., Komorowski J.C., Gardner J.E., Valdez-Moreno G. (2010), Eyewitness, stratigraphy, chemistry, and eruptive dynamics of the 1913 Plinian eruption of Volcán de Colima, México, *J. Volcanol. Geotherm. Res.*, *191*, 149-166, doi:10.1016/j.jvolgeores.2010.01.011.

Sawamura K., Sumi K., Ono K., Moritani T. (1970), Geology of the Shimoda District; quadrangle series, scale 1:50,000, Tokyo (8) No. 105, *Geological Survey of Japan*.

Scandone R., Malone S.D. (1985), Magma supply, magma discharge and readjustment of the feeding system of Mount St. Helens during 1980, *J. Volcanol. Geotherm. Res.*, *23*, 239-262.

Schasse H.W. (1987), Geologic map of the Mount Rainier quadrangle, Washington, 43 pp., 41 sheet pp, Division of Geology and Earth Resources.

Schmincke H.-U. (2004), Volcanism, 324 pp., Springer-Verlag.

Schumacher R., Schmincke H.U. (1991), Internal structure and occurrence of accretionary lapilli - a case study at Laacher See Volcano, *Bull. Volcanol.*, *53*, 612-634.

Schumacher R., Schmincke H.U. (1995), Models for the origin of accretionary lapilli, *Bull. Volcanol.*, *56*, 626-639.

Schuster J.E. (2005), Geologic map of Washington state, GM-53, Washington State Department of Natural Resources Division of Geology and Earth Resources, Olympia WA, United States (USA).

Sengupta S., Ghosh J.K., Mazumder B.S. (1991), Experimental-theoretical approach to interpretation of grain size frequency distributions, in *Principles, methods, and application of particle size analysis*, edited by J.P.M. Syvitski, p. 264-279, Cambridge Univ. Press, New York.

Sequeiros O.E., Spinewine B., Beaubouef R.T., Sun T., Garcia M.H., Parker G. (2010), Bedload transport and bed resistance associated with density and turbidity currents, *Sedimentology*, *57*, 1463-1490.

Shanmugam G., Spalding T.D., Rofheart D.H. (1993), Traction structures in deep-marine, bottom-current-reworked sands in the Pliocene and Pleistocene, Gulf of Mexico, *Geology*, *21*, 929-932.

Shanmugam G. (1997), The Bouma Sequence and the turbidite mind set, *Earth-Sci. Rev.*, *42*, 201-229.

Shanmugam G. (2002), Ten turbidite myths, *Earth-Sci. Rev.*, *58*, 311-341, doi:10.1016/S0012-8252(02)00065-X.

Shanmugam G. (2008), Deep-water bottom currents and their deposits, in *Contourites*, *Developments in Sedimentology*, vol. 60, edited by M. Rebesco, A. Camerlenghi, p. 59-81, Elsevier Science, Amsterdam, Netherlands.

Shea T., Houghton B.F., Gurioli L., Cashman K.V., Hammer J.E., Hobden B.J. (2010), Textural studies of vesicles in volcanic rocks: An integrated methodology, *J. Volcanol. Geotherm. Res.*, *190*, 271-289.

Shepherd J.B., Aspinall W.P. (1982), Seismological studies of the Soufriere of St. Vincent, 1953-79: Implications for volcanic surveillance in the lesser Antilles, *J. Volcanol. Geotherm. Res.*, *12*, 37-55.

Simmons G.C., Van Noy R.M., Zilka N.T. (1983), Mineral resources of the Cougar Lakes-Mount Aix study area, Yakima and Lewis counties, Washington, *U.S. Geol. Surv. Bull.*, *1504*.

Smith G.A., Lowe D.R. (1991), Lahars: volcano-hydrologic events and deposition in the debris flow -hyperconcentrated flow continuum, in *Sedimentation in volcanic settings*, edited by R.V. Fisher, G.A. Smith, p. 59-70, SEPM, Tulsa; Special Publication, 45.

Smith J.G. (1989), Geologic map of upper Eocene to Holocene volcanic and related rocks in the Cascade Range, Washington, 61 pp, 61 sheet pp, U. S. Geological Survey, Reston, VA, United States (USA).

Sohn Y.K., Chough S.K. (1993), The Udo tuff cone, Cheju Island, South Korea; transformation of pyroclastic fall into debris fall and grain flow on a steep volcanic cone slope, *Sedimentology*, *40*, 769-786.

Sohn Y.K. (1997), On traction-carpet sedimentation, *J. Sediment. Res.*, *67*, 502-509.

Sohn Y.K., Park K.H., Yoon S.H. (2008), Primary versus secondary and subaerial versus submarine hydrovolcanic deposits in the subsurface of Jeju Island, Korea, *Sedimentology*, *55*, 899-924.

Sohn Y.K., Yoon S.H. (2010), Shallow-marine records of pyroclastic surges and fallouts over water in Jeju Island, Korea, and their stratigraphic implications, *Geology*, *38*, 763-766.

Sonder L.J., Jones C.H. (1999), Western United States extension: How the west was widened, *Annu. Rev. Earth Planet. Sci.*, *27*, 417-462.

Soule S.A., Fornari D.J., Perfit M.R., Rubin K.H. (2007), New insights into mid-ocean ridge volcanic processes from the 2005-2006 eruption of the East Pacific Rise, 9°46′N-9°56′N, *Geology*, *35*, 1079-1082.

Sparks R.S.J., Self S., Walker G.P.L. (1973), Products of ignimbrite eruptions, *Geology*, *1*, 115-118.

Sparks R.S.J. (1976), Grain-size variations in ignimbrites and implications for transport of pyroclastic flows, *Sedimentology*, *23*, 147-188.

Sparks R.S.J., Sigurdsson H., Carey S.N. (1980), The entrance of pyroclastic flows into the sea; I, Oceanographic and geologic evidence from Dominica, Lesser Antilles; Explosive volcanism in island arcs., *J. Volcanol. Geotherm. Res.*, *7*, 87-96.

Sparks R.S.J. (1997), Causes and consequences of pressurisation in lava dome eruptions, *Earth Planet. Sci. Lett.*, *150*, 177-189, doi:10.1016/S0012-821X(97)00109-X.

Stewart A.L., McPhie J. (2003), Internal structure and emplacement of an Upper Pliocene dacite cryptodome, Milos Island, Greece, *J. Volcanol. Geotherm. Res.*, *124*, 129-148, doi:10.1016/S0377-0273(03)00074-X.

Stewart A.L., McPhie J. (2004), An Upper Pliocene coarse pumice breccia generated by a shallow submarine explosive eruption, Milos, Greece, *Bull. Volcanol.*, *66*, 15-28.

Stine C.M. (1987), Stratigraphy of the Ohanapecosh formation North of Hamilton Buttes, Southcentral Washington, M.Sc. thesis, 83 pp, Portland State University.

Stow D.A.V. (1994), Deep sea processes of sediment transport and deposition, in *Sediment transport and depositional processes*, edited by K. Pye, p. 257-291, Blackwell Scientific Publications, Edinburgh.

Stow D.A.V., Taira A., Ogawa Y., Soh W., Taniguchi H., Pickering K.T. (1998), Volcaniclastic sediments, process interaction and depositional setting of the Mio-Pliocene Miura Group, SE Japan, *Sediment. Geol.*, *115*, 351-381.

Stow D.A.V., Ogawa Y., Lee I.T., Mitsuzawa K. (2002), Neogene contourites, Miura-Boso forearc basin, SE Japan, in *Memoirs of the Geological Society of London*, vol. 22, edited, p. 409-419.

Stow D.A.V., Faugères J.-C. (2008), Contourite facies and the facies model, in *Contourites*, *Developments in Sedimentology*, vol. 60, edited by M. Rebesco, A. Camerlenghi, p. 223-256, Elsevier Science, Amsterdam, Netherlands.

Stow D.A.V., Hunter S., Wilkinson D., Hernández-Molina F.J. (2008), The nature of contourite deposition, in *Contourites*, *Developments in Sedimentology*, vol.

60, edited by M. Rebesco, A. Camerlenghi, p. 143-156, Elsevier Science, Amsterdam, Netherlands.

Sumner E.J., Talling P.J., Amy L.A. (2009), Deposits of flows transitional between turbidity current and debris flow, *Geology*, *37*, 991-994.

Swanson D.A. (1965), The middle and late Cenozoic volcanic rock of the Tieton River area, south-central Washington, Doctoral thesis, 333 pp, Johns Hopkins University, Baltimore.

Swanson D.A. (1966), Tieton volcano, a Miocene eruptive center in the Southern Cascade Mountains, Washington, *Geol. Soc. Am. Bull.*, *77*, 1293-1314.

Swanson D.A. (1978), Geologic map of the Tieton River area, Yakima County, South-central Washington, U. S. Geological Survey.

Swanson D.A. (1996), Geologic map of the Packwood Lake Quadrangle, southern Cascade Range, Washington, 25 pp, 22 sheets pp, U. S. Geological Survey, Reston, VA, United States (USA).

Swanson D.A., Moore R.B., Banks N.G. (1997), Geologic map of the Packwood Quadrangle, southern Cascade Range, Washington, 18 pages, 12 sheets pp, U. S. Geological Survey, Reston, VA, United States (USA).

Swanson S.E., Kienle J. (1988), The 1986 eruption of Mount St. Augustine; field test of a hazard evaluation, *J. Geophys. Res.*, *93*, 4500-4520, doi:10.1029/JB093iB05p04500.

Tabor R.W., Frizzell V.A., Jr., Vance J.A., Naeser C.W. (1984), Ages and stratigraphy of lower and middle Tertiary sedimentary and volcanic rocks of the central Cascades, Washington; application to the tectonic history of the Straight Creek Fault, *Geol. Soc. Am. Bull.*, *95*, 26-44.

Tabor R.W., Frizzell V.A., Jr., Booth D.B., Waitt R.B. (2000), Geologic map of the Snoqualmie Pass 30x60 minute quadrangle, Washington, 57 pp, U. S. Geological Survey, Reston, VA, United States (USA).

Takahashi M., Saito K. (1997), Miocene intra-arc bending at an arc-arc collision zone, central Japan, *Isl. Arc*, *6*, 168-182, doi:10.1111/j.1440-1738.1997.tb00168.x.

Talling P.J., Amy L.A., Wynn R.B. (2007), New insight into the evolution of large-volume turbidity currents: Comparison of turbidite shape and previous modelling results, *Sedimentology*, *54*, 737-769.

Talling P.J., Wynn R.B., Schmmidt D.N., Rixon R., Sumner E., Amy L. (2010), How did thin submarine debris flows carry boulder-sized intraclasts for remarkable distances across low gradients to the far reaches of the Mississippi fan?, *J. Sediment. Res.*, *80*, 829-851.

Tamura Y. (1990), Mode of emplacement and petrogenesis of volcanic rocks of the Shirahama Group, Izu Peninsula, Japan, Ph.D. thesis, 179 pp, University of Tokyo, Japan.

Tamura Y., Koyama M., Fiske R.S. (1991), Paleomagnetic evidence for hot pyroclastic debris flow in the shallow submarine Shirahama Group (Upper Miocene-Pliocene), Japan, *J. Geophys. Res.*, *96*, 21779-21787, doi:10.1029/91JB02258.

Tamura Y. (1994), Genesis of island arc magmas by mantle-derived bimodal magmatism: evidence from the Shirahama Group, Japan, *J. Petrol.*, *35*, 619-645, doi:10.1093/petrology/35.3.619

Tamura Y. (1995), Liquid lines of descent of island arc magmas and genesis of rhyolites: evidence from the Shirahama Group, Japan, *J. Petrol.*, *36*, 417-434, doi:10.1093/petrology/36.2.417

Tamura Y., Nakamura E. (1996), The arc lavas of the Shirahama Group, Japan: Sr and Nd isotopic data indicate mantle-derived bimodal magmatism, *J. Petrol.*, *37*, 1307-1319, doi:10.1093/petrology/37.6.1307

Tanguy J.C. (1994), The 1902-1905 eruptions of Montagne Pelée, Martinique: anatomy and retrospection, *J. Volcanol. Geotherm. Res.*, *60*, 87-107.

Tani K., Fiske R.S., Tamura Y., Kido Y., Naka J., Shukuno H., Takeuchi R. (2008), Sumisu volcano, Izu-Bonin arc, Japan: Site of a silicic caldera-forming eruption from a small open-ocean island, *Bull. Volcanol.*, *70*, 547-562.

Tani K.F., R. S., Dunkely D.J., Ishizuka O., Oikawa T., Isobe I., Tatsumi Y. (2011), The Izu Peninsula, Japan: Zircon geochronology reveals a record of intra-oceanic rear-arc magmatism in an accreted block of Izu-Bonin crust, *Earth Planet. Sci. Lett.*, doi:10.1016/j.epsl.2010.12.052.

Taron J., Elsworth D., Thompson G., Voight B. (2007), Mechanisms for rainfall-concurrent lava dome collapses at Soufrière Hills Volcano, 2000-2002, *J. Volcanol. Geotherm. Res.*, *160*, 195-209, doi:10.1016/j.jvolgeores.2006.10.003.

Taylor B. (1992), Rifting and the volcanic-tectonic evolution of the Izu-Bonin-Mariana Arc, *Proc. Ocean Drill. Program: Sci. Results*, *126*, 627-652.

Textor C., Graf H.F., Herzog M., Oberhuber J.M., Rose W.I., Ernst G.G.J. (2006), Volcanic particle aggregation in explosive eruption columns. Part I: Parameterization of the microphysics of hydrometeors and ash, *J. Volcanol. Geotherm. Res.*, *150*, 359-377.

Trofimovs J., Amy L., Boudon G., Deplus C., Doyle E., Fournier N., Hart M.B., Komorowski J.C., Le Friant A., Lock E.J., Pudsey C., Ryan G., Sparks R.S.J., Talling P.J. (2006), Submarine pyroclastic deposits formed at the Soufrière Hills volcano, Montserrat (1995-2003): What happens when pyroclastic flows enter the ocean?, *Geology*, *34*, 549-552.

Trofimovs J., Sparks R.S.J., Talling P.J. (2008), Anatomy of a submarine pyroclastic flow and associated turbidity current: July 2003 dome collapse, Soufrière Hills volcano, Montserrat, West Indies, *Sedimentology*, *55*, 617-634.

Valentine P.C., Cooper R.A., Uzmann J.R. (1984), Submarine sand dunes and sedimentary environments in Oceanographer Canyon, *J. Sediment. Petrol.*, *54*, 704-715.

Van Den Berg E.H., Meesters A.G.C.A., Kenter J.A.M., Schlager W. (2002), Automated separation of touching grains in digital images of thin sections, *Comput. Geosci.*, *28*, 179-190.

Vance J.A., Clayton G.A., Mattinson J.M., Naeser C.W. (1987), Early and middle Cenozoic stratigraphy of the Mount Rainier-Tieton River area, southern Washington Cascades, *Bull. - Wash., Div. Geol. Earth Resour.*, *77*, 269-290.

Verplanck E.P., Duncan R.A. (1987), Temporal variations in plate convergence and eruption rates in the Western Cascades, Oregon (USA), *Tectonics*, *6*, 197-209.

Villemant B., Boudon G. (1998), Transition from dome-forming to plinian

eruptive styles controlled by H_2O and Cl degassing, *Nature*, *392*, 65-69, doi:10.1038/32144.

Visher G.S. (1969), Grain size distributions and depositional processes, *J. Sediment. Petrol.*, *39*, 1074-1106.

Volentik A.C.M., Bonadonna C., Connor C.B., Connor L.J., Rosi M. (2010), Modeling tephra dispersal in absence of wind: Insights from the climactic phase of the 2450BP Plinian eruption of Pululagua volcano (Ecuador), *J. Volcanol. Geotherm. Res.*, *193*, 117-136.

Walker G.P.L. (1971), Grain-size characteristics of pyroclastic deposits, *J. Geol.*, *79*, 696-714.

Walker G.P.L., Croasdale R. (1971), Two Plinian-type eruptions in the Azores, *J. Geol. Soc. (London, U. K.)*, *127*, 17-55.

Walker G.P.L. (1972), Crystal concentration in ignimbrites, *Contrib. Mineral. Petrol.*, *36*, 135-145.

Walker G.P.L. (1973), Explosive volcanic eruptions - a new classification scheme, *Geol. Rundsch.*, *62*, 431-446.

Walker G.P.L. (1981), Generation and dispersal of fine ash and dust by volcanic eruptions, *J. Volcanol. Geotherm. Res.*, *11*, 81-92, doi:10.1016/0377-0273(81)90077-9.

Walker G.P.L. (1983), Ignimbrite types and ignimbrite problems, *J. Volcanol. Geotherm. Res.*, *17*, 65-88.

Walker G.P.L. (1984), Characteristics of dune-bedded pyroclastic surge bedsets, *J. Volcanol. Geotherm. Res.*, *20*, 281-296.

Walker G.P.L. (1992), Morphometric study of pillow-size spectrum among pillow lavas, *Bull. Volcanol.*, *54*, 459-474.

Walton W.H. (1948), Feret's statistical diameter as a measure of particle size, *Nature*, *162*, 329-330, doi:10.1038/162329b0.

Warren W.C. (1941), Relation of the Yakima basalt to the Keechelus andesitic series [Washington], *J. Geol.*, *49*, 795-814.

Weirich F.H. (1988), Field evidence for hydraulic jumps in subaqueous sediment gravity flows, *Nature*, *332*, 626-629, doi:10.1038/332626a0.

Weirich F.H. (1989), The generation of turbidity currents by subaerial debris flows, California, *Geol. Soc. Am. Bull.*, *101*, 278-291.

Wells R.E. (1990), Paleomagnetic rotations and the Cenozoic tectonics of the Cascade Arc, Washington, Oregon, and California, *J. Geophys. Res.*, *95*, 19409-19417, doi:10.1029/JB095iB12p19409.

Wells R.E. (1998), Fore-arc migration in Cascadia and its neotectonic significance, *Geology*, *26*, 759-762.

Wentworth C.K. (1922), A scale of grade and class terms for clastic sediments, *J. Geol.*, *30*, 377-392.

Wetzel A. (2009), The preservation potential of ash layers in the deep-sea; the example of the 1991-Pinatubo ash in the South China Sea, *Sedimentology*, *56*, 1992-2009.

White J.D.L. (2000), Subaqueous eruption-fed density currents and their deposits, *Precambrian Res.*, *101*, 87-109, doi:10.1016/S0301-9268(99)00096-0.

White J.D.L., Manville V., Wilson C.J.N., Houghton B.F., Riggs N.R., Ort M. (2001), Settling and deposition of AD 181 Taupo pumice in lacustrine and associated environments, in *Volcaniclastic sedimentation in lacustrine settings*, vol. 30, edited by S.P.o.t.I.A.o. Sedimentologists, p. 141-150.

White J.D.L., Smellie J.L., Clague D.A. (2003), Introduction: A deductive outline and topical overview of subaqueous explosive volcanism, in *Explosive Subaqueous Volcanism*, *Geophysical Monograph*, vol. 140, edited by J.D.L. White, et al., p. 1-23, AGU, Washington, D.C.

White J.D.L., Houghton B.F. (2006), Primary volcaniclastic rocks, *Geology*, *34*, 677-680, doi:10.1130/G22346.1.

Whitham A.G., Sparks R.S.J. (1986), Pumice, *Bull. Volcanol.*, *48*, 209-223.

Whitham A.G. (1989), The behaviour of subaerially produced pyroclastic flows in a subaqueous environment: Evidence from the Roseau eruption, Dominica, West Indies, *Mar. Geol.*, *86*, 27-40.

Wiesner M.G., Yubo W., Lianfu Z. (1995), Fallout of volcanic ash to the deep South China Sea induced by the 1991 eruption of Mount Pinatubo (Philippines), *Geology*, *23*, 885-888.

Wilson C.J.N., Walker G.P.L. (1985), The Taupo eruption, New Zealand. I. General aspects, *Philos. Trans. R. Soc., A*, 1529.

Wilson C.J.N. (2001), The 26.5 ka Oruanui eruption, New Zealand: An introduction and overview, *J. Volcanol. Geotherm. Res.*, *112*, 133-174, doi:10.1016/S0377-0273(01)00239-6.

Wilson C.J.N., Hildreth W. (2003), Assembling an ignimbrite: Mechanical and thermal building blocks in the Bishop Tuff, California, *J. Geol.*, *111*, 653-670.

Winters W.J. (1984), Stratigraphy and sedimentology of Paleogene arkosic and volcaniclastic strata, Johnson Creek-Chambers Creek area, southern Cascade Range, Washington, 160 pp, Portland State University, Portland.

Wise W.S. (1970), Cenozoic volcanism in the Cascade Mountains of southern Washington, 45 pp pp, Washington (State) Department of Natural Resources Division of Geology and Earth Resources, Olympia WA United States (USA).

Wohletz K.H., Sheridan M.F., Brown W.K. (1989), Particle size distributions and the sequential fragmentation/transport theory applied to volcanic ash, *J. Geophys. Res.*, *94*, 15703-15721, doi:10.1029/JB094iB11p15703.

Wolfe E.W., Hoblitt R.P. (1996), Overview of the eruptions, in *Fire and mud; eruptions and lahars of Mount Pinatubo, Philippines*, edited by C.G. Newhall, R.S. Punongbayan, p. 3-20, Philippine Institute of Volcanology and Seismology and University of Washington.

Woods A.W., Koyaguchi T. (1994), Transitions between explosive and effusive eruptions of silicic magmas, *Nature*, *370*, 641-642, doi:10.1038/370641a0.

Woods A.W. (2010), Turbulent plumes in nature, *Annu. Rev. Fluid. Mech. 42*, 391-412, doi:10.1146/annurev-fluid-121108-145430.

Wright A.C., Black P.M. (1981), Petrology and geochemistry of Waitakere group, North Auckland, New Zealand, *N. Z. J. Geol. Geophys.*, *24*, 155-165.

Wright I.C. (1996), Volcaniclastic processes on modern submarine arc stratovolcanoes: Sidescan and photographic evidence from the rumble IV and V volcanoes, southern Kermadec Arc (SW Pacific), *Mar. Geol.*, *136*, 21-39.

Wright I.C. (2001), In situ modification of modem submarine hyaloclastic/pyroclastic deposits by oceanic currents: An example from the southern Kermadec arc (SW Pacific), *Mar. Geol.*, *172*, 287-307.

Wright I.C., Gamble J.A., Shane P.A.R. (2003), Submarine silicic volcanism of the Healy caldera, southern Kermadec arc (SW Pacific): I - Volcanology and eruption mechanisms, *Bull. Volcanol.*, *65*, 15-29.

Wright I.C., Chadwick Jr W.W., de Ronde C.E.J., Reymond D., Hyvernaud O., Gennerich H.H., Stoffers P., Mackay K., Dunkin M.A., Bannister S.C. (2008), Collapse and reconstruction of Monowai submarine volcano, Kermadec arc, 1998-2004, *J. Geophys. Res., [Solid Earth Planets]*, *113*, B08S03, doi:10.1029/2007JB005138.

Yamada E. (1984), Subaqueous pyroclastic flows: their development and their deposits, in *Marginal basin geology*, vol. 16, edited by B.P. Kokelaar, M.F. Howells, p. 29-35, Blackwell Scientific; Geological Society Special Publication.

Yamada E., Sakaguchi K. (1987), Stratigraphy and geological structure of the Neogene formations, southwestern part of the Izu Peninsula, Japan, *Chishitsu Chosajo Geppo = Bulletin of the Geological Survey of Japan*, *38*, 357-383.

Yamagishi H. (1987), Studies on the Neogene subaqueous lavas and hyaloclastites in Southwest Hokkaido, *Chika Shigen Chosajo Hokoku (Hokkaido) = Report of the Geological Survey of Hokkaido*, *59*, 55-117.

Yamazaki T., Kato I., Muroi I., Abe M. (1973), Textural analysis and flow mechanism of the Donzurubo subaqueous pyroclastic flow deposits, *Bull. Volcanol.*, *37*, 231-244, doi:10.1007/BF02597132.

Yuasa M., Murakami F., Saito E., Watanabe K. (1991), Submarine topography of seamounts on the volcanic front of the Izu-Ogasawara (Bonin) Arc, *Chishitsu Chosajo Geppo = Bulletin of the Geological Survey of Japan*, *42*, 703-743.